ABSTRACT

Fluorometric detection of industrially important small molecules and metal ions using phenol-based probe molecules with applications in real samples

Submitted by: **Snigdha Roy**

This thesis represents some fluorescence techniques towards analytical detection of different environmentally important metal ions and small molecules which possess serious effects on our health. We have designed some simple phenol based fluorescent probes. The thesis consist of five chapters which are outlined below:

Chapter 1 includes theoretical and technical features of fluorescence spectroscopy as well as general approaches towards designing of fluorescence sensors. It also includes literature overview on some chemo-sensors based on phenolic moiety. Furthermore, it discussed previous studies in brief related to fluorometric detection of Al^{3+} and small molecules like water and methanol using different fluorescent probes.

Chapter 2 describes the materials and experimental methods for whole thesis work. It also describes the synthesis protocols of different fluorescent probes along with their characterization methods. Further the detail procedures for preparation of various analytical samples are included.

Chapter 3 highlights a convenient fluorometric procedure for the detection of soluble Al^{3+} in alcohol medium using a newly synthesized phenolic Schiff base molecule containing coumarin moiety as aluminium fluorosensor. The probe is operable in alcohol medium for early stage detection of micro-level alcoholate corrosion in terms of fluorometrically soluble aluminium alkoxide. Simultaneous monitoring of wet and dry corrosion facility is utilized to identify the alcoholate corrosion in its embryonic stage for commercial aluminium alloy.

Chapter 4 reports a very simple fluorescence probe method for the detection of trace moisture in polar aprotic solvents using a diformyl phenol derivatives. The probe exhibits water induced spectral blue shift in the UV-vis absorption spectra. Such spectral changes causes water% dependent linear emission intensity response which is utilized for the detection of moisture ratiometrically. The method due to its detection simplicity can be applied to detect water adulteration in different food stuffs.

Chapter 5 highlights a unique fluorescence method for detection of trace amount of methanol in ethanol and isopropanol medium using Al^{3+}-complexes of phenolic Schiff base. The detection is mediated by the presence of various extent of water in the medium. Thus, we have shown that the method is very useful to detect methanol poisoning in different alcoholic beverages and hand sanitizers containing high water background.

Dr. Partha Pratim Parui
12/5/22
Professor
Department of Chemistry
Jadavpur University, Kolkata-700032

Snigdha Roy
12/05/2022

Fluorometric Detection of Industrially Important Small Molecules and Metal Ions Using Phenol-based Probe Molecules with Applications in Real Samples

THESIS SUBMITTED FOR THE DEGREE OF

DOCTOR OF PHILOSOPHY (SCIENCE)

By

SNIGDHA ROY

DEPARTMENT OF CHEMISTRY
JADAVPUR UNIVERSITY
KOLKATA -700032
INDIA

May, 2022

CERTIFICATE FROM THE SUPERVISOR

This is to certified that the thesis entitled *"Fluorometric Detection of Industrially Important Small Molecules and Metal Ions Using Phenol-based Probe Molecules with Applications in Real Samples"* submitted by **Snigdha Roy** who got her name registered on June, 2017 for the award of Ph. D. (Science) degree of Jadavpur University, is absolutely based upon her own work under the supervision of **Prof. Partha Pratim Parui** and that neither this thesis nor any part of it has been submitted for any degree/diploma or any other academic award anywhere before.

Prof. Partha Pratim Parui 12/5/22
Supervisor

Dr. Partha Pratim Parui
Professor
Department of Chemistry
Jadavpur University, Kolkata-700032

DECLARATION

I hereby declare that the work incorporated in the present thesis entitled "*Fluorometric detection of industrially important small molecules and metal ions using phenol-based probe molecules with applications in real samples*" has been performed by me in the department of chemistry, Jadavpur University under supervision of Prof. Partha Pratim Parui. Neither this thesis nor any part of thereof has been submitted for any degree or whatsoever.

To possess the general practice of reporting scientific observations, due acknowledgement has been made whenever the work defined is based on the results of other investigators. Any oversight or error in judgment is apologized.

Date   12/05/2022

Snigdha Roy

Dedicated to my Father & Mother

Anything good that has come to my life has been because of you

ACKNOWLEDGEMENTS

I am extremely grateful towards my beloved husband and my parent-in-law for providing me the environment to continue my study.

At final I am exceedingly beholden to my parents, brother for their endless love, courage, unconditional support, each word of console and heartening in my whole life. It is most precise to devote my soul to the wagging tail and pawing of my sweet pets late. Jack & Tango and all the voiceless for always fill my heart without trying. Finally, I praise God for blessing me towards success and keeping me and my family safe.

12/05/22

(Snigdha Roy)
Department of Chemistry
Jadavpur University
Kolkata – 700032

PREFACE

The work bring about in this present thesis entitled "***Fluorometric Detection of Industrially Important Small Molecules and Metal Ions Using Phenol‑based Probe Molecules with Applications in Real Samples***" was begin in April, 2017 and accomplished in the Department of Chemistry, Jadavpur University, Kolkata- 700032.

This thesis introduces some methods of fluorescence techniques for detection of different environmentally vital metal ions as well as small molecules which imposed serious effects on our health and to aid this, we have designed some simple fluorescence probes. We designed phenolic Schiff-base molecule containing coumarin moiety as an aluminium fluorosensor for early detection of micro-level alcoholate corrosion fluorometrically in terms of soluble aluminium alkoxide. The wet and dry corrosions for aluminium alloys are estimated simultaneously to obtain valuable information on alloy specific finding of alcoholate corrosion in its embryonic stage. Fluorescence probe method is also introduced for the detection of trace moisture in polar aprotic solvents. For the moisture detection purpose, we have synthesized a very simple fluorescence probe which possess water% induced spectral blue shift in the absorption spectra as well as linear emission intensity response. The simplicity of the detection methodology can be highly useful to detect water adulteration in food stuffs. By exploiting alcohol coordinated Al^{3+}-complexes of phenolic Schiff-base molecular probe, a trace methanol is detected in ethanol or isopropanol medium in the presence of large water background. The methodology is shown to be highly useful to detect trace amount of methanol contamination in alcoholic beverages and hand sanitizers.

LIST OF ABREVIATIONS

ε	......	Extinction coefficient
τ	......	Fluorescence lifetime
Td	......	Tetrahedral
Oh	......	Octahedral
k_{nr}	......	Rate constant of non-radiative process
Φ	......	Fluorescence quantum efficiency or Fluorescence quantum yields
PET	......	Photo-induced electron transfer
FRET	......	Forster or Fluorescence resonance energy transfer
ICT	......	Intra and intermolecular charge transfer
PIT	......	Photo-induced charge transfer
ESPT	......	Excited state intra-molecular proton transfer
CHEF	......	Chelation enhanced fluorescence emission
AIE	......	Aggregation induced emission
LMCT	......	Ligand to metal charge transfer transition
NIR	......	Near infrared
ESCT	......	Excited state charge transfer
DFP	......	4-Methyl-2,6-diformylphenol
HMBDC	......	((6Z)-6-(2-hydroxy-3-(hydroxymethyl)-5-methylbenzylideneamine) -2H-chromen-2-one)
HHMB	......	2-hydroxy-3-(hydroxymethyl)-5-methylbenzaldehyde
6-ACO	......	6-amino coumarin

A⁻	......	Deprotonated AH
MOFs	......	Metal organic frameworks
PPY	......	Pyrazole unit
PPi	......	Inorganic pyrophosphate
CN⁻	......	Cyanide ion
SO₃²⁻/HSO₃²⁻	......	Sulphite-bisulphite
H₂O₂	......	Hydrogen peroxide
N₂H₄	......	Hydrazine
H₂PO₄	......	Dihydrogen phosphate
PBS	......	Phosphate buffered saline
DMSO	......	Dimethyl sulphoxide
MeOH	......	Methanol
EtOH	......	Ethanol
ⁱPrOH	......	Isopropanol
THF	......	Tetrahydrofuran
AcOH	......	Acetic acid
DMF	......	Dimethyl formamide
MeCN	......	Acetonitrile
n-PrOH	......	n- propanol
ᵗBuOH	......	Tertiary butanol
SOCl₂	......	Thionyl dichloride
TEA	......	Triethyl amine
DCM	......	Dichloromethane

$CaCl_2$ ......   Calcium chloride

EDTA   ......   Ethylene diamine tetraacetate

Na_2SO_4 ......   Sodium sulphate

Al-7075   ......   Aluminium based alloy

$Al(OR)_3$ ......   Aluminium alkoxide

CONTENTS

in polar aprotic solvents with the application in foodstuffs

LIST OF PUBLICATIONS (APPENDIX)

LIST OF PUBLICATIONS

1. **S. Roy**, S. Das, R. Majumder, A. Ray and P. P. Parui, *RSC Adv.*, 2020, **10**, 23245.

2. **S. Roy**, S. Das, A. Ray and P. P. Parui, *New J. Chem.*, 2021, **45**, 4574

3. **S. Roy**, S. Das, A. Ray and P. P. Parui, *RSC Adv.*, 2021, **11**, 30093.

4. **S. Roy**, S. Das, A. Ray and P. P. Parui, (To be submitted).

5. R. Majumder, **S. Roy**, K. Okamoto, S. Nagao, T. Matsuo and P. P. Parui, *Langmuir,* 2020, **36**, 426−434.

6. Y. Sarkar , **S. Roy** , R. Majumder , S. Das , D. V. Bhalani , A. Ray , S. K. Jewrajka and P. P. Parui, *Soft Matter*, 2020, **16**, 798-809

7. P.P. Parui, A. Ray, S. Das, Y. Sarkar, T. Paul, **S. Roy**, R. Majumder and J. Bandyopadhyay, *New J. Chem.*, 2019, **43**, 3750.

Chapter 1

Common aspect about small molecules and metal ions sensing: background, literature overview, extent and goal

1.1. Introduction

Rapid modernization introduces ions and molecules to redistribute in the environment and thus frequently offers adverse effects on living system and its surrounding.[1] Additionally, the exposure and adulteration of industrially and biologically hazardous elements may also alter industrial and physiological activities of human being.[2-4] Thus the detection of those ions/molecules possess a potential impact on chemical research.[5] Researchers have focused to design various types of small molecule chemical sensors to detect different environmentally or industrially important metal ions and small molecules.[6-8] In this context, the fluorescence based chemo-sensing procedures are extremely advantageous because of its simplicity, prompt responsive ability, as well as immune sensitive nature with non-destructive property. Moreover, its high detection sensitivity makes it more useful and offer to be act as a better alternative over other techniques.[9-13] Therefore designing of a suitable fluorescence chemo-sensing probe molecules is very demanding.[14-16] Some reviews of previous research works as well as brief outlines of present work based on the above said issues have been discussed in this thesis.

1.2. Fluorescence spectroscopy: theoretical and technical features

Fluorescence technique is one of the most reliable and convenient process both in environmental as well as biological domain for the detection of low concentration of analytes with high accuracy.[17] Fluorescence spectroscopy is concerned to the interaction of the light with matter. When a matter is exposed to light, some of the light may be absorbed, some may scattered or simply emit depending upon the nature of the matter and incident light.[18-19] The light absorption promotes the molecule in its excited electronic state. Since the probability of finding the molecule is maximum in the midpoint of the lowest vibrational state of singlet ground state, therefore the most probable transition originates from the midpoint of ground state. The upward vertical transition occurs by following the Franck Condon principle. The electronic transition involves the excitation of a bonding electron into the vacant antibonding or high energy orbital, and thus the equilibrium intermolecular distance is to be slightly greater than that of the excited singlet state. The excited molecules are subjected to collision with the surrounding molecules and gives up energy in different pathways. The molecules step down the ladder of vibrational levels by the process of radiation less decay or vibrational relaxation to the lowest vibrational level of the excited electronic state. Vibrational relaxation also takes place by phosphorescence *via* intersystem

crossing, forming excimer or exciplex, transforming electron or photon/energy, internally and photochemical transferring charges (Fig. 1). The surrounding molecules however might be unable to accept the larger energy differences needed to reach the molecule in the ground electronic state, and thus the molecules emits its excess energy in the form of radiation called fluorescence radiation. Therefore, fluorescence is the transition between two spin states of same multiplicity. Fluorescence occur at a lower energy than the incident radiation because the emissive transition occurs after some vibrational energy has been lost into the surrounding.
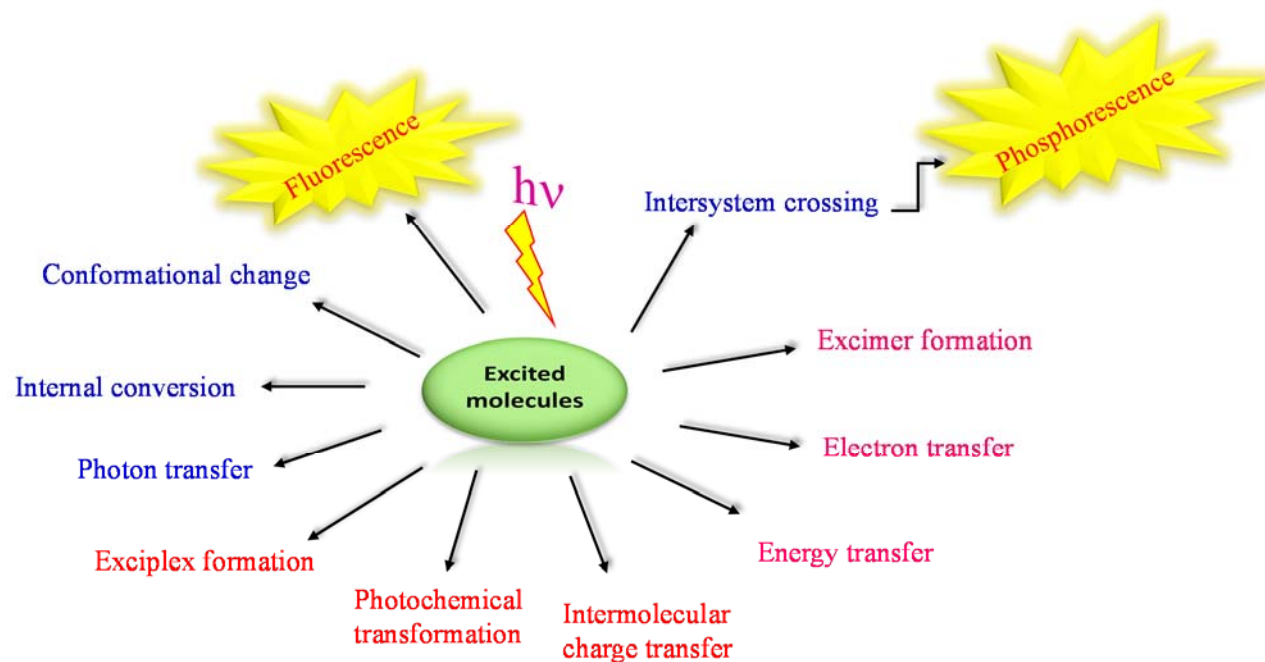
Fig. 1. Possible pathways of vibrational relaxation process

A Jablonski diagram is a simplified portrayal of relative positions of the electronic energy levels of a molecule proposed by Professor Alexander Jablonski in 1935. Vibrational levels of a given electronic state lie above each other. Illustration of the electronic states of a molecule and various transitions can be explained by Jablonski diagram (Fig. 2).
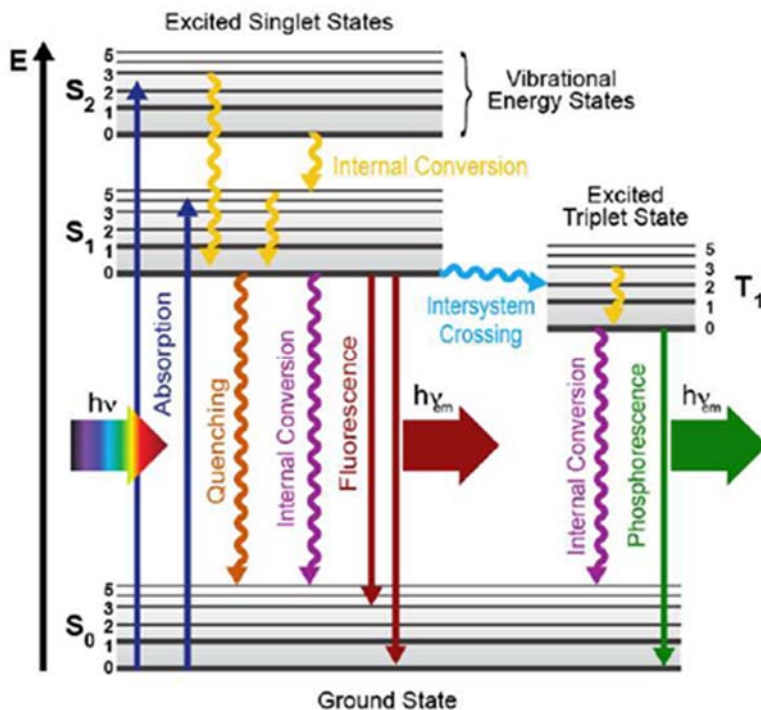
Fig. 2. Jablonski diagram of various photophysical process
(https://www.simtrum.com/WebShop/SolutionInfo.aspx?id=1669)

1.2.1. Fluorescence decay time or fluorescence lifetime

The fluorescent chemical compound that can emit its excitation energy in the form of light is known as fluorescence. In addition to the fluorescence intensity value, fluorescence decay time called fluorescence lifetime is very important parameter to analyze the molecular properties as well as its surrounding environments. The fluorescence lifetime is a measure of the time which a molecule spends in the excited state before returning to the ground state by emitting a photon in the form of light. The lifetime is affected by various external conditions like temperature, polarity or presence of fluorescence quenchers. The lifetimes of the excited species can vary from several picoseconds to hundreds of nanoseconds. The intrinsic or natural radiative lifetime (τ_n) in the absence of any competitive deactivation process is solely defines as,

$$\tau_n = \frac{1}{k_r}$$

Where k_r is the rate constant of radiative process. However, the actual average lifetime (τ) of an excited species defined as,

$$\tau_n = \frac{1}{k_r + k_{nr}}$$

Where k_{nr} is the rate constant of non-radiative process. The lifetime value is actually found to be less as compared to the natural radiative lifetime or intrinsic lifetime of that species owing to occurrence of other competitive deactivation pathway.[20-21]

1.2.2. Fluorescence quantum efficiency or fluorescence quantum yields

The fluorescence quantum efficiency (Φ) may be defined as the number of moles reacted per Einstein of the light absorbed,

$$\Phi = \frac{Number\ of\ molecules\ reacting\ in\ a\ time}{Number\ of\ quanta\ of\ light\ absorbed\ in\ the\ same\ time}$$

or,

$$\Phi = \frac{Rate\ of\ the\ reaction}{I_{abs}}$$

Basically fluorescence quantum efficiency is the measure of fluorescence efficiency of a fluorophore. If quantum efficiency is zero then the molecule is non-fluorescent. It may have value less than one, equal or greater than unity. When molecules simply re-emit its energy, collide with each other or may decompose through pre-dissociation then quantum efficiency have a value less than one.[22-25]

1.2.3. Fluorescence quenching

A variety of molecular interactions which causes to decrease the fluorescence intensity of any fluorophore is known as fluorescence quenching. Different types of excited state reactions, molecular reorganization, ground or excited state complexion, energy transmission, exciplex formation are responsible for the intensity quenching due to efficient non-radiative transitions to the ground state. Those short range interaction between excited species and quencher allows their electron cloud to interact and make the quenching process favorable. Temperature and pressure also sometimes affect for the quenching of fluorescence intensity. Different types of ions or small

organic molecules (amides, bromates, iodide, peroxides, nitroxides, and acrylamide) or even some gases such as molecular oxygen can act as efficient fluorescence quenchers. However, for effective fluorescence sensing methodology, analyte induced fluorescent enhancement behavior is more promising than that of the fluorescent quenching observation.[26] Thus, designing of "turn-on" fluorescence probe is more suitable as compare to the "turn-off" probes.

1.2.4. Mechanism of Fluorescence sensing

Fluorometric chemical sensing with an ultra-high sensitivity is considered to be one of the most convenient approaches.[27] Besides that, fluorescent chemo-sensor needs to fulfill some basic criteria, such as binding selectivity and sensitivity. It can be achieved by a specific affinity for the relevant target along with an unperturbed fluorescence signal from the effect of environmental interferences. The molecular sensor of this type is able to produce a detectable change upon its binding with an analyte.[28] Moreover, it possess stability against illumination. There are many different mechanism possible for energy transfer between donor and acceptor moiety in such fluorescent chemo-sensor. These are photo-induced electron transfer (PET), Forster resonance energy transfer (FRET), intra and inter molecular charge transfer (ICT), photo induced charge transfer (PCT), excited state proton transfer (ESPT).[29] A brief discussion about them are given as follows.

1.2.4.1. Photo-induced electron transfer (PET)

Photo-induced charge transfer (PET) processes consist of electron donation from the excited state of donor moiety to the acceptor moiety. As a result of PET, a charge separation is produced, which implies a redox reaction happening in the excited state. Generation of fluorescence takes place by the possible restriction of PET through inhibiting the donation of non-bonding electrons from donor moiety to the acceptor moiety. This process is mostly affected by polarity of the solvent. In more polar solvents electron transfer process become easier than less or nonpolar solvents with making the overall PET process favorable.[30]

1.2.4.2. Forster or fluorescence resonance energy transfer (FRET)

Forster or fluorescence resonance energy transfer is a mechanism that describe the energy transfer between two light sensitive molecules. Basically, the transformation of excitation energy of a

donor fluorophore moiety is takes place to a neighboring acceptor fluorophore moiety in a non-radiative fashion through a long range dipole-dipole interaction. In FRET process, both the chromophores are fluorescent in nature. This type of energy transferring process among different donor-acceptor moieties is very important towards designing of appropriate chemo-sensing probe molecules. This process of energy transfer is extremely sensitive with respect to slight changes in intramolecular distance between donor and acceptor units. For this reason this process is very much applicable to measure the dynamic activities of biological molecules.[31-32]

1.2.4.3. Intra and intermolecular charge transfer (ICT)

Charge transfer process is basically an electron relocation process, where the transformation of electron takes place from one part of a donor moiety to a different part of acceptor moiety. This type of electron transformation can be happened by intra or intermolecular way. When charge distribution in an excited molecule produces a very large excited state dipole moment, the intramolecular charge transfer takes place. However, when an excited molecule and its neighboring molecule behave like a donor-acceptor, then intermolecular charge transfer can take place. During the formation of π-electron conjugated system (contains electron rich as well as electron deficient skeleton) if direct attachment of fluorophore with the receptor happened then ICT can take place. Both inter- and intra-molecular charge transfer systems consist of donor acceptor moiety together.[33]

1.2.4.4. Photo-induced charge transfer (PCT)

Many biological process, electrophotography and photography are highly related with the photo-induced charge transfer process. Conjugation between electron donating group like $-OR, -NH_2$, $-NR_2$ and electron accepting group like $-NO$, $-CN$, $>C=O$ makes the process feasible. Electronic excitation causes the movement of electron from one orbital to other with simultaneous change in dipole moment. Increasing solvent polarity causes a bathochromic shift or red shift of emission wavelength. Excitation produces a partially positive character on the donor group owing to transfer of charge from donor to acceptor. This type of partial positive charge on donor atom makes the donor atom less desire to bind with metal ion.[34]

1.2.4.5. Excited state intramolecular proton transfer (ESIPT)

When photo-excited molecules relax their energy through tautomerization by transferring a proton from one to another moiety within the molecule then this process is known as excited state intramolecular proton transfer. The most common tautomerization is the keto-enol tautomerism. Molecules which possess ESIPT nature possess extremely larger Stokes shift compare to those observed for other known fluorescent molecules. Sometimes they exhibits dual fluorescence properties in which shorter-wavelength results from the original tautomer and longer-wavelength results from proton-transferred tautomer.[35]

1.3. General methodologies towards designing fluorescent sensors

Compounds that contains a binding site as well as fluorophore moiety with showing a well interaction ability between these two sites are considered as fluorescent chemosensor.[36] The fluorescent sensor is basically converts a molecular recognition to results a quantifiable fluorescent signal changes.[37] Nowadays, this type of sensor is turn into a potential tool in various analytical research fields. Construction of optical sensor is based on different chemical approaches to detect different analytes. The main important methodologies are chemo-dosimeter, binding site-signaling approach as well as displacement approach. The method of chemo-dosimeter is very useful approach concerning an analyte recognition with a simultaneous irreversible transduction of a noticeable signal changes. Chemo-dosimeter (fluorescence sensor) interacts with analytes with simultaneously breaking or forming of covalent bonds. This type of interaction leads to significant chemical modification and a product that has absolutely different properties compare to that of the starting material. Another type of method known as binding site-signaling approach, where covalent linkage generates among binding sites and signaling subunit, and subsequently fluorescence of the signaling unit is generated by the interaction of analyte and binding site. On the other hand, for displacement approach, a regeneration of fluorescence due to decomplexation is resulted in the presence of analytes.

In recent times, researcher have focused towards development of fluorescent chemo-sensor as it has extended application towards industrial as well as biological sphere.[38-39] Biologically/industrially important various types of cations, anions and small molecules have been recognized by this technique in a selective and sensitive way. Herein, three main sensing protocol for detection and estimation of ions and molecules are shown below (Fig. 3.1-3.3).
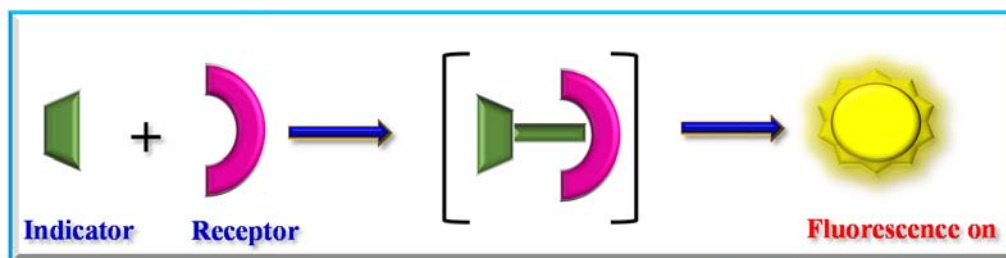
Fig. 3.1. Chemodosimeter approach
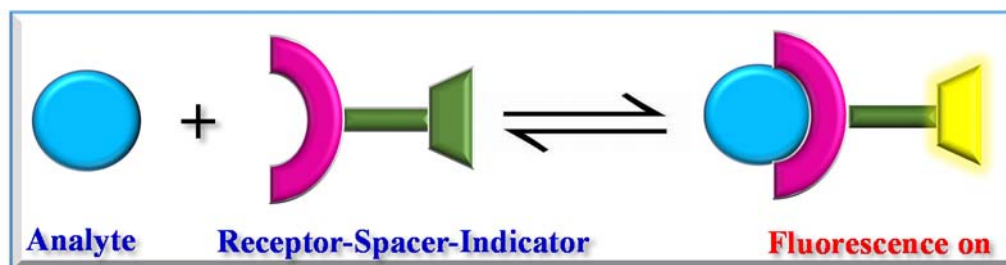
Fig. 3.2. Binding site-signaling approach
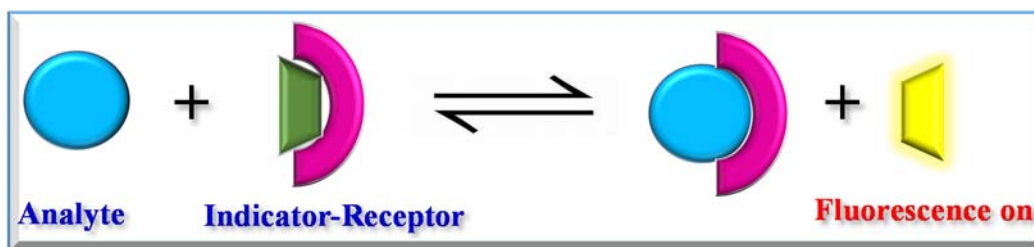
Fig. 3.3. Displacement approach

1.4. Phenol based probe as chemo-sensors

For development of diverse ions/molecules selective fluorescent chemo-sensors, different fluorophoric platforms have been used. Among them phenol based molecules are very well known, where the conversion from phenol to phenolate form is the main driving force for the generation of fluorescence. A large number of fluorescence chemo-sensor based on phenolic chromophore moieties have been reported in the recent past. As for example different derivatives of 4-methyl-2,6-diformylphenol (DFP) containing phenolic moiety are very purposeful for detection of cations, anions and small neutral molecules by a "turn-on" fluorescence method.[40] A novel fluorescent sensor **L1** based on a coumarin moiety is introduced by Y. Jiang *et al.* This probe has the ability

to combine selectively with Hg^{2+} among different other metal ions with a 'turn-on' yellow fluorescence intensity due to restriction of PET process.[41]
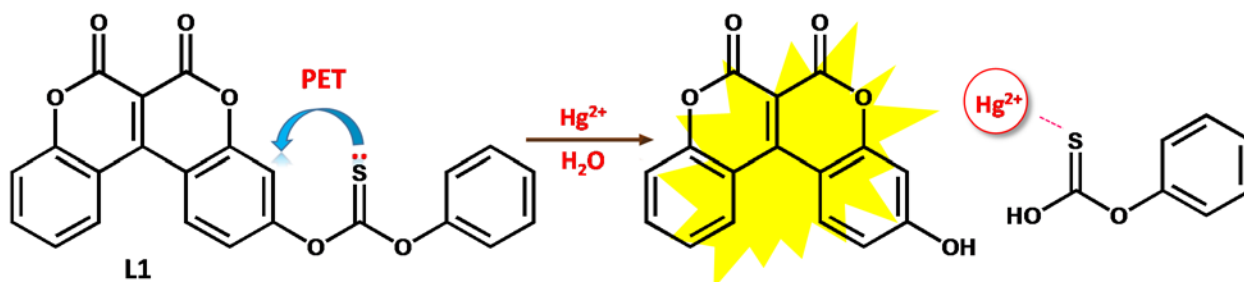
An interesting near infrared fluorosensor **L2** containing 6-hydroxyindole-BODIPY is reported by L. Chao and his research group for sensing Hg^{2+} by monitoring fluorescence enhancement at 637 nm due to the restriction of PET process.[42] B. Gao *et al.* have designed a 7-hydroxy coumarin based chemo-dosimeter **L3** which can detect Hg^{2+} with a colorimetric response in aqueous medium.[43] Another chemo-dosimeter **L4** based on benzothiazole with two recognition sites selective for Hg^{2+} and Cu^{2+} respectively is proposed by B. Gu and co-workers. The probe irreversibly binds with Hg^{2+} to produce a ratiometric fluorescence response. On the other hand, the reversible binding with Cu^{2+} results in quenching of fluorescence intensity. In live cell imagining studies, a naked eye visual color change from green to blue upon binding with Hg^{2+} is detected. Whereas in the presence of Cu^{2+} the ligand changes its color from green to colorless.[44]

L3

L4
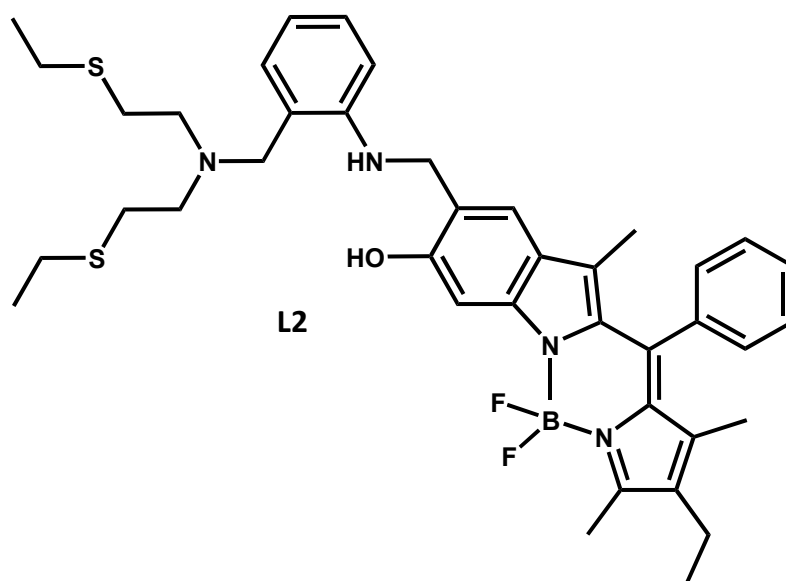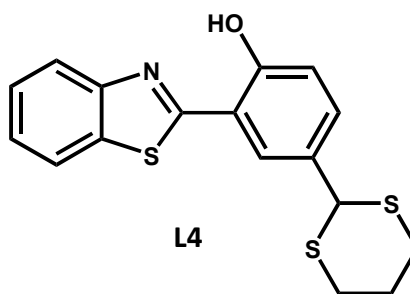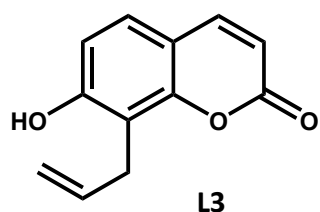
J. Z. Li and co-workers have designed a dicyanoisophorone-based near-infrared fluorescent probe (**L5**) which can act as a dual sensor for Cu^{2+} and S^{2-}. Additionally, the binding of **L5** with Cu^{2+} generates a change in color from light yellow to brown, whereas the introduction of S^{2-} in that system containing **L5**-Cu^{2+} complex results in conversion of brown to light yellow color.[45]
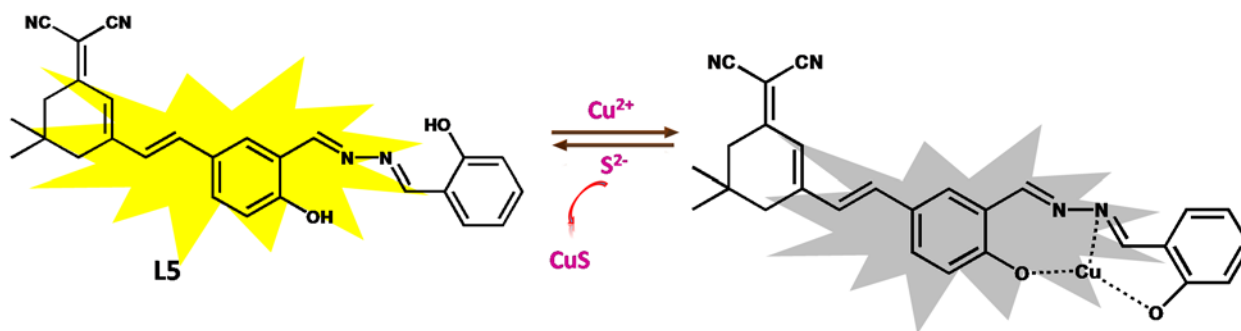
J. M. V. Ngororabanga and co-workers have proposed a simple coumarin-based Cu^{2+} selective turn-off fluorosensor (**L6**) in water medium. The binding of Cu^{2+} with the probe molecule allows an appreciable amount of charge transfer from the fluorophore excited state to the d-orbital of Cu(II) and thus facilitates the PET process to observe fluorescence quenching.[46] Another colorimetric chemo-sensor (**L7**) based on a julolidine (heterocyclic aromatic organic compound) and naphthalene moiety for detection of Cu^{2+} in aqueous methanol solution is reported by D. J. Fanna *et al*.

L6

L7
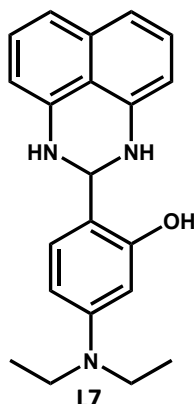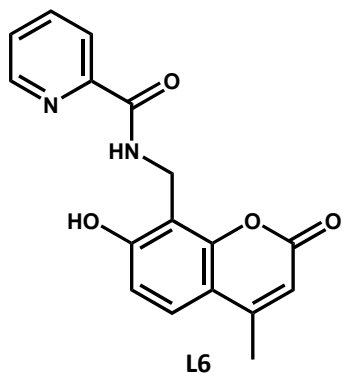
Upon binding with Cu^{2+} the probe possess a distinct color change from colorless to yellow.[47] Another two interesting fluorescent probes, **L8** and **L9** containing an amino-quinoline moiety have proposed by P. Wang and co-worker. An intramolecular charge transfer transition (ICT) in the ligand moiety is responsible for the fluorescence response of the probe molecule. Furthermore, in the presence of Cu^{2+} as well as citrate ion, the probe behave as a turn-off to turn-on colorimetric as well as fluorometric response. Inhibition of the ICT process is mainly responsible for the fluorescence quenching upon the coordination with Cu^{2+}. The citrate ion remove the Cu^{2+} reversibly to make the ligand free and thus regenerate the fluorescence signal of the probe.[48]

L8   **L9**
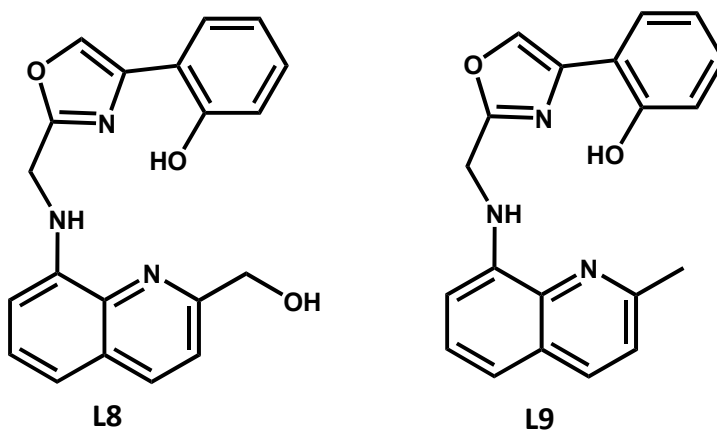
Recently, phenolic imine containing **L10** and **L11** have reported by O. G. Beltran *et al.* as a turn-off fluorescent probe towards the detection of Cu^{2+} and Fe^{3+}. They have reported that **L11** selectively sense Cu^{2+} whereas **L10** acts as a dual sensor towards Cu^{2+} and Fe^{3+}. **L10** in buffer medium undergo a hydrolysis reaction to produce 3-amino-7-hydroxycoumarin, which selectively bind with Cu^{2+} as well as Fe^{3+} and quenched the fluorescence intensity. On the other hand **L11** can only bind with Cu^{2+} with showing quenching of fluorescence intensity.[49]

L10   **L11**
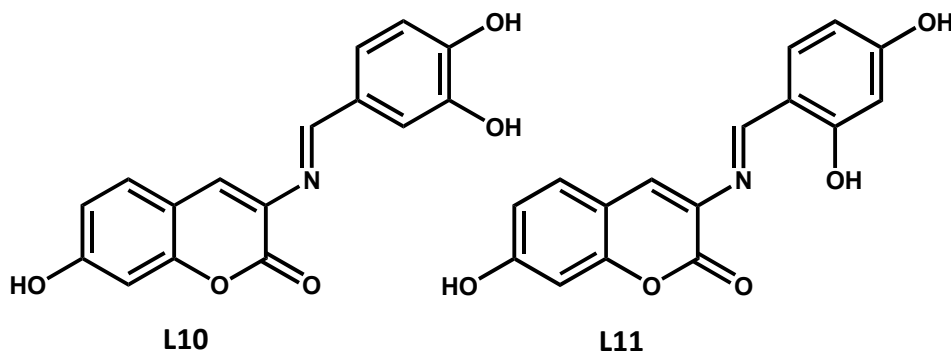
In addition, a new chemo-sensing ligand **L12** containing coumarin moiety is developed by W. Wang *et al.*. The probe exhibits a fast and reversible sensing *via* turn "off-on" response towards Fe^{3+} and inorganic pyrophosphate (PPi). Upon binding of Fe^{3+} with **L12**, the strong fluorescence intensity of **L12** become quenched either by paramagnetic quenching effect of Fe^{3+} and/or *via* LMCT process. However, regeneration of this fluorescence can take place by the interaction of PPi with **L12**-Fe^{3+} complex, where the displacement of Fe^{3+} from the complex set the ligand free.[50]
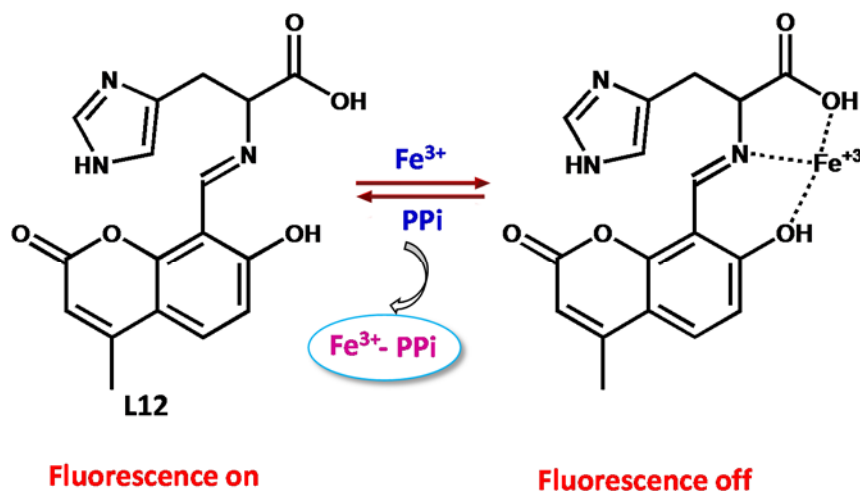
S. Gharami *et al.* synthesized another interesting coumarin moiety based fluorescent probe (**L13**) containing azo-phenol unit, which selectively sense Mg^{2+} by forming **L13**-Mg^{2+} complex and furthermore the Mg^{2+}-complex is used to detect F^- selectively among the presence of other anions. The probe itself shows very weak emission due to the PET process, but after binding with Mg^{2+} the PET process become restricted and chelation enhanced fluorescence (CHEF) takes place.[51] However in the presence of F^- ion the Mg^{2+} form MgF_2 and set the ligand free and thus the emission intensity again weaken.

12
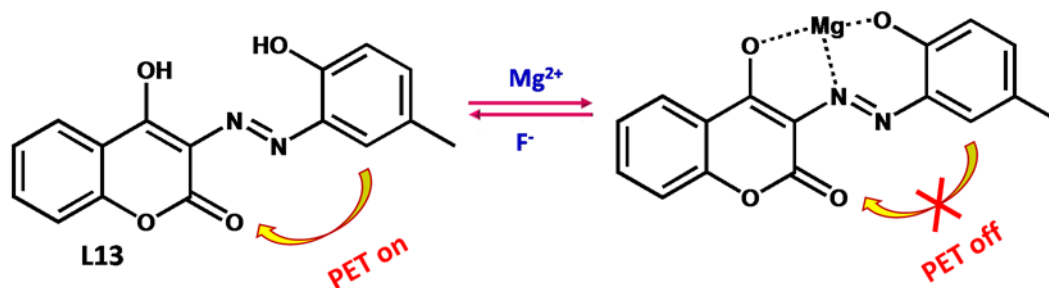
Various other types of anion sensing fluorescent probe molecules are also reported based on phenol moiety. G. mahalaxmi *et al.* design a naphthoquinone-imine based highly selective fluorescence "turn-on" probe (**L14**) for the detection of CN^- in aqueous medium. In the presence of CN^- ion, the three hydroxyl group in the probe molecule simultaneously loose H^+ for three alike CN^- ion. The deprotonations facilitate the activation of the rings by increasing the electron density in those moiety to result an appreciable enhancement of fluorescence intensity at 528 nm. Moreover, a green coloration from a colorless state under UV light upon interaction with CN^- is also noticed.[52] Another important ligand (**L15**) based on indole-naphthalene moiety is proposed by Y. Yue *et al.* with a characteristics of red fluorescence emission towards the sensing of CN^- ion. Due to the presence of polar CN^- ion, the ring becomes deactivated with creating an electron deficient site for nucleophilic addition by CN^- ion.
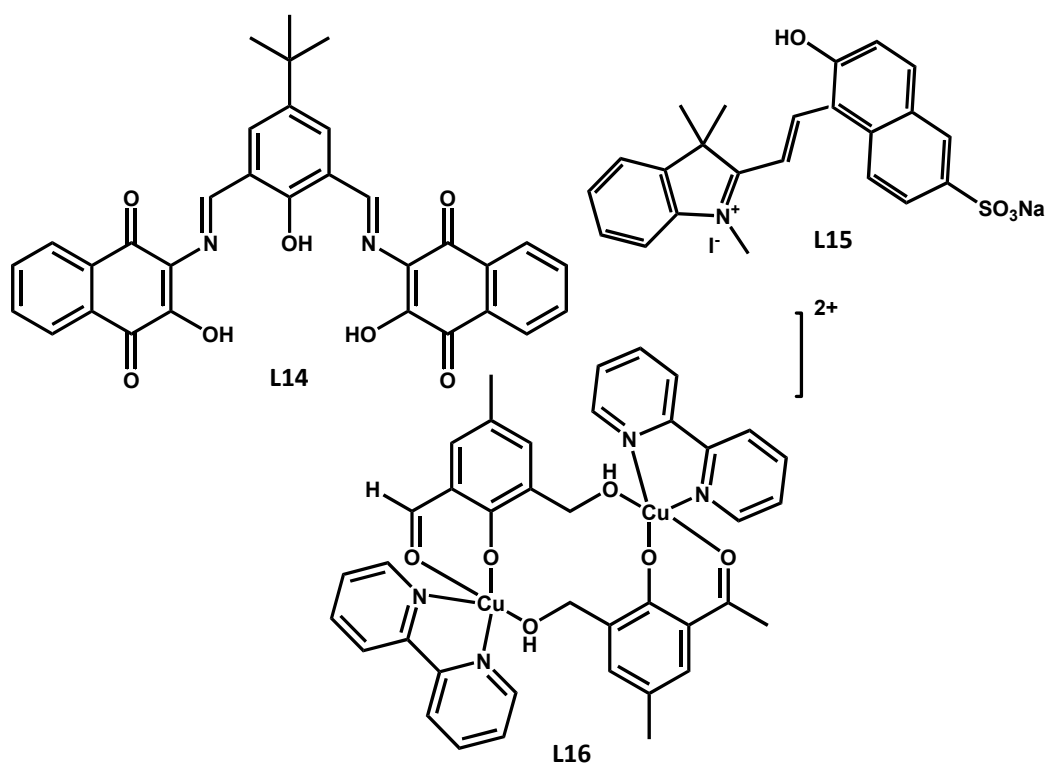
Such chemical changes restricts the intra-molecular charge transfer process (ICT) and subsequently quenching of the intense fluorescence intensity at 606 nm is detected.[53] Recently S. Das *et. al.* have reported a dimeric hydroxyl-methyl benzaldehyde based Cu-complex molecule as a fluorescence probe **L16** for the detection of CN⁻. This probe exhibits a fluorescence "off-on" response towards CN⁻ ion in aqueous medium. An irreversible dimer to monomer complex structural transformation in aqueous medium is mainly responsible for the sensing of CN⁻ ion. During interaction of CN⁻ ion with the complex, Cu^{2+} is displaced from the monomeric form of the probe and generate the fluorogenic phenolate moiety to observe large increase of fluorescence intensity.[54]

A near-infrared fluorescent probe (**L17**) based on IR-780 (a heptamethine cyanine fluorescent probe) is designed by D. Li *et al.* The probe can selectively identify SO_3^{2-}/HSO_3^{2-} by following a colorimetric response from light blue to light green colorization.[55] Y. H. Qin *et al.* have reported another interesting colorimetric fluorescence probe **L18** consisting a hemicyanin (group of acentric cationic dye) moiety which can detect SO_3^{2-}/HSO_3^-. Nucleophilic addition of SO_3^{2-}/HSO_3^{2-} with the C=C bond in the probe molecule and subsequent restriction of ICT process is mainly responsible for the color changing phenomenon.[56]

L18

L17
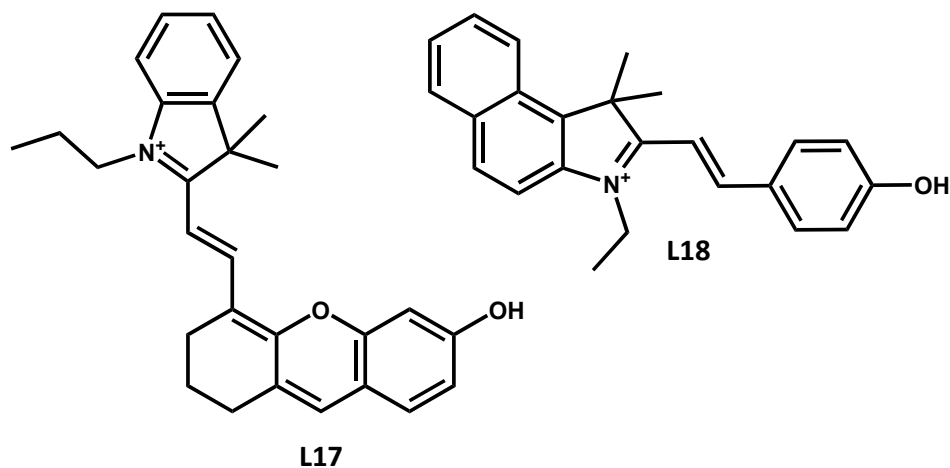
Beside the detection of ions, phenol based fluorescence probes are also employed for detection of small molecules, which possess both industrial as well as biological importance. A very important metal based fluorescent probe **L19** is introduced by Y. Hitomi *et al.* for detection of H_2O_2. The combination of 7-dihydroxyphenoxazine derivative as a fluorescence indicator site along with an

iron complex as a reaction site can have the ability to detect H_2O_2. In the presence of H_2O_2, the iron complex vigorously react to produce an oxidant species which furthermore undergoes an intramolecular conversion from 3,7-dihydroxyphenoxazine moiety to Resorufin. Such chemical conversion results change in fluorescence character from pink to bright red. So they propose that the generation of Resorufin is mainly responsible for the fluorometric response of the probe upon binding with H_2O_2.[57]

L19
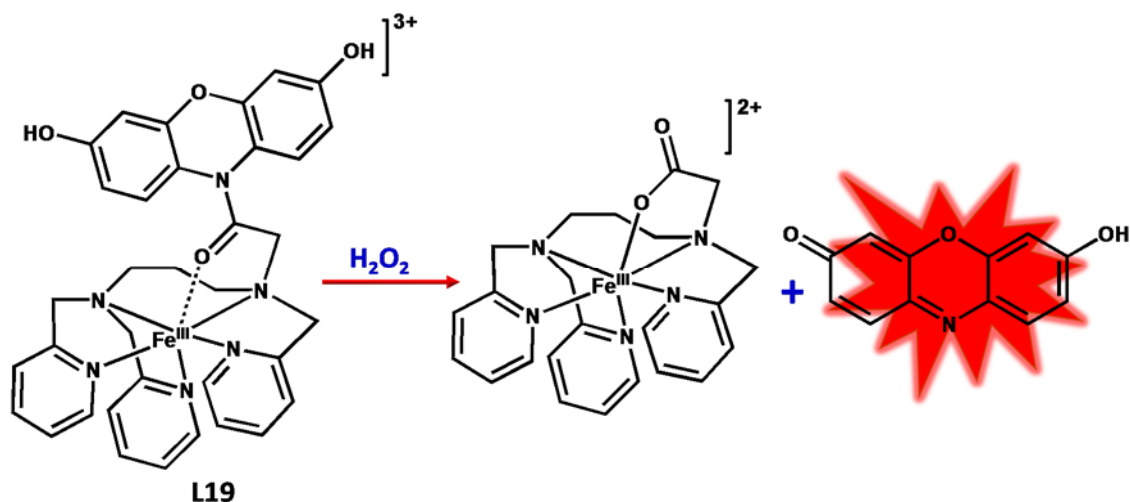
Another set of Schiff base-Cu^{2+} complexes acting as very efficient fluorescence probes (**L20** and **L21**) consisting diformyl phenol moiety are designed by S. Das *et al.* for the detection of cysteine (Cys) and glutathione (GSH) in 100% aqueous medium *via* a turn "off-on" fluorescence mode. **L20** selectively recognizes Cys over GSH *via* decomplexation process. The sensing response is observed due to large steric crowding created by the bulky tri-peptide GSH around the Cu^{2+} center during their decomplexation interaction. On the other hand, smaller Cys molecule can successfully interact with Cu^{2+} in **L20** followed by hydrolysis of the ligand to produce fluorogenic 4-methyl-2,6-diformyl phenol. Furthermore, **L21** recognizes GSH over Cys because the interaction of **L21** with Cys leads to the formation of a non-fluorescent stable cyclic thiazolidine derivative. However, the interaction with GSH produce the same fluorogenic 4-methyl-2,6-diformyl phenol.[58]

L20

L21
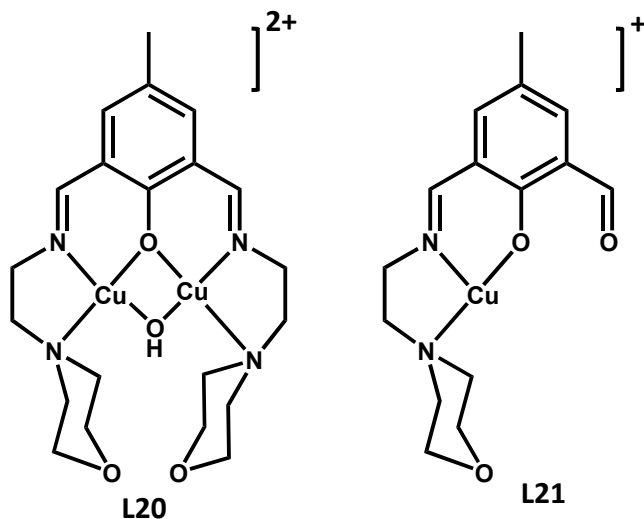
Y. Sarkar *et. al.* have demonstrated an unique boric acid (BA) sensing methodology in aqueous medium using a simple phenolic Schiff base fluorescent probe (**L22**) containing an aromatic aldimine domain. Inhibition of intra-ligand excited state electron or charge transfer (ESCT) mechanism is responsible for boric acid mediated fluorescence enhancement for the probe molecule.[59]

L22

L23

L24
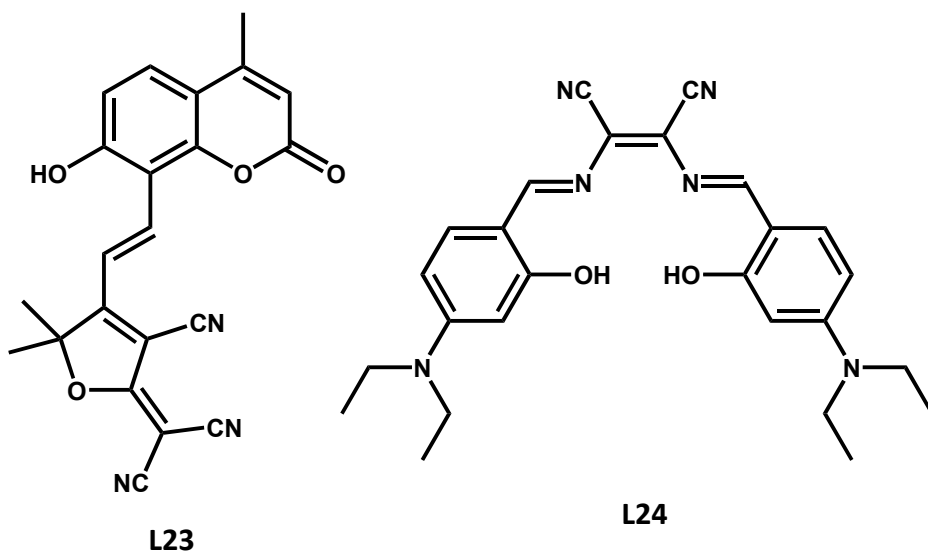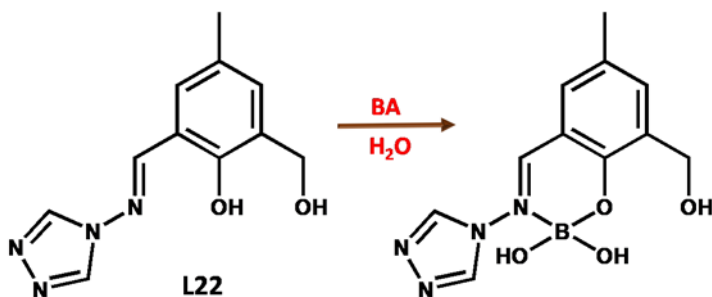
S. Jhang *et al.* have reported detection of hydrazine by a simple coumarin based turn-on fluorescent probe **L23** with a very distinct colorimetric response. The interaction of **L23** with hydrazine exhibits an achromatic to atrovirens color change under an ambient light condition whereas a very weak to brilliant blue fluorescence intensity change is observed under 365 nm ultraviolet lamp.[60] H. Xu *et al.* have also reported a ratiometric fluorescence probe (**L24**) based on hydroxyl benzylidine-maleonitrile moiety for sensing hydrazine. Intra molecular charge transfer (ICT) and excited state intramolecular proton transfer (ESIPT) processes in the presence of hydrazine are mainly responsible for the generation of red fluorescence intensity.[61] In addition, a distinct colorimetric response from purple to yellow is observed in the presence of hydrazene. Y. Jung *et al.* have reported another turn-on fluorescence probe (**L25**) based on napthaldehyde moiety which can specifically detect malononitrile in aqueous medium *via* an intramolecular cyclisation process. The approach of the malononitrile detection includes through a cascade reaction which generates a red-emitting iminobenzo coumarin fluorophore.[62]

L25
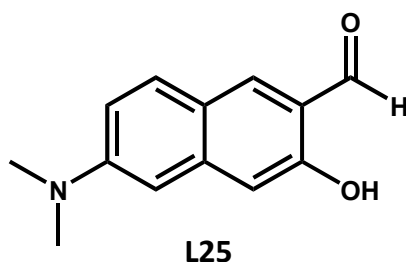
1.5. A short review on Al^{3+} sensor

Aluminium has versatile applications in our daily life starting from food industry to pharmaceutical industry. Beside many scientific evidences, it is found that aluminium can improve our health, although it is also well known that aluminium exposure can damage our health.[63] Some beneficial effect of aluminium includes the food and beverage packaging, due to providing safe barriers to bacteria contamination and also purifying drinking water. High levels of aluminium in the body have been shown to have neurotoxic effects, effects on bone and reproduction. Aluminium used as an active ingredient in some antiperspirants can cause breast cancer.[64] Thus, the evolution of fluorescent chemosensor with high selectivity for Al^{3+} has been a vital research area. Till date major research works related to aluminium sensing are devoted in the fields of medical diagnostics, environmental monitoring and toxicological analysis. Thus, even a trace aluminium level imposed

a potential effect. For this reason researchers have focused to develop effective probes which can able to detect aluminium and allow the in-depth understanding of its effect in biological as well as environmental area. Some of them are discussed very briefly in this context.

H. Xu *et al.* is proposed a novel purin based Schiff base fluorescence probe (**A1**) which possess reversible fluorescence property as well as a colorimetric response towards detection of Al^{3+} in 9:1 DMSO/water mixed medium. The enhancement of fluorescence intensity is due to the inhibition of PET as well as ESIPT processes. However, in the presence of F^-, the **A1**-Al^{3+} complex act as a "turn-off" fluorescence sensor for F^- following through the displacement of Al^{3+}.[65]

A1   **A2**
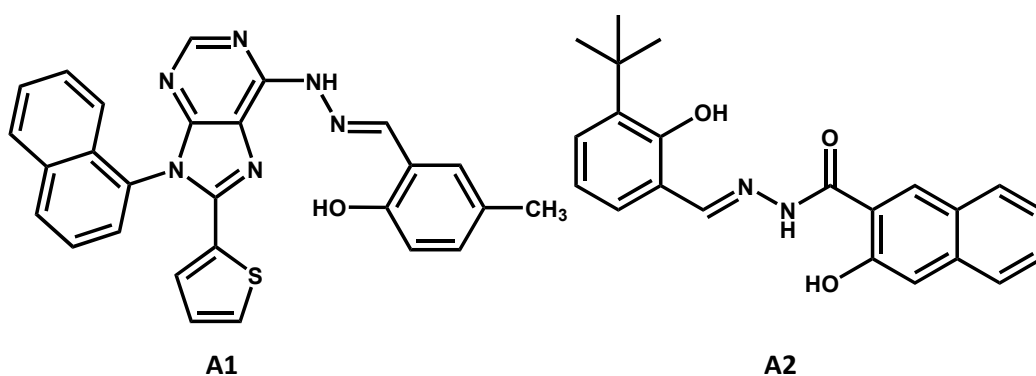
Another fluorescence probe molecule (**A2**) containing an acyl-hydrazone is introduced by D. Choe *et al.* in methanol medium. The probe possess the same reversible "turn-on" fluorescence property towards Al^{3+} along with a turn-off nature for **A2**-Al^{3+} complex in presence of $H_2PO_4^-$.[66] Y. Zhu *et al.* designed a phenolic-imine based fluorescent probe (**A3**) which selectively identify Al^{3+} in PBS (phosphate buffered saline)-DMSO 3:1 (v/v) medium due to the restriction of ESIPT and PET processes.[67] Another fluorosensor (**A4**) based on coumarin moiety is developed by S. M. Hossain and co-workers can detect Al^{3+} in DMF/water mixed medium. In the presence of Al^{3+}, the main responsible processes for the increasing the emission intensity are ICT, C=N isomerization along with CHEF (chelation enhanced fluorescence emission) .[68]

A3   **A4**
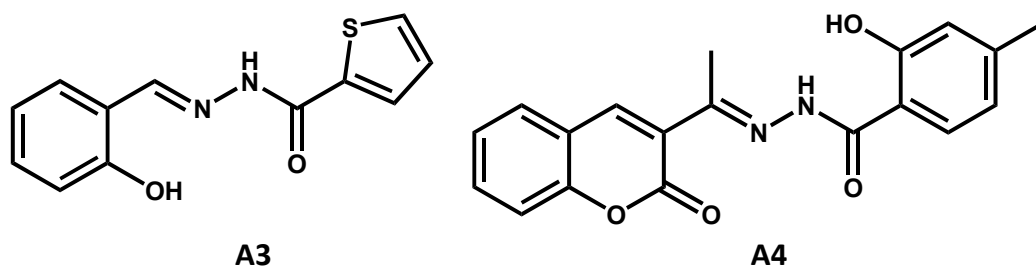
The fluorescent probe **(A5)** based on hydroxyl-quinoline moiety is proposed by L. Tian *et al.* which in aqueous medium can selectively detect Al^{3+} with an enhanced emission intensity. This is solely due to the occurrence of CHEF process induced by the restriction of the PET upon binding with Al^{3+}.[69]

A5   A6
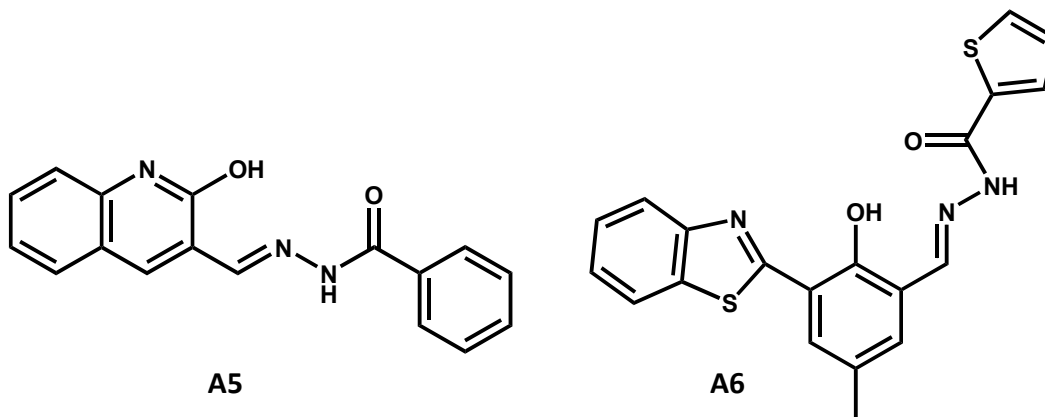
Furthermore, a fluorescence ratiometric detection of Al^{3+} in aqueous medium is introduced by Y. cheng and coworkers using a benzylidine based novel fluorescence probe **A6**. The probe **A6** shows an ESIPT and aggregation-induced emission (AIE) to result a noticeable emission intensity changes at 568 nm. Upon addition of Al^{3+}, a continuous generation of intensity at 476 nm along with depletion of the 568 nm band is observed in the emission spectra.[70] D. P Singh *et al.*, is utilized Al^{3+} induced keto-enol tautomerization in a dihydrazide based fluorescent probe **(A7)** for fluorometric detection of Al^{3+} in 2:3 (v/v) ethanol/water mixed medium. In the presence of Al^{3+}, the chelation of Al^{3+} with **A7** not only restrict the ICT process but also provides rigidity of the moiety which restricts the C=N isomerization with resulting the enhancement of the fluorescence intensity.[71] A benzophenone based Schiff base fluorosensor **(A8)** is reported by B. Naskar and co-worker to monitor Al^{3+} concentration in buffer medium. A possible ESIPT process along with C=N isomerization generates a non-fluorescent behavior. Upon binding with Al^{3+} both the ESIPT as well as the C=N isomerization become restricted to obtain a highly enhanced fluorescence intensity known as chelation enhanced fluorescence emission (CHEF).[72] Another fluorescent sensor **A9** based on imino-naphthalene-2-ol moiety for the detection of Al^{3+} in 1:1 (v/v) MeOH and water mixed medium is proposed by S. Sarma *et al.* **A9** exhibits a reversible fluorescence sensing property. It possess a "turn-on" fluorescence response towards Al^{3+} at 517 nm, where the probe

can be regenerated by interaction with EDTA molecule.[73] An alizarin-complex **A10** is designed by Y. Wang *et al.* to detect Al^{3+} by following a ratiometric response in EtOH and water (4:1, v/v) mixed medium.
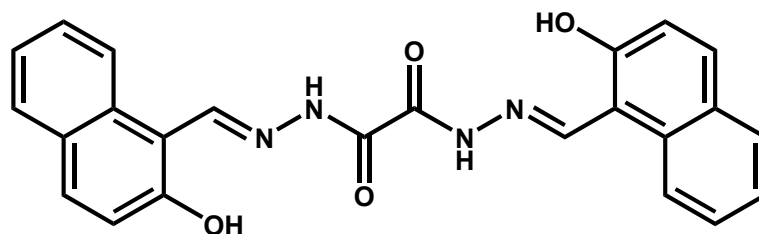
A7
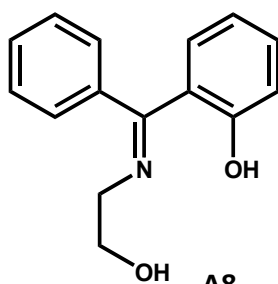
A8
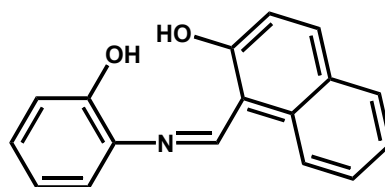
A9
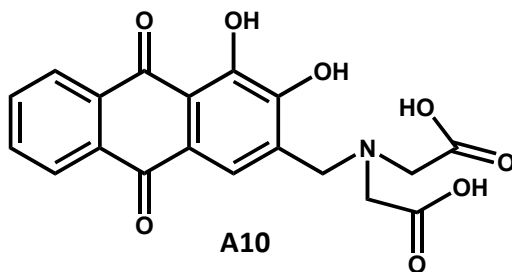
A10

In the presence of Al^{3+}, a continuous generation of an emission band at 558 nm takes place with simultaneous depletion of the characteristic emission intensity at 487 nm. This results in a conversion of blue to orange-yellow fluorescence of **A10** due to formation of **A10**-Al^{3+} complex, which can be virtually visible by naked eye.[74] Another Schiff base "turn-on" fluorosensor (**A11**) is synthesized by Y. Wang *et al.* and identified about 41-fold emission intensity enhancement after binding with Al^{3+} in methanol medium. Binding with Al^{3+} activates the ICT process but an ESIPT process simultaneously restricted, which leads to an enhancement of fluorescence intensity at 545 nm due to the complexation.[75] C. X. Wang and co-workers are used a DSPE (1,2-distearoyl-sn-glycero-3-phoshphorylethanolamine)–PEG (poly(ethylene glycol)) phospholipid polymer as a transporter of fluorescence sensing dye (DSPE-PEG- **A12)**. This DSPE-PEG-**A12** can detect Al^{3+}

in tetrahydrofuran and water (2:3, v/v) mixed medium by following an emission intensity increase at 447 nm due to restriction of PET and ESIPT processes.[76]

A11

A12
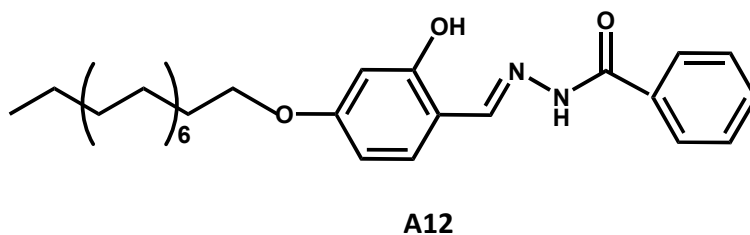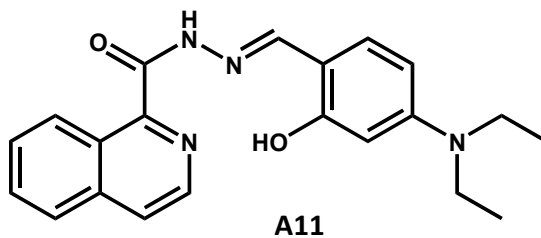
M. Wang *et al.* have reported tetra-styrene based optical fluorescent probe (**A13**). The probe has shown a remarkable aggregation induced change in emission characteristics in 9:1 (v/v) methanol and water mixed medium. It possess a strong emission intensity at 521 nm by restricting the PET process.[77] M. Kumar *et al.* have reported another very simple salicaldehyde based fluorescent probe (**A14**) which shows Al^{3+} induced a "turn-on" fluorescence response at 462 nm in water/ethanol (1:9 v/v) mixed medium owing to formation of a 2:1 **A14**-Al^{3+} stoichiometric complex. Probe **A14** after binding with Al^{3+} ion possess a naked eye detectable cyan color fluorescence emission at 462 nm due to inhibition of CHEF process.[78]

A13

A14
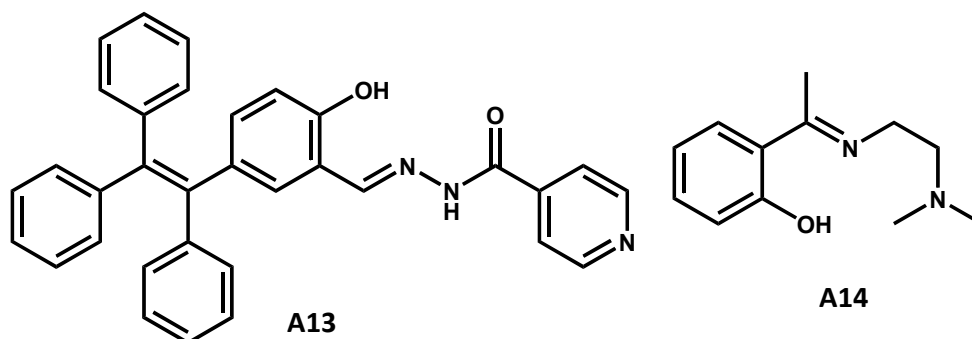
L. Wang *et al.* introduced an interesting phthalazine derivative as fluorescent probe (**A15**) that can detect Al^{3+} in water/ethanol (9.9:0.1, v/v) mixed medium with a "turn-on" fluorescence emission.

The fluorescence generation is solely due to an inhibition of ICT and generation of CHEF during the complexation of **A15** and Al^{3+} ion in a 2:1 binding ratio.[79] Moreover, B. Sen *et al.* reported another "turn-on" fluorescence probe **A16** containing coumarin moiety which can detect Al^{3+} by restricting the C=N isomerization process with facilitating CHEF process during the chelation with **A16** in methanol/buffer (9:1 v/v) mixed solvent.[80]

A15   A16
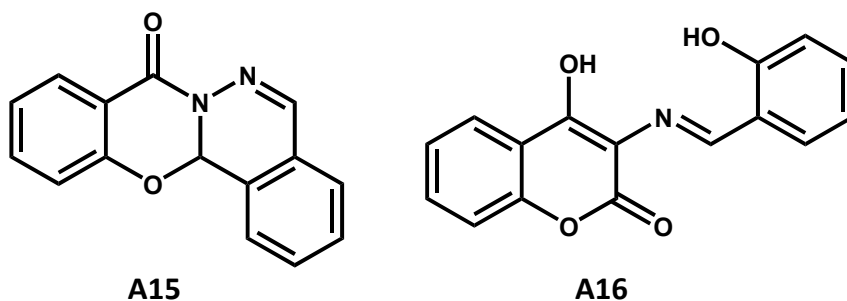
1.6. A short review on moisture sensor

Presence of moisture in all over air as well as surroundings makes it more prone to easily act as adulterants. Determination of water contaminants in various chemical compounds is very crucial particularly towards several industrial production of fine chemicals and foods.[81] Therefore chemical sensors that can able to alter optical response by tracing small to smallest amount of water are potentially important. A chemo-dosimeter based on salicaldehyde derivative (**W1**) for the detection of water in different organic solvents especially for methanol medium has been reported by G. Men and co-workers. A ratiometric fluorescence response with simultaneous disappearance of intensity at ~450 nm accompanied by continuous enhancement of intensity at ~505 nm in methanol medium upon a gradual water addition have noticed. This enhanced fluorescence intensity is caused by the breaking of imine-linkage in the probe molecule in the presence of water.[82] L. McDonald *et al.* have designed a moisture detecting hydrazine based fluorosensing probe (**W2**) effective in acetonitrile medium with a "turn-on" fluorescence response. In the presence of water, the probe exhibits a temperature dependent different emission behavior. The operation of ESIPT (excited state intramolecular proton transfer) process at low solution temperature is important to observe the emission at ~524 nm, while PET is dominant at higher temperature to have an emission maxima at ~475 nm.[83] A simple anthaquinone based reversible fluorescent probe (**W3**) has been introduced by P. Kumar *et al.* The probe possess an anion induced

22

deprotonation of phenolic-OH to exhibit a light blue color followed by water mediated protonation with resulting a pale yellow colorization. This water induced spectral changeover is useful for the detection of water in various organic solvents by following the colorimetric response.[84]

W1

W2

W3
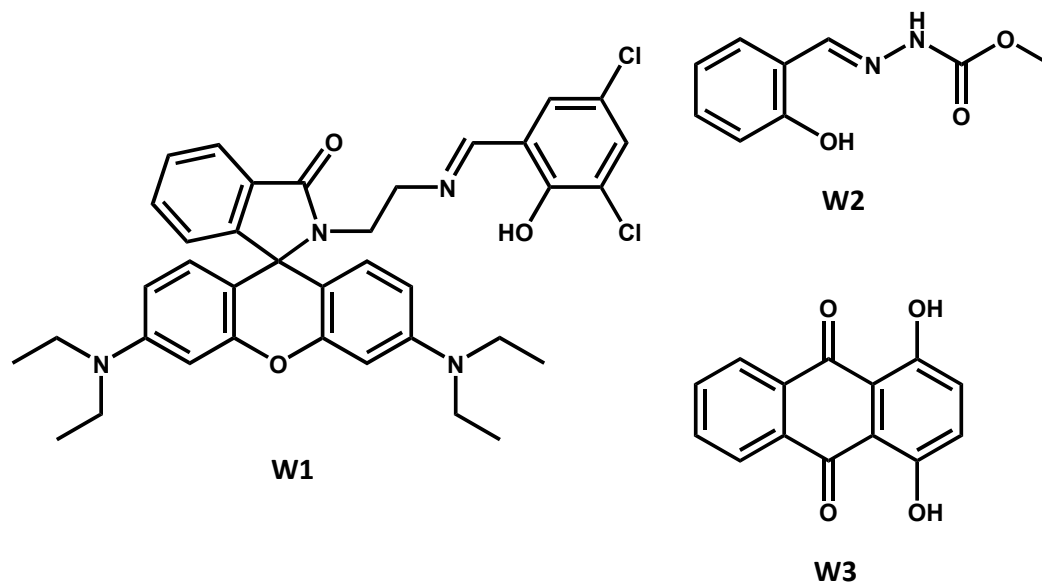
Another fluorene based fluorescent probe (**W4**) has been reported by P. Kumar and co-workers for detecting water in acetonitrile medium. Aggregation of probe molecules and subsequently a twisted intramolecular charge transfer process are responsible for the fluoro-sensing activity. Water sensitivity of **W4** have a dual nature. Lower water contamination leads to an increase in emission intensity with forming intense yellow color. However, the presence of large amount of water leads to undergo hydrolysis of the imine group which results emission intensity quenching with disappearing of yellow color.[85]

W4
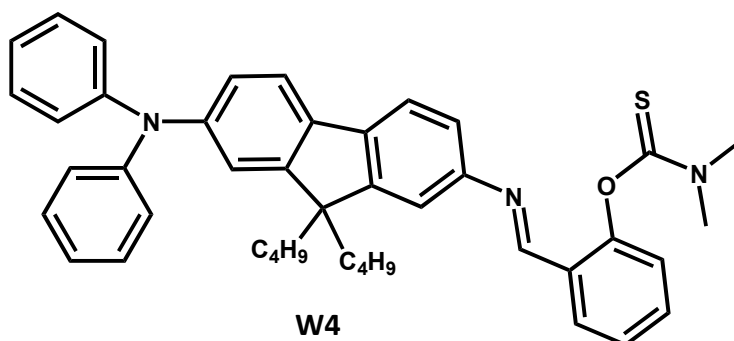
A dansyl moiety appended iron(III) complex fluorescent probe (**W5**) is reported by P. Kumar *et al* for the detection of water. In the presence of water, a probable displacement of the Fe^{3+} from

the **W5** complex leads to generate of strong fluorescence intensity.[86] J. Feng *et al.* have designed a julolidine based Al^{3+}-docketed fluorescent probe (**W6**) for the detection of trace amount of water in methanol medium *via* a colorimetric response. In methanol medium, probe **W6** undergoes complexation with Al^{3+} to result a large enhancement of emission intensity accompanied by a red shift in emission maxima from 540 to 570 nm. As a consequence a color transformation from yellowish green to orange is observed.

W5

W6
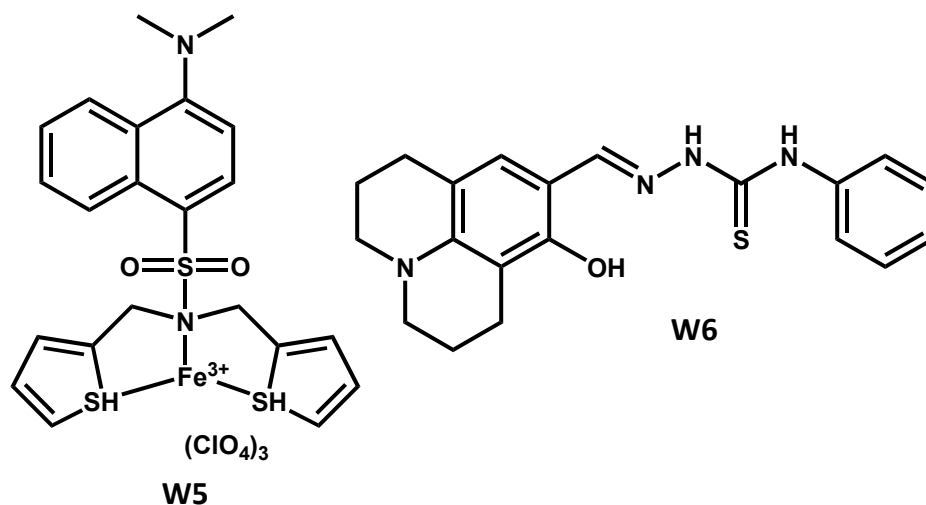
An addition of water to the **W6**-Al(III) complex leads to dissociation of the complex and sets the ligand free. As a result the emission intensity become quenched and the yellowish green color of the free ligand appears once again. This overall colorimetric and fluorometric responses are therefore utilize to work as water sensor in methanol medium.[87] Moreover, L. Chen *et al.* have designed a microporous and reversible Zn-metal organic framework (**W7**) possess ultrafast switchable luminescence characteristics towards detection of water.

W7
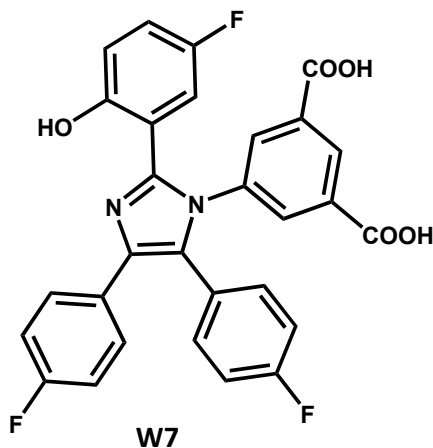
Upon binding with water molecule, the ESIPT process become on, whereas elimination of water lead to off the ESIPT process. As a result a single crystal to another single crystal transformation takes place, which produced a dual color photoluminescence cycles.[88]. Merocyanin based dye molecules (**W8** and **W9**) are synthesized by S. Cha *et al.* for detecting water in solution. Due to negative solvatochromic nature of both **W8** and **W9**, a huge blue shift in the position of absorption maxima is resulted due to changing solvent polarity by increasing amount of water content.[89] Another negative solvatochromic signaling merocyanin dye (**W10**) is proposed by H. park *et al.* for investigating water content in different organic solvents with a prominent colorimetric response.[90]

W8   **W9**   **W10**
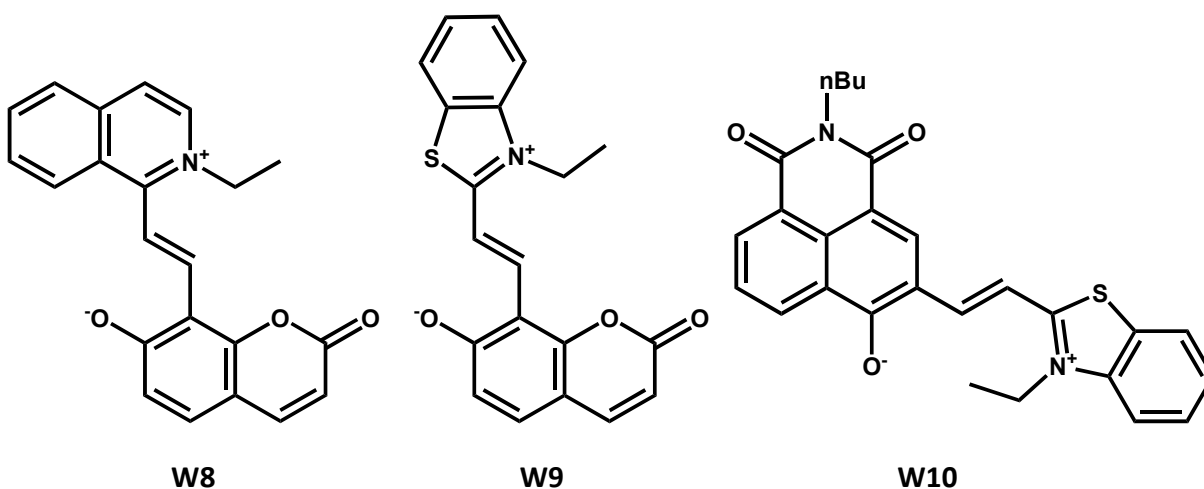
Z. Li and co-workers have reported three different hetero aryl-napthalimide based water detecting fluorescent probes (**W11, W12** and **W13**). They found that on moving from **W11** to **W13** the emission intensity gradually decreases upon increasing the solvent polarity and this decreasing tendency is highest for **W13**. The highest electron withdrawing effect for **W13** due to presence of the hetero aryl group attached to the napthalimide segment is responsible for the water sensing activity. This electron withdrawing effect of the heteroaryl group enhances the change in the dipole moment upon light excitation of **W13**.[91] D. Yang have reported a ratiometric dansyl and rhodamine moiety based fluorescent probe (**W14**) and light excitation induced FRET process is utilized towards the detection of water in organic solvents. In the presence of water, a continuous generation of emission intensity at ~620 nm along with simultaneous reduction of intensity at ~520 nm is identified owing to opening of the spiro-lactum ring.[92]

W11   **W12**   **W13**
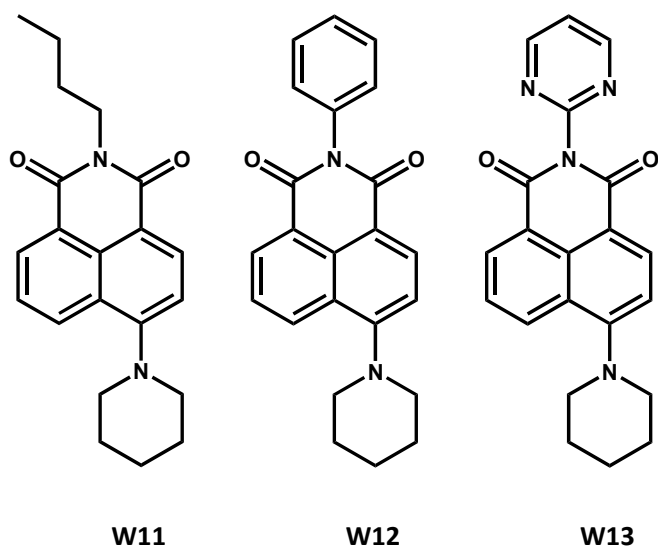
P. Kumar have designed Sudan-III and Alizarin-S based derivatives **W15** and **W16** as reversible colorimetric sensors to detect moisture in organic solvents. Here also an anion induced deprotonation and moisture induced protonation are responsible to observe water induced spectrophotometric changes.[93]

W14

W15   **W16**
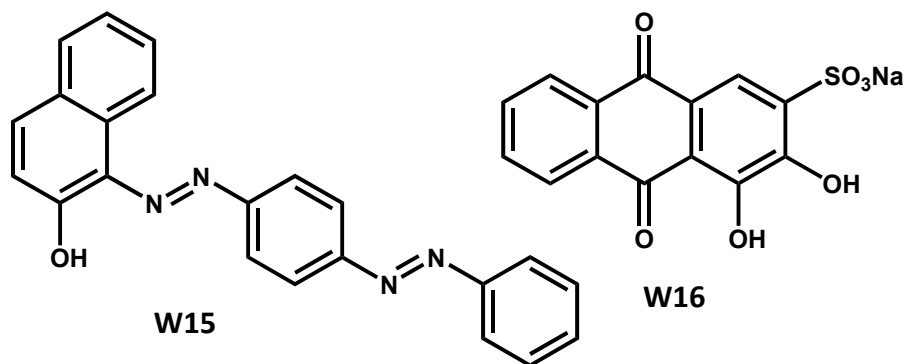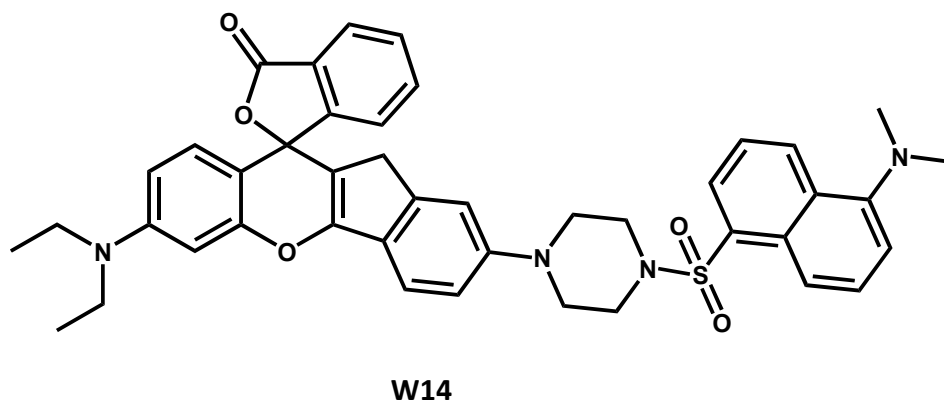
J. S. Kim *et al.* have reported an 8-hydroxy quinolone derivative (**W17**) for the detection of trace water in acetonitrile, THF and dioxane mediums by monitoring the fluorescence intensity quenching phenomenon. In acetonitrile and dioxane medium, the emission bands at 463 nm and 442 nm drastically decreases upon addition of less than 1% water in the medium. On the other hand, the same phenomenon of intensity quenching due to water addition in THF medium occurs at 410, 434, 458 and 498 nm.[94]

W17
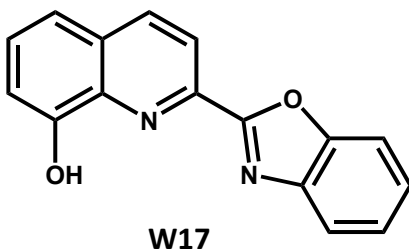
F. Wu *et al.* have identified a NIR-emitter di-ketopyrrole derivative (**W18**) as an efficient water detecting probe. The water sensing properties of the probe **W18** are relying on water induced ESIPT along with AIE process along with large Stoke shifts in fluorescence spectra.[95]

W18
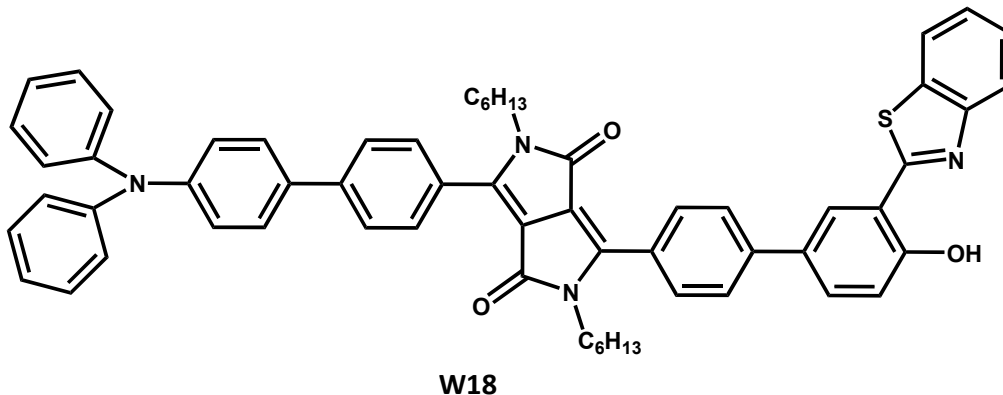
1.7. A short review on methanol sensor

Producing ethanol as a beverage by fermentation process is an ancient tradition in various parts of the world from household level to large industrial scale. In all over the world, indigenous people are involved in the traditional alcohol fermentation.[96] One of the most toxic alcohol is methanol which can be found primarily in alcoholic beverages produced by natural fermentation or distillation process. Although methanol and ethanol are chemically similar, only ethanol is edible. Ethanol fermentation is used to produce beer, wine and spirits and other alcoholic beverages. The

methanol contamination in alcoholic drinks made from home-distilled spirits is a serious concern.[97-98] As a result, methanol detection in ethanol is to be very crucial for put an end to the incidences of methanol contamination in traditional alcoholic beverages.

Q. Li and co-workers introduces a twisted-planar dimeric hexaphyrin (one type of porphyrinoid) based organic framework which basically exist as a trans-configuration. Introduction of methanol in this dimeric system produces two isomeric dimeric forms containing methoxy moiety and converts to cis-configuration. Further this methanol mediated configurational changes accompanied by a green to brown color changes.[99] P. F. Pereira and co-workers proposed a cyclic voltammetric method for simultaneous detection of methanol and ethanol in fuel ethanol. They have kept fuel ethanol in an electrochemical cell and both NaOH and methanol as an electrolyte. Ethanol has identified selectively at +0.19 V and for both methanol and ethanol it is at +1.20 V. Finally they performed a current subtraction to obtain the relative percentages of ethanol and methanol in the ethanol fuel.[100] Further J. v. d. Broek and co-workers have designed a handheld and inexpensive methanol detector consisting a tiny packed bed of tenax (porous polymer based on 2,6-diphenylphenol). It also consists a highly sensitive, yet non-specific micro-sensor comprising of flame-made Pd-doped SnO_2 nanoparticle on inter-digitated sensing electrodes. It is specified for the detection of methanol in a particular concentration range in the presence of higher ethanol percentage.[101] A. T. Guntner and co-workers have reported an inexpensive but compact device for the quantification of methanol in hand sanitizers by headspace analysis. It consist of a separation column of tenax particles along with a chemo-resistive gas sensor made up of Pd-doped SnO_2 nanoparticles integrated into a smart phone-assisted analyzer with validated performance for alcoholic sanitizers.[102] A. Kumar and co-workers have introduced a poly-indole deposited substrate integrated waveguide (SIW) for quantitative and qualitative methanol gas sensing. The probe deposited in the micro-well etched at an intense electric field region of microwave based cavity resonator. This results a sensing response for variation of dielectric property caused by the adsorption and desorption of methanol gas.[103] G. P. Dias and co-workers have quantified methanol content in gasoline and ethanol based fuels by using HPLC with refractive index detection methods. They have measure the ethanol content in gasoline containing methanol as adulterant.[104]

A pentacene-quinone derivative **M1** as a selective fluorescence sensor for the detection of methanol is reported by M. Zhao *et al.* **M1** possess a methanol mediated keto/enol tautomerization

and subsequently switching of ICT process generates strong fluorescence intensity along with a colorimetric response visible by naked-eye.[105]

V. Kumar and co-workers have reported a highly sensitive fluorometric and colorimetric methanol sensing procedure by exploiting a Schiff base molecule consisting a rhodamine scaffold (**M2**). In the presence of methanol, a nucleophilic attack on the electrophilic carbonyl center and subsequent conversion from the closed spiro-form to open-chain conformation is responsible for the sensing response.[106]
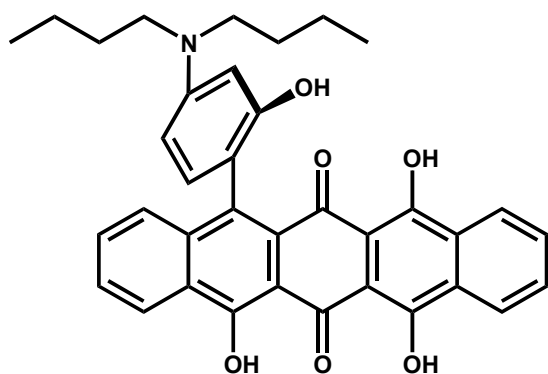
M1
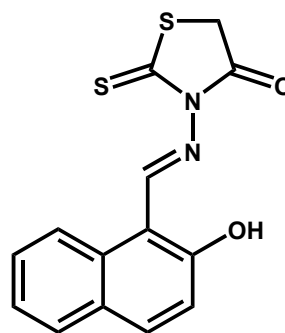
M2
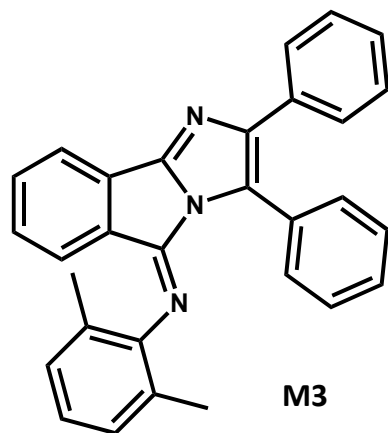
M3
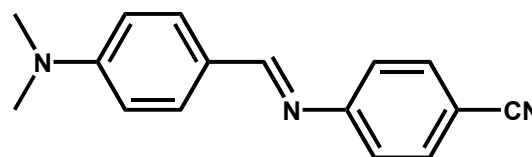
M4
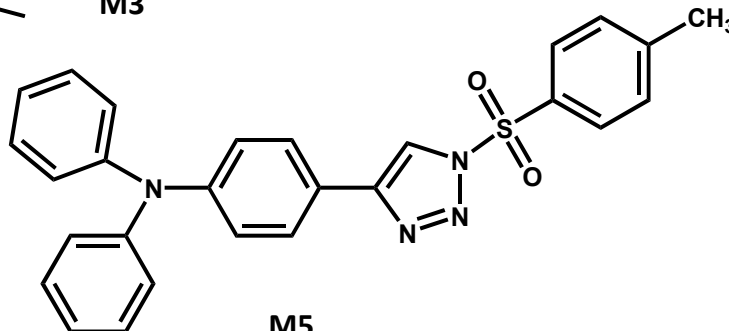
M5

An interesting fluorescent probe containing imidazole-isoindole imine scaffolds **M3** is used to detect trace amount of methanol by F. Ahmadi *et al.* This solvatochromic dye molecule in the presence of methanol exhibits enhancement of emission intensity with an appreciable blue shift due to the hydrogen bonding interaction in between methanol and **M3**.[107] R. Zhao *et al.* have reported a fluorescent probe (**M4**) which shows aggregation induced remarkable emission (AIE) intensity increase in response to the presence of methanol vapor. A hydrogen bonding interaction between methanol molecule and probe is responsible for the sensing response.[108] Applying the concept of click chemistry, Z. Hu *et al.* have reported a highly sensitive methanol detecting fluorescent probe **M5**. The combine features of structural conformation, conjugation along with solvent polarity and hydrogen bonding ability are mainly responsible for the emission response of probe **M5** towards methanol.[109]

Another set of ratiometric fluorescence probes for methanol detection based on flavonoid moiety are proposed by T. Qin *et al.* They designed two separate ligands **M6** and **M7** for methanol detection. **M6** exhibits strong hydrogen bond interaction with alcohol molecule and therefore restrict the ESIPT process with activating a fast and precise emission enhancement. In compare to other alcohol, methanol induces large change in emission properties including naked eye detection facility. This phenomenon is not feasible for probe **M7** due to the lack of such H-bonding.[110]
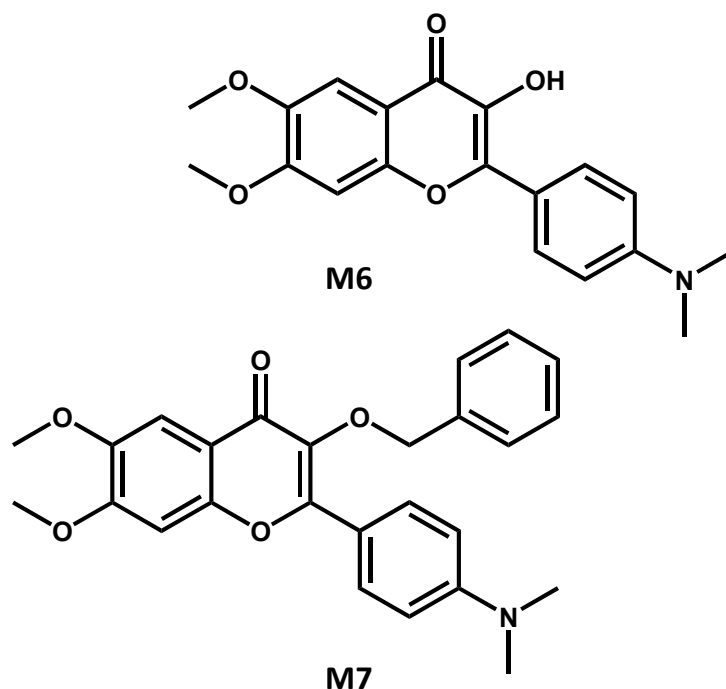
A set of imidazole moiety contained dyes (**M8-M11**), as ratiometric fluorescence indicator for methanol are reported by S. Swaminathan *et al.* A potential intermolecular hydrogen bonding interaction in between methanol and the probes lead to restrict the ICT process and thus generating strong emission intensity.[111]

M8

M9

M10

M11
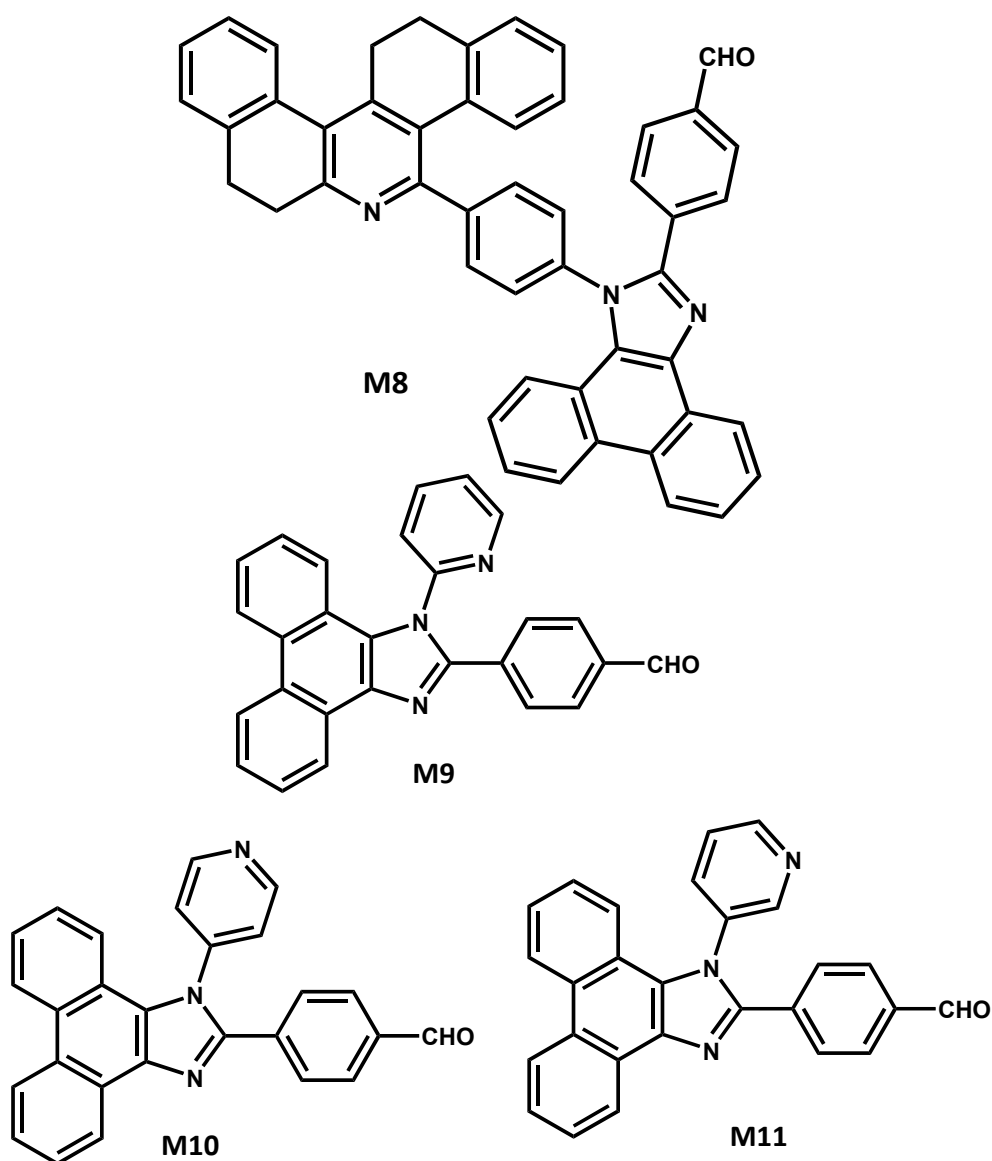
1.8. Scope and objectives of the present thesis

Fluorescence probe based chemo-sensing can be one of the best known technique to detect different metal ions and small molecules with potential industrial and biological importance. In

this work we have synthesized various "turn-on" fluorescent probes containing phenolic Schiff base moiety or simple aldehydic phenol as the basic architecture. The sensing responses are relying upon a large enhancement of fluorescence intensity owing to interaction of the detecting ions/molecule with the probe molecule. The fluoro-sensing phenomenon is further applied to analyze real analytical samples.

Basic intention of the present thesis work is the synthesis of fluorogenic phenol-based probe molecules which exhibits turn "off-on" fluorogenic activity upon exposing to a matrix of either industrially/biochemically important metal ions or small molecules. Depending on stereo-electronic factors, a particular ion/molecule from the chosen matrix can bind selectively with the probe to generate strong fluorescence intensity. Strategic utilization of such synthesized phenol-based ligand for specific ion/molecule selective turn "off-on" fluorescent chemo-sensing is the main objective of the present work. Side-by-side mechanistic approach to address the probable cause of selectivity as well as sensitivity for particular ion/molecule must also be offered with the aid of both theoretical and analytical investigations.

1.9. Thesis overview

This thesis has shaped into five major chapters.

Outline of Chapter 1

Chapter **1** contains a brief introduction of my work. In addition to theoretical and technical features of fluorescence spectroscopy, overall general methodologies towards designing fluorescent sensor are also discussed in this chapter. It also cover some literature survey on phenol based probe as metal ion as well as small molecule sensors. Some previously reported work related to Al^{3+} ion, water and methanol detections are also discussed here. The scope and objectives of the current work has been demonstrated on this context.

Outline of Chapter 2

This chapter describes the materials and methods as well as all experimental procedures used in this work.

Outline of Chapter 3

Nowadays for go-green mission, biofuels like ethanol, methanol replaces fossil fuels. Majority of the fuel tanks are made up with metallic aluminium which can easily prone to corrode with forming Al(OR)$_3$ due to prolong exposure in biofuels. The corrosion can leads to result severe disasters. Therefore, optimization is essential for reducing such critical engineering disasters by identifying such alcohol induced aluminium corrosion as in its nascent stage. So far, a huge number of fluorescent probes for Al^{3+} have been employed either in the biological field or environmental area, but barely focused on studies related to alcoholate corrosion. We have proposed a fluorescence probe method to detect Al^{3+} ion. The probe form alcohol specific Al^{3+} complex by the reaction with different soluble Al^{3+} salts, mainly, Al(OR)$_3$ to generate strong fluorescence enhancement by inhibiting the PET process in the probe molecule. The detection methodology is suitably tuned to monitor the alcoholate corrosion by fluorometrically estimating Al(OR)$_3$ formation under an inert condition, with a high sensitivity. Furthermore the methodology is extended for applications towards aluminium based alloy.

Outline of Chapter 4

Currently moisture adulteration in different organic solvents as well as food products causes major problem for chemical and food industries. So a suitable water detection methodology is always very demanding industrially. We have reported a simple water detecting fluorescence probe, 4-methyl-2,6-diformyl phenol (AH) for estimating a trace amount of moisture contamination in different polar aprotic solvents as well as food samples with a high precision. With increasing water% (v/v), the phenolate-form of the probe possess a large spectral blue shift from 485 to 440 nm both in the absorption and fluorescence excitation spectra due to the formation of H-bond with water molecule. However, due to the dissociation of the H-bond in the excited state the emission spectra are found to remain unchanged. Furthermore, the gradual blue-shift of the excitation band with the increase in water% (v/v) imposed an opposite emission intensity varying behavior, from increasing to decreasing fashion, owing to the change in the excitation wavelength from 440 to 485 nm. Such emission behavior are further normalized to achieve water% mediated a highly enhanced linear emission response. This improved sensitivity allow us to estimate water% in various moisture-sensitive edible oils and dairy foods.

Outline of Chapter 5

Recognition of methanol (MeOH) in ethanol (EtOH) or isopropanol (^{i}PrOH) medium comprising water is very important towards detection of MeOH poisoning in alcohol containing beverages and hand sanitizers. Though chemical sensing approaches are very sensitive and also easy to perform, the chemical resemblances among those alcohols make MeOH detection very difficult particularly in the presence of water. For this reason, we have introduced a fluorometric detection of a trace amount of MeOH in EtOH/^{i}PrOH in presence of water by using alcohol coordinated Al^{3+}-complexes of an aldehydic phenol ligand having a dangling pyrazole unit. The presence of MeOH in EtOH/^{i}PrOH results in a transformation of the complex geometry from tetrahedral (Td) to octahedral (Oh) by replacing the coordinated EtOH/^{i}PrOH by MeOH molecules. The Td-complex possess fluorescence whereas the Oh-species did not, due to the intramolecular photo-induced electron transfer (PET). Upon interaction of the Oh species with water, its one MeOH coordination is interchanged with a water molecule after that the proton transfer from the water to pyrazole-N produces strong fluorescence intensity by restricting the PET. However, the interaction with water dissociates the Td-complex to exhibit quenching of fluorescence intensity. The water mediated reversal of the fluorescence signal from the decrease to increase between the absence and presence of MeOH is exploited to identify MeOH in EtOH/^{i}PrOH medium as well as commercial alcoholic drinks containing high percentage of water.

1.10. Reference

1. S. Moitra, P. D. Blanc and S. Sahu, *Thorax*, 2013, **68**, 565–570. doi:10.1136/thoraxjnl-2012-203029.

2. S. Bansal, A. Singh, M. Mangal, A. K. Mangal and S. Kumar, *Crit. Rev. Food Sci. Nutr.*, 2017, **57**, 1174.

3. L. Luo, B. Wang, J. Jiang, Q. Huang, Z. Yu, H. Li, J. Zhang, J. Wei, C. Yang, H. Zhang, L. Dong and S. Chen, *Front. Pharmacol.*, 2021, **11**, 1. doi:10.3389/fphar.2020.595335.

4. M. Mazumdar, D. C. Bellinger, M. Gregas, K. Abanilla, J. Bacic and H. L. Needleman, *Environ. Health.*, 2011, **10**, 1. doi:10.1186/1476-069x-10-24.

5. C. J. Chang, T. Gunnlaugsson and T. D.James, *Chem. Soc. Rev.*, 2015, **44**, 4176.

6. P. D. Beer and P. A. Gale, *Angew. Chem. Int. Ed.,* 2001, **40**, 486.

7. A.P. De Silva, H.Q.N. Gunaratne, T. Gunnlaugsson, A.J.M. Huxley, C.P. McCoy, J.T. Rademacher and T.E. Rice, *Chem. Rev.*, 1997, **97**, 1515.

8. A. G. Amer, A. A. Hamid, M. A. Khateeb, Z. A. Tahat, M. Qudah, S. M. Obeidat and A. M. Rawashdeh, *J. Inorg. Chem.*, 2011, **201**, 1.

9. J. S. Kim and D. T. Quang, *Chem. Rev.*, 2007, **107**, 3780.

10. X. Chen, T. Pradhan, F. Wang, J. S. Kim and J. Yoon, *Chem. Rev.*, 2012, **112**, 1910.

11 J. Chan, S. C. Dodani and C. J. Chang, *Nat. Chem.*, 2012, **4**, 973.

12. H. Kobayashi, M. Ogawa, R. Alford, P. L. Choyke and Y. Urano, *Chem. Rev.*, 2010, **110**, 2620.

13. H.-W. Liu, L. Chen, C. Xu, Z. Li, H. Zhang, X.-B. Zhang and W. Tan, *Chem. Soc. Rev.*, 2018, **47**, 7140.

14. D. Maity, T. Govindaraju. *Chem. Commun.*, 2012, **48**, 1039.

15. A. S. Rao, D. Kim, T. Wang, K. H. Kim, S. Hwang and K. H. Ahn. *Org. Lett.*, 2012, **14**, 2598.

16. B. Chowdhury, S. Khatua, R. Dutta, S. Chakraborty and P. Ghosh. *Inorg. Chem.*, 2014, **53**, 8061.

17. D. Skoog, J. F. Holler and D. M. West. *Fundamentals of Analytical Chemistry*, 7th ed., Thomsen learning, 2007, 601.

18. A. Bose, I. Thomas, K. G and E. Abraham, *Int. J. Adv. Pharm. Anal.*, 2018, **8**, 1.

19. K. Naresh. *J. Chem. Pharm. Sci*, 2014, 18. ISSN: 0974-2115.

20. L. Liu and Z. Yang, *Inorganica Chim. Acta*, 2018, **469**, 588.

21. M. Y. Berezin and S. Achilefu. *Chem. Rev.*, 2010, **110**, 2641.

22. K. Rurack, Part of the Springer Series on Fluorescence book series. 2008, **5**, 101. DOI: 10.1007/4243_2008_019.

23. Compendium of Chemical Terminology, 2nd ed. (the "Gold Book"), Compiled by A. D. McNaught and A. Wilkinson, Accessed August 2021.

24. J. R. Lakowicz. Principles of Fluorescence Spectroscopy. 3rd ed. Springer New York; 2006.

25. B. Valeur and M. N. Berberan-Santos. Molecular Fluorescence: Principles and Applications. 2nd ed. Wiley-VCH Verlag GmbH & Co. KGaA; 2012.

26. C. Hariharan, V. Vijaysree and A.K. Mishra. *J. Luminescence*, 1997, **75**, 205.

27. G-Y. Li and K-L. Han. *WIREs Comput Mol Sci*, 2018, **8**, 1-17. 8:e1351. doi: 10.1002/wcms.1351.

28. A. W. Czarnik, *Acc. Chem. Res.*, 1994, **27**, 302.

29. M. Formica, V. Fusi, L. Giorgi and M. Micheloni, *Coord. Chem. Rev.*, 2012, **256**, 170.

30. H. Neuweiler, M. Sauer, *Curr. Pharm. Biotechnol.*, 2004, **5**, 285.

31. A. Hillisch, M. Lorenz and S. Diekmann, *Curr. Opin. Struct. Biol.*, 2001, **11**, 201.

32. C. Ma, F. Zeng, L. Huang, and S. Wu. *J. Phys. Chem. B*, 2011, **115**, 874.

33. R. Misra and S. P. Bhattacharyya, 2018 Wiley-VCH Verlag GmbH & Co. KGaA. DOI: 10.1002/9783527801916.

34. B. Valeur and I. Leray, 2001, **1**. Springer, Berlin, Heidelberg.

35. J. Zhao, S. Ji, Y. Chen, H. Guo and P. Yang . *Phys. Chem. Chem. Phys.*, 2012, **14**, 8803.

36. D. Wu, A. C. Sedgwick, T. Gunnlaugsson, E. U. Akkaya, J. Yoon and T. D. James. *Chem. Soc. Rev.*, 2017, **46**, 7105.

37. A. W. Czarnik, *Acc. Chem. Res.*, 1994, **27**, 302.

38. K. Kaur, R. Saini, A. Kumar, V. Luxami, N. Kaur, P. Singh and S. Kumar, *Coord. Chem. Rev.*, 2012, **256**, 1992.

39. P. R. Dongare and A. H. Gore, *ChemistrySelect*, 2021, **6**, 5657.

40. P. Roy, *Coord. Chem. Rev.*, 2021, **427**, 213562.

41. Y. Jiang, H. Li, R. Chen, W. Liu, C. Chen, Z. Li and W. Liu, *Spectrochim. Acta A Mol. Biomol.,* 2021, **251**, 119438.

42. C. Zhao, K. Li, N. Xie, M. Zhao and S. Peng, *J. Photochem. Photobiol. A.*, 2014, **290**, 72.

43. B. Gao, W. T. Gong, Q. L. Zhang, J. W. Ye and G. L. Ning, *Sens. Actuators B Chem.,* 2012, **162**, 391.

44. B. Gu, L. Huang, W. Su, X. Duan, H. Li and S. Yao, *Anal. Chim. Acta*, 2017, **954**, 97.

45. J. Z. Li, T. H. Leng, Z. Q. Wang, L. Zhou, X. Q. Gong, Y. J. Shen and C. Y. Wang, *J. Photochem. Photobiol. A: Chem.,* 2019, **373**, 146.

46. J. M. V. Ngororabanga, C. Moyo, E. Hosten, N. Mama and Z. R. Tshentu, *Anal. Methods*, 2019, **11**, 3857.

47. D. J. Fanna, L. M. P. Lima, A. R. Craze, A. Trinchi, G. Wei, J. K. Reynolds and F. Li, *J. Incl. Phenom. Macrocycl. Chem.* 2019, **94**, 141.

48. P. Wang, K. Yao, J. Fu, Y. Chang, B. Li and K. Xu, *Spectrochim. Acta A Mol. Biomol. Spectrosc.*, 2019, **211**, 9.

49. O. G. Beltran, B. K. Cassels, C. Perez, N. Mena, M. T. Nunez, N. P. Martinez, P. Pavez and M. E. Aliaga, *Sensors*, 2014, **14**, 1358.

50. W. Wang, J. Wu, Q. Liu, Y. Gao, H. Liu and B. Zhao, *Tetrahedron Lett.,* 2018, **59**, 1860.

51. S. Gharami, D. Sarkar, P. Ghosh, S. Acharyya, K. Aich, N. Murmu and T. K. Mondal, *Sens. Actuators B Chem.*, 2017, **253**, 317.

52. G. Mahalakshmi, P. S. Kumar, P. RajaLakshmi, M. Seenivasaperumal and K. P. Elango, *Methods Appl. Fluoresc.*, 2019, 7, 025003.

53. Y. Yue, F. Huo, C. Yin, J. Chao and Y. Zhang, *Sens. Actuators B Chem.*, 2015, **212**, 451.

54. S. Das, S. Biswas, S. Mukherjee, J.Bandyopadhyay, S. Samanta, I. Bhowmick, D.K. Hazra, A. Ray and P. P. Parui, *RSC Adv.,* 2014, **4**, 9656.

55. D. Li, X. Tian, Z. Li, J. Zhang, and X. Yang, *J. Agric. Food Chem.* 2019, **67**, 3062.

56. Y. H. Qin, X. Yi. Jiang, Y. F. Que, J. Yi. Gu, T. Wu, A. Aihemaiti, K. X. Shi, W. Yu. Kang, B. Y. Hu, J. S. Lan, Y. Ding and T. Zhang, *Molecules* 2019, **24**, 4011.

57. Y. Hitomi, T. Takeyasu, T. Funabiki, and M. Kodera, *Anal. Chem.* 2011, **83**, 9213.

58. S. Das, Y. Sarkar, S. Mukherjee, J. Bandyopadhyay, S. Samanta, P. P. Parui and A. Ray. *Sens. Actuators B Chem.,* 2015, **209**, 545.

59. Y. Sarkar, S. Das, R. Datta, S. Chattopadhyay, A. Ray and P. P. Parui, *RSC Adv.*, 2015, **5**, 51875.

60. S. Zhang, Y. Xie and L. Yan, *Spectrochim. Acta A Mol. Biomol.*, 2020, **230**, 118028.

61. H. Xu, Z. Huang, Y. Li, B. Gu, Z. Zhou, R. Xie, X. Pang, H. Li and Y. Zhang, *Analyst*, 2018, **143**, 4354.

62. Y. Jung, N. K. Park, S. Kang, Y. Huh, J. Jung, J. K. Hur and D. Kim, *Anal. Chim. Acta,* 2020, **1095**, 154.

63. M. Kawahara, K. Konoha, T. Nagata and Y. Sadakane, *Biomed. res. trace elem.,* 2007, **18**, 211.

64. C. A. Shaw and L. Tomljenovic, *Immunol. Res.*, 2013, **56**, 304.

65. H. Xu, W. Chen, L. Ju and H. Lu, *Spectrochim. Acta A Mol. Biomol. Spectrosc.* 2021, **247**, 119074. DOI: 10.1016/j.saa.2020.119074.

66. D. Choe and C. Kim, *Mater.* 2021, **14**, 6392.

67. Y. Zhu, X. Gong, Z. Li, X. Zhao, Z. Liu, D. Cao and R. Guan, *Spectrochim. Acta A Mol. Biomol. Spectrosc.,* 2019, **219**, 202.

68. S. M. Hossain, K. Singh, A. Lakma, R. N. Pradhan and A. K. Singh, *Sens. Actuators B Chem.*, 2017, **239**, 1109.

69. L. Tian, J. Xue and Z-Y. Yang, *Tetrahedron Lett.*, 2018, **59**, 4110.

70. Y. Chen, T. Wei, Z. Zhang, T. Chen, J. Li, J. Qiang, J. Lv, F. Wang and X. Chen, Ind. Eng. *Chem. Res.*, 2017, **56**, 12267.

71. D. P. Singh and V. P. Singh, *J. Lumin.*. 2014, **155**, 7.

72. B. Naskar, R. Modak, Y. Sikdar, D. K. Maiti, A. Bauza, A. Frontera, A. Katarkar, K. Chaudhuri and S. Goswami, *Sens. Actuators B Chem.*, 2017, **239**, 1194.

73. S. Sarma, A. Bhowmik, M. J. Sarma, S. Banu, P. Phukan and D. K. Das, *Inorganica Chim. Acta*, 2018, **469**, 202.

74. Y. Wang, L. J. Hou, Y-B. Wu, L. L. Shi, Z. Shang and W. J. Jin, *J. Photochem. Photobiol.*, 2014, **281**, 40.

75. Y. Wang, Z. Y. Ma, D. L. Zhang, J. L. Deng, X. Chen, C. Z. Xie, X. Qiao, Q. Z. Li and J.Y. Xu, *Spectrochim. Acta A Mol. Biomol. Spectrosc.*, 2018, **195**, 157.

76. C. X. Wang, B. Wu, W. Zhou, Q. Wang, H. Yu, K. Deng, J. Mi. Li, R. Xi. Zhuo and S.W. Huang, *Sens. Actuators B Chem.*, 2018, **271**, 225.

77. M. Wang, L. Lu, W. Song, X. Wang, T. Sun, J. Zhu and J. Wang, *J. Lumin.*, 2021, **233**, 117911.

78. M. Kumar, A. Kumar, Md. S. H. Faizi, S. Kumar, M. K. Singh, S. K. Sahu, S. Kishor and R. P. John, *Sens. Actuators B Chem.*, 2018, **260**, 888.

79. L. Wang, W. Qin, X. Tang, W. Dou, W. Liu, Q. Teng and X. Yao, *Org. Biomol. Chem.*, 2010, **8**, 3751.

80. B. Sen, S. K. Sheet, R. Thounaojam, R. Jamatia, A. K. Pal, K. Aguan and S. Khatua, *Spectrochim. Acta A Mol. Biomol. Spectrosc.*, 2017, **173**, 537.

81. H. S. Jung, P. Verwilst, W. Y. Kim and J. S. Kim, *Chem. Soc. Rev.*, 2016, **45**, 1242.

82. G. Men, G. Zhang, C. Liang, H. Liu, B. Yang, Y. Pan, Z. Wang and S. Jiang, *Analyst*, 2013, **138**, 2847.

83. L. McDonald, J. Wang, N. Alexander, H. Li, T. Liu and Yi Pang, *J. Phys. Chem. B*, 2016, **120**, 766.

84. P. Kumar, A. Ghosh and D. A. Jose, *Analyst*, 2019, **144**, 594.

85. P. Kumar, V. Kumar, N. Kaur, S. M. Mobin, P. Kaur and K. Singh, *Anal. Chim. Acta.*, 2022, **1189**, 339211.

86. P. Kumar, S. Gadiyaram and D. A. Jose, *ChemistrySelect*, 2020, **5**, 10648.

87. J. Feng, L. X. Duan, Z. B. Shang, J. B. Chao, Y. Wang and W. J. Jin, *Spectrochim. Acta A Mol. Biomol. Spectrosc.*, 2018, **201**, 185.

88. L. Chen, J.W. Ye, H. P. Wang, M. Pan, S.Y. Yin, Z. W. Wei, L.Y. Zhang, K. Wu, Y. N. Fan and C.Y. Su, *Nat. Commun..* DOI: 10.1038/ncomms15985.

89. S. Cha, M. G. Choi, H. R. Jeon and S-K Chang, *Sens. Actuators B Chem.*, 2011, **157**, 14.

90. H. Park and S-K Chang, *Dyes Pigm.*, 2015, **122**, 324.

91. Z. Li, Q. Yang, R. Chang, G. Ma, M. Chen and W. Zhang, *Dyes Pigm.* , 2011, **88**, 307.

92. D. Yang, X.T. Wu, X. J. Cao and B. X. Zhao, Dyes Pigm., 2019, **170**, 107558.

93. P.Kumar, R. Sakla, A. Ghosh and D. A. Jose, *ACS Appl. Mater. Interfaces*, 2017, **9**, 25600.

94. J. S. Kim, M. G. Choi,Y. Huh, M. H. Kim, S. H. Kim, S. Y. Wang and S. K. Chang, *Bull. Korean Chem. Soc.*, 2006, **27**, 2058.

95. F. Wu, L. Wang, H. Tang, and D. Cao, *Anal. Chem.*, 2019, **91**, 5261.

96. Elijah Ige, Ohimain SpringerPlus, 2016, 5:1607,1-10. DOI 10.1186/s40064-016-3303-1.

97. S. K. Tulashie., A. P. Appiah , G. D. Torku1 , A. Y. Darko and A. Wiredu, *Int. J. Food Contam.* 2017, **4**, 1.

98. G. Botelho, O. Anjos, L. M. Estevinho and I. Caldeira, *Process.* 2020, **8**, 1609.

99. Q. Li, C. Li, G. Baryshnikov, Y. Ding, C. Zhao, T. Gu, F. Sha, X. Liang, W. Zhu, X. Wu, H. Ågren, J. L. Sessler, and Y. Xie, *Nat. Commun,* 2020, **11**, 5289 | https://doi.org/10.1038/s41467-020-19118-9 | www.nature.com/naturecommunications.

100. P. F. Pereira, R. M.F. Sousa, R. A. A. Munoz, E. M. Richter, *Fuel*, 2013, **103**, 725.

101. J. v. d. Broek, S. Abegg, S. E. Pratsinis and A.T. Güntner, *Nat. Commun*, 2019 https://doi.org/10.1038/s41467-019-12223-4.

102. A. T. Guntner, L. Magro, J. v. d. Broek and S. E. Pratsinis, *iScience* 2021, **24**, 102050, (http://creativecommons.org/licenses/by/4.0/).

103. A. Kumar, C. Wang, F-Y. Meng, C-P. Jiang, G-F. Yan, M. Zhao, C-Q. Jing and L. Wang, *ACS Sens.* 2020, 5, **12**, 3939–3948.

104. G. P. Dias, R. C. d. Santos, R. C. Carvalho, C. G. de Souza, A. P. F. d. Santos, D. F. de A. Luiz A. d'Avila. *J. Braz. Chem. Soc.*, 2020, **31,** 1055. https://doi.org/10.21577/0103-5053.20190272.

105. M. Zhao, Y. Yue, C. Liu, P. Hui, S. He, L. Zhaoac and X. Zeng, *Chem. Commun.*, 2018, **54**, 8339.

106. V. Kumar, S. Kundu, B. Sk and A. Patra, *New J. Chem.*, 2019, **43**, 18582.

107. F. Ahmadi, H. R. Goli, Y. Balmohammadi, and A. Bazgir, *J. Org. Chem.* 2020, **86**, 146.

108. R. Zhaoa, M. Zhanga, Y. Liu, X. Zhanga, Y. Duana and T. Hana, *Sens. Actuators B Chem.* 2020, **319**, 128323.

109. Z. Wua, X. Fub and Y. Wanga. *Sens. Actuators B Chem.*, 2017, **245**, 406.

110. T. Qina, B. Liua, Y. Huang, K. Yang, K. Zhu, Z. Luo, C. Pan and L. Wang, *Sens. Actuators B Chem.***,** 2018, **277**, 484.

111. S. Sawminathan and S. Kulathu Iyer, *New J. Chem.*, 2021, **45**, 6033.

Chapter 2

Over-all analytical methods and chemicals

2.1. Chemicals and materials

All analytical grade chemicals and solvents from different commercial sources were used without additional purification. Solvents used for spectroscopic studies were dried precisely by standard procedures. Analytical grade acetyl acetone, p-cresol, hydrazine hydrate, triethyl amine (TEA) and anhydrous $AlCl_3$ were purchased from Sigma-Aldrich (USA). All required solvents dichloromethane (DCM), tetrahydrofuran (THF), thionyl chloride ($SOCl_2$) were obtained as analytical grade from E-Mark (India). HPLC grade solvents like dimethyl sulphoxide (DMSO), dimethyl formamide (DMF) methanol (MeOH), ethanol (EtOH), n-propanol (C_3H_7OH), isopropanol (^iPrOH), n-hexanol (C_6H_5OH), tertiary butanol (^tBuOH) were acquired from Sigma-Aldrich (USA) followed by drying process by 3Å molecular sieves.[1] For NMR studies deuterated solvents DMSO-d_6, CD_3OD were acquire from Cambridge Isotope Laboratories (USA). Pure Al sheet as well as Al-7075 was brought from Sigma-Aldrich (USA). Different alcoholic beverages vodka and wine and alcohol contained hand sanitizer, food samples like cheese, butter, coconut oil and ghee were obtained from various native sources. Milli-Q water (Millipore) with conductivity value of 18.2 MΩ.cm was used.

2.2. Synthesis of different probe molecules

2.2.1. Synthesis of AH

The preparation procedure of 4-methyl-2,6-diformyl phenol (AH) starting from p-cresol was already reported.[2] We have synthesized AH by using this procedure.^{1}H NMR (DMSO-d_6, 300MHz): δ = 2.081-2.091 (solvent peak), 2.227-2.345 (s, 3H,-ArCH$_3$), 2.501-2.519 and3.337 (trace amount of water in the solvent), 7.872-7.876 (s, 2 H, -Ar-H), 10.229-10.265 (s, 2 H-CHO), 11.401 (s, 1 H, -Ar-OH) Fig. 1 and Fig 2.
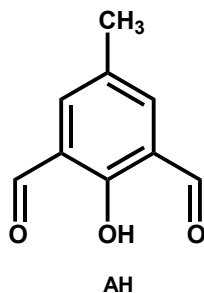
Fig. 1. Chemical structure of spectra of AH.
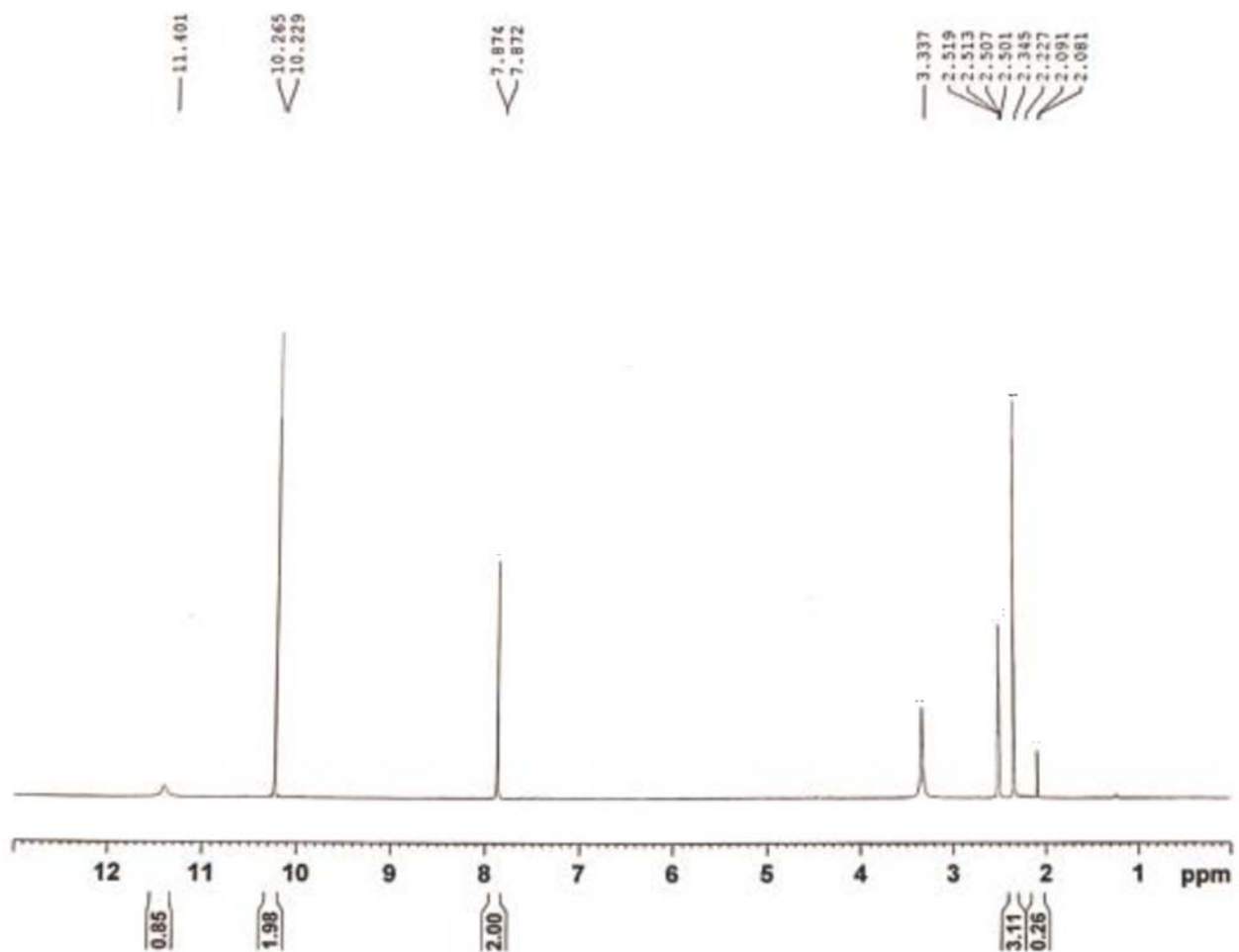
Fig. 2. ¹H-NMR spectra of AH in DMSO-d_6.

2.2.2. Synthesis of Schiff base (HMBDC)

2-hydroxy-3-(hydroxymethyl)-5-methylbenzaldehyde (HHMB) was synthesized from p-cresol by using the published procedure.[3] Synthesis of HMBDC ((6Z)-6-(2-hydroxy-3-(hydroxymethyl)-5-methylbenzylideneamine)-2H-chromen-2-one) was done by dropwise mixing 6-amino-2H-chromen-2-one (6-ACO) (0.04 g, 0.20mmol) to an anhydrous ethanolic solution of HHMB (0.04 g, 0.25 mmol), at ambient condition with constant stirring followed by an addition of 2 drops of AcOH. Then the reaction mixture was set for refluxed for 2 hour at 40°C followed by filtration. This filtrate was then evaporated by using a rotary evaporator to obtain the crude product as gel. Finally, it was purified by using column chromatography followed to get the pure HMBDC. The product also dried above CaCl$_2$ under vacuum (scheme 1). The structural analyses were checked by ¹H-NMR and ¹³C-NMR (DMSO-d_6, 300-MHz): 2.18-2.28 (s, 3H, ArCH$_3$), 2.48-3.31 (due to

42

trace H_2O in the solvent DMSO-d_6), 4.54-4.56 (d, 2H, CH_2-OH), 5.09 (t,1H, -CH_2-OH),6.53-6.57 (d,1H, -CH=CH), 7.29 (s,1H, -ArH), 7.36 (s,1H, -ArH), 7.47-7.50 (d,1H, -ArH), 7.69-7.71(d,1H, -CH=CH), 7.78 (s, 1H, ArH) 8.05-8.08 (d, 1H, -ArH), 8.96 (s, 1H, -N=CH), 13.14 (s,1H, -ArOH), ppm. ^{13}C NMR (DMSO-d_6, 75 MHz): 20.66, 57.82, 117.41, 117.91, 118.33, 119.83, 121.16, 125.53, 127.67, 130.23, 131.39, 132.49, 144.46, 144.63, 152.66, 155.66, 160.29, 165.04 ppm (Fig. 3).
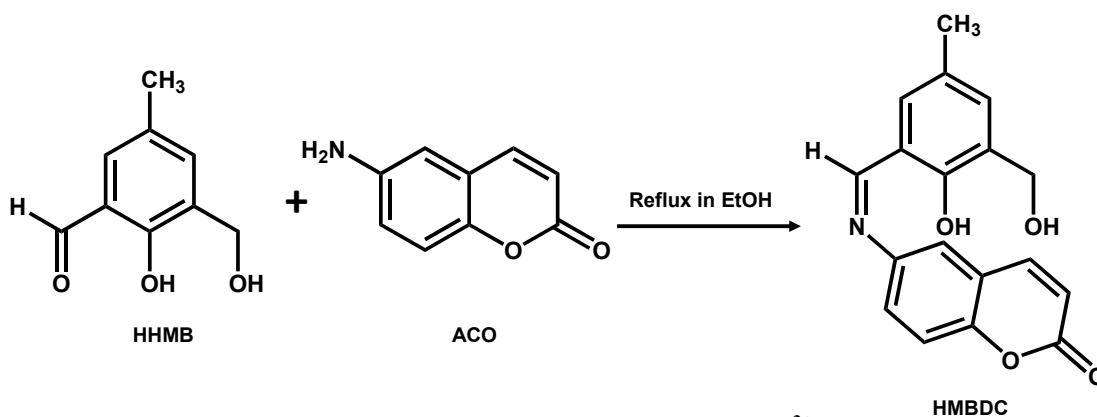
Scheme 1. Synthesis route of HMBDC and its complexation with Al^{3+}.
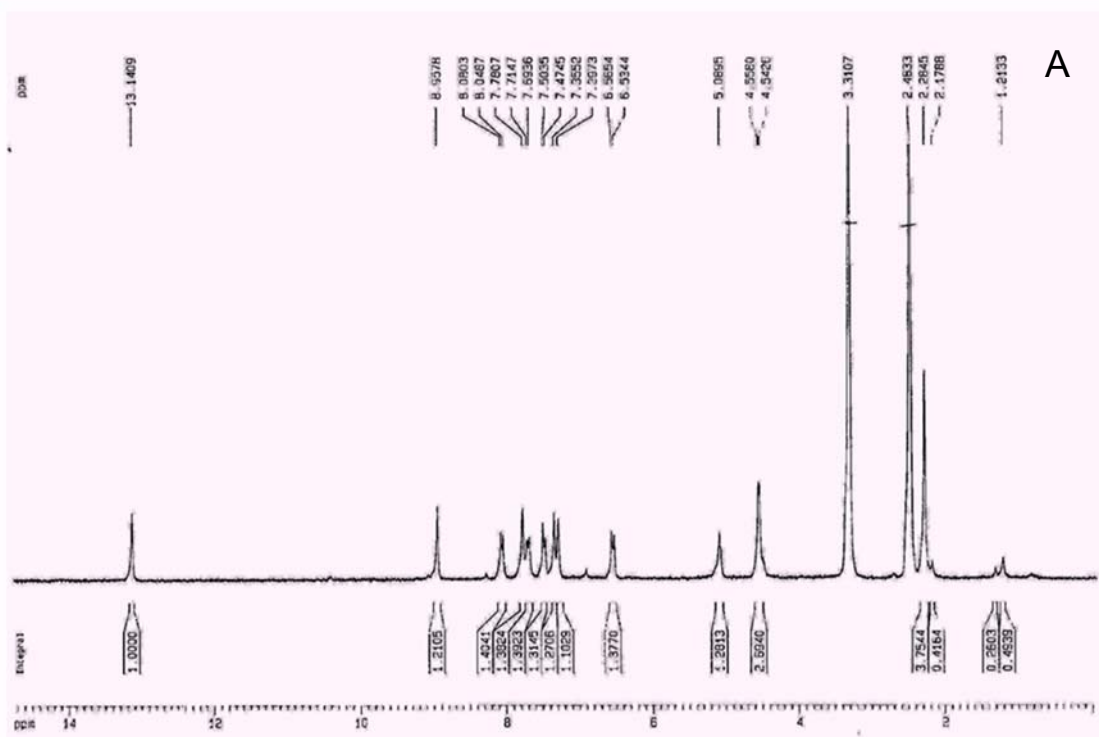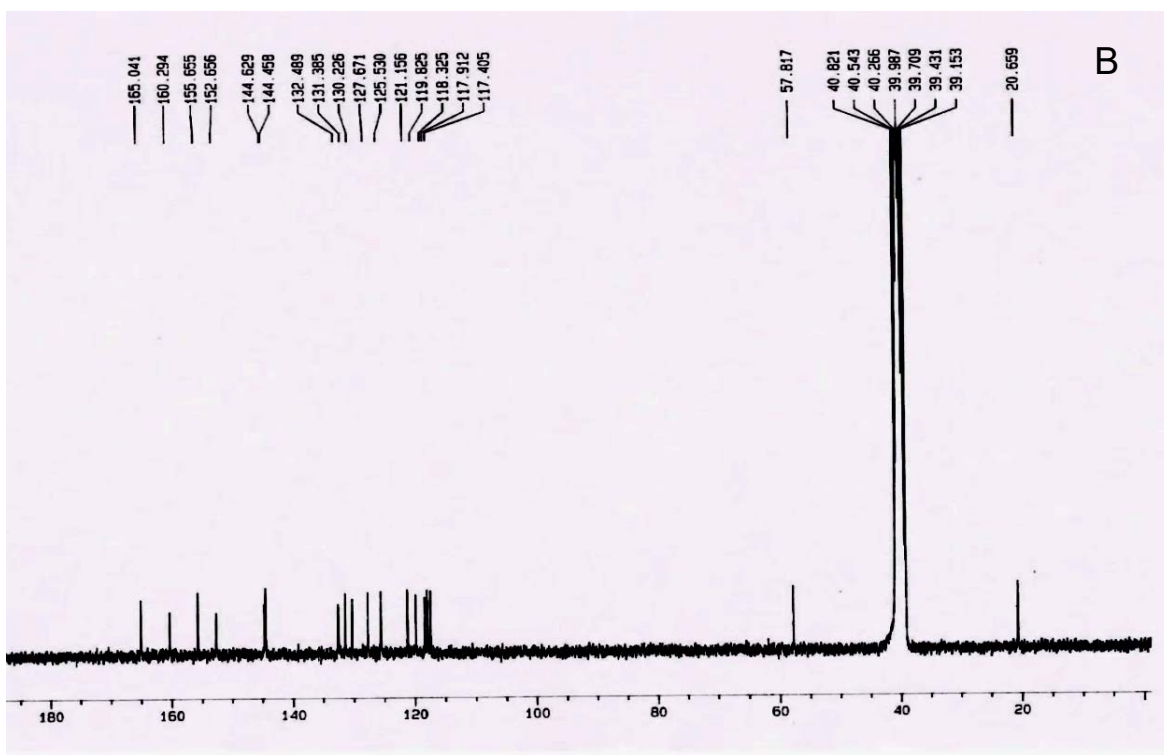
Fig. 3. (A) ^{1}H-NMR **(B)** ^{13}C-NMR spectra of HMBDC in DMSO-d_6.

2.2.3. Synthesis of Schiff base PPY

2-hydroxy-3-(hydroxymethyl)-5-methylbenzaldehyde (HHMB/**2**) and 3,5-dimethylpyrazole (**1**) were prepare by using published procedures.[4-5] For synthesizing of 3-(chloromethyl)-2-hydroxy-5-methylbenzaldehyde, HHMB (0.5 mol) was taken in 2 mL dichloromethane and the suspension gained was continued to stirred. Then freshly distilled SOCl$_2$ was added drop wise into DCM (final ratio of SOCl$_2$:DCM = 1:1) under vigorous stirring. After obtaining the yellow colored solution the reaction mixture was allowed to stir for another hour. Finally the excess SOCl$_2$ was detached and the solid residue was dissolved in 1 mL of DCM followed by dilution with 1 mL of hexane. The final solution was then set aside until it becomes evaporated to dry to obtain white crystals. After that, 1.84 g (10 mmol) of 3-(chloromethyl)-2-hydroxy-5-methylbenzaldehyde (HHMBCl/**3**) was dissolved in 5 mL of dry THF. Then, 0.96 g (10 mmol) of 3,5-dimethylpyrazole (Py) was poured in 20 mM of TEA. The solution of Py was mixed drop wise into the solution of HHMBCl, then the final mixture was allowed to stir for next 24 hour. This solution was then extracted from

44

brine solution and activated by using Na_2SO_4 to get the preferred product (PPY). The product was finally purified through column chromatography (Scheme 2). Structural analyses were checked by ^{1}H, ^{13}C-NMR. ^{1}HNMR (DMSO-d_6, 400 MHz): 2.08 (s, 3H, -ArCH$_3$), 2.23 (s, 6H,Py-2CH$_3$), 2.51 (solvent residual peak), 3.33 (due to trace H_2O), 5.14 (s, 2H, -CH$_2$-Ar), 5.86 (s,1H, Py-C=CH), 6.98 (s,1H, -ArH), 7.49 (s,1H, -ArH), 10.08 (s, 1H, -CHO), 11.12 (s,1H, -ArOH) ppm.^{13}C-NMR (DMSO-d_6, 75 MHz): 10.96, 13.82, 20.51, 39.51–40.90 (solvent residual peak), 46.51, 105.44, 121.82, 126.43, 129.27, 131.85, 136.95, 139.96, 139.79, 146.99, 156.36, 196.19 (Fig. 4).
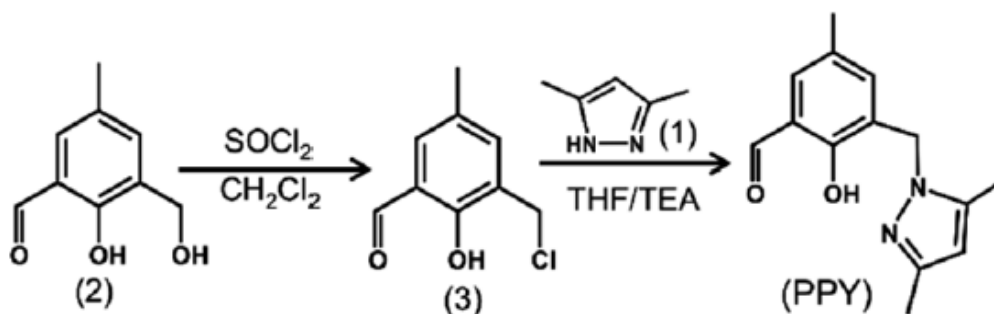
Scheme 2. Synthesis route of PPY.
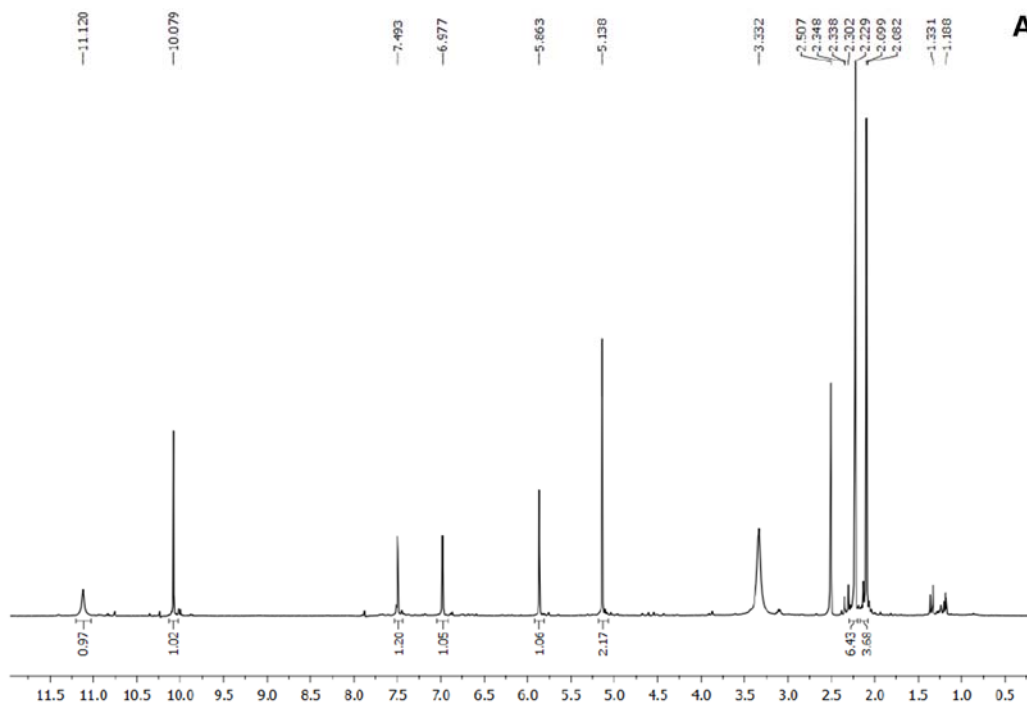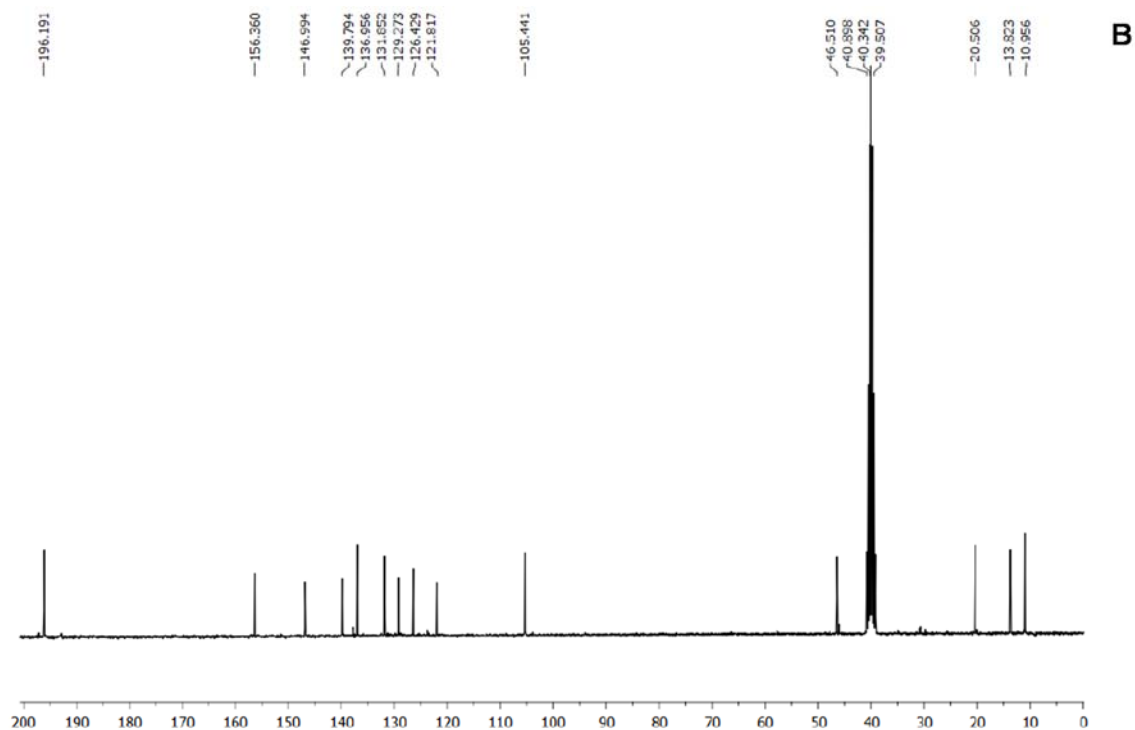
Fig. 4. (A) ^{1}H-NMR (B) ^{13}C-NMR spectra of PPY in DMSO-*d*6.

2.3. Preparation of different analytical samples

2.3.1. Preparation of food samples for moisture detection

All the food samples, such as cheese, butter, ghee as well as coconut oil were used as received from markets. The food samples were kept at 4°C in those commercially sealed container till use for the moisture analysis experiments. To extract free moisture present in food samples, various amounts of different food samples were mixed separately with 100 mL DMSO in a stoppered container under dry nitrogen conditions at room temperature (25°C). After that each sample mixture was heated at 60–70°C for complete liquefaction of those food samples, subsequently vigorous vortexing at that same temperature condition for 10 min to relocate entire free moisture from the food sample to the DMSO medium. Next, the solution was allowed to set till complete separation of the DMSO phase from rest of the solution. Then those DMSO phases were separated by using separating funnel, and used for fluorescence studies by addition of AH (0.5 μM) and KOH (10 μM).

46

2.3.2. Preparation of polar aprotic solvents for atmospheric moisture incorporation studies

40 mL of dry solvents (acetone, MeCN, DMF as well as DMSO) were poured individually in a 100 mL dry beaker having ~2.5 cm radius. Then each solvent was kept for incubation at open laboratory conditions possesses 75% (±5%) relative humidity at 25°C (±1°C) for different range of time intervals (12–120min). For determining atmospheric moisture absorption for those mediums, steady-state fluorescence emission and excitation spectra were performed by adding AH (0.5 μM) along with KOH (10 μM) to the bare-laboratory solvents at various time intervals (12–120 min). In case of acetone and MeCN, results of tiny volumes of solvent evaporation at the time of exposure to the open atmosphere on the moisture absorption values calculated from the fluorescence signal at different time gaps were incorporated to determine the time-dependent exact moisture incorporation values.

2.3.3. Generation of PPY/Al^{3+} in situ complex and its interaction with water

Stock solutions of AlCl$_3$ (1 mM) were prepared by taking appropriate amounts of AlCl$_3$ (anhydrous) in each of those different alcohol mediums then the mixtures were vortexed to solubilized completely. Individual stock solutions of 1mM PPY in each alcohol medium were prepared independently. Then the alcohol mediums were kept the same for to make stock solutions and reaction mediums. A part (10 μL or 4 μL) of the prepared stock solution of PPY (final concentration: 10 μM or 2 μM) was poured to each reaction medium (final volume 2 mL) having different amounts of AlCl$_3$ (5–200 μM) in absence or presence of water and/or MeOH in alcohol mediums at constant stirring condition, further the time-dependent PPY/Al^{3+} complexion kinetics were monitored by UV-vis absorption as well as fluorescence studies at 25°C.

2.4. Electrochemical studies/cyclic voltammetry (CV) studies

Cyclic voltammetry (CV) studies were performed by Auto-Lab (PG State 001) instrument by a platinum electrode (2-mm radius) as the working electrode finally the results were accumulated with reference to the standard calomel electrode. Hence, electrochemical properties of the corrosion medium towards the aluminium alloy (Al-7075) in absence and in presence of externally mixed water were studied by using cyclic voltammetric method for methanol/ethanol (4:1 v/v) medium equipped with a computer maintained Potentiostat/Galvanostat instrument (AUTOLAB, Netherland) accompanied by a conventional three electrode system kept at room temperature,

where supporting electrolyte was Tetrabutyl ammonium perchlorate. The Pt-wire was act as the working electrode and saturated calomel electrode (SCE) act as reference electrode and Pt-foil electrode (1 cm ×1 cm) behave as the counter electrode. The cell operation conditions were set for a scan area, −1.2V to 0.4 V; scan rate, 0.05 V/s.

2.5. UV-vis absorption and fluorescence studies

Throughout all the experiments UV-vis absorption studies were done by using a 1 cm path-length quartz cell with a double-beam spectrophotometer (Shimadzu, Japan; model TCC-240A) equipped by a thermos-statted cell holder. Steady-state fluorescence studies were performed by using a Perkin- Elmer LS-55 spectro-fluorimeter (PerkinElmer, USA) using a 1 cm path-length quartz cell. All the determining solutions were passed through a 0.45 mm filter (Millex, Millipore).

Fluorescence excitation as well as emission spectra for HHMB/AH were obtained for a fixed emission wavelength at 525 nm and excitation at 440 or 485 nm (excitation slit: 11; emission slit: 4). For HMBDC Fluorescence spectra were acquired upon excitation at 406 nm (excitation slit: 8, emission band pass: 3). In case of PPY fluorescence spectra were recorded by exciting at 402 nm (excitation slit: 10 or 8, and emission slit: 2 or 8). By retaining the same excitation and emission slit, time-dependent fluorescence intensities at 505 nm were recorded up to 60 min for excitation at 405 nm.

2.5.1. Limit of detection studies

The LOD for Al^{3+} detection by HMBDC, MeOH detection by PPY and for water by AH were obtained using the following equation[6]

$$\text{Detection limit (LOD)} = 3\sigma/k$$

Where, σ and k signify the experimental standard deviation and slope of 3 linear fitting curve.

2.5.2. Determination of fluorescence quantum yield

Fluorescence quantum yield (Φ) for the A^- (phenolate) form of AH (AH − 0.5 μM + KOH (10 μM)) was calculated by the procedure described earlier.[7] In short, 9,10-diphenylanthracene taken in an ethanol medium was act as the reference fluorophore with an emission quantum yield (Φ_r) = 0.95. The Φ_s was estimated using the following equation:

$$\Phi_s = [A_r F_s n_s^2 / A_s F_r n_r^2] \Phi_r$$

Where A signifies the absorbance at the excitation wavelength, also the integrated emission area is defined by F. n is the refractive index of that particular medium. Subscripts 'r' refer to the reference and 's' refer to sample molecule.

2.5.3. Fluorescence lifetime study

Fluorescence transient decays were studied by the time correlated single-photon counting (TCSPC) method. Where two different nano-second diodes (nano-LED; IBH, UK) with excitation at 450 and 490 nm were used as the light source. Fluorescence decays were monitored using a distinct Hamamastu photomultiplier tube (PMT) equipped with a TBX4 detection module (IBH, UK).The solutions for analysis were passed through a 0.45 mm filter (Millex, Millipore) before all the experiments. By using the in-built software the decays were evaluated. Fluorescence transient decays were monitored by using time correlated single-photon counting (TCSPC) method.

2.5.4. Fluorometric corrosion studies

A sheet of pure aluminium along its alloy that is, Al-7075 (composition: Al, 90%; Zn, 5.5%; Mg, 2.5%; Cu, 1.5 and Si, 0.5%) having similar dimension (3.5 cm × 1.5 cm × 0.2 cm) were grazed using an emery papers (400 grade) for surface polish purpose. The roughly polished metal sheets were washed thoroughly in acetone followed by sonication for 30 min. Then, those specimens were further washed by de-ionized water and finally dried in an oven at 60°C for 20 min. Weight of those metallic specimens were determined by using METTLER AE 240 balance. Those metallic coupons were then completely deep in 10 or 100 mL anhydrous methanol or 4:1 (v/v) methanol/ethanol mixed medium in air-tight measuring flux at the normal air as well as nitrogen conditions. For keeping appropriate normal air or nitrogen condition during the progress of corrosion (up to 30 days), the open air or nitrogen was purged in every 24 hour interval. Wherever, the minor change in solution volume was adjusted if necessary by adding proper amount of normal air- or nitrogen-saturated same solvent. To identify extent of Al(OR)$_3$ formation owing to the alcoholate corrosion, 30 mL of corrosion solution in every 3 day time-waits up to 18 or 30 days was taken out by a syringe then the fluorescence measurement was done after diluting the corrosion solution by 270 mL of parent solvent. For measuring the weight-loss due to corrosion, those

metallic sheets were taken out from the mediums after certain time-interval (after 18 days for pure aluminium sheet) then dried appropriately in an oven. Weight of those metallic sheets after the corrosion was assessed using the balance stated before.

2.6. ESI-MS⁺ and FT-IR study

ESI-MS$^+$ (positive mode) were performed by a QTOF Micro YA263 mass spectrometer. IR spectra for HHMB were recorded in methanol medium with and without Al^{3+} using a Perkin-Elmer Spectrum-2 spectrophotometer containing a Zn-Se ATR. Pyris6 TGA (Netherlands) instrument was used for thermo-gravimetric analysis (TGA).

2.7. Scanning electron microscopy

Surface characterization of aluminium based alloy, Al-7075, before as well as after corrosion were done by FESEM (JSM 6700F, JEOL Ltd. Tokyo, Japan).

2.8. Theoretical calculation

Density function theory (DFT) calculations were done by the Gaussian 09 Program for optimizing geometry by determining the structure of the hydrogen-bonded A^-/H_2O complex, alcohol coordinated Al^{3+}-HMBDC complex, (PPY/ROH/H_2O) complex.[8] Further Time-dependent DFT (TD-DFT) calculations were completed to obtain the lowest singlet excited states geometries and to acquire UV-vis absorption parameters of different probes and their respective complexes. For HHMB/AH the TD-DFT calculation was done in various solvents by using the CPCM solvent model. Whereas for HMBDC TD-DFT calculation was performed in methanol medium and for PPY methanol, ethanol as well as isopropanol mediums were chosen for TD-DFT calculations. The structural optimizations were carried out by considering the B3LYP exchange-correlation functional and different basis sets for each experiment in the solvent phase. For HHMB/AH 6-31G++(3d,3p) basis was set and the geometries were optimized. Geometry of HMBDC as well as its complex with Al^{3+} based on most acceptable structure was accomplish by allowing the 6-31G+(d,p) basis was set and the geometries were optimized. Whereas for PPY it was 6-31G basis function. In all the cases the global minima of all those species were definite by the positive vibrational frequencies.

2.9. References

1. Y. Hui and R. D. Webster, *Anal. Chem.*, 2011, **83**, 976.

2. R. R. Gagne, C. L. Spiro, T. J. Smith, C. A. Hamann, W. R. Thies and A. K. Schiemke, *J. Am. Chem. Soc.*, 1981,**103**, 4073.

3. E. Lambert, B. Chabut, S. C. Noblat, A. Deronzier, G.Chottard, A. Bousseksou, J. P. Tuchagues, J. Laugier, M. Bardet and J. M. Latour, *J. Am. Chem. Soc.*, 1997, **119,** 9424.

4. R. R. Gagne, C. L. Spiro, T. J. Smith, C. A. Hamann, W. R. Thies and A. K. Schiemke, *J. Am. Chem. Soc.*, 1981, **103**, 4073.

5. R. H. Wiley and P. E. Hexner, *Org. Synth.*, 1951, **31**, 43.

6. V. Thomsen, D. Schatzlein and D. Mercuro, *spectroscopy*, 2003, **18**, 112.

7. J. V. Morris, M. A. Mahaney and J. R. Huber, *J. Phys. Chem.*, 1976, **80**, 969.

8. M. J. Frisch and others, *Gaussian 09 Rev. A.1, Gaussian Inc., Wallingford CT*, 2009.

Chapter 3

Fluorometric detection of aluminium ion and its application for micro-level alcoholate corrosion

3.1. Introduction

Switching over from conventional fossil fuel to biofuel is of current interest owing to the maximum utilization of ecofriendly non-conventional energy.[1-2] Commercially produced less polluted biofuels such as methanol and ethanol, mixed with fossil fuels have an acceptable performance capacity for the gasoline engine.[3-6] Moreover, in comparison to the gasoline, methanol and ethanol have much higher octane rating or compression ratio to resist the knocking for better thermal efficiency.[7] Since most of the fuel tanks/pipes are made of aluminium or its alloys owing to its high strength-to-density ratio, the aluminium corrosion due to the formation of alkoxide (alcoholate or dry corrosion) during storage or even transportation of such bio-alcohols may cause leakage in the fuel tanks and in worst cases enough threat is speculated for fire and explosion.[8] Mechanical overloads, alloy impurities even at elevated temperatures are further contenders for accelerating the alcoholate corrosion.[9] However, a prolong exposure to the moisture retards the alcoholate corrosion by forming a protective layer of hydrated aluminium oxide in the metallic surface but moisture impurity in the fuel may damage the gasoline engine.[10] Hence, a maintenance optimization is crucial in critical engineering disasters by detecting alcoholate corrosion as in its nascent state with minimizing the chance of water contamination.[10-12]

Several electrochemical and mechanical methods have been exploited for decades to propose aluminium alcoholate and other corrosions;[6] yet the early detection of the alcoholate corrosion is still a challenging task due to the lack of sensitive analytical methods.[10,13-16] Here, the fluorescence technique may act as a better alternative owing to its simplicity and high sensitivity.[17-19] Till date, a large number of fluorescent probes for Al^{3+} have been exploited in the biological or environmental domain,[20-22] but has never focused on alcoholate corrosion studies. Based on this requirement, we synthesized a fluorescent probe, namely HMBDC ((6Z)-6-(2-hydroxy-3-(hydroxymethyl)-5-methylbenzylideneamine)-2H-chromen-2-one), to detect alcoholate corrosion with µg-level detection ability along with its retarding signature in the presence of moisture in a judicious way. Such novel method may lead to an early detection of alcoholate corrosion in a simpler way.

3.2. Result and discussion

3.2.1. Probe designing and solvent induced complexation with Al^{3+}

The non-fluorescent phenolic Schiff-base molecule containing a coumarin moiety (HMBDC) was prepared by condensing an equimolar mixture of 6-amino coumarin (6-ACO) and 2-hydroxy-3-(hydroxymethyl)-5-methylbenzaldehyde (HHMB) in dry ethanol (Scheme 1 and Fig. 3 of chapter 2).
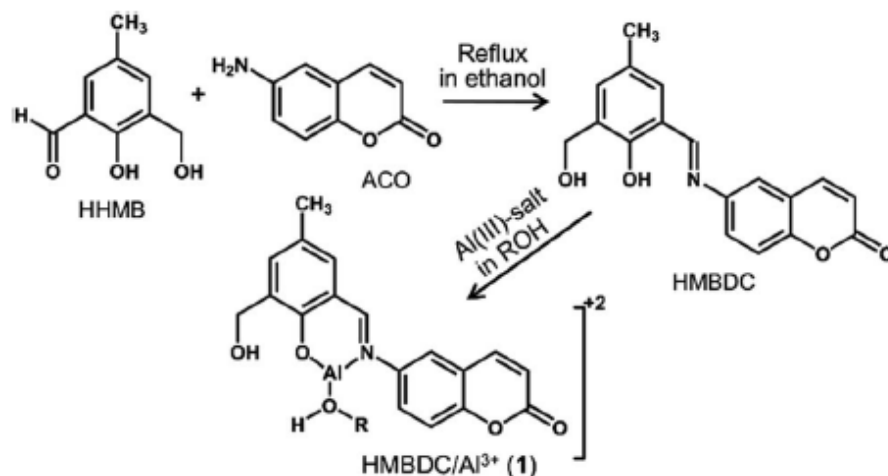
Scheme 1. Synthesis of HMBDC and its complexation with Al^{3+} in an alcohol solvent.

3.2.2. Solvent induced spectral response for HMBDC/Al^{3+}

Among various organic solvents, the interaction of HMBDC with Al^{3+} was observed only in the alcoholic medium according to the UV-vis studies (Fig. 1).
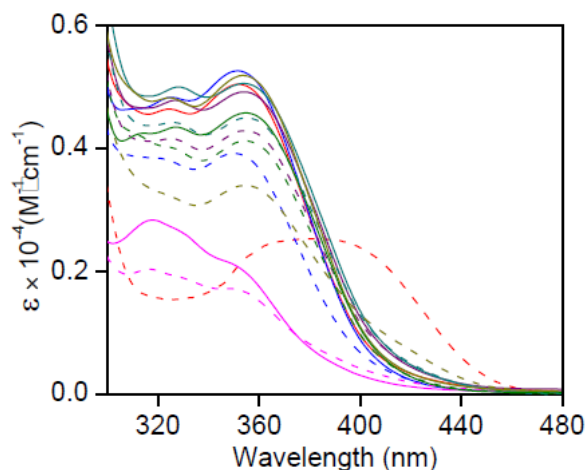
Fig. 1. Solvent dependent UV-vis absorption spectra of HMBDC in the absence (solid lines) and presence (broken lines) of Al(NO₃)₃ (8 equiv.) at 25°C: methanol (red), acetonitrile (blue), 1,4-dioxane (magenta), DMF (purple), DMSO (pink), ethanol (dark yellow) and THF (green).

In methanol, the absorption intensity at ~353 nm for HMBDC (5 μM) decreased gradually with the continuous addition of Al(NO₃)₃ until saturated at ~8-equiv., giving rise to a new peak at ~406 nm, where an isosbestic point at ~384 nm assures the formation of Al^{3+}/HMBDC complex (**1**) (Fig. 2A). Upon optimization of the complex formation affinity in various ethanol/methanol mixed media, highest reactivity with the lowest saturated Al^{3+} concentration (~5 equiv.) compared to that obtained in pure methanol was observed in a 4:1 methanol/ ethanol-mixed medium (Fig. 3). Most probably, more effective H-bonding interaction of the dimeric ethanol/methanol[23] with **1** (Al^{3+}/HMBDC complex of scheme 1) induces greater complex (**1**) stability, although the complex formation reactivity was much less in pure ethanol compared to the methanol medium (Fig. 2 and 1).
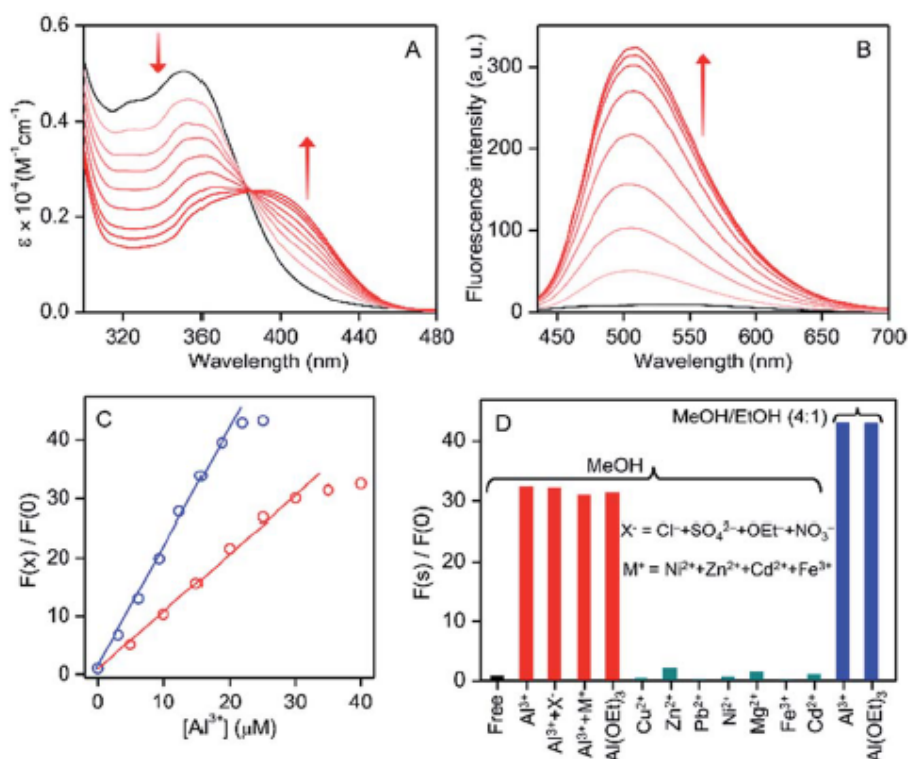
Fig. 2 (A) UV-vis absorption and (B) fluorescence spectra of HMBDC (5 μM) in the presence (red) and absence (black) of increasing concentration of Al(NO₃)₃ (0–40 μM) in anhydrous methanol at 25°C. The intensity changes with increasing Al^{3+} concentrations are indicated by arrows. (C) Al^{3+} concentration dependent relative increase in the fluorescence intensity with respect to its absence in methanol (red) or methanol/ethanol (4:1) (blue). (D) Fluorescence intensity ratios in presence and absence of various ions or mixture of ions in the mixed solvent (25 μM each; blue) or methanol (40 μM each; other colors) or are shown by bar-diagram.
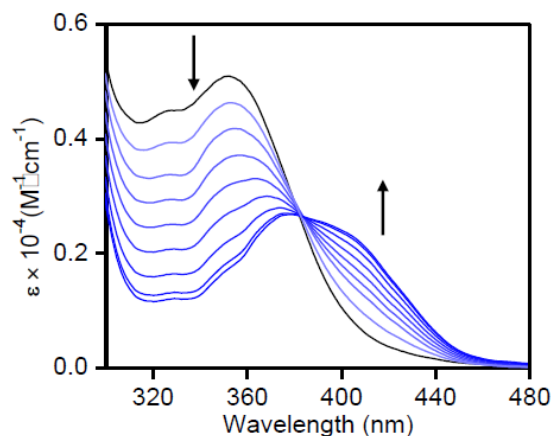
Fig. 3. UV-vis absorption spectra of HMBDC (5 µM) in the presence of increasing concentration of Al(NO$_3$)$_3$ (up to 25 µM) in 4:1 (v/v) methanol/ethanol mixed medium at 25°C. The increase or decrease of absorbance with increasing concentration of Al^{3+} is depicted by the arrows. The spectrum in the absence of Al^{3+} is shown by black.

In spite of the stronger H-bonding interactions of **1** with water compared to the methanol or ethanol, a complete dissociation of **1** in the presence of 20% (v/v) water in methanol (Fig. 4) suggests that, in addition to the solvent assisted H-bonded structural stability of **1**, alcohol molecule may also participate in the coordination with Al^{3+} to form **1**. Indeed, the possible methanol coordination is reflected in the ESI-MS$^+$ analysis. (Fig. 5).
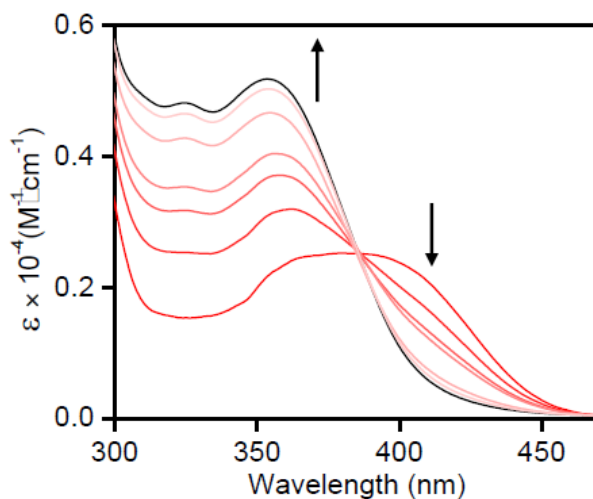
Fig. 4. UV-vis absorption spectral changes of HMBDC/Al^{3+} (5 µM with respect to HMBDC) in methanol by addition of increasing amount of water (0-20% (v/v)). The increase or decrease of absorbance with increasing percentage of water is depicted by the arrows. The spectrum of HMBDC in methanol is shown by black.
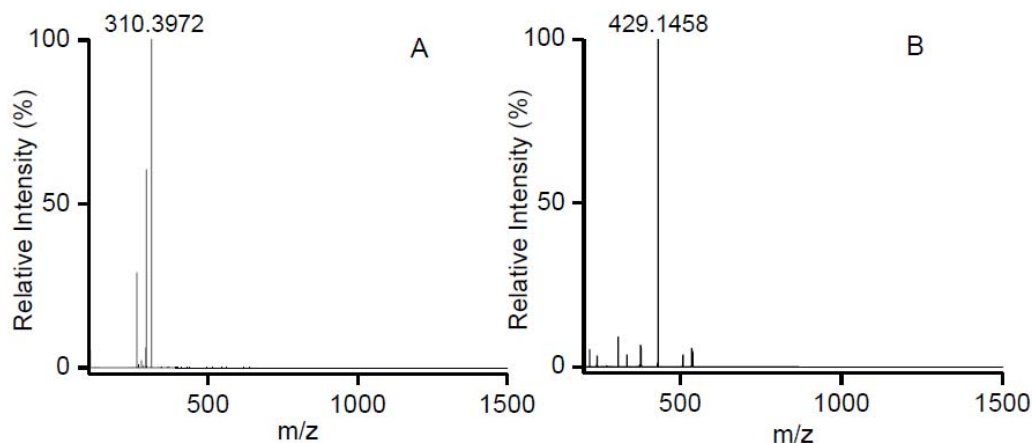
Fig. 5. ESI-MS$^+$ of HMBDC (A) (m/z for [HMBDC+H]$^+$ or [C$_{18}$H$_{16}$O$_4$N]$^+$: cal'd – 310.3207 (obs'd – 310.3972)) and HMBDC/Al^{3+} complex (B) (m/z for [HMBDC+Al+NO$_3$+CH$_3$OH]$^+$ or [C$_{19}$H$_{19}$O$_8$N$_2$Al]$^+$: cal'd – 429.3315 (obs'd – 429.1458) in MeOH.

In addition, the Job's plots in the absorption studies showed that the HMBDC formed 1:1 stoichiometric complex with Al^{3+} (Fig. 6).
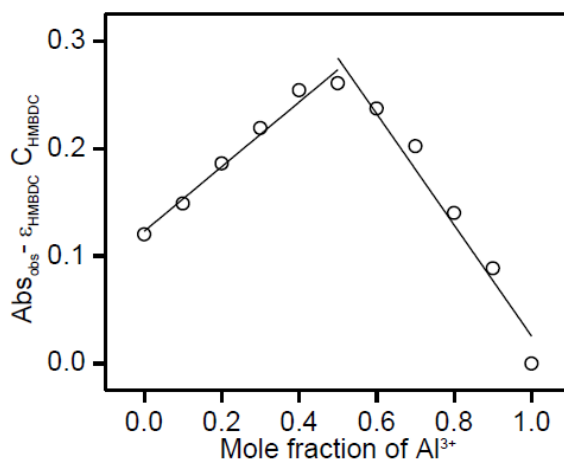
Fig. 6. Job's plot for defining binding stoichiometry of Al^{3+} to HMBDC in methanol medium, at 25°C.

3.2.3. DFT based theoretical calculations for complex structure

To elucidate the probable structure of **1**, we carried out the DFT-based theoretical calculation by considering the 1:1 stoichiometric Al^{3+}/HMBDC complex with or without methanol coordination. A stable structure of **1** was obtained when the oxygen atom of the methanol

56

molecule coordinates with Al^{3+} and other two coordination sites of Al^{3+} are occupied by the phenolic-oxygen and imine-nitrogen of HMBDC (Scheme 1, Fig. 7 and 8).
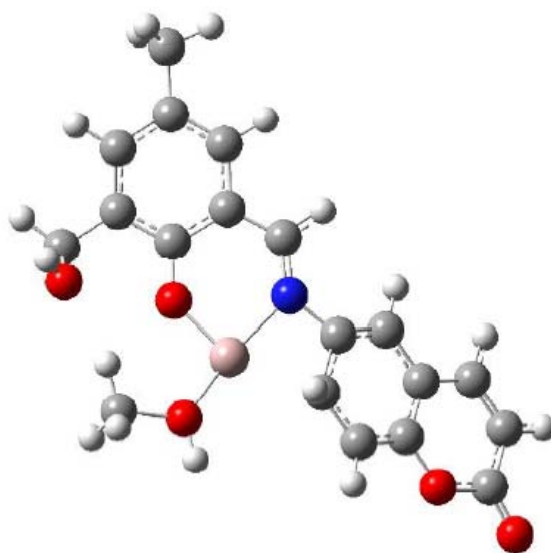
Fig. 7. Molecular view of HMBDC/Al^{3+} complex optimized with DFT-based theoretical calculation: (color code) white, H; gray, C; blue, N; red, O and light pink, Al.
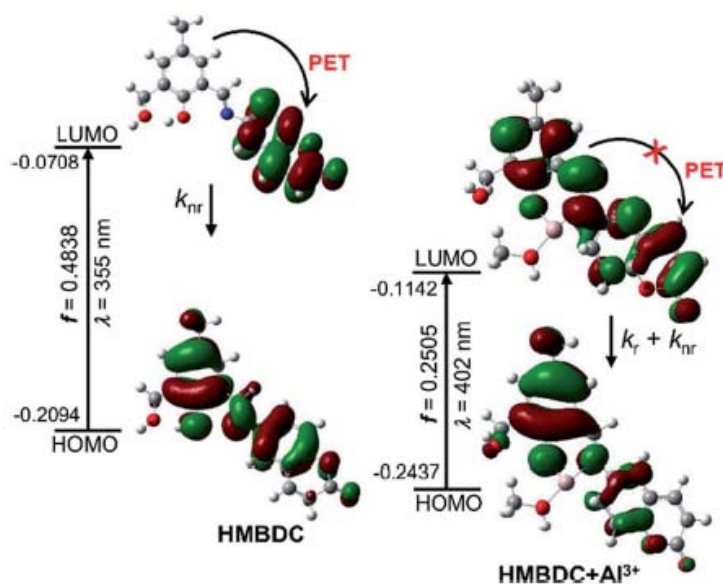
Fig. 8 Frontier molecular orbital profiles including various UV-vis absorption parameters of HMBDC (left panel) and HMBDC/Al^{3+} complex (right panel) based on TD-DFT (B3LYP/6-31G(d)).

Facile coordination of those hard donor sites of HMBDC towards harder Al^{3+} is susceptible towards alcohol assisted stabilization of **1**. The UV-vis absorbance at ~402 nm for **1** computed

from the time-dependent DFT (TD-DFT) calculations in methanol medium, where the HOMO (90)/LUMO (92) excitation nicely matched with the experimental absorbance at ~406 nm (Fig. 2 and 7). However, monitoring of the ^{1}H-NMR peak characterized for aldimine proton is a useful strategy to identify the bonding of the imine-N to Al^{3+}.[24] We observed that the aldimine proton peak intensity for HMBDC in CD_3OD was quenched to a great extent with a considerable down-field shift from 8.80 to 8.88 ppm in the presence of Al^{3+} (Fig. 9). The down-field shift is expected owing to the imine-N and Al^{3+} coordination, but intensity quenching does not follow the previous trend in the aprotic polar medium.[24] The generation of a partial positive charge at the N-centre upon its binding with the Al^{3+} may enhance the acidity of the aldimine proton to become labile for participating in the H/D exchange in a protic medium (CD_3OD), as reported previously for other allied systems.[25-26] These results strongly suggest the imine-N and Al^{3+} bonding in **1**. On the other hand, Al^{3+} induced large decrease in the IR intensity at ~3300 cm^{-1} for phenolic-OH also supports the phenoxide coordination (Fig. 10).
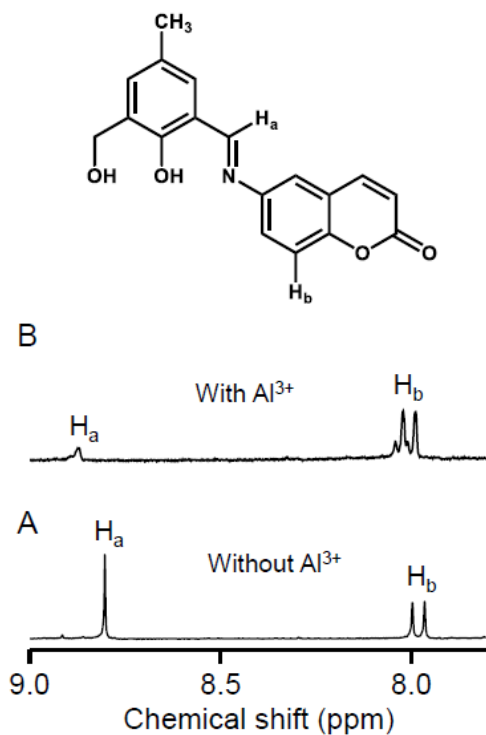
Fig. 9. 300 MHz ^{1}H-NMR (downfield region) spectra of HMBDC in (A) absence and (B) presence of 8.0 equiv. of Al(NO$_3$)$_3$ in CD$_3$OD.

The electronic distribution in the molecular orbital diagram (MO) of the HMBDC evaluated from the DFT calculation showed an intra-molecular photo-induced electron transfer (PET) from coumarin to the HHMB moiety, which makes the HMBDC non- fluorescent (Fig. 8). Al^{3+}

58

induced an instantaneous increase in the fluorescence intensity for HMBDC (5 μM) in the alcoholic medium (methanol/ethanol or their mixture) due to the formation of **1** (Fig. 2B and 11).
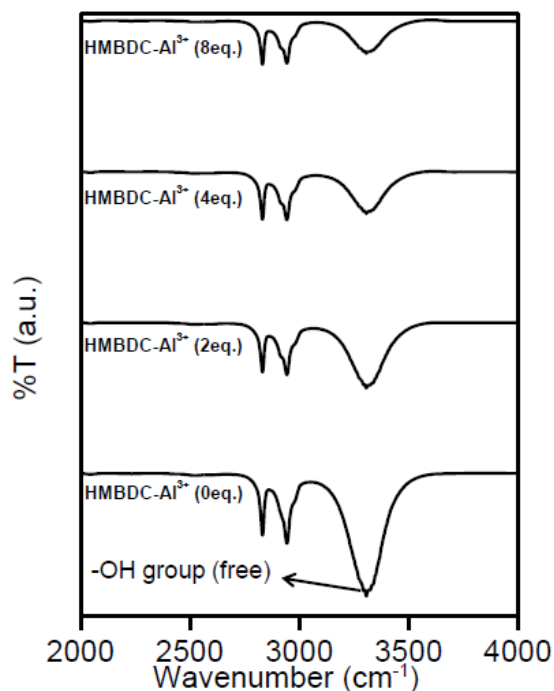
Fig. 10. FT-IR spectra of HMBDC in the absence and presence of various concentration of Al(NO₃)₃ in methanol medium.

A gradual fluorescence intensity increase at ~506 nm (λ_{ex} = 406 nm) of ~30-fold for 8 equiv. of Al^{3+} and ~40-fold for 5 equiv. of Al^{3+} was observed in the methanol and 4:1 (v/v) methanol/ethanol medium, respectively (Fig. 2 and 11B).
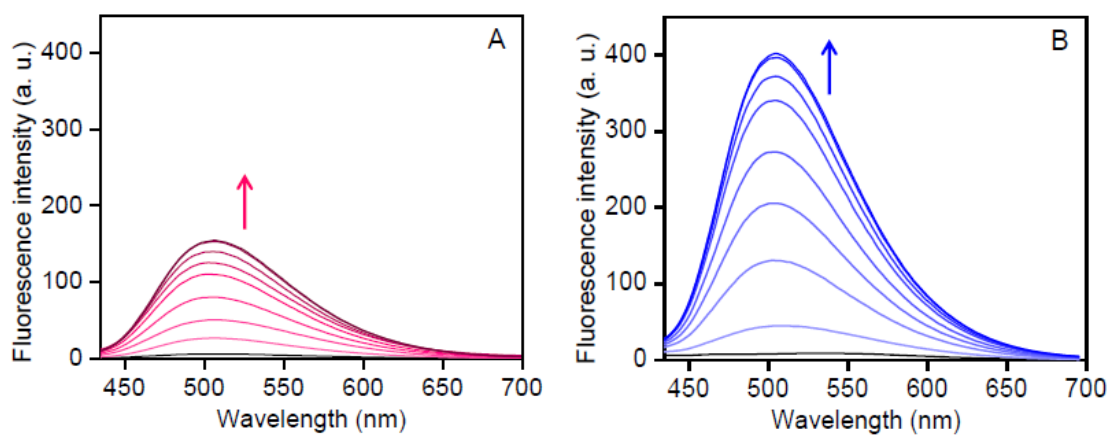
Fig. 11. Fluorescence spectra of HMBDC (5 μM) in presence of increasing concentration of Al(NO₃)₃ in (A) ethanol (up to 8 equiv.) and (B) methanol/ethanol (4:1 v/v) (up to 5 equiv.) at

59

25°C. The spectra without Al³⁺ are represented by black. The gradual increase of intensity with increasing concentration of Al³⁺ is showed by the arrow. The excitation wavelength was 406nm.

According to the HOMO and LUMO electronic distributions for **1** in the DFT studies, the PET process in HMBDC was highly restricted upon its binding with Al³⁺ in **1**, causing for the large increase in the fluorescence intensity (Fig. 8). However, the better fluorescence response (lower intensity-saturated Al³⁺ concentration and larger intensity increase) in the mixed medium than pure methanol may be associated with greater stability of **1**, as described in the previous section (Fig. 1). The fluorescence intensity increase remains invariant using other soluble Al(III)-salts (Fig. 2D and 12), which eliminates the role of counter anions for the increasing intensity. To ascertain the Al³⁺ selectivity, we performed similar fluorescence studies with other potentially interfering cations but failed to produce any noticeable fluorescence (Fig. 2D and 13). However, a linear intensity increase with the increase in the concentration of Al³⁺ up to 6 equiv. in methanol and 4 equiv. in the 4:1 methanol/ ethanol mixed medium can be useful for a ratiometric detection of unknown concentration of Al³⁺ (Fig. 2C), where the limit of detection[27] (LOD) of Al³⁺ with HMBDC in the methanol medium was found to be ~0.5 μM (*c.f.* details in chapter 2). Most importantly, HMBDC recognized Al³⁺ selectively from the mixture of various other cations, and also in presence of other soluble Al(III) salts, particularly, aluminium alkoxide (ethoxide) with similar accuracy (Fig. 2D and 13). Therefore, the Al(III) sensing ability for an alcoholate corrosion with an aluminium alloy must not be perturbed due to the interference of other leached cations. The dry alcoholate corrosion of aluminium or its alloy while forming soluble alkoxide $(Al(OR)_3)$ can be detected upon incubation in an anhydrous alcoholic medium. However, under a condition of prolonged incubation, the contamination of trace amounts of moisture may also trigger the conversion of $Al(OR)_3$ to $Al(OH)_3$, followed by the hydrated alumina $(Al_2O_3.xH_2O)$ coating on the metallic surface.[6] The formation of hydrated alumina can also be possible via the decomposition of $Al(OR)_3$.[6]

Fig. 12. Fluorescence spectra of HMBDC (5 µM) in the presence of various Al³⁺ salts (40 µM each): AlCl₃ (dark yellow), Al(NO₃)₃ (red), Al₂(SO₄)₃ (purple), and Al(OEt)₃, green.
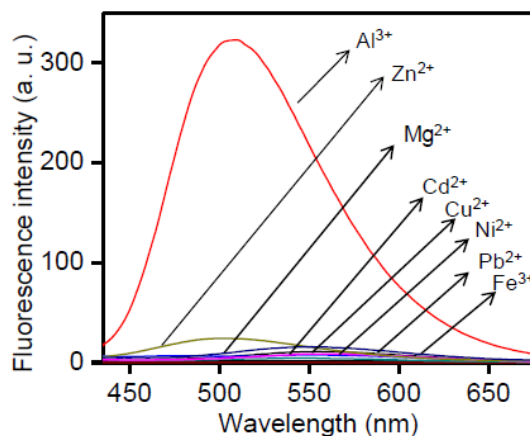
Fig. 13. Fluorescence spectra of HMBDC (5 *µ*M) in methanol medium containing different metal ions (40 µM each).

3.2.4. Detection of Alcoholate corrosion and correlation with weight loss experiments

To characterize the alcoholate corrosion as an exclusive process to the maximum limit, we minimized those wet-processes by allowing the corrosion under inert conditions. A previously grazed aluminium-sheet (dimension ~3.5×1.5×0.2 cm³; surface area ~12.5 cm²) was incubated for 18 days in 100 mL anhydrous methanol or methanol/ethanol (4:1) mixed solvent under nitrogen atmosphere by purging nitrogen every 24 h, where the small change in the solution volume if required was adjusted by injecting an appropriate amount of the nitrogen saturated anhydrous solvent. The amount of Al(OR)₃ (R = -Me, -Et) generated in the medium was estimated by monitoring the HMBDC (5 µM) fluorescence. After 10-fold dilution of the medium with the parent solvent, the amount of Al(OR)₃ formed or the alcoholate corrosion was estimated in every 3 days interval according to the amount of Al³⁺ obtained from the time dependent fluorescence responses (Fig. 14) as per the linear calibration plots in Fig. 2C multiplied by the dilution factor. linear increase in the normalized fluorescence intensity from ~3.5 to 16.8 and ~7.3 to 36.1 was observed with an increase in the incubation time period from 3 day to 18 day for methanol and methanol/ethanol (4:1) media (Fig. 15A and 14) respectively, which correspond to the linear increase in the Al³⁺ amount in the medium from ~3.2 to 16.6 µmol for either solvents (Fig. 15C). Indeed, the weight-loss of ~0.47 mg i.e., ~17.5 µmol was found to be closely similar with that of the increase in Al³⁺, revealing that not only the dry corrosion leads to the generation of Al³⁺ (Al(OR)₃) as the only product, but also HMBDC is highly effective for an accurate estimation of the alcoholate corrosion. In addition, the nice

61

correlation between the weight-loss and Al(OR)$_3$ amount also reveals that the decomposition of alkoxide into insoluble alumina is negligibly small during the whole corrosion time-course.

However, under open atmospheric conditions maintained by air purging (average relative humidity ~70%; average temperature 28°C) in every 24 h interval while maintaining other similar experimental conditions and analysis protocol, the specific corrosion rate (~2.0 μg per day per cm^2) up to 12 days, was found to be closely similar to that detected under the nitrogen atmosphere (Fig. 15C and 14).

Fig. 14. Fluorescence spectra of HMBDC for the corrosion of pure aluminium sheet (dimension: 3.5×1.5×0.2 cm^3). The spectra of HMBDC (5 μM) in alcohol medium (methanol or 4:1 (v/v) methanol/ethanol mixture) containing 10% corrosion solution of same solvent composition after undergoing the corrosion at every 3-days' time-interval up to 18 days at nitrogen or open air condition: (A) methanol in nitrogen condition; (B) methanol in open air condition; (C) 4:1 (v/v) methanol/ethanol medium at nitrogen condition, (D) 4:1 (v/v) methanol/ethanol medium at open air condition. The increase of intensity with increasing incubation time (3 to 18 days), are depicted by arrows.
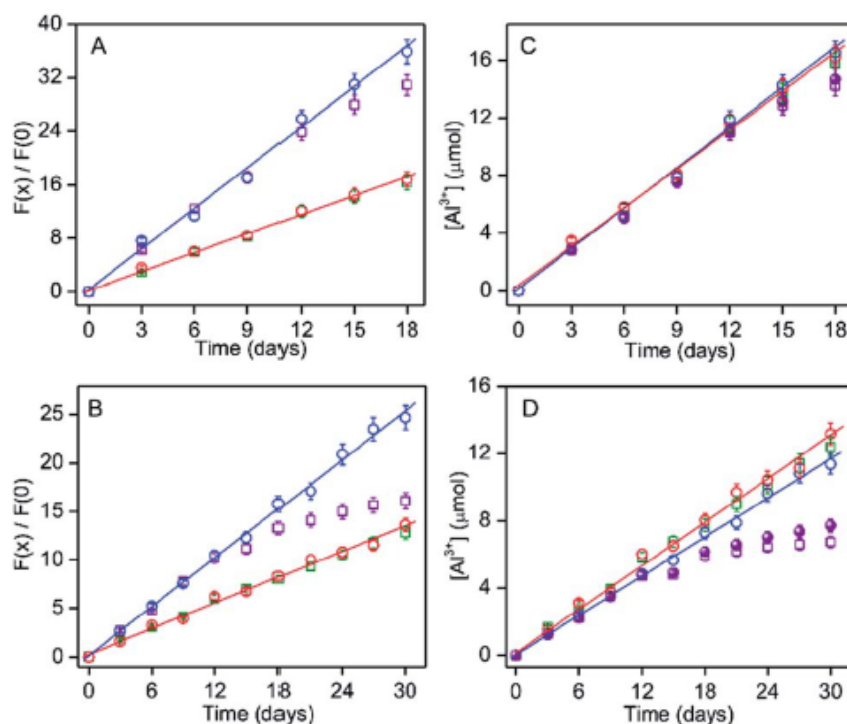
Fig. 15 (A and B) Extent of the fluorescence intensity increase due to corrosion-induced leached Al^{3+} ($F_{(x)}/F_{(0)}$) of HMBDC (5 μM) and (C and D) amount of Al^{3+} in the corrosion medium according to fluorescence response are plotted with various incubation times of pure aluminium sheet or its alloy (Al-7075) in different mediums/atmosphere conditions: nitrogen atmosphere in methanol (red) and methanol/ethanol (4:1) (blue); open atmosphere in methanol (green) and methanol/ethanol (4:1) (purple). The data at nitrogen conditions were only fitted linearly. (A and B) The fluorescence intensity of HMBDC (5 μM) was monitored after the 10-fold dilution of the corrosion medium with the same solvent. (C and D) The amount of Al^{3+} estimated as the amount obtained from the normalized intensity with comparing the linear plots in Fig. 1C multiplied by the dilution factor 10. The actual amount of alcoholate corrosions for the mixed medium under open atmosphere were depicted by solid circle (purple).

The results also indicate that the early stage of the alcoholate corrosion process (at least up to 12 days) for pure aluminium is not affected significantly by the atmospheric moisture content, although the final corrosion amount after 18 days incubation in normal atmosphere was slightly lower (~84%) for the mixed medium compared to that obtained for pure methanol (Fig. 15C). The decrease in the $Al(OR)_3$ amount can be affected by two processes: (a) $Al(OR)_3$ to insoluble $Al(OH)_3$ conversion due to the adsorbed moisture; (b) actual retardation of the corrosion rate due to the surface deposition of $Al(OH)_3$. The extent of the conversion of $Al(OR)_3$ to $Al(OH)_3$ in the corrosion medium under the open air condition can be assessed by estimating the fluorescence intensity at every 3 day time interval in the absence of aluminium sheet (from day-3 to day-18) with the addition of same amount of $Al(OEt)_3$ (3.2, 5.7, 8.0, 11.7, 14.2 and 16.4 μmol (final added amount) at day 0 (beginning of day 1), 3, 9, 12 and 15, respectively, in

63

100 mL mixed medium) as that of the alkoxide amount detected due to the corrosion under nitrogen condition (Fig. 16).

Fig. 16. Changes in fluorescence spectra of HMBDC due to various amount of Al(OEt)₃ addition at different time-intervals in 100 mL 4:1 (v/v) methanol/ethanol medium at open air condition. After addition of Al(OEt)₃ at day-0 (beginning of day 1), 3.2 µmol; day-3, 5.7 µmol; day-6, 8.0 µmol; day-9, 11.7 µmol; day-12, 14.2 µmol; day-15, 16.4 µmol, the fluorescence were monitored after (black) day-3, (red) 6, (blue) 9, (purple) 12, (green) 15, and (orange) 18, respectively. The fluorescence intensity of HMBDC (5 µM) were monitored after 10-fold dilution of the medium containing Al(OEt)₃ with the same solvent. The fluorescence were recorded before the addition of day-specific schedule Al(OEt)₃ amount (solid lines). The amount of Al(OEt)₃ represents sum of all additions. For comparison, the fluorescence spectra for the corrosion medium at the same time interval are depicted by the corresponding light color spectra (broken lines).

In comparison to the actual added Al(OEt)₃, any decrease in the Al(OEt)₃ amount upon such incubation should be added with the corrosion induced formation of Al(OR)₃ amount under nitrogen condition for respective time interval to obtain the actual alcoholate corrosion. The actual corrosion was found to be slightly higher than that estimated from the corrosion-induced Al(OR)₃ formation (Fig. 15C, solid symbol). According to the LOD of Al^{3+}, the detection of the alcoholate corrosion amount as minimum as ~0.1 µg mL^{-1} can be possible by monitoring the fluorescence response of HMBDC.

3.2.5. Real time detection of alcoholate corrosion using Al-7075 alloy

Alcoholate corrosion in a widely used aluminium alloy, Al-7075 (composition: Al, 90%; Zn, 5.5%; Mg, 2.5%; Cu, 1.5 and Si, 0.5%) was also studied. The previously grazed alloy sheet with same dimension and surface area as that of the pure aluminium sheet was incubated in 100 mL anhydrous methanol or 4:1 methanol/ ethanol under nitrogen as well as normal atmospheric conditions. The amount of the alcoholate corrosion in every 3 days interval up to 30 days was estimated by evaluating the fluorescence response of HMBDC (Fig. 15B and 17).

In comparison to the pure aluminium sheet, the increase in corrosion from ~1.5 to 4.0 µmol evaluated from the increase in the normalized fluorescence intensity (1.65 to 5.90 in methanol; 2.64 to 10.40 in methanol/ethanol (4:1) mixture) with the increase in the incubation time from day-3 to day-12 follows a similar linear relation regardless of the solvent compositions and atmospheric conditions (Fig. 15B and D), while the intrinsic rate of corrosion ~0.95 µg per day per cm^2 was more than 2-fold slower (Fig. 15C and D). The lower rate constant value for the alloy compared to pure aluminium indicates that the contamination of other metals in the alloy resists the early stage alcoholate corrosion process. However, under normal atmospheric condition, the corrosion amount vs. time relation deviates from the linearity after 12 days. Importantly, after 30 days of incubation, a large reduction in the $Al(OR)_3$ amount from ~11.38 to 6.64 µmol was estimated for the mixed medium, but the change was only from ~13.20 to ~12.33 µmol for pure methanol (Fig. 15D).
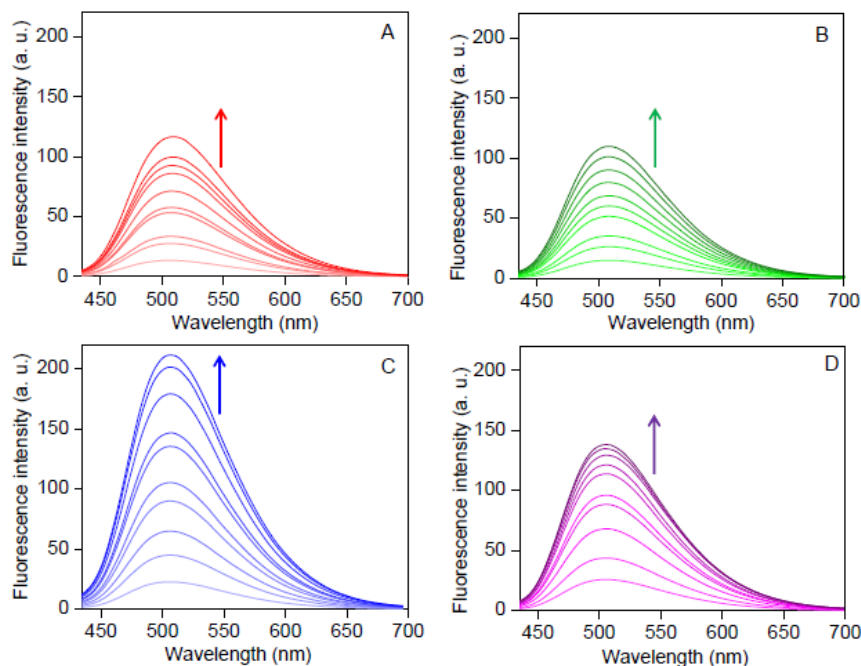
Fig. 17. Fluorescence spectra of HMBDC for the corrosion of aluminium alloy sheet, Al-7075 (dimension: 3.5×1.5×0.2 cm³). The spectra of HMBDC (5 μM) in alcohol medium (methanol or 4:1 (v/v) methanol/ethanol mixture) containing 10% corrosion medium of same solvent composition after undergoing the corrosion at every 3-days' time-interval up to 30 days at nitrogen or open air condition: (A) methanol in nitrogen condition; (B) methanol in open air condition; (C) 4:1 (v/v) methanol/ethanol medium at nitrogen condition, (D) 4:1 (v/v) methanol/ethanol medium at open air condition. The increase of intensity with increasing incubation time (3 to 30 days) are depicted by arrows.

By determining the hydration-induced conversion amount of Al(OR)$_3$ to Al(OH)$_3$ according to the procedure, as described before (Fig. 18), the actual alcoholate corrosion was found to decrease from ~11.38 to 7.70 µmol by changing the condition from nitrogen to open atmosphere after 30 days (Fig. 15D, solid symbol). Our study reveals that in comparison to pure methanol, the formation of Al(OH)$_3$ under open atmospheric condition retards the alcoholate corrosion largely due to the presence of more hygroscopic ethanol.[28] The deposition of Al$_2$O$_3$.xH$_2$O onto the alloy-surface is responsible for resisting the further alcoholate corrosion (Fig. 15D).[6]
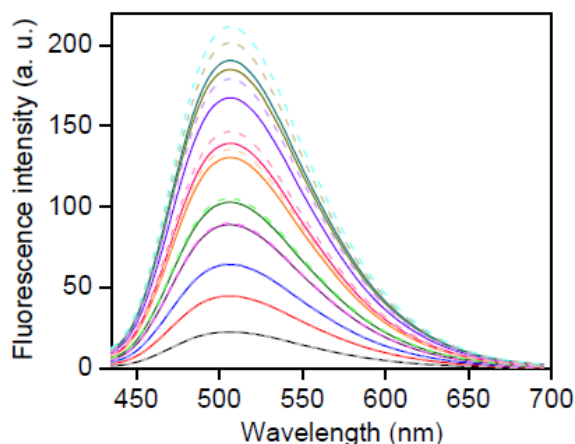
Fig. 18. Changes in fluorescence spectra of HMBDC due to various amount of Al(OEt)$_3$ addition at different time intervals in 100 mL 4:1 (v/v) methanol/ethanol medium at open air condition. After addition of Al(OEt)$_3$ in day-0 (beginning of day 1), 1.2 µmol; day-3, 2.4 µmol; day-6, 3.5 µmol; day-9, 4.8 µmol; day-12, 5.7 µmol; day-15, 7.2 µmol; day-18, 7.9 µmol; day- 21, 9.6 µmol; day-24, 10.8 µmol and day-27, 11.4 µmol, the fluorescence were monitored after day 3 (black), 6 (red), (blue) 9, (purple) 12, (green) 15, (orange) 18, (pink) 21, (violet) 24, (dark yellow) 27, and (dark cyan) 30, respectively. The fluorescence intensity of HMBDC (5 µM) were monitored after 10-fold dilution of the medium containing Al(OEt)$_3$ with the same solvent. The fluorescence were recorded before the addition of day specific schedule Al(OEt)$_3$ amount (solid lines). The amount of Al(OEt)$_3$ represents sum of all additions. For comparison, the fluorescence spectra for the corrosion medium at the same time interval as shown in Fig. 18, were depicted by corresponding light color spectra (broken lines).

In fact, the generation of more surface pits owing to the higher extent of the alcoholate corrosion in methanol over the mixed medium was also detected by naked eye (Fig. 19).
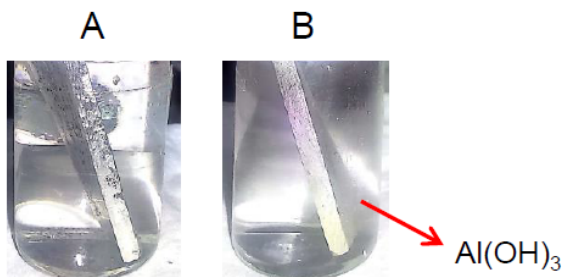
Fig. 19. Naked eye corrosion monitoring for Al-7075 sheet (dimension: 3.5×1.5×0.2 cm^3) after 30 days' time-period in 10 mL 4:1 (v/v) methanol/ethanol medium at (A) nitrogen and (B) open air conditions.

The surface morphology in the SEM studies showed that the alloy surface was little bit smoother after the corrosion in the mixed medium (Fig. 20), justifying our proposition for the surface deposition of $Al_2O_3 \cdot xH_2O$.
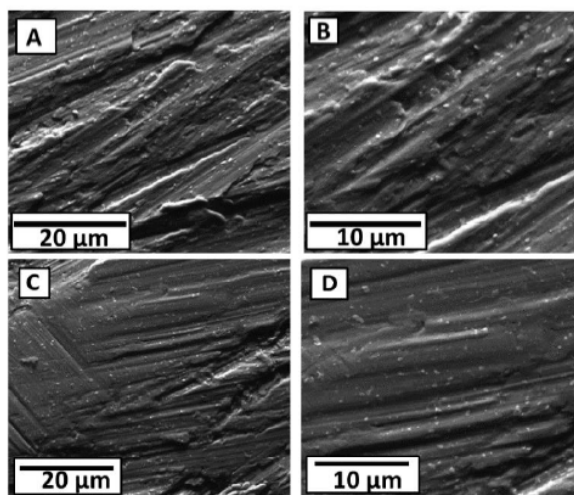
Fig. 20. FESEM images of Al-7075 alloy (A,B) before and after (C,D) corrosion in (A,C) methanol and (B,D) 4:1 (v/v) methanol/ethanol medium.

On the other hand, cyclic voltammetric studies in the corrosion medium exposed to normal atmospheric conditions identified an irreversible cathodic peak at ~ -0.7 V due to the formation of insoluble $Al(OH)_3$ in addition to the conversion from Al to Al^{3+}, but such irreversible peak was not observed for the medium exposed to nitrogen (Fig. 21). Moreover, the formation of white gelatinous precipitate of $Al(OH)_3$ in the mixed medium was clearly visible by naked eye under normal atmospheric conditions (Fig. 19B). All those results strongly support that the initiation of the wet-process by forming $Al(OH)_3$ inhibits the alcoholate corrosion rate.
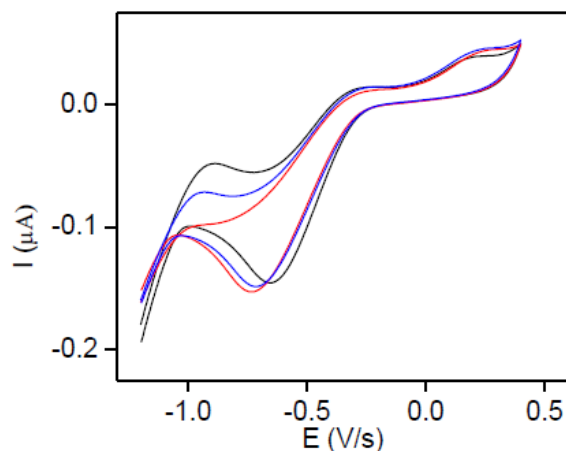
Fig. 21. Cyclic voltammetric studies in the corrosion medium for (4:1) methanol/ethanol solution with Al-7075 alloy: (red) under nitrogen atmosphere and (blue) under open air condition. The cyclic voltagram of the corrosion medium in presence of externally added 2% water was depicted by black for comparison. Tetrabutyl ammonium perchlorate used as the supporting electrolyte. The potential were measured using platinised platinum electrode against saturated calomel electrode at 25°C. Scan region -1.2 to 0.4 V and scan rate 0.05 V/Sec.

3.3. Conclusions

In conclusion, a phenolic Schiff-base consisting of a coumarin unit as a fluorescent sensor for Al^{3+} operable only in the alcoholic medium is synthesized to monitor dry alcoholate corrosion. The photo-induced electron transfer process in the probe molecule exhibits Al^{3+} induced large increase of fluorescence intensity, lifted by its complexation with Al^{3+}, which was further stabilized by the coordination and H-bonding interaction with the solvent molecule. The alcohol specific complex formation and subsequent fluorescence generation was suitably tuned to monitor the alcoholate corrosion by fluorometrically estimating aluminium alkoxide formation with a sensitivity of ~10 µg L^{-1}. However, the simultaneous participation of small extent of the wet-process ($Al(OR)_3$ to $Al(OH)_3$ conversion) and its deposition in metal surface, particularly for the alloy, inhibits the dry alcoholate corrosion. The alloy specific detection of the early stage alcoholate corrosion is in progress to obtain suitable material useful as a biofuel container.

3.4. References

1. J. Xuan, D. Y. C. Leung, M. Ni and M. K. H. Leung, *Renew. Sustain. Energy Rev.*, 2009, **13**, 1301.

2. F. H. Shinya and Y. KenjiImou. *Bioresour. Technol.*, 2010, **101**, 109.

3. L. Matejovsky, J. Macak, M. Pospisil, P. Baros, M. Stas and A. Krausova, *Energy Fuels*, 2017, **31**, 10880.

4. R. H. Borgwardt, *Ind. Eng. Chem. Res.*, 1998, **37**, 3760.

5. B. Shayan, S. M. Seyedpour, F. Ommi, S. H. Moosavy and M. Alizadeh, *Int. J. Automot. Mech. Eng.*, 2011, **1**, 3.

6. J. H. Lunsford, *Catal. Today*, 2000, 63, 165.

7. M. B. Çelik, B. Ozdalyan and F. Alkan, *Fuel*, 2011, **90**, 1591.

8. K. Wagner, K. Eppel, T. Troßmann and C. Berger, *Energy Mater. Mater. Sci. Eng. Energy Syst.*, 2008, **3**, 227.

9. K. Eppel, M. Scholz,T. Troßmann and C. Berger, Proceedings: EUROCORR, 2009, Nice, p. 9.

10. J. Linder, thesis on, Alcoholate corrosion of aluminium in ethanol blends, Master thesis, KTH Royal Institute of Technology, Div. Surface and Corrosion Science, Stockholm, 2012.

11. P. B. L. Fregolente, M. R. Wolf Maciel and L. S. Oliveira, *Braz. J. Chem. Eng.*, 2015, **32**, 895.

12. S. K. Thangavelu, A. S. Ahmed and F. N. Ani, *Int. J. Energy Res.*, 2016, **40**, 1704.

13. L. Kruger, F. Tuchscheerer, M. Mandel, S. Muller and S. Liebsch, *J. Mater. Sci.*, 2012, **47**, 2798.

14. O. Seri and Y. Kido, *Mater. Trans.*, 2009, **50**, 1433.

15. Corrosion resistance of aluminium and protective measures where appropriate, First Edition: 2011 © AFSA Compiled and published by the Aluminium Federation of South Africa

16. G. R. Kramer, C. M. Mendez and A. E. Ares, *Mat. Res.*, 2018, **21**, 1.

17. S. Das, Y. Sarkar, S. Mukherjee, J. Bandyopadhyay, S. Samanta, P. P. Parui and A. Ray, *Sens. Actuators, B*, 2015, **209**, 545.

18. P. P. Parui, A. Ray, S. Das, Y. Sarkar, T. Paul, S. Roy, R. Majumder and J. Bandyopadhyay, *New J. Chem.*, 2019, **43**, 3750.

19. P. A. Anna, P. Paul and W. R. David, Anal. Chem., 1997, **69**, 1635.

20. A. Gupta and N. Kumar, *RSC Adv.*, 2016, **6**, 106413.

21. Q. Jiang, M. Li, J. Song, Y. Yang, X. Xu, H. Xu and S. Wang, *RSC Adv.*, 2019, **9**, 10414.

22. H. L. Nguyen, N. Kumar, J.-F. Audibert, R. Ghesami, J.-P. Lefevre, M.-H. Ha-Thi, C. Mongin and I. Leray, *New J. Chem.*, 2019, **43**, 15302.

23. I. A. Finneran, P. B. Carroll, G. J. Mead and G. A. Blake, *Phys. Chem. Chem. Phys.*, 2016, **18**, 22565.

24. S. Sahana, S. Bose, S. K. Mukhopadhyay and P. K. Bharadwaj, *J. Lumin.*, 2016, **169**, 334.

25. R. Casasnovas, M. Adrover, J. Ortega-Castro, J. Frau, J. Donoso and F. Mu~noz, *J. Phys. Chem. B*, 2012, **116**, 10665.

26. B. Setner, M. Wierzbicka, L. Jerzykiewicz, M. Lisowski and Z. Szewczuk, *Org. Biomol. Chem.*, 2018, **16**, 825.

27. V. Thomsen, D. Schatzlein and D. Mercuro, *Spectroscopy*, 2003, **18**, 112.

28. B. Tan, P. Melius and P. Ziegler, *J. Chromatogr. Sci.*, 1982, **20**, 213.

Chapter 4

A unique fluorescence method for the real-time detection of trace water in polar aprotic solvents with the application in foodstuffs

4.1. Introduction

An effective analytical procedure for the estimation of trace water in organic solvents displays a direct impact in chemical research, industry and food inspection.[1–5] For organic synthesis, in particular the synthesis of organometallic compounds, moisture-free solvents are essential to obtain the optimum product yield.[6-7] Carboxylic ester and imine functional compounds are highly susceptible to hydrolysis even in the presence of trace amounts of moisture during their storage in organic solvents.[8] The moisture contamination in oil can be a major problem in the petroleum industry due to emulsification and phase separation processes,[9-10] resulting in the blockage of fuel pipe, and subsequent engine damage or failure.[11-12] Furthermore, the estimation of water in food samples is very important for various reasons:[13–17] (a) optimum moisture level in foods is essential for to sustain an appropriate test, texture and appearance, and most vital nutritional values; (b) food manufacturers often incorporate inexpensive water ingredients illegally as much as possible in foods for their profit; (c) trace water affects microbial food degradation or water rancidity, especially for pure oil-based food materials;[15–17] (d) food processing operations such as transferring through pipes, packaging and mixing also affect the estimation.

The Karl Fischer titration is one of the best known methods for the estimation of moisture in organic Gas chromatography is another well-acquainted classic option.[19-20] However, certain limitations in those methods such as time consumption, inability for real-time analysis, specialized equipment design requirement, difficulties in sample preparation, and rigorous data handling are major concerns for easy and cost-effective moisture detection for applied analytical samples.[21-22] Fluorescence technique may opt as a better alternative owing to its simplicity and rapid response, and non-destructive fabrication and most importantly its high sensitivity.[23–25] Consequently, a number of research groups currently switch their focus to various kinds of commercially viable fluorescence-based water sensing procedures. Up to now, a number of fluorosensing mechanisms, such as intramolecular charge transfer (ICT)[26-27] photo-induced electron transfer (PET),[1,28] excited-state intra-molecular proton transfer (ESIPT),[29-30] H-bonding interaction,[5,31-32] aggregation-induced emission (AIE)[33–35] and Forster resonance energy transfer (FRET),[36-37] have been reported to detect trace water in organic solvents. Water fluorosensors based on chemical rearrangements such as ring opening of cyclic rhodamine derivatives,[38] hydrolytic cleavages of Schiff bases[39-40] and hydration of aldehyde functionality[41] have also been reported. In addition, researchers constructed various metal/ligand complexes or metal organic frameworks (MOFs)[42-43] as water fluorosensors.

Among the various water sensing fluorescent probe molecules reported in the literature, some exhibit very high detection sensitivity (~0.001% or even below), although often the high detection accuracy is restricted to specific solvent systems.[14,44–46] However, the requirement of multi-step complex synthesis procedures for the preparation of probe molecules makes the overall moisture detection procedure inconvenient for routine analytical purpose.[34,37,41–43] In most cases, the detection methodologies are relying only upon a single emission/excitation band originated by the association/interaction of water with the recognition site of a probe molecule.[26–32,34–38,41-42] Therefore, it is not always straightforward to recognize the actual cause for the observed fluorescence response between the inhomogeneous probe distribution in the solution due to sample micro-heterogeneity and any moisture affected changes. In addition, photo-bleaching of the probe molecule and instrumental parameters[44] are often troublesome to assess the actual fluorosensing response induced by water incorporation.

In this study, a simple 4-methyl-2,6-diformyl phenol fluorescent probe (AH) was exploited to detect trace water in several polar aprotic organic solvents with high precision (detection limit ~0.01–0.04% (v/v)). The phenolate form of the probe molecule (A^-) exhibits a water-induced spectral blue-shift to various extents in the UV-vis absorption and fluorescence excitation spectra from ~470–490 nm to 440–450 nm depending on various polar aprotic organic solvents due to the formation of an A^-/H_2O H-bonded complex. Although both A^-/H_2O and free A^- show identical fluorescence emission characteristics, an opposite emission intensity changing pattern, from a gradually increasing to a decreasing trend with the increase in water%, was detected upon switching the excitation wavelength from 440 to 485 nm. Water induced emission intensity changes of A^- and A^-/H_2O species for each water% value were combined together to obtain a normalized single spectral profile, and thus the water% induced emission increase manifested considerably with eliminating the probe concentration dependency on the intensity response. Moreover, such normalization eventually produces linear intensity changes dependent on water%, which are effective to estimate water% ratiometrically. In addition, a large spectral blue-shift of ~25 nm in the excitation spectra induced by only a small quantity of water (2–5% v/v) can also be suitably tuned for its detection purpose. The water detection procedure was applied to monitor real-time atmospheric moisture incorporation in common polar aprotic solvents and moisture analysis studies in various food samples useful for water rancidity.

4.2. Results and discussion

4.2.1. Solvent-induced spectral shifts of the phenolate form of AH

AH deprotonated partially around neutral pH (pKa ~ 7.1) in an aqueous buffer according to the pH-dependent changeover of UV-vis absorption intensities between ~350 nm for the phenol form (AH) and ~440 nm for the phenolate form (A$^-$) (Fig. 1).
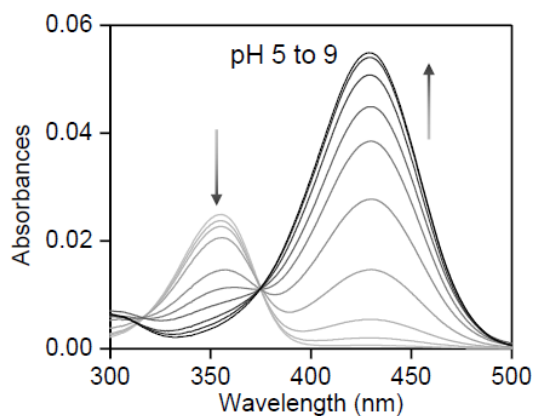
Fig. 1. pH dependent UV-vis absorption spectra of AH (6 μM) in 20 mM HEPES buffer, at 25°C. The pH of buffer solution was adjusted by an addition of NaOH. The increase or decrease of absorbance with increasing pH is depicted by arrows.
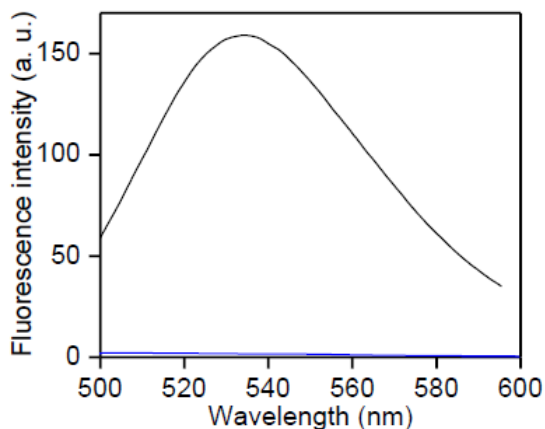
Fig. 2. Fluorescence emission spectra of AH (0.5 μM) in the absence (blue) and presence (black) of KOH (10 μM) in water. Excitation wavelengths: 350 nm (blue) and 440 nm (black).

73

A⁻ exhibited a strong fluorescence intensity (quantum yield (Φ) ~ 0.4) (cf. Experimental section), but AH did not (Fig. 2).[47] Consistent with the earlier reports, an additional absorption intensity at ~485 nm with appreciable quenching of the intensity at ~350 nm for AH (6 µM) was identified in the DMF or DMSO medium even in the absence of the base (Fig. 3A).[48-49] The appearance of band at ~485 nm is mainly due to partial deprotonation of AH induced by the basic solvent character,[50] since the spectral shape and position did not change except a large increase in its intensity by an addition of base (KOH, 15 µM) in DMF or DMSO (Fig. 3B). This proposition is further supported by the base-induced similar spectral shift from ~350 nm to 470–480 nm for other non-basic aprotic solvents (acetone, MeCN) (Fig. 3B)
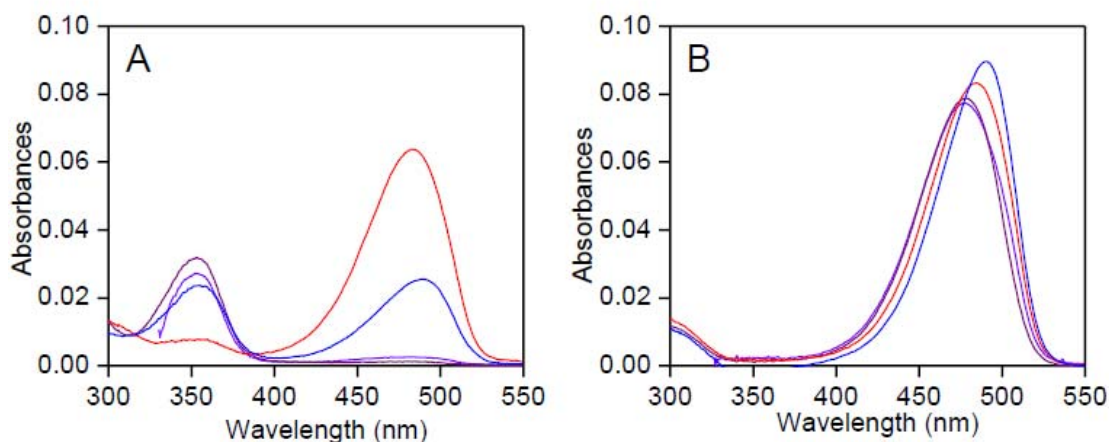
Fig. 3. Different aprotic solvent dependent UV-vis absorption spectra of AH (6 µM) in (A) the absence and (B) presence of KOH (15 µM) at 25°C: violet, acetone; purple, MeCN; red, DMF and blue, DMSO.

However, similar to the aqueous medium, a large blue-shifting of absorption band from 470–485 nm to 440–435 nm for the phenolate form (A⁻) was detected by changing the medium from aprotic to protic methanol or ethanol (Fig. 4). Previously, the solvent-induced large spectral blue-shift has been justified with presuming higher dipole moment of DMSO/DMF than the water molecule.[53] However, since the solvent-dependent absorption spectral shift is usually very nominal, the large spectral blue-shift is attributed to a specific A⁻/solvent interaction (Fig. 5 and Fig. 4).
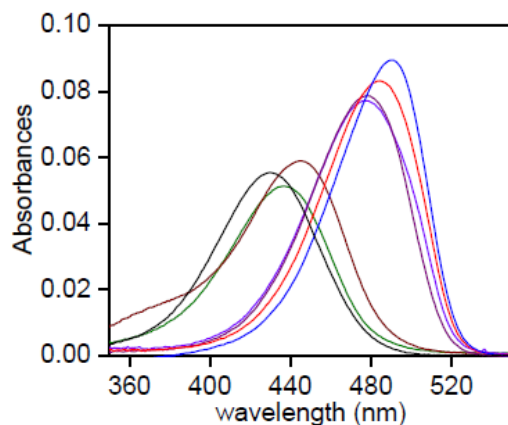
Fig. 4. Different protic solvent dependent UV-vis absorption spectra of AH (6 μM) in presence of KOH (15 μM) at 25°C: black, water; green, methanol; brown, ethanol. The spectra for aprotic solvents are shown for comparison (violet, acetone; purple, MeCN; red, DMF; blue, DMSO).
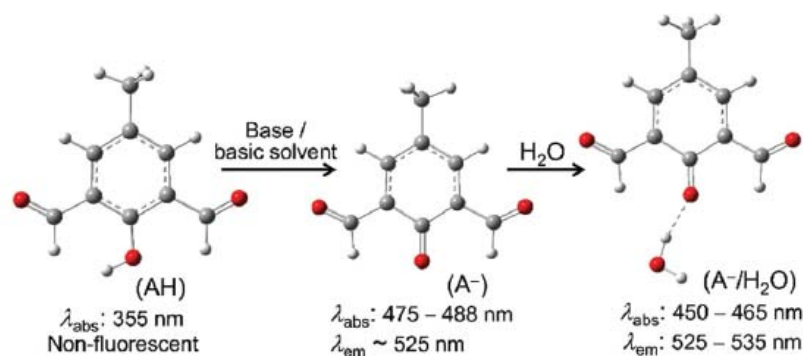
Fig.5. Schematic of base or basic solvent (DMSO/DMF)-induced complete/ partial deprotonation of AH (A⁻) and its H-bonding interaction with water. The DFT-optimized structures are shown (color index: C, gray; O, red; and H, white). The experimental UV-vis absorption (λ_{abs}) and emission (λ_{em}) wavelengths for different species are depicted in the lower panel. (cf.) The calculated absorption parameters are shown inin Table 2.

4.2.2. Formation of A⁻/H₂O complexes in aprotic solvents

The phenolic-OH deprotonated form of AH (A⁻) was confirmed with forming UV-vis intensity at 470–485 nm by addition of any base (KOH or TEA) to polar aprotic solvents (Fig. 5). However, TEA (THF-solubilized base) induced no spectral change in a relatively nonpolar THF medium, suggesting no such deprotonation reaction of AH (Fig. 6), presumably due to poor solvation of the negatively charged A⁻ species. The water-induced large blue-shift of the absorption band for A⁻ shows the interaction of A⁻ with the water molecule (Fig. 7).
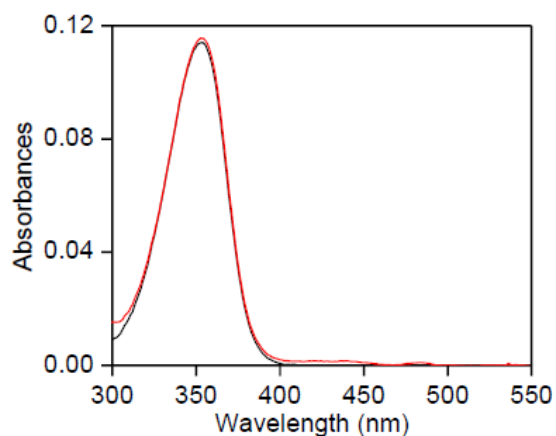
Fig. 6. UV-vis absorption spectra of AH (10 µM) in the absence (black) and presence of TEA (1 mM) (red) in THF medium at 25°C.

A similar UV-vis spectral blue-shift by water interaction was reported by C. Pinheiro *et al.*[6] Instead, the presence of water causes no spectral changes for the protonated AH form (Fig. 8), which excludes the possibility of water/AH interaction. Most probably, the large negative charge density at phenolate-O in A⁻ may induce efficient H-bonding affinity with the water molecule to form an A⁻/H_2O complex.

Fig. 7. UV-vis absorption spectra of AH (6 μM) in the presence of KOH (15 μM) and various water% (v/v) in different solvents: (A) acetone (water%: 0.1, 0.3, 0.6, 1.0, 1.5, 2.0, 3.5, 6.0, 8.5 and 11.0); (B) MeCN (water%: 0.1, 0.3, 0.6, 1.5, 2.5, 6.5 and 9.0); (C) DMF (water%: 0.1, 0.4, 1.0, 1.5, 2.7, 4.8, 6.5, 8.5 and 10.0) and (D) DMSO (water%: 0.3, 0.9, 1.4, 2.0, 3.2, 5.1, 6.3, 8.5, 6.3, 10.0 and 12.3). (A–D) The gradual spectral blue-shift with the increase in water% is depicted by arrows. The spectra in the absence of water are shown in black.
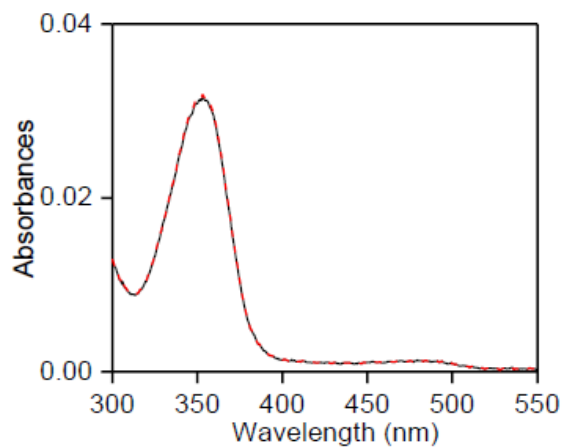
Fig. 8. UV-vis absorption spectra of AH (6 μM) in the absence (black) and presence of 1% (v/v) water (red, broken line) in MeCN medium at 25°C.

77

To avoid any significant change of general solvent properties, UV-vis absorption spectral changes of A^- (AH (6 μM) + KOH (15 μM)) in different polar aprotic solvents (acetone, MeCN, DMF and DMSO) were monitored in the presence of low amounts of water up to ~6–12% (v/v). With the increase in water% in solvents (0.1–6.0% for acetone, 0.1–8% for MeCN, 0.1–12% for DMF and 0.3–12% DMSO), the absorption band of A^- gradually blue-shifted from 475 to 488 nm maximally up to ~445–450 nm (Fig. 7). The spectrum at the highest water% for each aprotic solvent was found to be closely similar to that obtained in a pure aqueous medium (Fig. 7 and Fig. 4). Upon reverse solvent addition, i.e., each aprotic solvent (~10% (v/v)) in an aqueous medium causes an insignificantly small spectral wavelength shift (Fig. 9), indicating that A^- involves a specific interaction with water in the aprotic solvents. Notably, the observed small spectral changes between the aprotic medium in the presence of the highest water% and in pure water can be explained by their general solvent properties, even though the same species, namely, A^-/H_2O complex, can be expected in both types of solvents (Fig. 7 and Fig. 9).
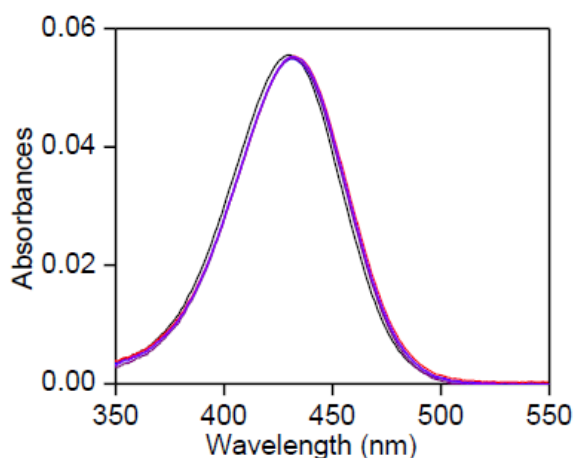
Fig. 9. UV-vis absorption of AH (6 μM) in the presence of KOH (15 μM) and 10% (v/v) different aprotic solvents in water at 25°C: violet, acetone; purple, MeCN; red, DMF; blue, DMSO. The spectrum in the absence of aprotic solvent is depicted in black.

However, the replacement of water with other protic solvents such as methanol or ethanol, in the aprotic solvents showed a similar spectral blue-shift up to ~435 nm (Fig. 10), while the blue-shift requires much higher alcohol% (~23–25% (v/v)) than water% (6–12%) presumably due to weaker interaction ability of A^- with the alcohol molecules. Most probably, A^- participates in the H-bonding interaction with water molecules, which may increase the $S_0 - S_1$

transition energy for the phenolate chromophore moiety to attribute for the 30–50 nm spectral blue-shift (Fig. 5). Since the water molecule itself participates in the H-bonding interaction with large affinity in the aprotic solvents, the fraction of H-bonded A^- was found to be enhanced with the increase in water% due to the formation of more number of A^-/H_2O H-bonded complexes than its dissociation affected by the increased ratio of the water amount in the solvent composition. The H-bonding interaction of A^- with water molecules was also examined by steady-state and time-resolved fluorescence methods. The deprotonated A^- species exhibited a strong emission intensity at 525–535 nm in different solvents (acetone, MeCN, DMF, DMSO and water) (Fig. 11).
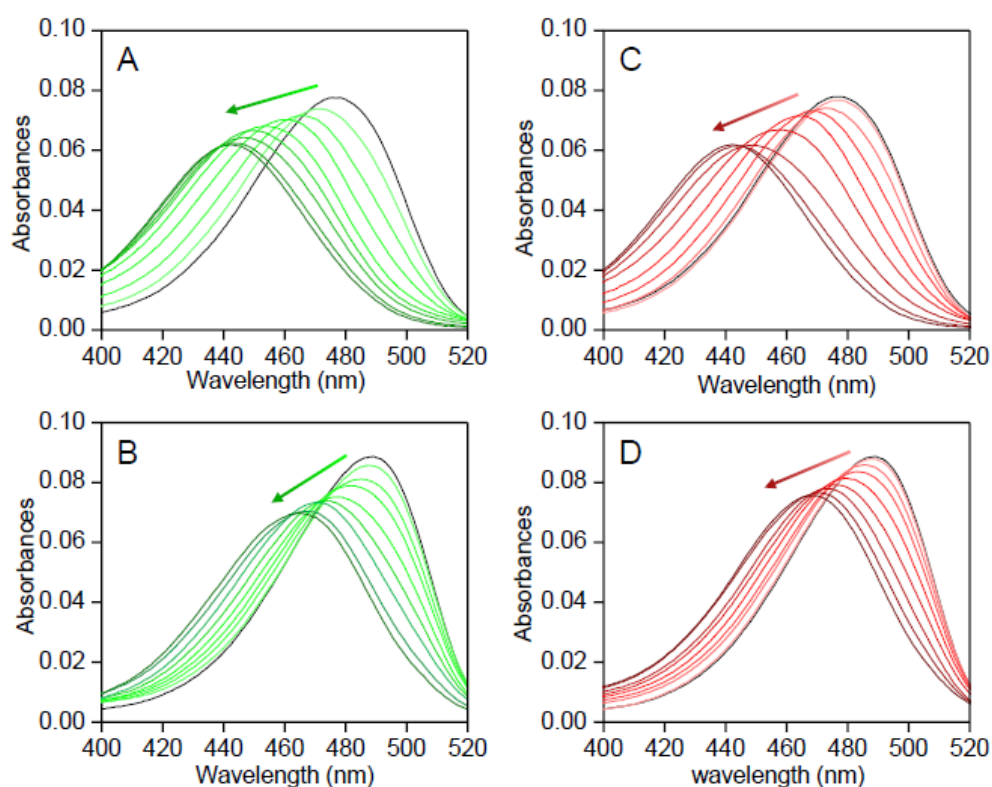
Fig. 10. UV-vis absorption spectra of AH (6 µM) in the presence of KOH (15 µM) under various amount of (A,B) methanol% or (C,D) ethanol% (v/v) in (A,C) MeCN or (B,D) DMSO medium (methanol% at 25°C: 1.0, 3.0, 6.0, 9.0, 12.0, 15.0, 18.0, 23.0; ethanol%: 1.0, 2.0, 5.0, 8.0, 12.0, 16.0, 20.0, 25.0). (A-D) The gradual spectral blue shift with increasing alcohol% is depicted by arrow. The spectra in the absence of alcohol are shown in black.
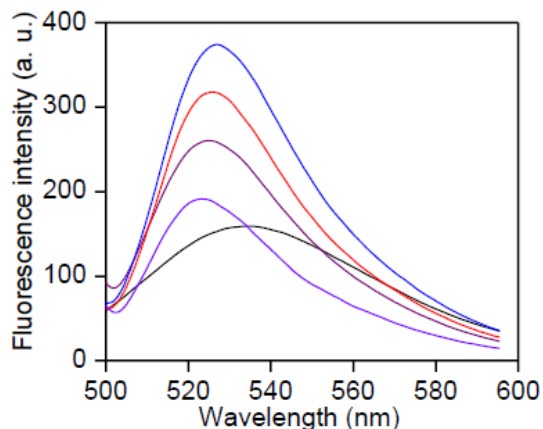
Fig. 11. Fluorescence emission spectra of AH (0.5 μM) in the presence of KOH (10 μM) in various aprotic solvents at 25°C: black, water; violet, acetone; purple, MeCN; red, DMF; blue, DMSO. Excitation wavelengths: 440 nm for water and 485 nm for aprotic solvents.

The excitation spectra of deprotonated A⁻ for the emission at 525 nm showed an intensity at 470–490 nm for different aprotic solvents, whereas in the water medium the peak shifted to ~440 nm (Fig. 12), which is consistent with the observed absorption wavelength shift by changing an aprotic to water medium (Fig. 7 and Fig. 4).
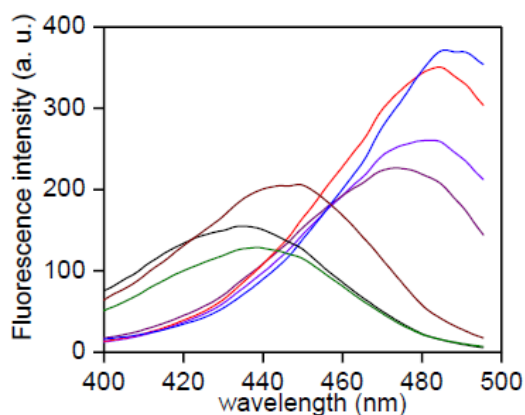
Fig. 12. Fluorescence excitation spectra of AH (0.5 μM) in the presence of KOH (10 μM) in various solvents at 25°C: black, water; green, methanol; brown, ethanol; violet, acetone; purple, MeCN; red, DMF; blue, DMSO. Emission wavelength was 525 nm.

Similar to the absorption studies, the fluorescence excitation band gradually blue-shifted up to ~445–450 nm by a gradual increase in water% up to 6–12% (v/v) in different aprotic solvents (Fig. 7 and Fig. 13).
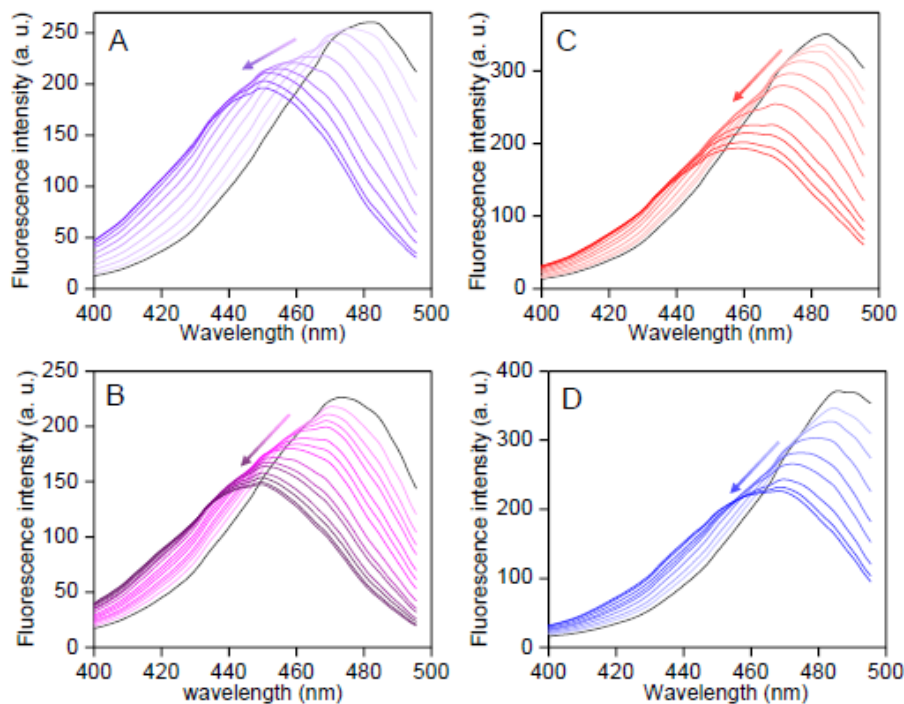
Fig. **13.**

Fluorescence excitation spectra of AH (0.5 µM) in the presence of KOH (10 µM) under various water% (v/v) in different solvent system: (A) acetone (water%: 0.1, 0.3, 0.6, 1.1, 1.8, 3.0, 4.5, 8.0 and 11.5); (B) MeCN (water%: 0.1, 0.2, 0.3, 0.4, 0.6 0.8, 1.0, 1.5, 2.0, 2.5, 3.0, 4.0, 4.7 and 5.5); (C) DMF (water%: 0.2, 0.4, 0.8, 1.5, 2.5, 4.0, 6.5, 8.0, 10.0 and 12.0) and (D) DMSO (water%: 0.5, 1.0, 2.0, 3.5, 5.0, 7.5, 10.0 and 11.4). (A-D) The spectra in the absence of water are shown in black. The gradual blue shift for the excitation intensity with increasing water% are depicted by arrows. Emission wavelength was 525 nm.

These results corresponded well with that interpreted from the absorption studies for the formation of the H-bond in the A^-/H_2O complex (Fig. 5). However, no emission wavelength shift under a particular water% value in the aprotic media was detected by the change in the excitation wavelength from 440 to 485 nm (Fig. 14). The result indicates that the emissive properties are similar between free A^- and A^-/H_2O H-bonded complexes.

81
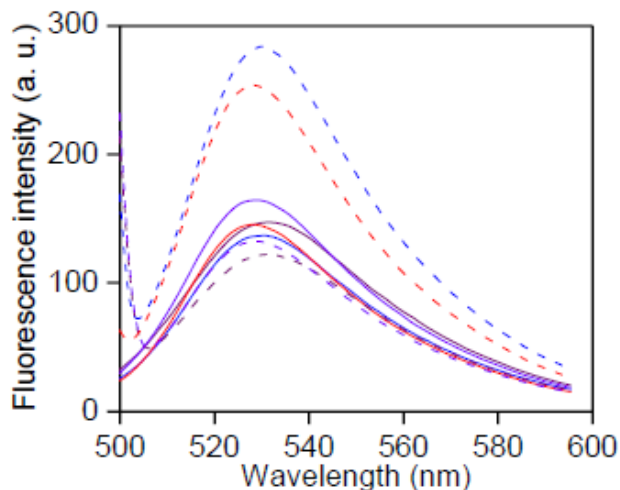
Fig. 14. Excitation wavelength dependent fluorescence emission spectra of AH (0.5 µM) in the presence of KOH (10 µM) and various water% (v/v) in different aprotic solvents at 25°C: (violet) 1.1% water in acetone; (purple) 1.0% water in MeCN; (red) 1.5% water in DMF and (blue) 3.5% water in DMSO. Excitation wavelengths were 440 nm (solid lines) and 485 nm (broken lines).

Different water%-dependent fluorescence transient decays for A^- in the aprotic solvents were monitored at 530 nm for excitations at ~450 nm and ~490 nm. For either excitation, a mono-exponential decay with unchanged fluorescence lifetime (τ) values was noticed at each water% value (Fig 15), where the t value was found to increase gradually with the increase in water% from 0 up to 8%; from ~3.3 to 5.7 ns for acetone, ~3.8 to 5.7 ns for MeCN, ~3.8 to 5.9 ns for DMF and 4.1 to 5.9 ns for DMSO (Table 1). The similar τ value between two different excitations (450 and 490 nm) especially when the A^-/H_2O complex and free A^- coexist at the water% value below 4% strongly justify our proposition that the emission of the A^-/H_2O complex originated from the excited state of free A^- after breaking of the H-bond in the excited state (Fig. 16 and Fig. 15). However, an expected stronger electrostatic interaction of A^- with the water molecule than any of those aprotic solvent molecules may increase the local water concentration surrounded to A^- largely than remaining of the solution even for a small increase of water% in the solution. Presumably, the higher water accumulation around A^- may affect greater solvation induced its higher excited state stability to observe the gradual increase in the τ value with the increase in the water% value. Moreover, the τ value for the A^- species in a pure aqueous medium is ~4.7 ns which is significantly lower than that observed in various aprotic solvents containing 8% water (~5.9 ns) probably due to a significant decrease in non-radiative decay rate from the aprotic solvents to water (Fig. 15 and Table 1).
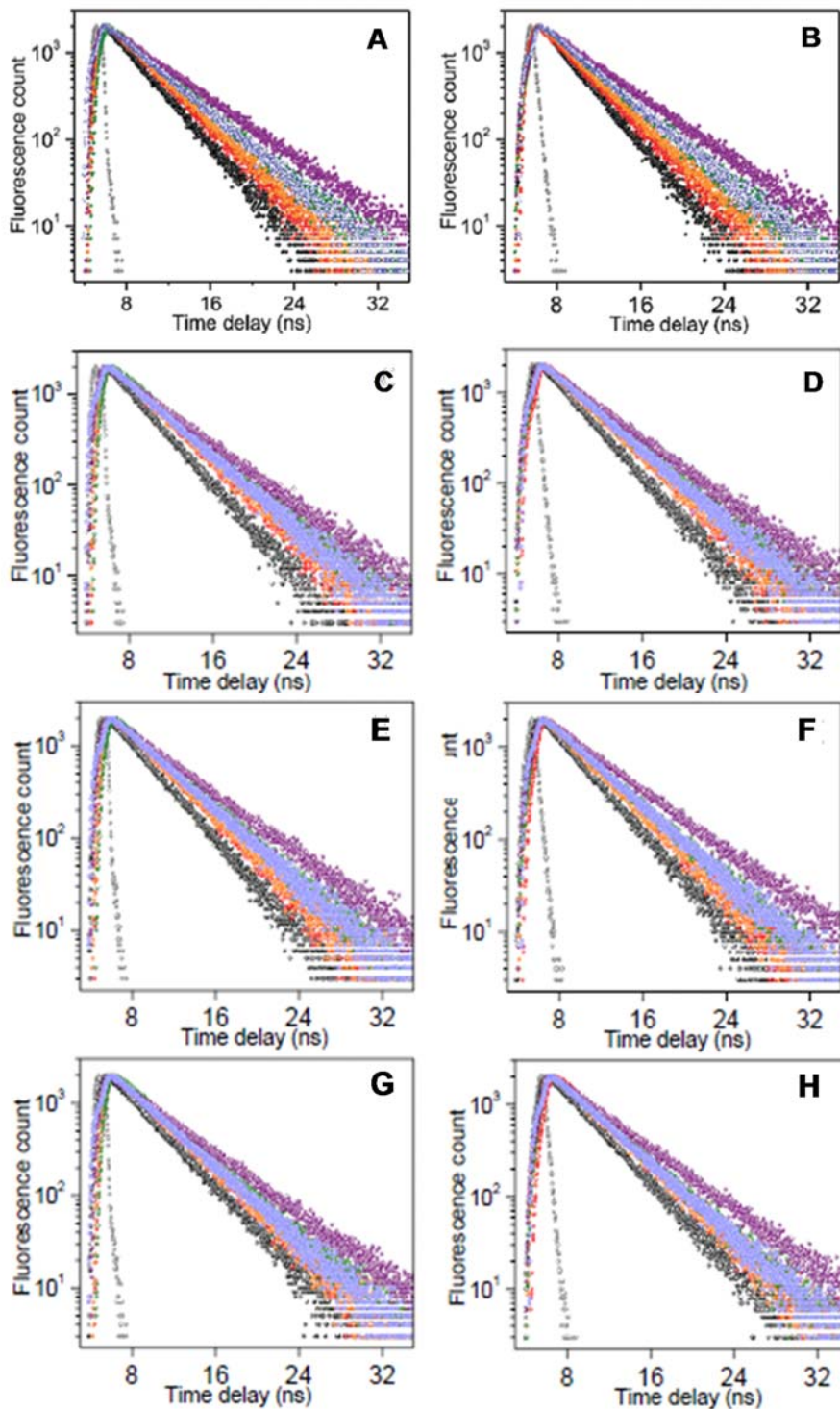
Fig. 15. Excitation wavelength dependent relative fluorescence transients of AH (6 µM) in the presence of KOH (15 µM) in various solvents under various water% (v/v): in (AB) acetone (red, 1.0%; orange, 2%; green, 4%; purple, 8%). (C,D) MeCN (red, 1.0; orange, 2.0; green, 4.0; purple, 8.0), (E,F) DMF (red, 1.5%; orange, 3.0%; green, 7.0%; purple, 13%), (G,H) DMSO (red, 1.5%;

orange, 3.0%; green, 7.0%; purple, 13%). Excitation wavelengths were (A- G) 450 nm and (B-H) 490 nm. The fluorescence transient in absence of water and pure water medium were illustrated in black and blue, respectively, for contrast. The fluorescence obtained at 525 nm. The scattering profile was revealed in grey.

Table 1. Emission lifetime values of A⁻ in various polar aprotic solvents having different water% (v/v)[a]

Solvent	Lifetime (τ/ns) Water% (v/v)				
	0.0	1.0	2.0	4.0	8.0
Acetone	3.34 (3.34)	4.03 (4.03)	4.22 (4.22)	4.77 (4.77)	5.71 (5.71)
MeCN	3.83 (3.83)	4.38 (4.38)	4.54 (4.54)	4.97 (4.97)	5.75 (5.75)
DMF	3.85 (3.85)	4.39 (4.39)	4.47 (4.77)	4.87 (4.87)	5.87 (5.87)
DMSO	4.09 (4.09)	4.57 (4.57)	4.60 (4.60)	4.86 (4.86)	5.87 (5.87)
Water[b]	4.75 (4.75)	—	—	—	—

[a] The emission obtained at 525 nm for the excitations at 450 nm and 490 nm. The τ values in brackets were for the excitation at 490 nm.
[b] τ values in pure water solvent.

Fig. 16.

Excitation wavelength-dependent fluorescence emission spectra of AH (0.5 μM) in the presence of KOH (10 μM) and various water% (v/v) values in different solvents: (A and E) acetone (water%: 0.1, 0.3, 0.6, 1.1, 1.8, 3.0, 4.5, 8.0 and 11.5); (B and F) MeCN (water%: 0.1, 0.2, 0.3, 0.4, 0.6 0.8, 1.0, 1.5, 2.0, 2.5, 3.0, 4.0, 4.7 and 5.5); (C and G) DMF (water%: 0.2, 0.4, 0.8, 1.5, 2.5, 4.0, 6.5, 8.0, 10.0 and 12.0); (D and H) DMSO (water%: 0.5, 1.0, 2.0, 3.5, 5.0, 7.5, 10.0 and 11.4). The spectra in the absence of water are depicted in black. The gradual increase or decrease in intensities with the increase in water% values is indicated by arrows. Excitation wavelengths were 440 nm (A–D) and 485 nm (E–H).

4.2.3. Theoretical studies for H-bonding interaction in A⁻/H₂O

85

To identify the probable H-bonding mode in the A⁻/H₂O complex, DFT-based theoretical calculations were performed considering the most probable H-bonding interaction between phenolate-O and one hydrogen atom of water molecules (Fig. 5 and Fig. 17A). The ground-state structures in the gas phase for free A⁻ and A⁻/H₂O complex were optimized using the B3LYP 6-31G++(3d,3p) basis set (Fig. 17A).
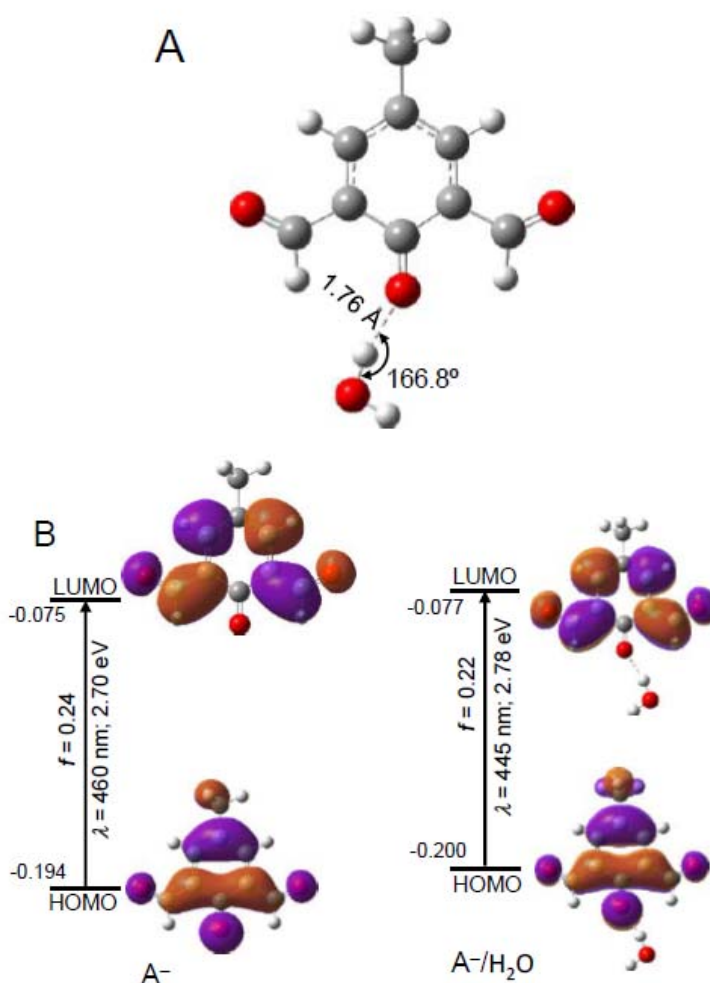
Fig. 17. (A) DFT-optimized structure of A⁻/H₂O H-bonded complex. The H-bond and its respective angles were revealed in single broken line and curved lines, respectively; color index: C, gray; O, red and H, white. (B) Frontier molecular orbital profiles (HOMO/LUMO) including different UV-vis absorption parameters of A⁻ (left panel) and A⁻/H₂O complex (right panel) based on TD-DFT (B3LYP/6-31G++ (3d,3p)) calculations.

To correlate the experimental UV-vis absorption parameters, TD-DFT calculations (B3LYP, 6-31G++(3d,3p) basis function) on the optimized ground-state geometries were performed in the solution phase considering the CPCM solvent model for acetone, MeCN and DMSO, and

the calculated values of various absorption parameters are depicted in Table 2 and Fig. 17B). The electric charge densities in HOMO/LUMO both for A⁻ and A⁻/H₂O are centered within the diformyl-phenolate unit (Fig. 17B). The excitation wavelengths for A⁻ species in different aprotic solvents (acetone, DMF and DMSO) were computed to be ~455– 460 nm due to the HOMO (43) to LUMO (44) electronic transition (Table 2). However, the A⁻/H₂O H-bonded complex exhibited the absorption intensity at ~443-445 nm for HOMO (48) to LUMO (49) transition (Table 2). Although the energy of LUMO is comparable between A⁻ (-0.075 eV) and A⁻/H₂O (-0.077 eV), a considerable decrease in the HOMO energy by 0.006 eV for A⁻ upon its H-bond interaction with water causes for the spectral blue-shift (Fig. 17B). The calculated spectral blue-shift from free A⁻ species to its water-complex well corresponded with the water-induced experimental blue-shift of the UV-vis absorption (or fluorescence excitation) band of the A⁻ species in the aprotic solvents (Table 2). In addition, the experimental UV-vis molar extinction coefficient (ε) values also well matched with those values calculated theoretically (Table 2). The results justify the proposed H-bonding mode of the water molecule with A⁻.

Table 2. Solvent based experimental (exp.) along with TD-DFT calculated (cal.) wavelengths of UV-vis absorption band (λ_{max}) as well as molar extinction coefficients (ε) for the deprotonated form of AH (A⁻) along its H-bonded complex with water (A⁻/H₂O)[a]

	Absorbance parameters							
	A⁻				A⁻/H₂O			
	λ_{max} (nm)		$\varepsilon \times 10^4$ (M⁻¹ cm⁻¹)		λ_{max} (nm)		$\varepsilon \times 10^4$ (M⁻¹ cm⁻¹)	
Solvent	Exp.	Cal.	Exp.	Cal.	Exp.	Cal.	Exp.	Cal.
Acetone	477	458	1.32	0.91	450	444	1.19	0.80
MeCN	478	457	1.34	0.91	445	443	1.06	0.80
DMF	485	—	1.39	—	457	—	1.16	—
DMSO	489	460	1.50	0.95	463	445	1.21	0.90
Water	—	—	—	—	443	443	1.20	0.87

[a]**Experimental UV-vis parameters for A⁻ (in absence of water) and A⁻/H₂O (in presence of maximun water% value) acquired according to Fig. 7.**

4.2.4. Detection of water in polar aprotic solvents

Water-induced fluorescence response for A⁻ remained similar on the nature of base (KOH or TEA) used in the polar aprotic solvents (Fig. 18). Thus, the addition of base attributes no other role except for the deprotonation of the phenolic-OH moiety in AH.
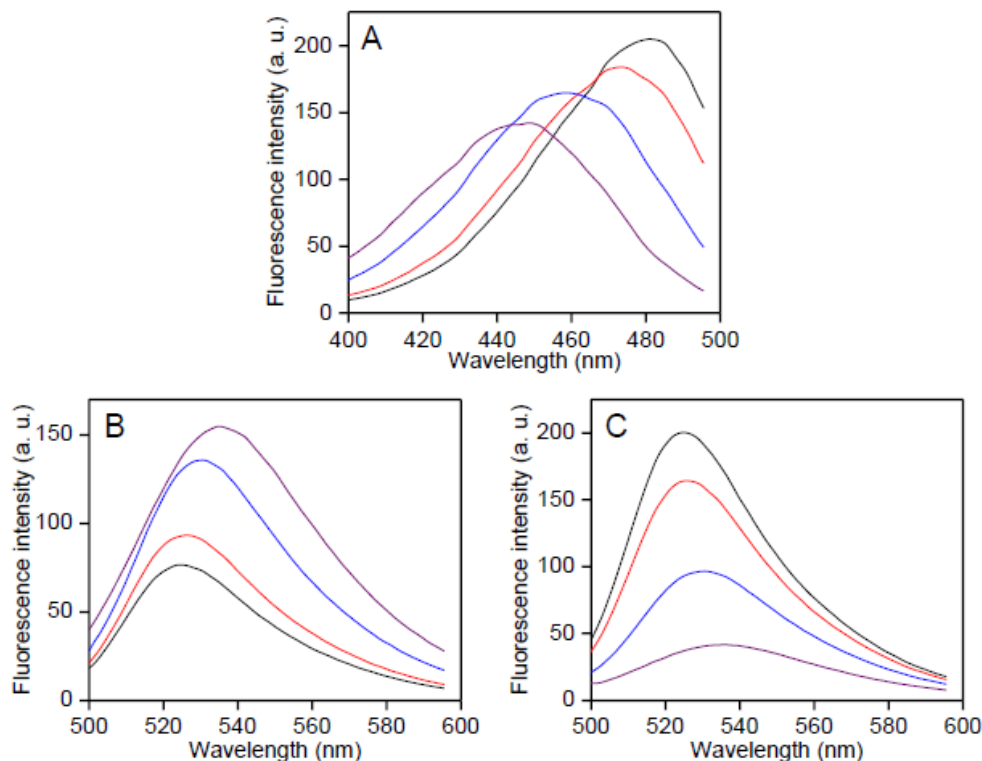
Fig. 18. Fluorescence (A) excitation spectra as well as (B,C) excitation wavelength based (B: 440 nm and C: 485 nm) emission spectra of AH (0.5 μM) containing TEA (1 mM) under different water% (v/v) in MeCN solvent: water%: red, 0.3; blue, 1.0 and purple, 6.0. The spectra in absence of water were shown in black. (A)The emission wavelength was 525 nm.

The conversion from free A^- to H-bonded A^-/H_2O species by the addition of water attributes the blue shifting of the fluorescence excitation (or UV-vis absorption) band from ~485 to 440 nm for the fluorescence emission at 525 nm (Fig. 13), where the excitation band intensity at ~485 and ~440 nm were assigned to the ground-state free A^- and A^-/H_2O species, respectively. In contrast, their emissive properties, e.g., its intensity-wavelength (~530 nm) and lifetime values for different excitation wavelengths at 440 and 485 nm are observed to be identical due to the excited-state H-bond dissociation, as discussed before (Fig. 14, 15 and Table 2). Consequently, with the increase in water% in the solution (up to 6–12% (v/v)), the more amount of free A^- to A^-/H_2O conversion in the ground state resulted in a gradual increase in the emission intensity at ~530 nm for a fixed wavelength excitation of the A^-/H_2O species at 440 nm (Fig. 16A–D), whereas the emission intensity was found to decrease gradually during the excitation of reduced amount of free A^- species with the 485 nm light (Fig. 4E–H). It is noteworthy to mention here that the base induced formation of de deprotonated A^- species is

not possible in relatively nonpolar aprotic solvents (THF) (Fig. 6); thus, the operable solvent condition for the detection of moisture should be polar aprotic in nature.

The effect of water-induced changes in the equilibrium concentration of the free A^- and A^-/H_2O complex on emission intensity changes for the two separate excitation (440 and 485 nm) can be combined together by including the effect of both the intensity changes in a single spectrum (Fig. 16 and 19A–D (right spectra)). For each water% value, the emission spectrum for excitation at 440 nm was divided by the maximum intensity value in the absence of water, and the resulting spectrum (F $_{(\lambda)}$/F$_0$ (λ_{ex} = 440 nm)) was further divided by the extent of emission intensity decrease factor with respect to the zero water condition for excitation at 485 nm (F$_{max}$/F$_0$ (λex = 485 nm)) to obtain the normalized emission spectrum ((F$_{(\lambda)}$/F$_0$)/(F$_{max}$/F$_0$)) (Fig. 19A–D (right spectra)). Such normalization procedure not only is helpful to manifest the water-induced emission response and its detection sensitivity, but also causes the water%-dependent linear emission response (Fig. 19E–H). In addition, such normalization procedure eliminates the AH concentration dependency during the ratiometric detection of water in the solution with heterogeneous distribution of probe molecules (Fig. 19). The maximum normalized intensity value at ~530 nm increased more than 5.5- and 5.7-fold in the presence of 6.0% and 7.5% water in acetone and MeCN, respectively (Fig. 19E and F However, the extent of increased intensities, maximally up to ~3.5-fold for acetone and 3.3-fold for MeCN, in the presence of various amounts of added water% up to 2% (v/v), maintains a very well behaved linear correlation with a residual of fitting R^2 ~ 0.995–0.997 and slope ~1.24 volume%$^{-1}$ (acetone) or 1.20 volume%$^{-1}$ (acetonitrile) (Fig. 19E and F). In comparison, the water%-dependent normalized emission intensity increase was found to be relatively less for the other aprotic solvents (DMF and DMSO) (Fig. 19G and H); maximum up to ~4.3- fold for DMF and 3.8-fold for DMSO. Nevertheless, the linear intensity increasing region expanded up to much higher water% value; ~6% for DMF and ~12% for DMSO medium (R^2 ~ 0.995 and slope 0.34 volume%$^{-1}$ (DMF) or 0.21 volume%$^{-1}$ (DMSO)) than that observed for acetone or MeCN solvent (Fig. 19G and H).

The water amount-dependent linear emission intensity changes can be highly useful for the ratiometric detection of unknown water% in the aprotic solvents. Based on the water induced minimum extent of detectable unambiguous fluorescence response, the limit of detection (LOD) was evaluated using the eqn. LOD = 3σ/k, where σ and k represent the standard deviation for the emission measurements and the slope value of the linear fitting curve, respectively (Fig. 19E–H).
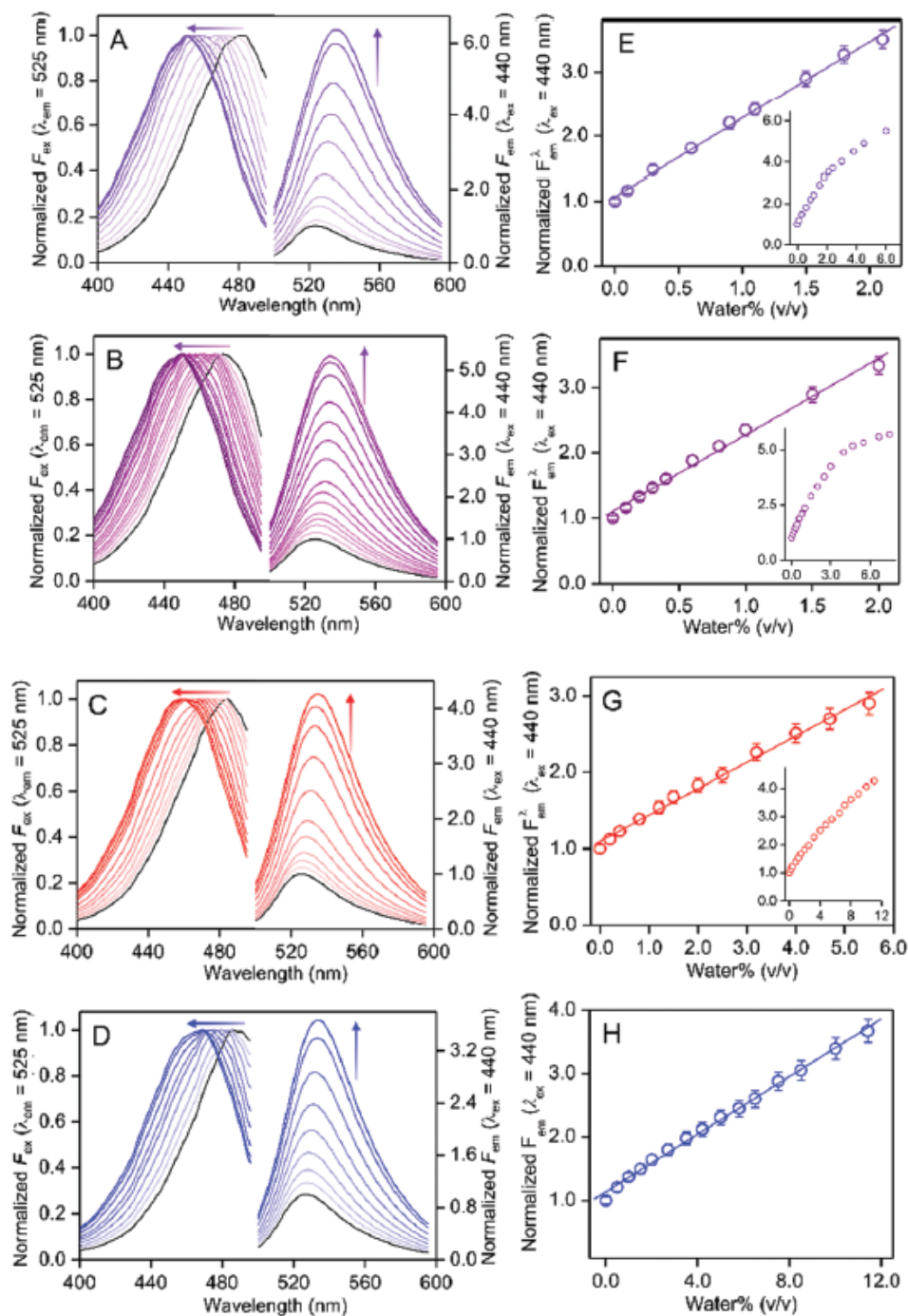
Fig. 19 (A–D) Normalized fluorescence excitation (left part) as well as emission (right part) spectra of AH (0.5 µM) in presence of KOH (10 µM) also different water% (v/v) values in various solvents: (A) acetone (water%: 0.1, 0.3, 0.6, 1.1, 1.8, 3.0, 4.5, 8.0 and 11.5); (B) MeCN (water%: 0.1, 0.2, 0.3, 0.4, 0.6 0.8, 1.0, 1.5, 2.0, 2.5, 3.0, 4.0, 4.7 and 5.5); (C) DMF (water%: 0.2, 0.4, 0.8, 1.5, 2.5, 4.0, 6.5, 8.0, 10.0 and 12.0) and (D) DMSO (water%: 0.5, 1.0, 2.0, 3.5, 5.0, 7.5, 10.0 and 11.4). The spectra in absence of water were illustrated in black. (E–H) The normalized intensities were plotted against water% (v/v) as well as fitted linearly up to definite water% range: (E) acetone; (F) MeCN; (G) DMF and (H) DMSO. The variations for other higher water% were shown in inset of E–G. (A–D) every fluorescence excitation spectrum for the emission at 525 nm was normalized by its maximum intensity value. For normalization of emission spectra, every emission spectrum for excitation at 440 nm was divided by the maximum intensity value in absence of water. Further the resulting spectrum was divided by the extent of emission intensity reducing factor with respect to zero water condition for excitation at 485 nm. The steady blue shift in the excitation spectra or the enhancements in the emission intensity with the increasing water% were illustrated in arrows.

The LOD values for the detection of water% were evaluated to be ~0.01% for acetone and MeCN, whereas it was ~0.04% (v/v) for DMF and DMSO. To check the reversibility in the water detection, fluorescence studies for AH (0.5 µM) in the presence of KOH (10 µM) were performed at a certain water% value (1.8% for acetone; 1.5% for MeCN; 2.5% for DMF and 3.5% for DMSO), and followed by the addition of a specific amount of the same
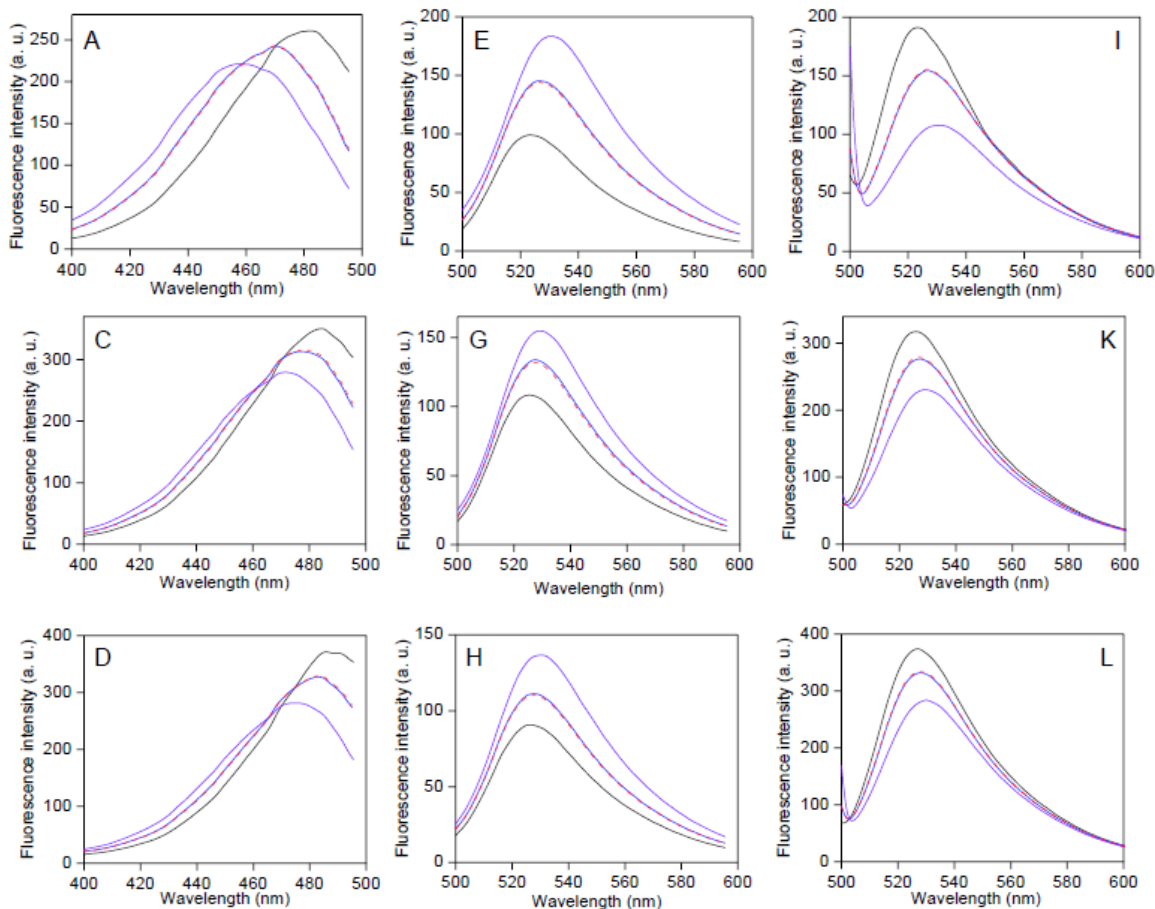
Fig. 20. Fluorescence (A-D) excitation as well as (E-L) excitation wavelength based emission spectra (E-H: 440 nm; I-L: 485 nm) of AH (0.5 μM) in presence of KOH (10 μM) along different water% (v/v) in different solvent mediums: (A,E,I) acetone; (B,F,J) MeCN; (C,G,K) DMF; (D,H,L) DMSO. The spectra in presence of 1.8%, 1.5%, 2.5% and 3.5% water for acetone, MeCN, DMF and DMSO, respectively, (violet), followed by adding up respective similar solvents having identical probe concentration to alters the water concentrations 0.6%, 0.6%, 0.8% and 1.0% respectively (broken red) were illustrated. The spectra in the presence of 0.6%, 0.6%, 0.8% and 1.0% for acetone, MeCN, DMF and DMSO, respectively, were displayed in blue. The spectra in absence of water were shown in black for contrast.

solvent without water but containing identical probe concentrations to reach a certain value of water% below that of the respective initial value (0.6% for acetone and MeCN; 0.8% for DMF and 1.0% for DMSO). Fluorescence excitation and emission spectra of final water-diluted solutions were found to be nicely matched with the corresponding known spectra at an identical water% value (Fig. 20), showing that the water association with A⁻ is reversible in nature. In addition to the emission intensity changes, the wavelength shift of fluorescence excitation or UV-vis absorption band may also be beneficial for the detection of water%. About ~25 nm blue shift for the addition of ~2% water in acetone and MeCN or ~15 and 20 nm blue-shift for the addition of ~5% water for DMF and DMSO, respectively, was detected (Fig. 21). The extent of blue-shift in the absorption or excitation spectra was plotted against the water% value in different aprotic media (Fig. 6), and the data points were fitted with a single exponential curve. The phenomenon of such a large wavelength shift induced by the presence of a relatively low water amount (<2% (v/v) for acetone and acetonitrile; <4% for DMF and DMSO) can be exploited for the detection of lower water amounts (Fig. 21).
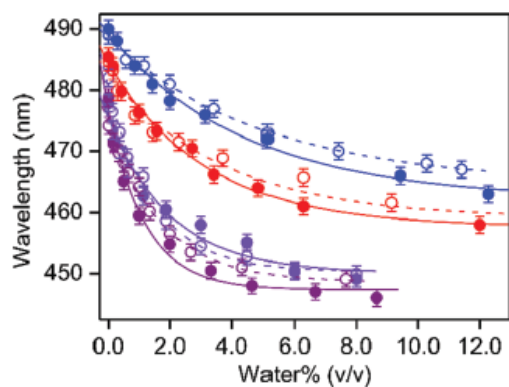
Fig. 21. Water% (v/v) based shift in the fluorescence excitation wavelength (hollow circles, broken lines) for the emission at 525 nm and UV-vis absorption wavelength (solid circles, solid lines) for AH in presence of KOH in various solvents was plotted: violet, acetone; purple, MeCN; red, DMF; blue, DMSO. The data points were fitted in single exponential curves.

4.2.5. Real-time moisture analysis in polar aprotic solvents

Polar aprotic organic solvents exhibit high moisture affinity, and thus, require special arrangement to preserve them under the moisture-free condition for prolonged period of time. It has been reported that a considerable extent of moisture incorporation in the solvents may happen even for their short-time exposure in an open atmosphere.[19,21] Using the present water detection protocol, the real-time atmospheric moisture incorporations in the aprotic solvents under the open laboratory atmospheric condition were monitored.

The amount of moisture incorporations is highly dependent on the relative atmospheric humidity and temperature. As described in detail in the experimental section, all the solvents were dried meticulously and stored in a closed glass container in a nitrogen atmosphere with 3 Å molecular sieves up to not more than 12 hours. No moisture incorporation during the solvent preservation was confirmed from the unchanged emission response for A⁻ (Fig. 22).
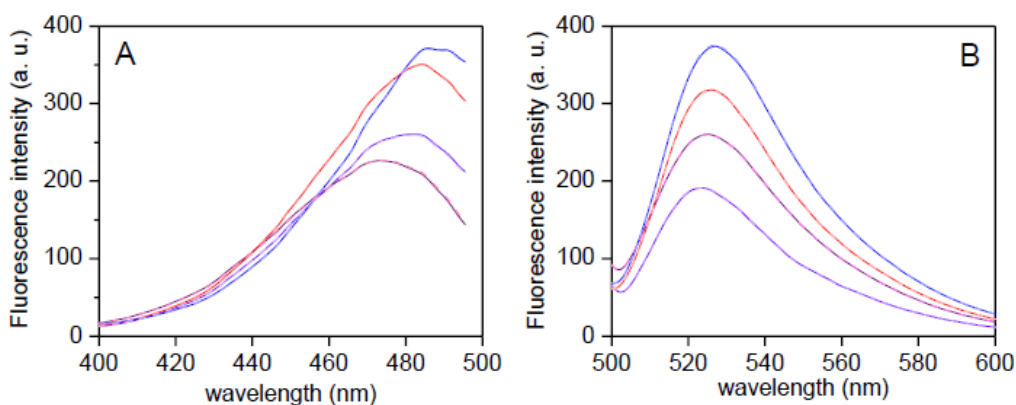
Fig. 22. Fluorescence (A) excitation and (B) emission spectra of AH (0.5 μM) in presence of KOH (10 μM) in various solvents before (solid lines) and after (broken and corresponding light colour lines) incubation under dry nitrogen in presence of 3Å molecular sieves for 12 hour: violet, acetone; purple, MeCN; red, DMF; blue, DMSO. Excitation as well as emission spectra were recorded towards the fixed emission wavelength at 525 nm (A) as well as excitation wavelength at 485 nm (B), respectively.

We exposed each dried solvent (~40 mL) containing A⁻ (AH (0.5 μM) + KOH (10 μM)) in a 100 mL beaker with a diameter of ~5 cm for different time intervals up to 2 hours in the open laboratory atmosphere with 75% (±5%) relative humidity at 25°C (± 1°C). The amount of moisture incorporation was estimated by evaluating the normalized excitation and emission spectra determined from the time-dependent emission spectra of A⁻ upon excitation at 440 nm and 485 nm, as described in the previous section (Fig. 23). The normalized emission intensity at its intensity maxima at 525–530 nm increased gradually with the increase in exposure time

intervals up to 120 min, where the extent of intensity increase depends on the specific solvent system; 1.91-fold for acetone and 1.95-fold for MeCN, 1.40-fold for DMF and 1.37-fold for DMSO for 120 min exposure (Fig. 23).
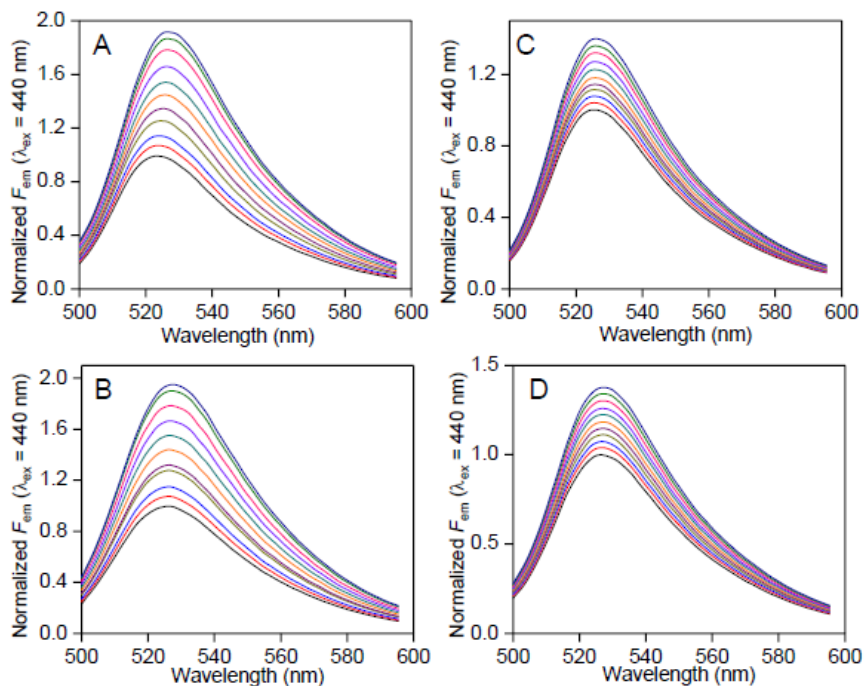
Fig. 23. Normalized fluorescence emission spectra of AH (0.5 µM) in presence of KOH (10 µM) in various aprotic solvents after open atmosphere exposure in 75% (±5%) relative humidity at 25°C (±1°C): (A) acetone; (B) MeCN; (C) DMF and (D) DMSO. (A-D) The solvent were exposed towards various time gaps (in min): (red) 12; (blue) 24; (dark yellow) 36; (purple) 48; (orange) 60; (dark cyan) 72; (violet) 84; (pink) 96; (green) 108 and (dark blue) 120. The spectra without exposure were shown in black. For normalization of emission spectra, every emission spectrum for excitation at 440 nm was divided by maximum intensity value in absence of water, the resulting spectrum was then divided by extent of emission intensity decrease factor with respect to zero water condition for excitation at 485 nm.

The gradual increase in the normalized emission intensity with the time period of atmospheric exposure suggests a greater extent of atmospheric moisture incorporation (Fig. 24A). In addition, the gradual blue-shift in the excitation spectra (from ~474 to 467 nm for acetone; ~482 to 472 nm for MeCN; ~485 to 477 nm for DMF and ~489 to 484 nm for DMSO) with the increase in exposure time intervals also indicates an increase in the moisture content in solvents (Fig. 24B).

94
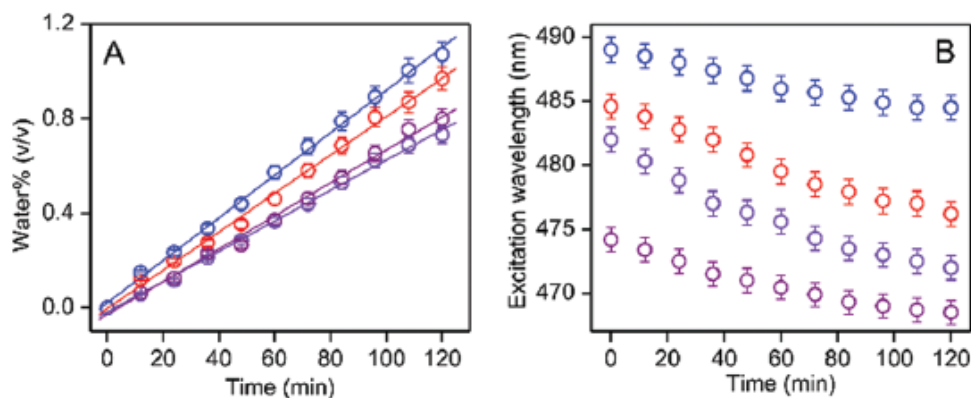
Fig. 24 (A) Plots of water% (v/v) incorporation and (B) wavelength of fluorescence excitation band for the emission at 525 nm in different aprotic solvents over time upon exposure under open laboratory atmosphere at 25°C (±1°C) and 75% (±5%) relative humidity condition: violet, acetone; purple, MeCN; red, DMF; blue, DMSO.

However, the precise amount of atmospheric moisture incorporation for each solvent system was evaluated by correlating the time-dependent normalized emission intensities at 525– 530 nm, according to Fig. 19E–H. It is noteworthy to mention here that the effect of small volume changes, particularly for acetone and MeCN, upon exposure to the open atmosphere, on the relative changes of normalized emission intensities was also considered during the estimation of moisture incorporation from the normalized emission intensity value. With the increase in the exposure time from 12 to 120 min, the amount of moisture intake increased along with maintaining a fairly well linear correlation from ~0.05 to 0.73% (v/v) for acetone, ~0.06 to 0.80% for MeCN, ~0.11 to 0.97% for DMF and ~0.14 to 1.07% for DMSO (Fig. 24.A).

To justify the generality of the present methodology in terms of detection accuracy and applicability, we also performed similar atmospheric moisture incorporation studies in the presence of externally added water-spike of 1% before exposing each solvent to the open atmosphere (Fig. 25 and Table 3).
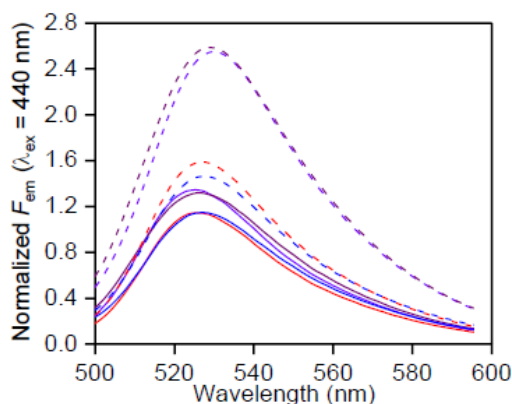
Fig. 25. Normalized fluorescence emission spectra of AH (0.5 µM) in presence of KOH (10 µM) in various aprotic solvents (violet, acetone; purple, MeCN; red, DMF; blue, DMSO) after open atmosphere exposure for 48 min (relative humidity 75% (±5%)) at 25°C (±1°C) (solid lines) without along (broken lines) with 1% (v/v) water spikes. For normalization of emission spectra, every emission spectrum for excitation at 440 nm was divided by the maximum intensity value in absence of water, the resulting spectrum was further divided by the extent of emission intensity decrease factor with respect to zero water condition for excitation at 485 nm.

Notably, the subtracted amount of water-spike from the total recovered water% obtained fluorometrically was found to well match with that evaluated under the condition of without water-spikes (Table 3). The results indicate the generality that various extents of contaminated water from different sources can be easily monitored by this method. Based on the atmospheric moisture incorporation capabilities for different aprotic solvents, the relative hygroscopicity scale can be drawn as DMSO > DMF > MeCN > acetone, which is consistent with the earlier reports.[19,21]

Table 3. Approximated water amount incorporated in different aprotic solvents for open atmosphere exposure in absence (A_0) as well as presence (A_T) of 1% water-spike

Solvent	Exposure time (min)^a	A_0 (v/v %)	A_T (v/v %)	$A_T - 1.0$ (v/v %)
Acetone	24	0.11	1.10	0.10
	48	0.28	1.23	0.23
	72	0.43	1.40	0.40
MeCN	24	0.13	1.13	0.13
	48	0.27	1.28	0.28
	72	0.46	1.46	0.46
DMF	24	0.20	1.22	0.22
	48	0.35	1.38	0.38
	72	0.58	1.60	0.60
DMSO	24	0.23	1.22	0.22
	48	0.44	1.41	0.41
	72	0.68	1.66	0.66

^{a}Exposure under relative humidity ~75%, temperature ~ 25°C

4.2.6. Moisture analysis in different food samples

The moisture content in various processed food items is one of the key parameter from legal and economic point of view.[13,51] There are ample possibility to differ the total moisture content from its recommended tolerant limit particularly in diary food items (butter, cheese and ghee (commonly popular in India and south Asian countries)) or coconut oil, obtained from high water content raw materials. Moreover, higher moisture content than its tolerant limit of ~0.3% in pure oil-based ghee and coconut oil are highly susceptible to undergo microbial degradation or water rancidification during their preservation for prolonged time period.[15–17,52–54]

Therefore, the quality control of the foods relies heavily on cost-effective convenient moisture detection methods.
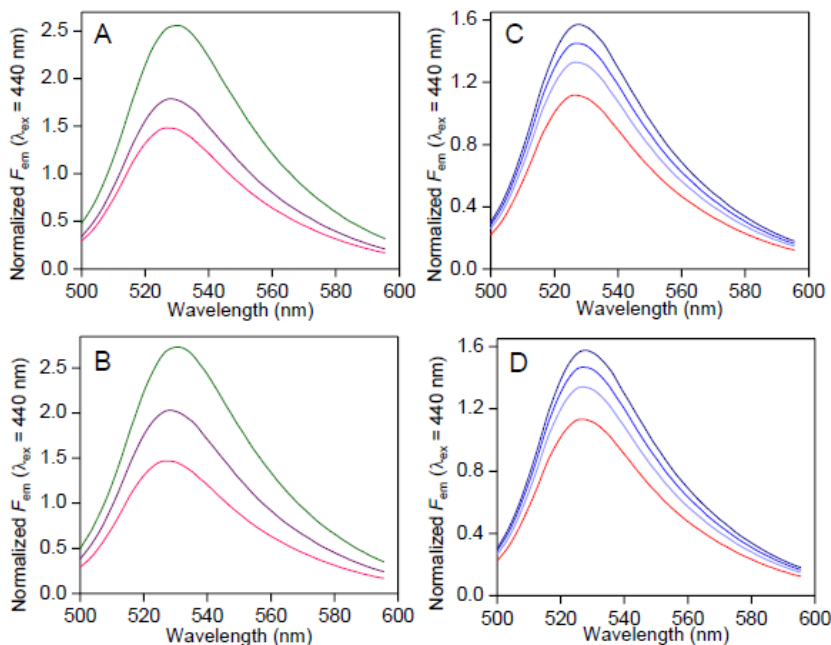
Fig. 26. Normalized fluorescence emission spectra of AH (0.5 µM) in presence of KOH (10 µM) in 100 mL DMSO containing different quantity of various food samples: (A) butter: (red) 10 gm, (purple) 20 gm and (green) 40 gm; (B) cheese: (red) 4 gm, (purple) 10 gm and (green) 20 gm; (C) ghee: 100 gm in absence (red) and presence of different externally added water spikes (light blue, 0.5%; blue, 1.0%; dark blue, 1.5% (v/v)); (D) coconut oil: 100 gm in the absence (red) and the presence of different external added water-spikes (light blue, 0.5%; blue, 1.0%; dark blue, 1.5% (v/v)). (A-D) The spectra were noted for the DMSO medium after separating it from the food sample solution. For the normalization of emission spectra, every emission spectrum for the excitation at 440 nm were divided by the maximum intensity value in absence of water and the resultant spectrum were further divided by the extent of emission intensity decreasing factor with respect to the zero water condition for excitation at 485 nm.

The total moisture contents in those food items (butter, cheese, ghee and coconut oil) available in the market were estimated using the present water detection protocol. For the chosen food samples, most of the food components either insoluble or sparingly soluble in the DMSO medium, and thus, the general solvent properties of DMSO are not expected to differ appreciably even in their presence in large excess, making DMSO a preferred solvent over the other aprotic solvents. In addition, the water-induced linear emission response spanning up to the large water-ratio value of ~12% (v/v) for DMSO is an additional advantage for its use as a suitable medium to detect widely different moisture contents in different food items varying

from the very low (ghee or coconut oil) to large value (butter or cheese). The moisture content of a food material is defined using the following equation:

$$\% \, Moisture = (m_w/m_{sample}) \times 100$$

Where, m_w and m_{sample} represent the mass of water and mass of the sample, respectively. The water% in various food samples was analysed by mixing different amounts of each food sample in 100 mL DMSO medium according to the protocol described in the Experimental section. The content of free water molecules in ghee or coconut oil is much lower than that in cheese or butter. Therefore, a lower amount of butter (10, 20 and 40 g) or cheese (4.0, 7.5 and 15 g) than ghee or coconut oil (100 g each) was mixed with the DMSO solvent for effective fluorescence studies to estimate the moisture content in those foodstuffs. Fluorescence spectra were recorded with the DMSO phase in the presence of AH (0.5 μM) and KOH (10 μM) (*cf.* chapter 2). The relative moisture amounts in different food samples obtained by evaluating the normalized fluorescence intensities are listed in Table 3 (Fig. 26). The moisture amounts were found to be ~15% for butter and ~48% for cheese irrespective of different quantities of each sample taken (butter sample: 10, 20 and 40 g; cheese sample: 4.0, 7.5 and 15.0 g) in 100 mL DMSO medium (Table 4). However, low moisture amounts of ~0.3% and 0.4% were estimated for ghee and coconut oil, respectively (Table 4 and Fig. 26 (C and D)).

Table 4 Estimated water percentages in commercial food samples

Sample	Amount[a] (g)	Water-spike[b] (%, v/v)	Total water[c] (%, w/w)	A_T–A_0[d] (%, w/w)
Butter	10.0	—	15.0 ± 0.2	—
	20.0	—	14.9 ± 0.2	—
	40.0	—	15.4 ± 0.2	—
Cheese	3.0	—	48.2 ± 0.3	—
	7.5	—	48.5 ± 0.3	—
	15.0	—	47.1 ± 0.3	—
Ghee	100	0	0.32 ± 0.04	—
		0.50	0.79 ± 0.04	0.47
		1.00	1.34 ± 0.06	1.02
		1.50	1.83 ± 0.06	1.51
Coconut oil	100	0	0.40 ± 0.04	—
		0.50	0.87 ± 0.05	0.47
		1.00	1.41 ± 0.06	1.01
		1.50	1.88 ± 0.06	1.48

ᵃ Mass taken in 100 mL of DMSO solvent.
ᵇ Volume% of water with respect to the DMSO volume.
ᶜ quantity of water with respect to 100 g of food sample.
ᵈ Subtracted value of estimated water% without water spiking from the total estimated water%.

As described earlier, higher moisture contamination in pure oil based commercial ghee or coconut oils make them susceptible to water rancidity. To validate our method with detecting higher water%, we introduced additional 0.5, 1.0 or 1.5% water-spike in the DMSO medium containing ghee or coconut oil sample (Fig. 26). The recovered moisture amount after subtracting the actual moisture present, i.e., 0.3–0.4% (estimated without water-spike) in the commercial sample, from the estimated total found water% were closely similar to the amount of respective amounts of water-spikes (Table 4). The results strongly indicate that the present moisture detection protocol can be applied to arrest the water rancidity by identifying the contamination of higher moisture% than its permissible limit for those essentially moisture-free food items with great accuracy.

4.3. Conclusions

We demonstrated a sensitive fluorometric method for the detection of trace moisture in various common aprotic solvents using a simple aldehydic phenol probe molecule. The phenolate form of the probe participates in the H-bonding interaction with water in the aprotic medium to exhibit a large blue-shift, from ~485 nm to 440 nm, in the absorption or fluorescence excitation spectra, although both H-bonded and free phenolate forms of probe show similar emission characteristics owing to the dissociation of the H-bond in the excited state. The water induced spectral blue-shift and subsequent emission intensity increase and decrease for excitation at 440 nm and 485 nm, respectively, and they were utilized for the detection of moisture. Both those emission intensities changes for two different excitations were combined in a single spectral profile to enhance the detection sensitivity eliminating the dependency of the probe concentration for the ratiometric detection of moisture even in complex heterogeneous samples. The atmospheric moisture incorporation kinetics was evaluated for various aprotic solvents. Moreover, we estimated the water amount in butter or cheese with a relatively high water content and edible coconut oil or ghee food samples with a low water content. We have also shown that the present water detection protocol is highly effective to check water rancidity in ghee and coconut oil during their manufacture from high-water content raw materials.

4.4. References

1. H. S. Jung, P. Verwilst, W. Y. Kim and J. S. Kim, *Chem. Soc.* Rev., 2016, **45**, 1242.

2. N. L. T. Padivitage, J. P. Smuts and D. W. Armstrong, Specification of drug substances and products: development and validation of analytical methods, Elsevier, Amsterdam, 2013.

3. T. Kodama, M. Takeuchi, N. Wakiyama and K. Terada, *Int. J. Pharm.*, 2014, **469**, 59.

4. W. E. Lee, Y. J. Jin, L. S. Park and G. Kwak, *Adv. Mater.*, 2012, **24**, 5604.

5. C. Pinheiro, J. C. Lima and A. J. Parola, *Sens. Actuators, B*, 2006, **114**, 978.

6. E. W. Abel, F. G. A. Stone and G. Wilkinson, Comprehensive Organometallic Chemistry II, Pergamon, Oxford, 1995.

7. H. W. Roesky, M. G. Walawalkar and R. Murugavel, *Acc. Chem. Res.*, 2001, **34**, 201.

8. S. Das, Y. Sarkar, S. Mukherjee, J. Bandyopadhyay, S. Samantab, P. P. Parui and A. Ray, *Sens. Actuators, B*, 2015, **209**, 545.

9. F. G. Golding, M. Giallorenzo, N. Moreno and V. Chang, *Sens. Actuators, A*, 1995, **47**, 337.

10. R. Liu, X. Xi and C. Liang, *Proc. SPIE-Int. Soc. Opt. Eng.*, 1991, **1572**, 399.

11. A. M. Araujo, L. M. Santos, M. Fortuny, R. L. F. V. Melo, R. C. C. Coutinho and A. F. Santos, *Energy Fuels*, 2008, **22**, 3450.

12. N. S. Foster, J. E. Amonette, T. Autrey and J. T. Ho, *Sens. Actuators, B*, 2001, **77**, 620.

13. J. M. deMan, J. W. Finley, W. J. Hurst and C. Y. Lee, *Principles of Food Chemistry, Food Science Text Series*, 2018, DOI: 10.1007/978-3-319-63607-8.

14. P. Kumar, R. Kaushik, A. Ghosh and D. A. Jose, *Anal. Chem.*, 2016, **88**, 11314.

15. K. Aysegul and J. Issa, *J. Dairy Technol.*, 2008, **61**, 300–306.

16. N. Suwarat and W. Tungjaroenchai, *Int. J. Biosci., Biochem. Bioinf.*, 2013, **3**, 332.

17. E. Lu¨ck and G. W. R. Lipinski, Foods, 3. Food Additives, Ullmann's Encyclopedia of Industrial Chemistry, 2002, Wiley- VCH, Weinheim, DOI: 10.1002/14356007.a11_561.

18. H. A. Frediani, *Anal. Chem.*, 1952, **24**, 1126.

19. B. Tan, P.Melius and P. Ziegler, *J. Chromatogr. Sci.*, 1982, **20**, 213.

20. J. M. Hogan, R. A. Engel and H. F. Stevenson, *Anal. Chem.*, 1970, **42**, 249.

21. Y. Hui and R. D. Webster, *Anal. Chem.*, 2011, **83**, 976.

22. H. S. Peng, X. H. Li, F. T. You, F. Teng and S. H. Huang, *Microchim. Acta*, 2013, **180**, 807.

23. P. P. Parui, Y. Sarakar, R. Majumder, S. Das, H. Yang, K. Yasuhara and S. Hirota, *Chem. Sci.*, 2019, **10**, 9140.

24. Y. Sarkar, R. Majumder, S. Das, A. Ray and P. P. Parui, *Langmuir*, 2018, **34**, 6271.

25. S. Roy, S. Das, R. Majumder, A. Ray and P. P. Parui, *RSC Adv.*, 2020, **10**, 23245.

26. A. P. de Silva, H. Q. N. Gunaratne, T. Gunnlaugsson, A. J. M. Huxley, C. P. McCoy, J. T. Rademacher and T. E. Rice, *Chem. Rev.*, 1997, **97**, 1515.

27. C. G. Niu, A. L. Guan, G. M. Zeng, Y. G. Liu and Z. W. Li, *Anal. Chim. Acta*, 2006, **577**, 264.

28. Y. Ooyama, M. Sumomogi, T. Nagano, K. Kushimoto, K. Komaguchi, I. Imae and Y. Harima, *Org. Biomol. Chem.*, 2011, **9**, 1314.

29. H. Mishra, V. Misra, M. S. Mehata, T. C. Pant and H. B. Tripathi, *J. Phys. Chem. A*, 2004, **108**, 2346.

30. W. Liu, Y. Wang, W. Jin, G. Shen and R. Yu, *Anal. Chim. Acta*, 1999, **383**, 299.

31. C. Pinheiro, J. C. Lima and A. J. Parola, *Sens. Actuators, B*, 2006, **114**, 978.

32. S. Cha, M. G. Choi, H. R. Jeon and S. K. Chang, *Sens. Actuators, B*, 2011, **157**, 14.

33. W. Chen, Z. Zhang, X. Li, H. Agren and J. Su, *RSC Adv.*, 2015, **5**, 12191.

34. D. W. Cho, New J. Chem., 2014, **38**, 2233.

35. M. Tanioka, S. Kamino, A. Muranaka, Y. Shirasaki, Y. Ooyama, M. Ueda, M. Uchiyama, S. Enomoto and D. Sawada, *Phys. Chem. Chem. Phys.*, 2017, **19**, 1209.

36. D. Yang, X. J. Cao, X. T. Wu, Z. X. Yang and B. X. Zhao, *Anal. Methods*, 2019, **11**, 3079.

37. D. Yang, X. T. Wu, X. J. Cao and B. X. Zhao, *Dyes Pigm.*, 2019, **170**, 1075582.

38. M. G. Choi, M. H. Kim, H. J. Kim, J. E. Park and S. K. Chang, *Bull. Korean Chem. Soc.*, 2007, **28**, 1818.

39. G. Men, G. Zhang, C. Liang, H. Liu, B. Yang, Y. Pan, Z. Wang and S. Jiang, *Analyst*, 2013, **138**, 2847.

40. W. Y. Kim, H. Shi, H. S. Jung, D. Cho, P. Verwilst, J. Y. Lee and J. S. Kim, *Chem. Commun.*, 2016, **52**, 8675.

41. S. A. Poteet and F. M. MacDonnell, *Dalton Trans.*, 2013, **42**, 13305.

42. L. Chen, J. W. Ye, H. P. Wang, M. Pan, S. Y. Yin, Z. W. Wei, L. Y. Zhang, K. Wu, Y. N. Fan and C. Y. Su, *Nat. Commun.*, 2017, **8**, 15985.

43. B. Li, W. Wang, Z. Hong, E. S. M. E. Sayed and D. Yuan, *Chem. Commun.*, 2019, **55**, 6926.

44. R. Kaushik, R. Sakla, N. Kumar, A. Ghosh, V. D. Ghule and D. A. Jose, *Sens. Actuators, B*, 2021, **328**, 129026.

45. T. I. Kim and Y. Kim, *Anal. Chem.*, 2017, **89**, 3768.

46. M. H. Lee, J. S. Kim and J. L. Sessler, *Chem. Soc. Rev.*, 2015, **44**, 4185.

47. S. Mitra, R. Das and S. Mukherjee, *J. Photochem. Photobiol., A*, 1994, **79**, 49.

48. A. Mandal and S. Mukherjee, *Chem. Phys. Lett.*, 2001, **343**, 265.

49. M. Mukhopadhyay, D. Banerjee and S. Mukherjee, *J. Phys. Chem. A*, 2006, **110**, 12743.

50. H. Shen, L. Zhang and A. Eisenberg, *J. Am. Chem. Soc.*, 1999, **121**, 2728.

51. S. K. Lee, S. Anema and H. Klostermeyer, *Int. J. Food Sci. Technol.*, 2004, **39**, 763.

52. R. L. Bradley, *J. AOAC Int.*, 2001, **84**, 569.

53. M. L. Serunjogi, R. K. Abrahamsen and J. Narvhus, *Int. Dairy J.*, 1998, **8**, 677.

54. A. Kirazci and I. Javidipour, *Int. J. Dairy Technol.*, 2008, **61**, 300.

Chapter 5

Fluorometric detection of trace methanol in ethanol and isopropanol for application in alcoholic beverages and hand sanitizers

5.1. Introduction

Worldwide, hundreds of economically constrained people are dying every year because of consumption of methanol (MeOH) contaminated illicit liquors.[1–3] In the countryside, use of crude fermentation methods and improper distillation are the main culprits for the MeOH contamination in ethanol (EtOH). In some cases, unavoidable MeOH formation during standard fermentation processes is also a major concern.[4] Consumption of MeOH beyond a certain permissible limit (1−2 mL per kg body mass) directly affects the central nervous system, by inhibiting the activity of cytochrome c oxidase, causing hypoxia, acidosis or even a painful death.[5–9] Even a minute amount of MeOH ingestion, approximately 10 mL of dietary intake, is potent enough to cause some adverse effects.[10-11] The use of much less expensive MeOH is a very common illegal practice used to alter the EtOH strength in alcoholic beverages to give a higher profit. Nevertheless, in recent times during the COVID-19 pandemic, a large number of poisonous MeOH containing hand sanitizers were seized worldwide, even after repeated warnings from the FDA.[12] Because the use of costly EtOH and isopropanol (^{i}PrOH) based hand sanitizers has significantly increased to help combat the COVID-19 pandemic, indiscriminate commercial production inevitably increases the chance of using MeOH containing cheaper hand sanitizers.[12]

The MeOH, EtOH and ^{i}PrOH are all chemically similar in nature.[13–15] Thus, using a reaction based chemical sensor, MeOH detection in commercial alcoholic beverages and hand sanitizers containing a large amount of EtOH/^{i}PrOH as well as water is an extremely challenging task.[16–18] In the search for an alternative method of detection, researchers focused on various other analytical procedures, such as different types of mass spectrometry (MS)[19–21] gas chromatography,[22–24] cyclic voltammetry,[25] capillary electrophoresis,[26] quartz crystal microbalances (QCMs) and so on.[27] However, costly sophisticated instrumentation, the requirement of skilled technicians or tedious standardizations for the previous methods are major disadvantages for using them in routine analysis. In view of their cost-effectiveness and easy detection protocol, the reaction based chemical sensing methods are far superior detection techniques.

Fluorometric chemical sensing because of its ultra-high sensitivity is considered to be one of the most effective methods. Despite this, few organic fluorescent probes for MeOH are reported in the literature and those that are have certain limitations.[17, 28–30] Different materials have also been used as MeOH fluorosensors such as a supramolecular ionic material by Zhang *et al.*,[31] bimetallic lanthanide-organic framework by Du *et al.*,[32] and nitrogen-doped oxidized

carbon dots by Latha *et al.*[33] In most of the cases MeOH is differentiated only from EtOH but not from ^{i}PrOH. The detection is based on either an increase or decrease of the relative intensity changes between MeOH and EtOH but never in the opposite direction, that is an increase for one and a decrease for the other. In addition, the effect of a large amount of water in the sample being analyzed for MeOH, although useful in the preparation of alcoholic beverages and hand sanitizers, has not been thoroughly investigated. Thus, it is proposed that the MeOH detection based on water induced a reverse fluorescence response for the probe such as an increase in intensity in the presence of MeOH but a decrease in intensity in its absence for an EtOH/^{i}PrOH medium.

The aldehydic phenol ligand (PPY) and its alcohol coordinated Al(III)-complexes were strategically synthesized, and they exhibited a water mediated MeOH selective fluorometric response. The presence of MeOH in EtOH/^{i}PrOH induces a change in the complex geometry from a fluorescent tetrahedral (Td) form to a weakly fluorescent octahedral (Oh) form, which is due to the exchange of coordinated EtOH/^{i}PrOH by MeOH. The interaction of water with the Oh-species exhibited a strong fluorescence intensity because of the exchange of its one coordinated MeOH with a water molecule followed by an intramolecular proton transfer from the coordinated water to the ligand moiety. However, the less stable Td-complex in the absence of MeOH is dissociated by the water interaction to exhibit an intensity decrease. Such water induced opposite intensity changes between the absence and presence of MeOH are utilized to detect MeOH in EtOH/^{i}PrOH and in alcoholic beverages/hand sanitizers in a water medium.

5.2. Results and discussion

5.2.1. Probe design for MeOH detection

The synthesis route of the Al^{3+} binding aldehydic phenol ligand consisting of a dangling pyrazole unit (PPY) is shown in Scheme 2 of chapter 2. It has recently been reported that the Al^{3+} ion exhibits a strong complex formation affinity with phenolic Schiff-base molecules by binding to phenolic-O and imine-N in alcohol solvents, and the rest of the Al(III)-coordination sites were filled by alcohol molecules.[34] In this research, the aldehydic moiety was deliberately not converted into the corresponding imine functionality of PPY, in order to achieve a reduced complex formation affinity due to the weaker interaction ability of aldehydic-O than that of the imine-N. Thus, upon the addition of a trace amount of the MeOH in the EtOH/^{i}PrOH medium, a spontaneous conversion from a structurally fragile Td geometry to a relatively stable Oh symmetrical PPY/Al^{3+} complex is possible due to the exchange of coordinated EtOH/^{i}PrOH

by MeOH molecules. The reaction of water with PPY/Al^{3+} induces a fluorescence increase for the Oh species, but an intensity decrease for the Td complex. The MeOH induced the reversal of the fluorescence intensity change due to the change of the Al(III) geometry which was utilized for the detection of trace MeOH in EtOH/^{i}PrOH.

5.2.2. The PPY/Al^{3+} complex formation and its interaction with water

In the presence of anhydrous AlCl$_3$ (200 μM), the UV-vis absorption intensity at ~340 nm for PPY (10 μM) in alcohol solvents decreased gradually with time (up to 60 min), upon the formation of a new intensity at 405–410 nm through an isosbestic point at ~378 nm (Fig. 1 and 2), indicating that PPY was involved in a complex formation reaction with the Al^{3+} ion by a kinetically slow process. The amount of complex formation was evaluated directly by judging the relative intensity changeover from ~340 nm to the 405–410 nm absorption band, because both intensities are not overlapped by each other (Fig. 1). However, to estimate the equilibrium between PPY and its Al(III)–complex in the presence of various amount of AlCl$_3$ (20–200 μM), the intensity values when the reaction attained equilibrium in nearly in 60 min were evaluated (Fig. 1 and Fig. 3). It should be noted that a large amount of Al^{3+} (~200 μM, 20 equiv.) was required to react all the PPY with Al^{3+} in an MeOH medium (Fig. 1 and 3), which suggested that the interaction of PPY with the Al^{3+} ions was not only kinetically slow but also thermodynamically weak in nature.
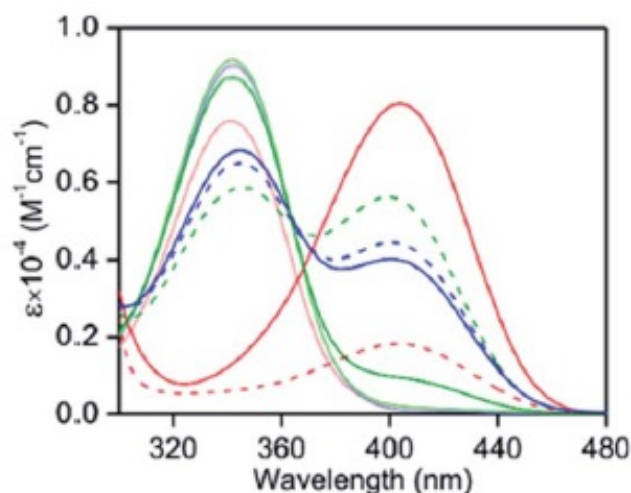
Fig. 1. The UV-vis absorption spectra of PPY (10 μM) in the presence (solid lines) and absence (broken lines) of 2.5% (v/v) water containing anhydrous AlCl$_3$ (200 μM) at 25°C: red, MeOH; blue, EtOH and green, ^{i}PrOH. The spectra were collected during the 60 min of AlCl$_3$ addition.

The spectra of PPY in the absence of AlCl₃ and water are depicted in their respective light colors for comparison.
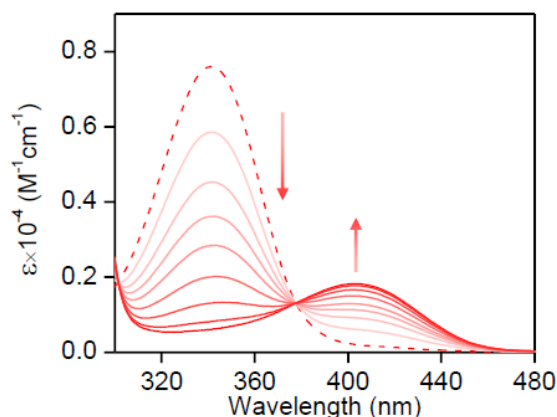
Fig. 2. UV-vis absorption spectra of PPY (10 μM) at various reaction times (2-60 min) of AlCl₃ (200 μM) addition in MeOH solvent at 25°C. The increase or decreasing intensities with the reaction time are shown by arrows. The spectrum in the absence of AlCl₃ is depicted in broken.

However, large fractions of unreacted PPY ~60% in EtOH and ~50% in ^{i}PrOH medium were identified in the presence of the same concentration of Al^{3+} (20 equiv.) (Fig.1). This result indicates that the complex formation affinity was reduced even more in the EtOH/^{i}PrOH than in the MeOH medium. In spite of inadequate complex formation in the EtOH or ^{i}PrOH solvents, the intensity at ~405 nm for the PPY/Al^{3+} complex was ~3-fold larger, i.e., there was a 6−7 times higher molar extinction coefficient (ε) value (~1.1×10^4 M^{-1} cm^{-1}), than that observed in MeOH (~0.17×10^4 M^{-1} cm^{-1}) (Fig. 1).

Fig. 3. UV-vis absorption spectra of PPY (10 μM) in the presence (solid) various amount of anhydrous AlCl₃ (20-200 μM) addition in MeOH solvent at 25°C. The spectra were collected in 60 min of AlCl₃ addition. The increase or decreasing intensities with the increase of AlCl₃ amount are shown by arrows. The spectrum in the absence of AlCl₃ is depicted in broken.

Although phenolate-O and Al^{3+} bond formation was quite obvious, the formation of aldehydic-O with the Al^{3+} bond was assured by an up-field ^{1}H-NMR chemical shift from ~9.91 to 9.53 ppm, which was presumably due to an Al^{3+} binding induced, increased negative charge density at the aldehydic-O (Fig. 4 and 5 compared with theoretical calculation section).
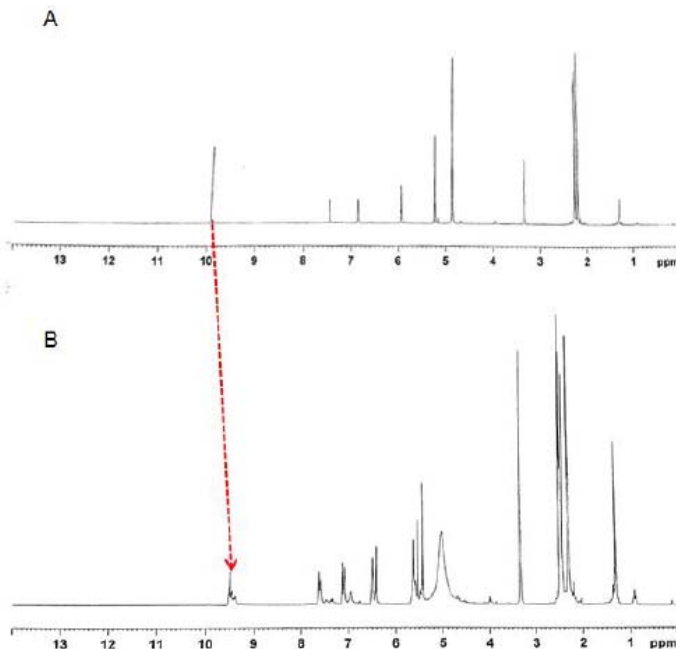
Fig. 4. ^{1}H-NMR spectrum of PPY (1 mM) in (A) the absence and (B) presence of AlCl₃ (20 mM) in CD₃OD.
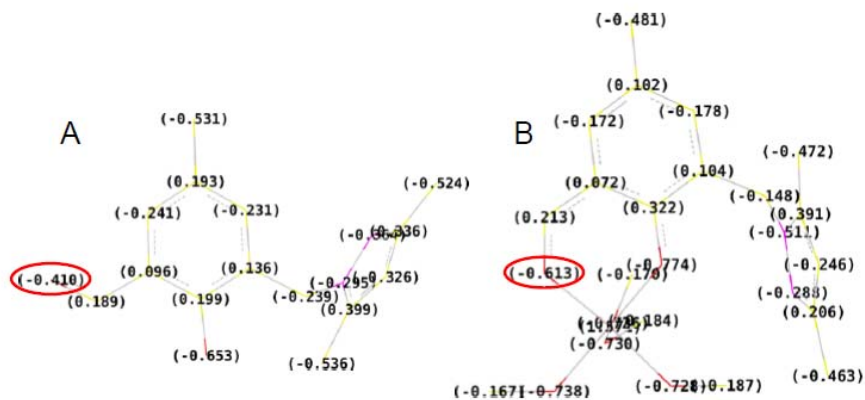
Fig. 5. Mulliken atomic charge values for the optimized geometries of (A) PPY and (B) PPY/Al³⁺ complex containing coordination of 4 MeOH molecules obtained from DFT based theoretical calculations (B3LYP/6-31G). Color index for atoms: H, cyan; C, yellow; N, pink and O, red. H atoms are removed in optimized structure for clarity. The charge values on carbonyl-O atoms are depicted by red circles.

106

Furthermore, a 1:1 PPY to Al^{3+} binding with a reflection of coordinated alcohol molecules (maximum up to four MeOH molecules (m/z calc. for $[PPY + 4MeOH + Al + Cl]^+$: 433.873, found: 433.912) and two EtOH molecules (m/z calc. for $[PPY + 2EtOH + Al + Cl]^+$: 397.854, found: 397.823)) were recognized in the ESI-MS$^+$ studies (Fig. 6B and D)).
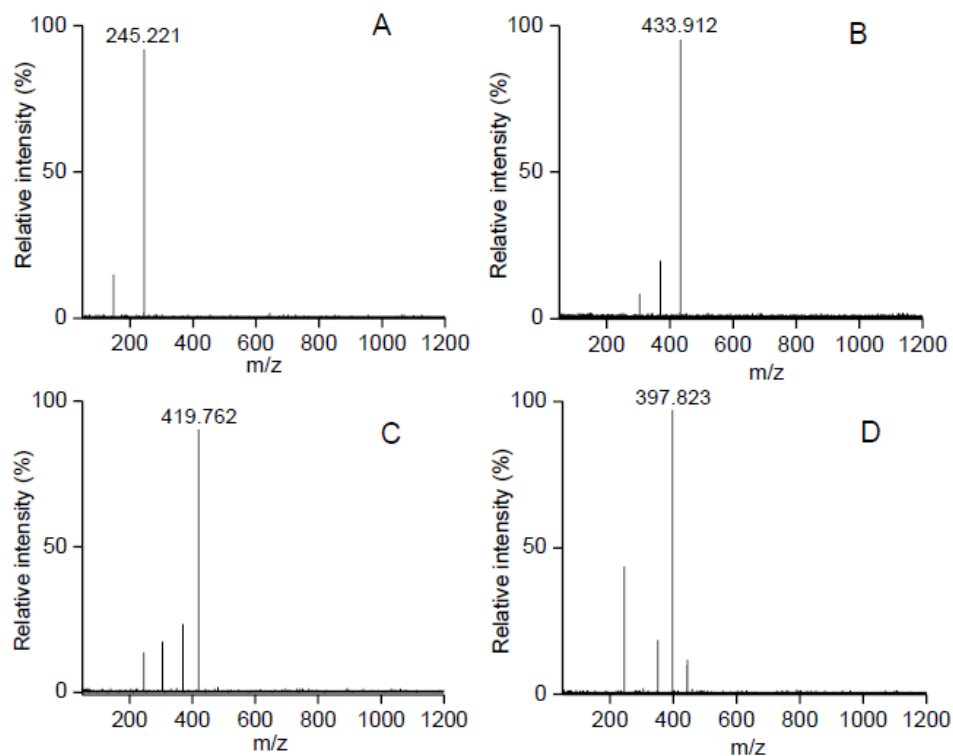
Fig. 6. ESI-MS$^+$ of PPY (A) (m/z for [PPY+H]$^+$: cal'd – 245.281 (obs'd – 245.221)) and PPY/Al^{3+} complex in (B) MeOH (m/z for [PPY+Al+Cl+4CH$_3$OH]$^+$: cal'd – 433.873 (obs'd – 433.912)), (C) MeOH/water (water: 2% (v/v)) (m/z for [PPY+Al+Cl+H$_2$O+3CH$_3$OH]$^+$: cal'd – 419.842 (obs'd – 419.762)) and (D) EtOH (m/z for [PPY+Al+Cl+2C$_2$H$_5$OH]$^+$: cal'd – 397.854 (obs'd – 397.823)).

The results indicated that the saturation of the Al(III)-coordination was effected by the solvent alcohol molecules. The reaction of MeOH (1–20% (v/v)) with the solvent coordinated PPY/Al^{3+} in the presence of unreacted PPY in EtOH/^{i}PrOH showed a gradual decrease of both UV-vis intensities at ~340 nm of unreacted PPY and at ~403 nm of the PPY/Al^{3+} complex due to newly formed MeOH coordinated complexes and a replacement of coordinated EtOH/^{i}PrOH by MeOH molecules in the solvent coordinated PPY/Al^{3+}, respectively, (Fig. 7). The results justified the proposition that the stability or formation affinity was higher for MeOH coordinated PPY/Al^{3+} than for the EtOH/^{i}PrOH coordinated one.
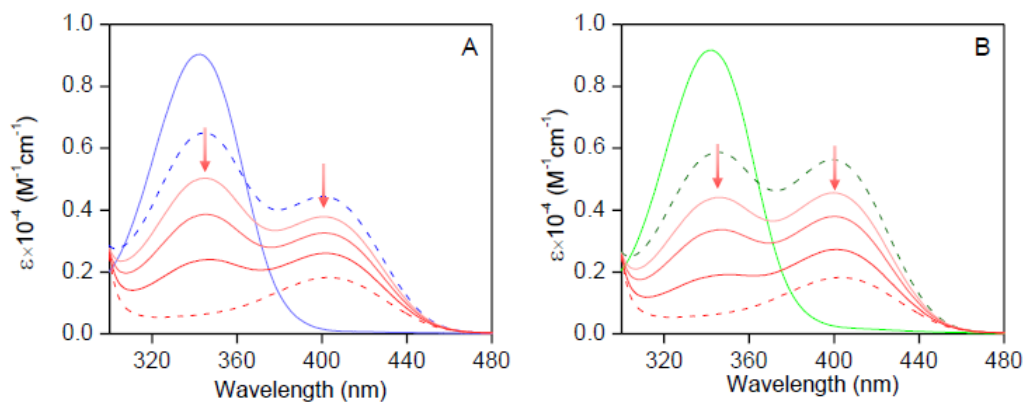
Fig. 7. UV-vis absorption spectra of PPY (10 μM) in 60 min of anhydrous AlCl₃ (200 μM) addition in EtOH or ⁱPrOH (broken blue: EtOH (A), broken green: ⁱPrOH (B)) at 25°C. (broken red: A and B) Spectra in MeOH are shown for comparison. (solid red: A and B) Spectra recorded in 60 min (120 min of AlCl₃ addition) upon addition of various amount of MeOH (5-20%) in (A) EtOH and (B) ⁱPrOH reaction mixture at 25°C. The spectra PPY in the absence of AlCl₃ and MeOH are shown in light blue (A) or light green (B). The spectra were collected in 60 min of AlCl₃ addition. The decreasing intensities with the increase of MeOH amount are shown by arrows.

The interaction of the PPY/Al^{3+} complex with water molecules in EtOH/ⁱPrOH medium showed an increase of absorption intensity at ~340 nm whereas a decrease in intensity at ~405 nm indicated the dissociation of the complex (Fig. 8).
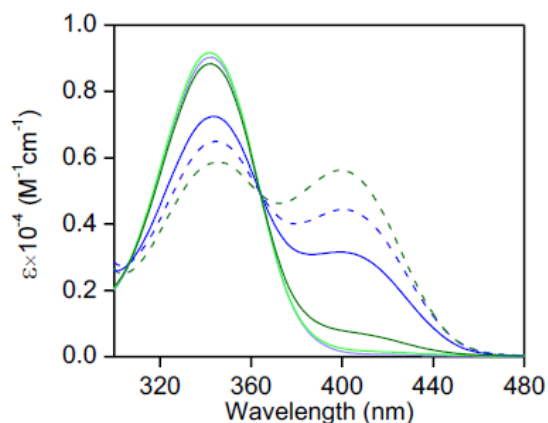
Fig. 8. UV-vis absorption spectra of PPY (10 μM) in 60 min of anhydrous AlCl₃ (200 μM) addition in (broken blue) EtOH and (broken green) ⁱPrOH at 25°C. Spectra recorded in 60 min (120 min of AlCl₃ addition) upon addition of 5% (v/v) water (solid blue) EtOH and (solid green) ⁱPrOH reaction mixture at 25°C. The spectra PPY in the absence of AlCl₃ and water are shown in light blue and light green (solid).

However, a similar water interaction in the MeOH medium caused a large increase of absorption intensity (~4-fold) at 405 nm without generating any absorption band at ~340 nm for free PPY (Fig. 1). This result shows that water reacted with the Al(III) center in the MeOH

coordinated PPY/Al^{3+} complex without disturbing the PPY and Al(III) interaction. Because of the greater stabilities of MeOH coordinated species, an incorporation of a water molecule in the Al(III) coordination site may occur by it replacing one coordinated MeOH molecule, and this phenomenon was verified from the ESI-MS$^+$ measurements (m/z calc. for [PPY + 3MeOH + H$_2$O + Al + Cl]$^+$: 419.842, found: 419.762) (Fig. 6C).

5.2.3. Solvent alcohol/water induced fluorescence response for PPY/Al^{3+}

The PPY exhibited no fluorescence intensity. With an addition of AlCl$_3$ (50 μM, 25 equiv.) in separate different alcohol mediums (MeOH, EtOH or ^{i}PrOH) containing PPY (2 μM), the fluorescence intensity at ∼510 nm was enhanced gradually with time until the intensity was nearly saturated in ∼60 min of Al^{3+} addition (Fig. 9A). However, the saturated intensity value varied widely depending on the alcohol medium. Compared to MeOH, ∼8- and 2-fold larger intensities were detected in ^{i}PrOH and EtOH, respectively, (Φ_F ∼0.013 for MeOH, ∼0.025 for EtOH, and ∼0.102 for ^{i}PrOH) (Fig. 9). Interestingly, the interaction of water with the PPY/Al^{3+} complex exhibited an increase of intensity in the MeOH medium but an intensity decrease in the EtOH/^{i}PrOH medium (Fig. 9).
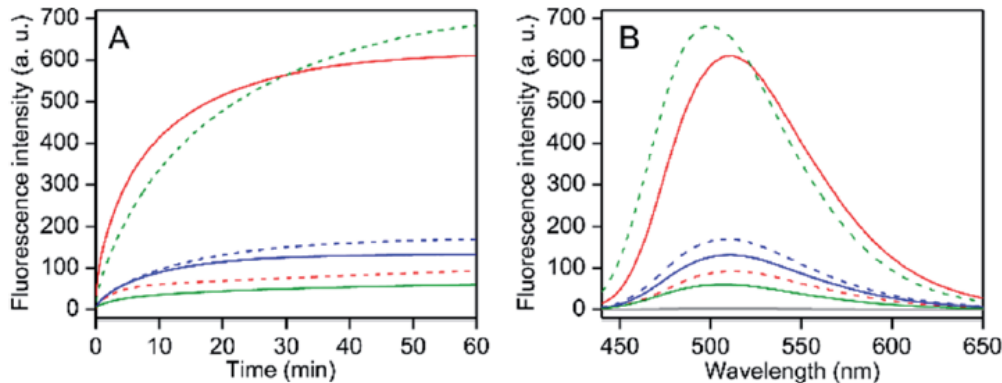
Fig. 9 (A) Time-dependent fluorescence intensity changes at 505 nm upon the addition of anhydrous AlCl$_3$ addition (50 μM), and (B) fluorescence spectra in 60 min of AlCl$_3$ addition in various alcohol solvents in the presence (solid line) and absence (broken line) of 2.5% (v/v) water containing PPY (2 μM) at 25 °C: red, MeOH; blue, EtOH and green, ^{i}PrOH. The spectrum in the absence of PPY is shown in grey (B). The excitation wavelengths were 405 nm in both (A and B).

An intensity increase of about 6-fold was observed in the MeOH medium containing ∼1.2% (v/v) water, whereas the intensity increased maximally up to ∼6.7-fold (Φ_F ∼0.09) in the presence of ∼2.5% water (Fig. 10). In contrast, intensity quenching, almost completely in ^{i}PrOH and ∼20% in EtOH solvents was detected by the addition of 5% water (Fig. 10).

Similarly to the EtOH/^{i}PrOH solvent, the water induced fluorescence decrease was noticed for other alcohols (n-PrOH, ^{t}BuOH, n-hexanol) (Fig. 11). Therefore, MeOH is a unique alcohol to use to show the water induced fluorescence increase.

Fig.10. The ratio of fluorescence intensities at 505 nm for the PPY/Al^{3+} complex in the presence of various amounts of water% and its absence are plotted with the value of water% (v/v) in different alcohol mediums at 25°C: red, MeOH; blue, EtOH and green, ^{i}PrOH. The intensity values in the absence and presence of different water% are collected in 60 min of anhydrous AlCl$_3$ (50 μM) addition in the medium containing PPY (2 μM). Inset: the Y-axis expanded plots for EtOH and ^{i}PrOH medium are shown for clarity. Excitation and emission wavelength were 405 and 505 nm, respectively. The data points for each alcohol solvent are fitted using a single exponentially-fitted method. The average value for each data point is obtained from triplicate measurements (n = 3).

Fig. 11. Fluorescence spectra of PPY/Al^{3+} in various alcohol medium in the absence (solid) and presence (broken) of 2.5% (v/v) water at 25ºC: purple, n-propanol; dark cyan, ^{t}BuOH and pink, n-hexanol).The spectra were reordered in 60 min of AlCl$_3$ (50 μM) addition. Excitation wavelength was 405 nm.

5.2.4. DFT theoretical calculations: complex structure vs. optical response

The Al(III) can exist as both Oh and Td geometric forms,[35-37]where the Oh symmetry is more preferred than the Td symmetry.[36,37]According to the results of the ESI-MS$^+$ studies,

coordination of four MeOH and two EtOH molecules in the respective solvents were identified (Fig. 6). Because PPY was acting as 1:1 bi-dentate ligand for Al^{3+}, the coordination of the four MeOH molecules was related to the Oh geometry of Al(III). However, the same number of alcohol molecules binding for bigger EtOH or ^{i}PrOH or any other alcohol molecules may not be a steric fit around the Al(III) coordination sphere, thus a less stable Td structure which would allow two EtOH/^{i}PrOH molecules was the most likely to occur (Scheme 1).

Using a DFT based theoretical calculation, it was identified that a possible Oh to Td structural interconversion for PPY/Al^{3+} was responsible for the alcoholic solvent dependent changes in UV-vis absorption and fluorescence properties, both in the presence and absence of water. The ground state geometries of four MeOH and two EtOH/^{i}PrOH molecules coordinated Oh and Td complexes, respectively, with common phenolic-O and aldehydic-O coordination were optimized using B3LYP density function and a 6-31G basis set. The UV-vis absorption properties for the Oh and Td structures were evaluated using the TD-DFT calculations on the optimized ground state structures. The calculated HOMO to LUMO electronic transitions at ~409 nm for both Oh and Td structures corresponded well with the respective experimental absorption wavelengths (Fig. 1, 12 and Scheme 1).
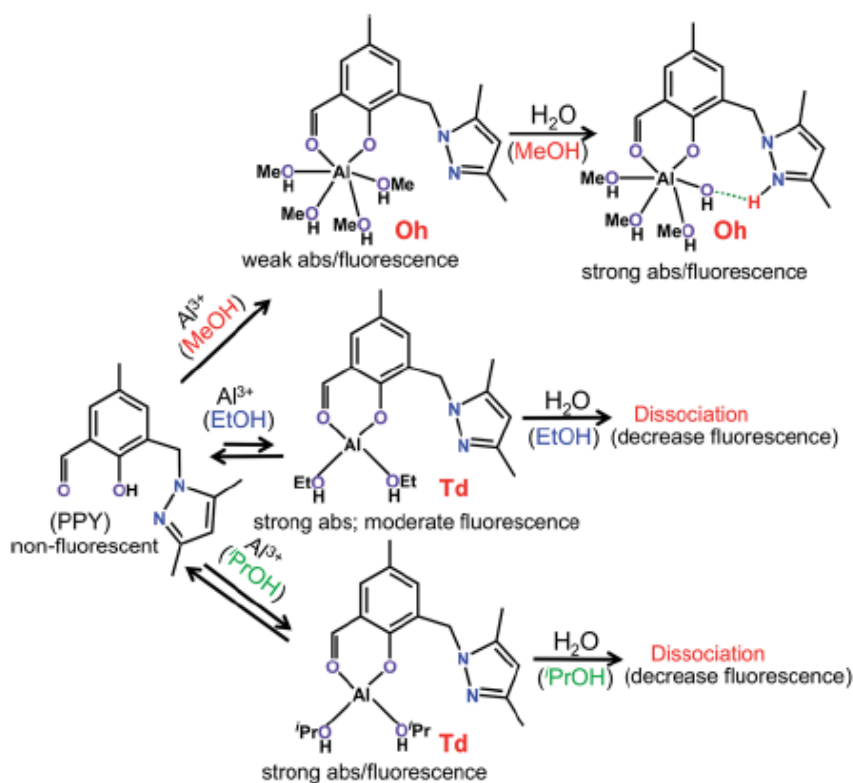
Scheme 1 Mechanistic view of alcoholic solvent selective formation of geometrically different PPY/Al^{3+} complexes and their reaction with water molecules. The Al(III) coordination saturation

for the octahedral (Oh) geometry in MeOH and the tetrahedral (Td) geometry in EtOH/ ^{i}PrOH medium are achieved by the coordination of four MeOH and two EtOH/^{i}PrOH molecules, respectively. The coordination geometry dependent relative UV-vis absorption (abs), and the emission parameters of the PPY/Al^{3+} complex are shown.

In a similar way to the experimentally observed UV-vis intensity increase at ~405 nm obtained by changing the solvent medium from MeOH to EtOH/^{i}PrOH, the HOMO / LUMO oscillator strength (f_{cal}) for the MeOH coordinated Oh geometry (~0.04) was found to be significantly lower than that detected for the EtOH/^{i}PrOH coordinated Td geometry (~0.07) (Fig. 12). When one coordinated MeOH close to the pyrazole-N was replaced by a water molecule, the optimized structure showed a proton transfer reaction from the coordinated water molecule to pyrazole-N, and a large increase of f_{cal} from ~0.04 to 0.09 was detected (Fig. 12 and Scheme 1).
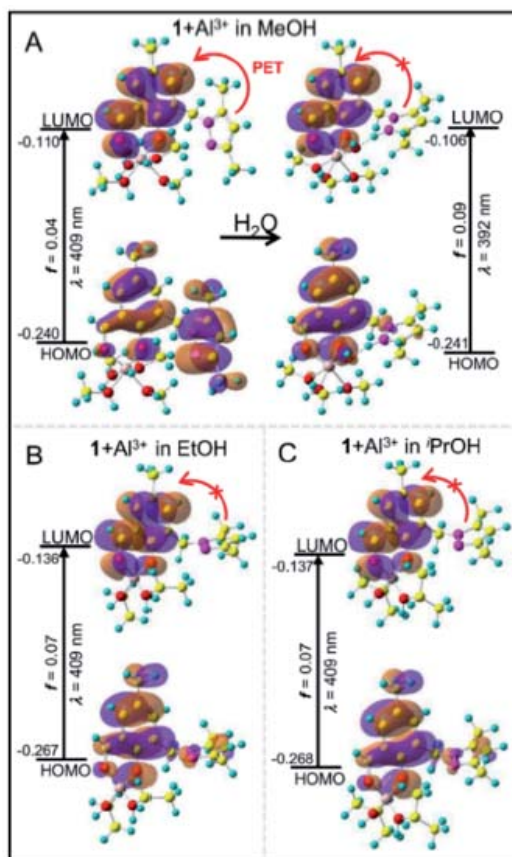
Fig.12. Frontier molecular orbital (FMO) profiles including different calculated UV-vis absorption parameters of MeOH (A: left upper panel) and MeOH/H$_2$O (A: right upper panel) coordinated Oh. The EtOH (B: left lower panel) and ^{i}PrOH (C: right lower panel) coordinated Td complexes based on DFT and TD-DFT (B3LYP/6-31G) calculations.

The increase of f_{cal} agreed well with the experimentally observed water induced large increase of UV-vis intensity in the MeOH medium (Fig. 1).

112

The efficient PET process from the pyrazole unit to the aldehydic phenol chromophore moiety made the PPY non- fluorescent (Fig. 13). For the MeOH coordinated Oh structure, the PET process did not disturb it significantly, and thus a weak fluorescence intensity was observed experimentally (Fig. 9 and 12).
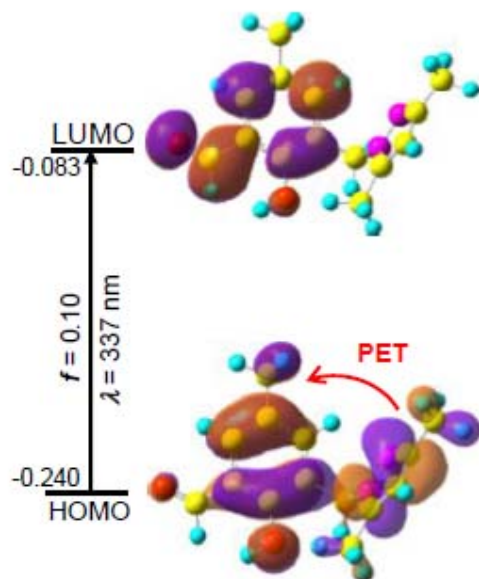
Fig.13. Frontier molecular orbital (FMO) profile including various UV-vis absorption parameters of PPY based on TD-DFT (B3LYP/6-31G) calculations. Color index for atoms: H, cyan; C, yellow; N, pink and O, red.

However, the electron distribution in both HOMO and LUMO for EtOH or ^{i}PrOH coordinated Td-species centered mostly at the aldehydic phenol chromophore, and the resultant suppression of the PET process made the Td complex highly fluorescent (Fig. 9, 12 and Scheme 1). Most interestingly, the calculations also identified that the PET process in the water substituted Oh species was eliminated, which clarified the probable reason for the water induced large increase of fluorescence intensity in the MeOH medium. All these studies suggested that the change of Al(III) geometry from Oh to Td be responsible for the alcohol solvent dependent change in optical response for the PPY/Al^{3+} complex.

5.2.5. Detection of MeOH in EtOH or ^{i}PrOH in the presence of water

It was found that the addition of water induced a fluorescence increase for MeOH coordinated Oh PPY/Al^{3+}, whereas the intensity decreased for the EtOH/^{i}PrOH coordinated Td complex (Fig. 10). An intensity increase of about 6.7-fold was found in MeOH/water mixed medium,

which remained unaffected within a water% of ~2.5%–11.0% (v/v), although the intensity decreased gradually as the water% was further increased (Fig. 10 and 14). However, for the water% amount above ~75%, the intensity value was found to be less in comparison to that observed in the absence of water (Fig. 14). It was also observed that the coordinated solvent in the PPY/Al^{3+} complex were replaced by MeOH from the EtOH/^{i}PrOH molecules with a subsequent change of complex geometry from Td to Oh by the addition of MeOH in EtOH/^{i}PrOH (Fig. 9, Scheme 1, and Fig. 7). Additionally, the residual unreacted PPY existed after the completion of a complex formation in EtOH/^{i}PrOH medium reacted further with Al^{3+} to form MeOH coordinated PPY/Al^{3+} in the presence of MeOH (Fig. 7).
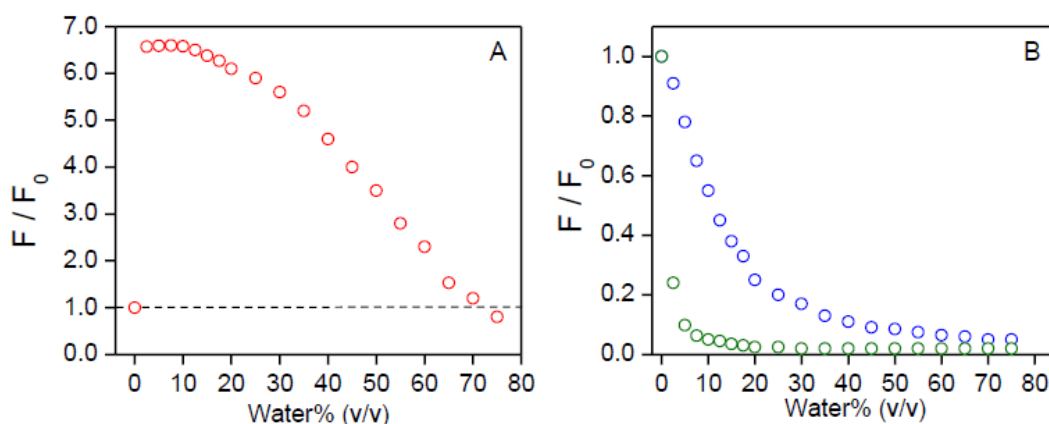
Fig. 14. The ratio of fluorescence intensities at ~505 nm for PPY/Al^{3+} in the presence of various amount of water% (v/v) and its absence are plotted with water% (v/v) in different alcohol mediums at 25°C: (A) red, MeOH; (B) blue, EtOH and (B) green, ^{i}PrOH. The intensity values in the absence and presence of different water% are collected in 60 min of anhydrous AlCl$_3$ (50 μM) addition in the medium containing PPY (2 μM). (A) The broken black line is shown to identify the extent the increase or decrease of intensity with respect to the intensity in the absence of water. Excitation wavelength was 405 nm.

Moreover, the presence of 10% MeOH in the solution with various EtOH/^{i}PrOH to water ratios showed that the presence of water effected different extents of intensity increase up to 70% water (Fig. 15). All these results strongly suggest that the relative percentage of coordinated Oh complex with respect to the EtOH/^{i}PrOH coordinated Td species should be much higher even in the presence of a low amount of MeOH in EtOH/^{i}PrOH. The water effected fluorescence intensity increased in the presence of various MeOH amounts was investigated for its potential use in the analytical detection of MeOH in EtOH/^{i}PrOH.
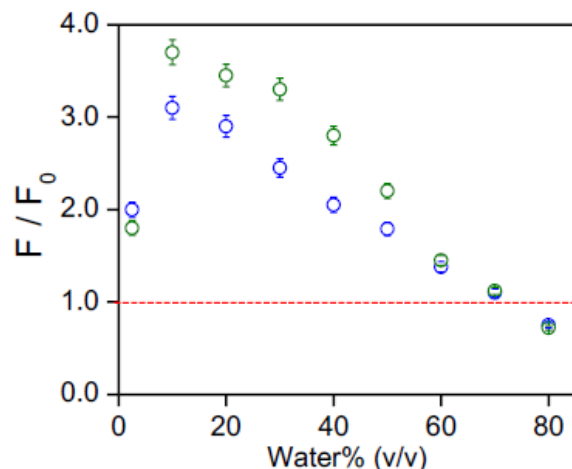
Fig.15. The ratio of fluorescence intensities at ~505 nm for PPY/Al^{3+} in the presence of various amount of water% (v/v) and its absence are plotted with water% (v/v) in different alcohol mediums containing 10% (v/v) MeOH at 25ºC: blue, EtOH and green, ^{i}PrOH. The intensity values in the absence and presence of different water% are collected in 60 min of anhydrous AlCl$_3$ (50 μM) addition in the medium containing PPY (2 μM). The broken red line is shown to identify the extent the increase or decrease of intensity with respect to the intensity in the absence of water. The average value for each data point is obtained from triplicate measurements (n = 3).

In the EtOH/^{i}PrOH medium containing water, the intensity ratios between the presence and absence of MeOH increased gradually with the increase of MeOH% (0.5–10% (v/v)) when the amount of any fixed water% value was within 2.5−55% (Fig. 16 and 17). The relative intensity enhancements depended on the water%. For a solution containing 10% MeOH, the relative intensity increments were ~2.0-, 3.1-, 2.5- and 1.5-fold for the EtOH system or ~1.8-, 3.7-, 3.5- and 2.2-fold for the ^{i}PrOH system in the presence of 2.5%, 10%, 25%, and 55% (v/v) of water, respectively (Fig. 16). The extent of the relative intensity increase with increasing MeOH% under various water% (2.5−55%) values followed a fairly good linear correlation (residual of fitting χ^2 ~ 0.99) for both the EtOH and ^{i}PrOH systems, where the water% dependent slope values were estimated to be ~0.10, 0.21, 0.15 and 0.08 for EtOH or ~0.08, 0.26, 0.25 and 0.12 for ^{i}PrOH in the presence of 2.5%, 10%, 25% and 55% water, respectively (Fig. 16). Using the linear calibration curve, the unknown amount of MeOH in the EtOH/^{i}PrOH solvent containing various water% can be evaluated ratiometrically.

Fig. 16. Relative fluorescence intensity changes between the presence and absence of MeOH for PPY/Al^{3+} are plotted with MeOH% (v/v) in (A) EtOH/water and (B) ^{i}PrOH/water mixed medium containing various amounts of water% (v/v): black, 2.5%; red, 10%; blue, 25%; orange, 55%. The identical value of water% before and after the MeOH spike was maintained by an addition of an appropriate amount of water in the spiked sample. The intensity values in the absence and presence of various MeOH% were collected during the addition of AlCl$_3$ (50 μM), over 60 min, to the medium containing PPY (2 μM). The data points for each solvent system are fitted with a linear equation. Excitation and emission wavelengths were 405 nm and 505 nm. The average value for each data point is obtained from triplicate measurements (n = 3).

Fig. 17. Fluorescence spectra for PPY/Al^{3+} in the presence of 10% (v/v) MeOH spikes in EtOH and ^{i}PrOH medium containing 5% (v/v) water. The corresponding spectra in the presence of 10% EtOH spikes instead of 10% MeOH spike are shown in broken blue and green. Excitation wavelength was 405 nm.

It was evident that the water amount present in the solution played the most critical role for the MeOH detection sensitivity, in which the sensitivity was at maximum at a water amount of ~10% (v/v) for both EtOH and ^{i}PrOH. Notably, the MeOH (10% v/v) also induced an

116

appreciable amount of increased fluorescence intensity for PPY/Al^{3+} and this was also observed in other alcohol mediums (n-PrOH, ^{t}BuOH and n-hexanol) containing 5% water (Fig. 18), which indicated that the MeOH detection selectivity of the PPY/Al^{3+} complex did not alter with the change of alcohol systems.
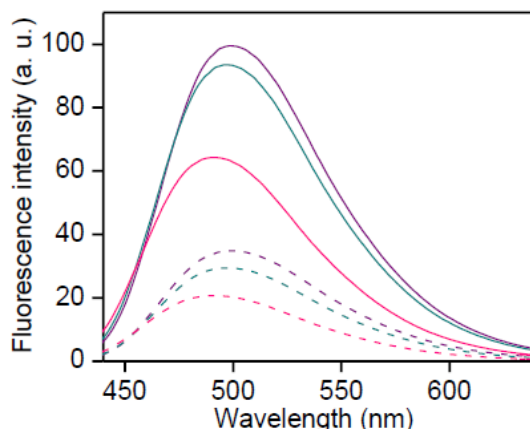
Fig. 18. Fluorescence spectra of PPY/Al^{3+} (PPY: 2 μM + AlCl$_3$: 50 μM) in various alcohol medium containing 2.5% water in the presence (solid) and absence (broken) of 10% MeOH at 25°C: purple, *n*-propanol; dark cyan, ^{t}BuOH and pink, *n*-hexanol. The spectra were reordered in 60 min of AlCl$_3$ (50 μM) addition. The identical value of water% before and after of MeOH spike was maintained by an appropriate amount of water addition in the spiked sample. Excitation wavelength was 405 nm.

However, to detect a low amount of MeOH or low LOD values, fluorescence studies conducted in the presence of very low PPY/Al^{3+} concentrations (0.1 μM PPY and 4 μM Al^{3+}) so that an appreciable fluorescence response can be observed even in the presence of much lower amount of MeOH. The fluorescence intensity changes in the presence of much lower amounts of MeOH (0.05−0.30%) are shown in Fig. 19). The LOD was evaluated using the equation: LOD = 3σ/k (*cf*. Experimental section/chapter 2). The LOD values for MeOH detection were estimated to be ~0.03%–0.06% depending on the solvent compositions.

The water% dependency variation of the fluorescence response for MeOH was interpreted by combining the water% dependent various extent of intensity increase for MeOH medium in the absence of EtOH/^{i}PrOH and the intensity decrease for EtOH/^{i}PrOH in the absence of MeOH (Fig. 10 and 14).

Fig. 19. (A,B) Relative fluorescence spectral changes between presence and absence of MeOH for PPY/Al^{3+} in the presence of various amount of MeOH spikes (0.05-0.30% (v/v)) in (A) EtOH and (B) ^{i}PrOH medium containing 10% (v/v) water at 25°C: red, 0.05%; blue, 0.10%; dark yellow, 0.15%; purple, 0.20%; green, 0.25% and violet, 0.30% MeOH. The spectra in the absence of MeOH spikes are shown in black. The identical value of water% before and after of MeOH spike was maintained by an appropriate amount of water addition in the spiked sample. The spectra in the absence and presence of various MeOH% are collected in 60 min of AlCl$_3$ (5 μM) addition in the medium containing PPY (0.1 μM). Excitation wavelength was 405 nm. The background fluorescence in the absence of probe was subtracted for each spectrum. (B) The maximum intensity values are plotted against the amount of MeOH spikes for (C) EtOH and (D) ^{i}PrOH. The data points are fitted by linear equation. The average value for each data point is obtained from triplicate measurements (n = 3).

The presence of a small amount of MeOH in the EtOH/^{i}PrOH medium replaced coordinated EtOH/^{i}PrOH with MeOH molecules in PPY/Al^{3+} to obtain a Td to Oh structural change. However, the existence of an EtOH/^{i}PrOH coordinated Td complex and its water interaction induced intensity decrease cannot be neglected entirely in the interpretation of the fluorescence response values in the presence of various amounts of MeOH and water. The presence of a water induced ~6.7-fold intensity increase remains unchanged between 2.5% and 10% of water for MeOH in the absence of EtOH/^{i}PrOH (Fig. 10 and 14 and the observed intensity was decreased by increasing the water% (2.5% to 10%) for EtOH/^{i}PrOH in the absence of MeOH,

which effects the enlargement of the MeOH detection slope value (~0.10 to 0.21 for EtOH and ~0.08 to 0.26 for ^{i}PrOH) by the increase of water%. Significantly higher slope changes for ^{i}PrOH medium: ~3.7-fold compared to ~2.1-fold for EtOH medium due to the increase of water% (2.5% to 10%) was rationalized by the increased water amount which induced a greater amount of intensity quenching for ^{i}PrOH (~90%) than the EtOH medium (45%) in the absence of MeOH (Fig. 16 and 14). However, any further increase of water% from 10% to 55% produced a larger intensity decrease for MeOH in the absence of EtOH/^{i}PrOH than for EtOH/^{i}PrOH in the absence of MeOH (Fig. 14), and thus a gradual decrease of the MeOH detection slope value from ~0.21 to 0.08 for EtOH and ~0.26 to 0.12 for ^{i}PrOH was observed.

5.2.6. The MeOH detection in alcoholic samples and sanitizers

The EtOH% in alcoholic beverages are dependent (5−70% (v/v)) on their classifications, and usually water is the rest of the liquid volume. However, according to WHO guidelines, the composition of hand sanitizers should be ~80% EtOH (v/v) or 75% ^{i}PrOH (v/v), glycerol (1.45% (v/v)), and H_2O_2 (0.125% (v/v)).[38] Spiked MeOH% in high and low EtOH% containing vodkas (~45% (v/v)) and wine (~15% (v/v)) samples, respectively, were estimated. As the MeOH detection sensitivity at above 55% (v/v) of water was comparatively low (Fig. 14 and Fig. 15), an external EtOH addition is required for the detection of MeOH in the wine samples. In addition, spiked MeOH was estimated both in the presence and absence of externally added EtOH to show the applicability of the method for alcoholic beverages containing higher EtOH%. However, the spiked MeOH amounts were estimated in EtOH- and ^{i}PrOH-based hand sanitizers without any further addition of external EtOH/^{i}PrOH.

To observe the MeOH induced fluorescence intensity increase, the water% before and after MeOH spikes in the hand sanitizer samples were maintained by addition of an appropriate amount of water in the spiked MeOH sample. With the increase of MeOH spikes from 0.5% to 10% in the vodka sample in the presence and absence of externally added 30% EtOH (total water ~25%), the relative fluorescence intensity between the presence and absence of MeOH was found to increase linearly from 1.04- to 1.77-fold and 1.08- to 2.45-fold, respectively (Fig. 20A−C). For a wine sample with the externally added 30% EtOH, the relative intensity also increased linearly from 1.05- to 1.78-fold (Fig. 21), where the slope value of the linear plots ~0.08 was found to be similar to that obtained for a known EtOH/water mixed medium (45% EtOH) or vodka (45% EtOH) sample (Fig. 16A).

119

Fig. 20. The relative fluorescence spectral changes between the presence and absence of MeOH for PPY/Al^{3+} with various MeOH spikes (0.5–10% (v/v)) in an alcoholic beverage (vodka: labelled EtOH% ∼ 45% (v/v)) in (A) the absence and (B) the presence of externally added 30% EtOH, and (D) EtOH or (E) ^{i}PrOH-based hand sanitizers (labelled ^{i}PrOH ∼75% and EtOH ∼80%) at 25 °C. The spectra in the absence of MeOH spikes are shown in black. The maximum intensity values for alcoholic beverages (C) and hand sanitizer (F) samples are plotted against the amount of the MeOH spikes. (A–C) Blue and red correspond to the presence and absence of externally added 30% EtOH, respectively. (D–F) Purple and green correspond to EtOH- and ^{i}PrOH based hand sanitizer, respectively. (A–F) The identical value of water% before and after of MeOH spike was maintained by using an appropriate amount of water addition in the spiked sample. The intensity increases with the increase of MeOH% are shown by arrows. The excitation wavelength was 405 nm. The average value for each data point is obtained from triplicate measurements (n = 3).

In addition, the slope values for vodka samples with 30% EtOH added externally (total EtOH, 75%) were also similar to the results obtained for the known 75% EtOH medium (Fig. 16A,

120

20B and C). All these results clearly showed that the presence of other chemicals in alcoholic beverages did not disturb the detection ability of the MeOH. Even without knowing the accurate water% value in the test sample, the estimation of MeOH contamination was possible from the correlation of fluorescence response of the test sample with the linear calibration plots for the corresponding MeOH free alcoholic beverages (Fig. 20C).
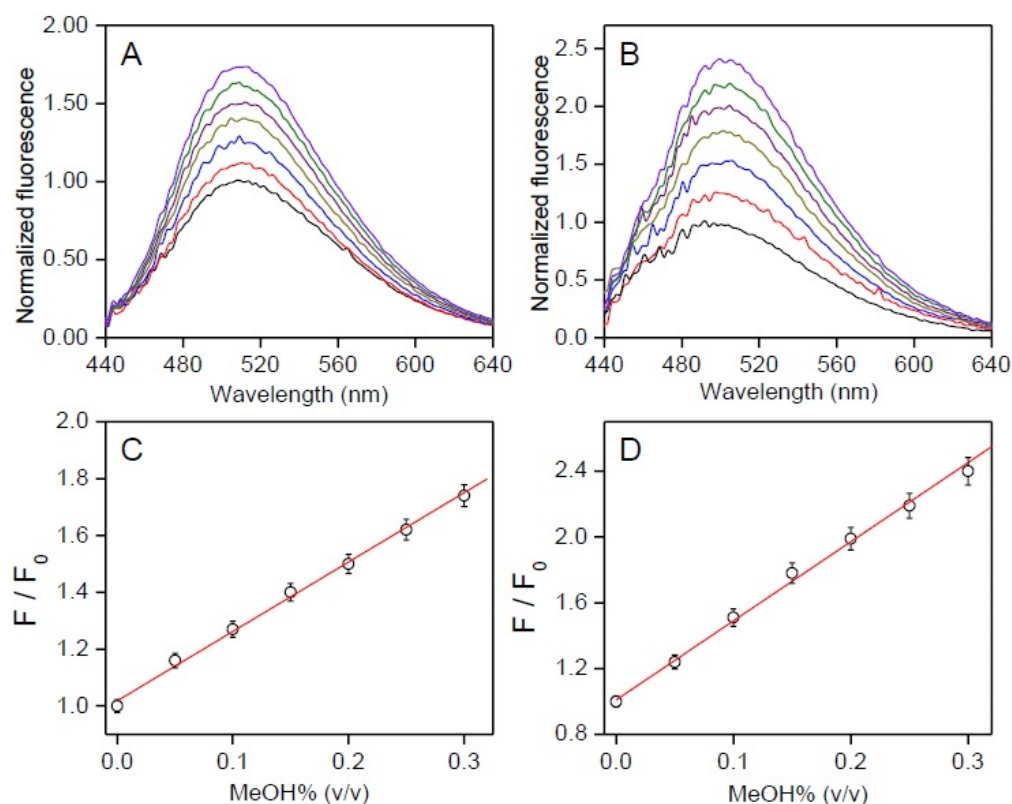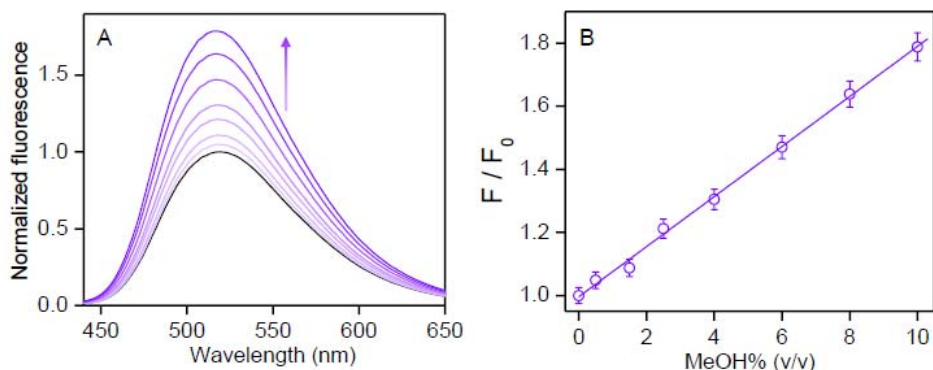

Fig. 21. (A) Relative fluorescence spectral changes between presence and absence of MeOH for PPY/Al^{3+} in the presence of various amount of MeOH spikes (0.5-10% (v/v)) in commercial wine (labelled EtOH% ~15% (v/v)) in presence of externally added 30% EtOH at 25°C. The spectra in the absence of MeOH spikes are shown in black. The identical value of water% before and after of MeOH spike was maintained by an appropriate amount of water addition in the spiked sample. The increase of intensities with the increase of spike MeOH amounts are shown by arrow. Excitation wavelength was 405 nm. (B) The maximum intensity values are plotted against the amount of MeOH spikes. The data points are fitted by linear equation. The average value for each data point is obtained from triplicate measurements (n = 3).

The fluorescence spectra for PPY/Al^{3+} in EtOH (80%) or ^{i}PrOH (75%) and a water mixed medium remain unchanged by the addition of glycerol (1.45% (v/v)) or H$_2$O$_2$ (0.125% (v/v)), both in the presence and absence of MeOH (Fig. 22), showing that the presence of glycerol and H$_2$O$_2$ in hand sanitizers did not affect the performance of the probe.
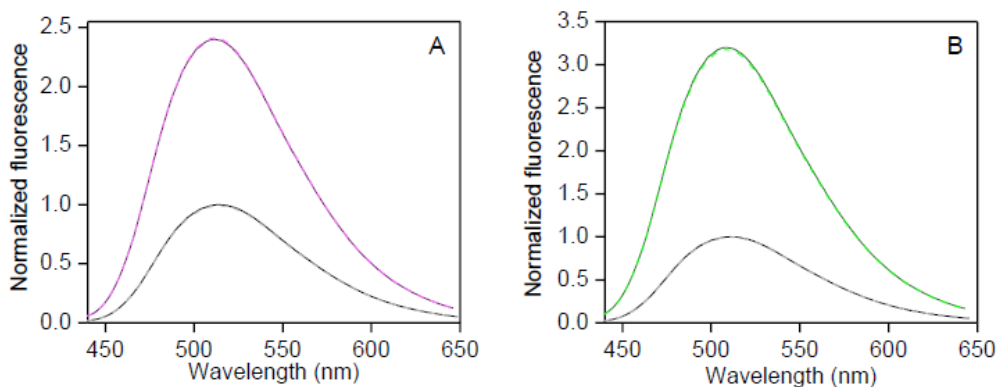
Fig. 22. Relative fluorescence spectral changes for PPY/Al^{3+} in the absence (black) and presence (A: purple and B: green) of 10% MeOH spikes in (A) EtOH/water (water: 80% (v/v)) and (B)

iPrOH (water: 75% (v/v)) medium containing 1.45% (v/v) glycerol and 0.125% (v/v) H₂O₂. The corresponding spectra in the absence of glycerol and H₂O₂ are shown in broken light colors. The identical value of water% before and after of MeOH spike was maintained by an appropriate amount of water addition in the spiked sample. Excitation wavelength was 405 nm.

The intensity increased linearly from ~1.05 to 2.38 for EtOH-based sanitizer or from ~1.08 to 3.22 for the iPrOH-based sanitizer because of the increase of the amount of MeOH spiking from 0.5% to 10% under the identical water% condition. The observed slope value of ~0.22 for the iPrOH-based sanitizer and of ~0.14 for the EtOH-based sanitizer were similar to that detected for the known 80% EtOH and 75% iPrOH medium, respectively (Fig. 16 and 20D–F). Therefore, an unknown amount of MeOH contamination in hand sanitizers could be estimated by correlating the intensity value of the test sample with the known linear calibration line obtained for the EtOH (or iPrOH) containing water or MeOH free standard for the EtOH (or iPrOH)-based hand sanitizer.

As in the procedure described previously, a low level of MeOH contamination in alcoholic beverages and sanitizer could be estimated using a low probe concentration (0.1 μM PPY and 4 μM Al³⁺). The MeOH induced fluorescence spectral changes in the presence of a lower amount of MeOH spikes (0.06–0.18% for a vodka sample and 0.03–0.10% for the iPrOH hand sanitizer) revealed that even a MeOH contamination of below 0.1 μM in alcoholic beverages and sanitizer can be estimated accurately by the present protocols (Fig. 23).

Fig. 23. (A,B) Relative fluorescence spectral changes between presence and absence of MeOH for PPY/Al³⁺ in the presence of various amount of MeOH spikes (0.03-0.18% (v/v)) in (A) commercial vodka (labelled EtOH% ~45% (v/v)) and (B) iPrOH-based hand sanitizers (labelled iPrOH ~75%) at 25°C: (A): red, 0.06%; blue, 0.12%; purple and 0.18% MeOH for vodka and (B): red, 0.03%; blue, 0.06%; purple and 0.10% MeOH for hand sanitizer. The spectra in the absence of MeOH spikes are shown in black. The identical value of water% before and after of MeOH spike was maintained by an appropriate amount of water addition in the spiked sample. The spectra in the absence and presence of various MeOH% are collected in 60 min of AlCl₃ (5 μM) addition in the

medium containing PPY (0.1 μM). The background fluorescence in the absence of probe was subtracted for each spectrum. Excitation wavelength was 405 nm.

The efficiency of probe recovery was also verified by conducting EDTA induced fluorescence intensity quenching studies in vodka and EtOH-based hand sanitizers. For both samples, MeOH induced ~90% of the increased intensity for PPY/Al^{3+} which was found to be quenched by the addition of EDTA, whereas the intensity recovered again upon further addition of Al^{3+} (Fig. 24). The EDTA induced displacement of PPY from the PPY/Al^{3+} complex again participated in complexation with the freshly added Al^{3+} to regain the fluorescence intensity by the reaction with MeOH present in solution. Thus, the probe can be reused on several occasions.
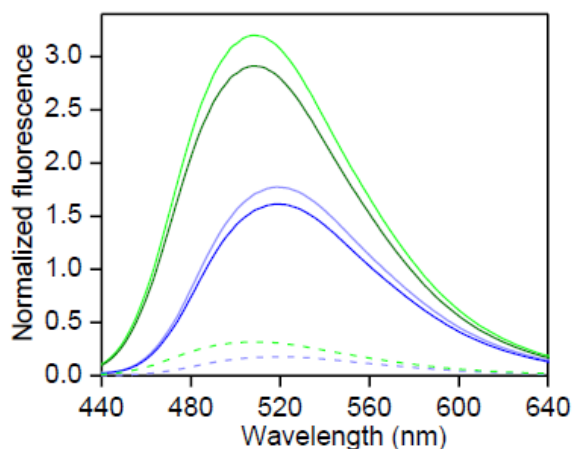
Fig. 24. Fluorescence spectra for PPY/Al^{3+} (PPY: 2 μM + AlCl$_3$: 50 μM) in (broken light blue) vodka or (broken light green) ^{i}PrOH-based sanitizer containing 10% MeOH and 50 μM EDTA. The corresponding spectra in the absence of EDTA are shown by solid light colors. Furthermore 100 μM of AlCl$_3$ was added in the solutions containing EDTA, and the spectra were recorded in 60 min of the AlCl$_3$ addition (solid blue for vodka and solid green for ^{i}PrOH-base sanitizer). Excitation wavelength was 405 nm.

5.3. Conclusions

A sensitive fluorometric MeOH detection method was demonstrated in EtOH/^{i}PrOH in a water medium using a 1:1 Al(III)- complex of an aldehydic phenol ligand containing a pyrazole unit (PPY). The complex adopted the MeOH coordinated weakly fluorescent octahedral (Oh) geometry from the fluorescent tetrahedral (Td) structure by an addition of MeOH in the EtOH/ ^{i}PrOH. The interaction of water with the Oh species causes a large fluorescence intensity increase due to the exchange of one coordinated MeOH by a water molecule, whereas a similar water interaction for the Td complex resulted in an intensity decrease due to its dissociation. The water mediated fluorescence intensity reversal due to the change in complex geometries

by the addition of MeOH was utilized to detect MeOH in EtOH/ⁱPrOH and various alcoholic beverages/hand sanitizers. Such water induced MeOH detection could be very useful industrially.

5.4. References

1. S. B. Jarwani, P. D. Motiani and S. Sachdev, *J. Emerg. Trauma Shock*, 2016, **6**, 73.

2. G. A. Beauchamp and M. Valento, *Emerg. Med. Pract.*, 2016, **18**, 1.

3. R. Paasma, K. E. Hovda, A. Tikkerberi and D. Jacobsen, *Clin. Toxicol.*, 2007, **45**, 152.

4. F. Bindler, E. Voges and P. laugel, *Food Addit. Contam.*, 1988, **5**, 343.

5. P. E. Hantson, *Bull Mem Acad R Med Belg*, 2006, **161**, 425.

6. D. G. Barceloux, G. R. Bond, E. P. Krenzelok, H. Cooper and J. A. Vale, *J. Toxicol. Clin. Toxicol.*, 2002, **40**, 415.

7. J. J. Liu, M. R. Daya and N. C. Mann, *J. Toxicol., Clin. Toxicol.*, 1999, **37**, 69.

8. F. Onder, S. Ilker, T. Kansu, T. Tatar and G. Kural, Int. Ophthalmol., 1998, **22**, 81.

9. J. A. Kruse, *Crit. Care Clin.*, 2012, **28**, 661.

10. C. S. Moon, *Ann Occup Environ Med*, 2017, **29**, 44.

11. D. Jacobsen and K. E. McMartin, *Med. Toxicol.*, 1986, **1**, 309.

12. L. Welle, A. Medoro and B. Warrick, *Ann. Emerg. Med.*, 2021, **77**, 131.

13. P. F. Pereira, R. M. F. Sousa, R. A. A. Munoz and E. M. Richter, *Fuel*, 2013, **103**, 725.

14. Methanol: colorless, mp¼_97.0 _C, bp ¼ 64.7 _C, d ¼ 0.79 g dm3, nD (at 20 _C) ¼ 1.33, dipole moment ¼ 1.70 D, dielectric constant ¼ 33, pKa ¼ 15.5.

15. Ethanol: colorless, mp ¼ _114.3 _C, bp ¼ 78.4 _C, d ¼ 0.799 g dm3, nD (at 20 _C) ¼ 1.36, dipole moment ¼ 1.69 D, dielectric constant ¼ 24.6, pKa ¼ 15.9.

16. G. J. Mohr, F. Lehmann, U. W. Grummt and U. E. Spichiger- Keller, *Anal. Chim. Acta*, 1997, **344**, 215.

17. S. H. Lim, L. Feng, J. W. Kemling, C. J. Musto and K. S. S. Suslick, *Nat. Chem.*, 2009, **1**, 562.

18. T. Qin, B. Liu, Y. Huang, K. Yang, K. Zhu, Z. Luo, C. Pan and L. Wang, *Sens. Actuators, B*, 2018, **277**, 484.

19. L. R. Cordell, H. Pandya, M. Hubbard, A. M. Turner and S. P. Monks, *Anal. Bioanal. Chem.*, 2013, **405**, 4139.

20. T. M. Allen, T. M. Falconer, M. E. Cisper, A. J. Borgerding and C. W. Wilkerson, Anal. Chem., 2001, **73**, 4830.

21. V. Shestivska, V. Kolivoska, J. Kubista, D. Smith and P. Spanel, *Rapid Commun. Mass Spectrom.*, 2020, **34**, 1.

22. M. L. Wang, Y. M. Choong, N. W. Su and M. H. Lee, *J Food Drug Anal*, 2003, **11**, 133.

23. M. Bursova, T. Hlozek and R. Cabala, *J. Anal. Toxicol.*, 2015, **39**, 741.

24. J. V. D. Broek, S. Abegg, S. E. Prastsinis and A. T. Guntner, *Nat. Commun.,* 2019, **10**, 1.

25. D. S. Park, M. S. Won, R. N. Goyal and Y. B. Shim, *Sens. Actuators, B*, 2012, **174**, 45.

26. M. S. F. Santos, E. T. D. Costa, I. G. R. Gutz and C. D. Garcia, *Anal. Chem.*, 2017, **89**, 1362.

27. C. Wang, F. Chen, X. W. He, S. Z. Kang, C. C. You and Y. Liu, *Analyst*, 2001, **126**, 1716.

28. V. Kumar, A. Kumar, U. Diwan, M. K. Singh and K. K. Upadhyay, *Org. Biomol. Chem.*, 2015, **13**, 8822.

29. Z. Wu, X. Fu and Y. Wang, *Sens. Actuators, B*, 2017, **245**, 406.

30. M. Zhao, Y. Yue, C. Liu, P. Hui, S. He, L. Zhao and X. Zheng, *Chem. Commun.*, 2018, **54**, 8339.

31. L. Zhang, H. Qi, Y. Wang, L. Yang, P. Yu and L. Mao, *Anal. Chem.*, 2014, **86**, 7280.

32. D. M. Chen, C. X. Sun, Y. Peng, N. N. Zhang, H. H. Si, C. S. Liu and M. Du, *Sens. Actuators B*, 2018, **265**, 104.

33. M. Latha, R. A. Devi, N. K. R. Bogireddy, S. E. S. Rios, W. L. Mochan, J. C. Uribe and V. Agarwal, *RSC Adv.*, 2020,**10**, 22522.

34. S. Roy, S. Das, R. Majumder, A. Ray and P. P. Parui, *RSC Adv.*, 2020, **10**, 23245.

35. J.-J. Delpuech, M. R. Khaddar, A. A. Peguy and P. R. Rubini, *J. Am. Chem. Soc.*, 1975, **97**(12), 3373.

36. E. Furia, A. Beneduci, N. Russo and T. Marino, *New J. Chem.*, 2018, **42**, 11006.

37. L. Malacaria, G. A. Corrente, A. Beneduci, E. Furia, T. Marinoand G. Mazzone, *Molecules*, 2021, **26**, 2603.

38. Guide to Local Production: WHO-recommended handrub formulations (PDF), World Health Organization, WHO/IER/ PSP/2010.5, WHO April, 2010.

ROYAL SOCIETY
OF CHEMISTRY

PAPER

An aluminium fluorosensor for the early detection of micro-level alcoholate corrosion†

Snigdha Roy,[a] Sanju Das,[ab] Rini Majumder,[a] Ambarish Ray‡*[b]
and Partha Pratim Parui 🆔 *[a]

The detection of the dry alcoholate corrosion of aluminium is vital to design a corrosion resistive aluminium alloy for the storage and transportation of biofuel (methanol or ethanol). By synthesizing an Al^{3+} fluorescent probe operable in an alcoholic medium, we quantified the alcoholate corrosion in terms of the fluorometrically estimated soluble alkoxide $(Al(OR)_3)$ generation under nitrogen atmosphere. With time, a linear increase in corrosion with specific aluminium dissolution rate constants $\sim$2.0 and 0.9 μg per day per cm^2 were estimated for aluminium and Al-7075 alloy, respectively. During open atmosphere monitoring, the adsorbed moisture converted small extent of $Al(OR)_3$ to the insoluble $Al(OH)_3$ at the alloy surface which retarded the alcoholate corrosion appreciably.

Switching over from conventional fossil fuel to biofuel is of current interest owing to the maximum utilization of eco-friendly non-conventional energy.[1] Commercially produced less polluted biofuels such as methanol and ethanol, mixed with fossil fuels have an acceptable performance capacity for the gasoline engine.[2] Moreover, in comparison to the gasoline, methanol and ethanol have much higher octane rating or compression ratio to resist the knocking for better thermal efficiency.[3] Since most of the fuel tanks/pipes are made of aluminium or its alloys owing to its high strength-to-density ratio, the aluminium corrosion due to the formation of alkoxide (alcoholate or dry corrosion) during storage or even transportation of such bio-alcohols may cause leakage in the fuel tanks and in worst cases enough threat is speculated for fire and explosion.[4] Mechanical overloads, alloy impurities even at elevated temperatures are further contenders for accelerating the alcoholate corrosion.[5] However, a prolong exposure to the moisture retards the alcoholate corrosion by forming a protective layer of hydrated aluminium oxide in the metallic surface but moisture impurity in the fuel may damage the gasoline engine.[6] Hence, a maintenance optimization is crucial in critical engineering disasters by detecting alcoholate corrosion as in its nascent state with minimizing the chance of water contamination.[6,7]

Several electrochemical and mechanical methods have been exploited for decades to propose aluminium alcoholate and

other corrosions;[6] yet the early detection of the alcoholate corrosion is still a challenging task due to the lack of sensitive analytical methods.[6,8] Here, the fluorescence technique may act as a better alternative owing to its simplicity and high sensitivity.[9] Till date, a large number of fluorescent probes for Al^{3+} have been exploited in the biological or environmental domain,[10] but has never focused on alcoholate corrosion studies. Based on this requirement, we synthesized a fluorescent probe, namely HMBDC ((6*Z*)-6-(2-hydroxy-3-(hydroxymethyl)-5-methylbenzylideneamine)-2*H*-chromen-2-one), to detect alcoholate corrosion with μg-level detection ability along with its retarding signature in the presence of moisture in a judicious way. Such novel method may lead to an early detection of alcoholate corrosion in a simpler way.

The non-fluorescent phenolic Schiff-base molecule containing a coumarin moiety (HMBDC) was prepared by condensing an equimolar mixture of 6-amino coumarin (6-ACO) and 2-hydroxy-3-(hydroxymethyl)-5-methylbenzaldehyde (HHMB) in dry ethanol (Scheme 1 and Fig. S1†) (*c.f.* ESI† for details). Among various organic solvents, the interaction of HMBDC with Al^{3+} was observed only in the alcoholic medium according to the UV-vis studies (Fig. S2†). In methanol, the absorption intensity at $\sim$353 nm for HMBDC (5 μM) decreased gradually with the continuous addition of $Al(NO_3)_3$ until saturated at $\sim$8-equiv., giving rise to a new peak at $\sim$406 nm, where an isosbestic point at $\sim$384 nm assures the formation of Al^{3+}/HMBDC complex (**1**) (Fig. 1A). Upon optimization of the complex formation affinity in various ethanol/methanol mixed media, highest reactivity with the lowest saturated Al^{3+} concentration ($\sim$5 equiv.) compared to that obtained in pure methanol was observed in a 4 : 1 methanol/ethanol-mixed medium (Fig. S3†). Most probably, more effective H-bonding interaction of the dimeric ethanol/methanol[11] with **1** induces greater complex (**1**) stability, although the complex

[a]Department of Chemistry, Jadavpur University, Kolkata 700032, India. E-mail: parthaparui@yahoo.com; Fax: +91-33-24146223; Tel: +91-9433490492

[b]Department of Chemistry, Maulana Azad College, Kolkta 700013, India. E-mail: r_ambarish@yahoo.co.in; Fax: +91-33-22268111; Tel: +91-9836650180

† Electronic supplementary information (ESI) available. See DOI: 10.1039/d0ra00619j

‡ Department of Chemistry, Barasat Govt. College, Kolkata 700124, India
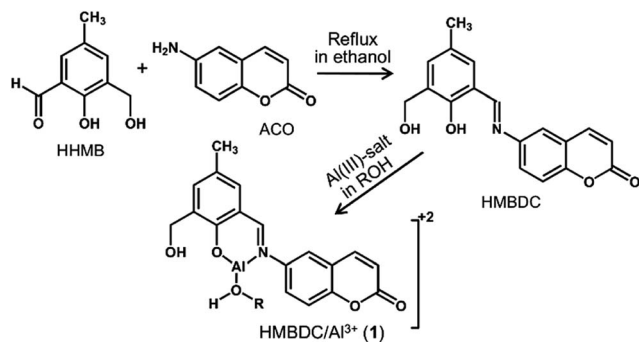
Scheme 1 Synthesis of HMBDC and its complexation with Al^{3+} in an alcohol solvent.

formation reactivity was much less in pure ethanol compared to the methanol medium (Fig. 1 and S2†).

In spite of the stronger H-bonding interactions of **1** with water compared to the methanol or ethanol, a complete dissociation of **1** in the presence of 20% (v/v) water in methanol (Fig. S4†) suggests that, in addition to the solvent assisted H-bonded structural stability of **1**, alcohol molecule may also participate in the coordination with Al^{3+} to form **1**. Indeed, the possible methanol coordination is reflected in the ESI-MS$^+$ analysis (Fig. S5B†). In addition, the Job's plots in the absorption studies showed that the HMBDC formed 1 : 1 stoichiometric complex with Al^{3+} (Fig. S6†). To elucidate the probable structure of **1**, we carried out the DFT-based theoretical calculation by considering the 1 : 1 stoichiometric Al^{3+}/HMBDC
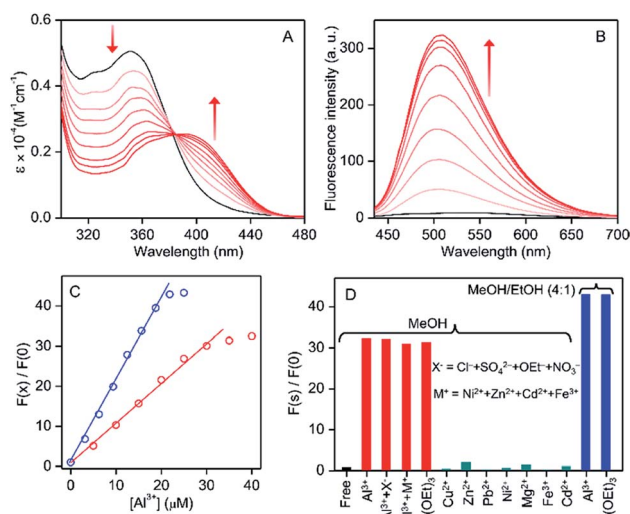
Fig. 1 (A) UV–vis absorption and (B) fluorescence spectra of HMBDC (5 μM) in the presence (red) and absence (black) of increasing concentration of $Al(NO_3)_3$ (0–40 μM) in anhydrous methanol at 25 °C. The intensity changes with increasing Al^{3+} concentrations are indicated by arrows. (C) Al^{3+} concentration dependent relative increase in the fluorescence intensity with respect to its absence in methanol (red) or methanol/ethanol (4 : 1) (blue). (D) Fluorescence intensity ratios in the presence and absence of various ions or mixture of ions in the mixed solvent (25 μM each; blue) or methanol (40 μM each; other colors) or are shown by bar-diagram.

complex with or without methanol coordination. A stable structure of **1** was obtained when the oxygen atom of the methanol molecule coordinates with Al^{3+} and other two coordination sites of Al^{3+} are occupied by the phenolic-oxygen and imine-nitrogen of HMBDC (Scheme 1, Fig. 2 and S7†). Facile coordination of those hard donor sites of HMBDC towards harder Al^{3+} is susceptible towards alcohol assisted stabilization of **1**. The UV-vis absorbance at ~402 nm for **1** computed from the time-dependent DFT (TD-DFT) calculations in methanol medium, where the HOMO (90) → LUMO (92) excitation nicely matched with the experimental absorbance at ~406 nm (Fig. 1 and 2). However, monitoring of the ^{1}H-NMR peak characterized for aldimine proton is a useful strategy to identify the bonding of the imine-N to Al^{3+}.[12] We observed that the aldimine proton peak intensity for HMBDC in CD_3OD was quenched to a great extent with a considerable down-field shift from 8.80 to 8.88 ppm in the presence of Al^{3+} (Fig. S8†); the down-field shift is expected owing to the imine-N and Al^{3+} coordination, but intensity quenching does not follow the previous trend in the aprotic polar medium.[12] The generation of a partial positive charge at the N-centre upon its binding with the Al^{3+} may enhance the acidity of the aldimine proton to become labile for participating in the H/D exchange in a protic medium (CD_3OD), as reported previously for other allied systems.[13] These results strongly suggest the imine-N and Al^{3+} bonding in **1**. On the other hand, Al^{3+} induced large decrease in the IR intensity at ~3300 cm^{-1} for phenolic-OH also supports the phenoxide coordination (Fig. S9†).

The electronic distribution in the molecular orbital diagram (MO) of the HMBDC evaluated from the DFT calculation showed an intra-molecular photo-induced electron transfer (PET) from coumarin to the HHMB moiety, which makes the HMBDC non-fluorescent (Fig. 2). Al^{3+} induced an instantaneous increase in the fluorescence intensity for HMBDC (5 μM) in the alcoholic medium (methanol/ethanol or their mixture) due to the formation of **1** (Fig. 1B and S10†). A gradual fluorescence intensity increase at ~506 nm (λ_{ex} = 406 nm) of ~30-fold for 8 equiv. of
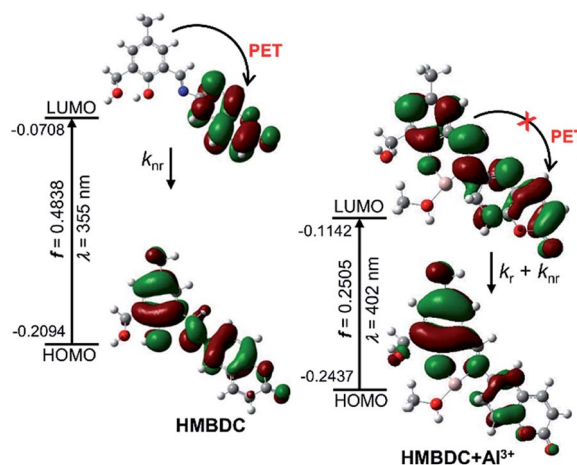
Fig. 2 Frontier molecular orbital profiles including various UV–vis absorption parameters of HMBDC (left panel) and HMBDC/Al^{3+} complex (right panel) based on TD-DFT (B3LYP/6-31G(d)).

Al^{3+} and ∼40-fold for 5 equiv. of Al^{3+} was observed in the methanol and 4 : 1 (v/v) methanol/ethanol medium, respectively (Fig. 1 and S10B†). According to the HOMO and LUMO electronic distributions for **1** in the DFT studies, the PET process in HMBDC was highly restricted upon its binding with Al^{3+} in **1**, causing for the large increase in the fluorescence intensity (Fig. 2). However, the better fluorescence response (lower intensity-saturated Al^{3+} concentration and larger intensity increase) in the mixed medium than pure methanol may be associated with greater stability of **1**, as described in the previous section (Fig. S2†). The fluorescence intensity increase remains invariant using other soluble Al(III)-salts (Fig. 1D and S11†), which eliminates the role of counter anions for the increasing intensity. To ascertain the Al^{3+} selectivity, we performed similar fluorescence studies with other potentially interfering cations but failed to produce any noticeable fluorescence (Fig. 1D and S12†). However, a linear intensity increase with the increase in the concentration of Al^{3+} up to 6 equiv. in methanol and 4 equiv. in the 4 : 1 methanol/ethanol mixed medium can be useful for a ratiometric detection of unknown concentration of Al^{3+} (Fig. 1C), where the limit of detection[14] (LOD) of Al^{3+} with HMBDC in the methanol medium was found to be ∼0.5 μM (*c.f.* details in ESI†). Most importantly, HMBDC recognized Al^{3+} selectively from the mixture of various other cations, and also in presence of other soluble Al(III) salts, particularly, aluminium alkoxide (ethoxide) with similar accuracy (Fig. 1D and S12†). Therefore, the Al(III) sensing ability for an alcoholate corrosion with an aluminium alloy must not be perturbed due to the interference of other leached cations.

The dry alcoholate corrosion of aluminium or its alloy while forming soluble alkoxide (Al(OR)$_3$) can be detected upon incubation in an anhydrous alcoholic medium. However, under a condition of prolonged incubation, the contamination of trace amounts of moisture may also trigger the conversion of Al(OR)$_3$ to Al(OH)$_3$, followed by the hydrated alumina (Al$_2$O$_3$·xH$_2$O) coating on the metallic surface.[6] The formation of hydrated alumina can also be possible *via* the decomposition of Al(OR)$_3$.[6] To characterize the alcoholate corrosion as an exclusive process to the maximum limit, we minimized those wet-processes by allowing the corrosion under inert conditions. A previously grazed aluminium-sheet (dimension ∼3.5 × 1.5 × 0.2 cm^3; surface area ∼12.5 cm^2) was incubated for 18 days in 100 mL anhydrous methanol or methanol/ethanol (4 : 1) mixed solvent under nitrogen atmosphere by purging nitrogen every 24 h, where the small change in the solution volume if required was adjusted by injecting an appropriate amount of the nitrogen-saturated anhydrous solvent. The amount of Al(OR)$_3$ (R = -Me, -Et) generated in the medium was estimated by monitoring the HMBDC (5 μM) fluorescence. After 10-fold dilution of the medium with the parent solvent, the amount of Al(OR)$_3$ formed or the alcoholate corrosion was estimated in every 3 days interval according to the amount of Al^{3+} obtained from the time-dependent fluorescence responses (Fig. S13†) as per the linear calibration plots in Fig. 1C multiplied by the dilution factor. A linear increase in the normalized fluorescence intensity from ∼3.5 to 16.8 and ∼7.3 to 36.1 was observed with an increase in the incubation time period from 3 day to 18 day for methanol and methanol/ethanol (4 : 1) media (Fig. 3A and S13†),

respectively, which correspond to the linear increase in the Al^{3+} amount in the medium from ∼3.2 to 16.6 μmol for either solvents (Fig. 3C). Indeed, the weight-loss of ∼0.47 mg *i.e.*, ∼17.5 μmol was found to be closely similar with that of the increase in Al^{3+}, revealing that not only the dry corrosion leads to the generation of Al^{3+} (Al(OR)$_3$) as the only product, but also HMBDC is highly effective for an accurate estimation of the alcoholate corrosion. In addition, the nice correlation between the weight-loss and Al(OR)$_3$ amount also reveals that the decomposition of alkoxide into insoluble alumina is negligibly small during the whole corrosion time-course.

However, under open atmospheric conditions maintained by air purging (average relative humidity ∼70%; average temperature 28 °C) in every 24 h interval while maintaining other similar experimental conditions and analysis protocol, the specific corrosion rate (∼2.0 μg per day per cm^2) up to 12 days, was found to be closely similar to that detected under the nitrogen atmosphere (Fig. 3C and S13†). The results also indicate that the early stage of the alcoholate corrosion process (at least up to 12 days) for pure aluminium is not affected significantly by the atmospheric moisture content, although the final corrosion amount after 18 days incubation in normal atmosphere was slightly lower (∼84%) for the mixed medium compared to that obtained for pure methanol (Fig. 3C). The decrease in the Al(OR)$_3$ amount can be affected by two
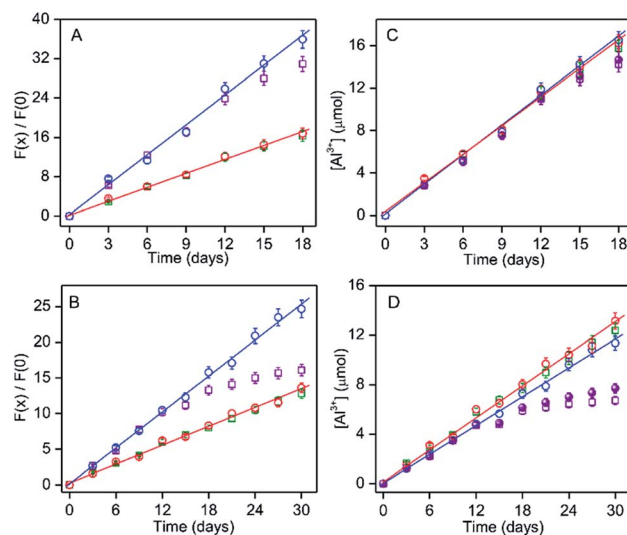
Fig. 3 (A and B) Extent of the fluorescence intensity increase due to corrosion-induced leached Al^{3+} ($F(x)/F(0)$) of HMBDC (5 μM) and (C and D) amount of Al^{3+} in the corrosion medium according to fluorescence response are plotted with various incubation times of pure aluminium sheet or its alloy (Al-7075) in different mediums/atmosphere conditions: nitrogen atmosphere in methanol (red) and methanol/ethanol (4 : 1) (blue); open atmosphere in methanol (green) and methanol/ethanol (4 : 1) (purple). The data at nitrogen conditions are only fitted linearly. (A and B) The fluorescence intensity of HMBDC (5 μM) were monitored after the 10-fold dilution of the corrosion medium with the same solvent. (C and D) The amount of Al^{3+} estimated as the amount obtained from the normalized intensity with comparing the linear plots in Fig. 1C multiplied by the dilution factor 10. The actual amount of alcoholate corrosions for the mixed medium under open atmosphere are depicted by solid circle (purple).

processes: (a) $Al(OR)_3$ to insoluble $Al(OH)_3$ conversion due to the adsorbed moisture; (b) actual retardation of the corrosion rate due to the surface deposition of $Al(OH)_3$. The extent of the conversion of $Al(OR)_3$ to $Al(OH)_3$ in the corrosion medium under the open air condition can be assessed by estimating the fluorescence intensity at every 3 day time interval in the absence of aluminium sheet (from day-3 to day-18) with the addition of same amount of $Al(OEt)_3$ (3.2, 5.7, 8.0, 11.7, 14.2 and 16.4 μmol (final added amount) at day 0 (beginning of day 1), 3, 9, 12 and 15, respectively, in 100 mL mixed medium) as that of the alkoxide amount detected due to the corrosion under nitrogen condition (Fig. S14†). In comparison to the actual added $Al(OEt)_3$, any decrease in the $Al(OEt)_3$ amount upon such incubation should be added with the corrosion induced formation of $Al(OR)_3$ amount under nitrogen condition for respective time interval to obtain the actual alcoholate corrosion. The actual corrosion was found to be slightly higher than that estimated from the corrosion-induced $Al(OR)_3$ formation (Fig. 3C, solid symbol). According to the LOD of Al^{3+}, the detection of the alcoholate corrosion amount as minimum as $\sim$0.1 μg mL^{-1} can be possible by monitoring the fluorescence response of HMBDC.

Alcoholate corrosion in a widely used aluminium alloy, Al-7075 (composition: Al, 90%; Zn, 5.5%; Mg, 2.5%; Cu, 1.5 and Si, 0.5%) was also studied. The previously grazed alloy sheet with same dimension and surface area as that of the pure aluminium sheet was incubated in 100 mL anhydrous methanol or 4 : 1 methanol/ethanol under nitrogen as well as normal atmospheric conditions. The amount of the alcoholate corrosion in every 3 days interval up to 30 days was estimated by evaluating the fluorescence response of HMBDC (Fig. 3B and S15†). In comparison to the pure aluminium sheet, the increase in corrosion from $\sim$1.5 to 4.0 μmol evaluated from the increase in the normalized fluorescence intensity (1.65 to 5.90 in methanol; 2.64 to 10.40 in methanol/ethanol (4 : 1) mixture) with the increase in the incubation time from day-3 to day-12 follows a similar linear relation regardless of the solvent compositions and atmospheric conditions (Fig. 3B and D), while the intrinsic rate of corrosion $\sim$0.95 μg per day per cm^2 was more than 2-fold slower (Fig. 3C and D). The lower rate constant value for the alloy compared to pure aluminium indicates that the contamination of other metals in the alloy resists the early stage alcoholate corrosion process. However, under normal atmospheric condition, the corrosion amount *vs.* time relation deviates from the linearity after 12 days. Importantly, after 30 days of incubation, a large reduction in the $Al(OR)_3$ amount from $\sim$11.38 to 6.64 μmol was estimated for the mixed medium, but the change was only from $\sim$13.20 to $\sim$12.33 μmol for pure methanol (Fig. 3D). By determining the hydration-induced conversion amount of $Al(OR)_3$ to $Al(OH)_3$ according to the procedure, as described before (Fig. S16†), the actual alcoholate corrosion was found to decrease from $\sim$11.38 to 7.70 μmol by changing the condition from nitrogen to open atmosphere after 30 days (Fig. 3D, solid symbol). Our study reveals that in comparison to pure methanol, the formation of $Al(OH)_3$ under open atmospheric condition retards the alcoholate corrosion largely due to the presence of more hygroscopic ethanol.[15] The deposition of $Al_2O_3 \cdot xH_2O$ onto the alloy-surface is responsible for resisting the further alcoholate corrosion[6] (Fig. 3D).

In fact, the generation of more surface pits owing to the higher extent of the alcoholate corrosion in methanol over the mixed medium was also detected by naked eye (Fig. S17†). The surface morphology in the SEM studies showed that the alloy surface was little bit smoother after the corrosion in the mixed medium (Fig. S18†), justifying our proposition for the surface deposition of $Al_2O_3 \cdot xH_2O$. On the other hand, cyclic voltammetric studies in the corrosion medium exposed to normal atmospheric conditions identified an irreversible cathodic peak at $\sim$−0.7 V due to the formation of insoluble $Al(OH)_3$ in addition to the conversion from Al to Al^{3+}, but such irreversible peak was not observed for the medium exposed to nitrogen (Fig. S19†). Moreover, the formation of white gelatinous precipitate of $Al(OH)_3$ in the mixed medium was clearly visible by naked eye under normal atmospheric conditions (Fig. S17B†). All those results strongly support that the initiation of the wet-process by forming $Al(OH)_3$ inhibits the alcoholate corrosion rate.

In conclusion, a phenolic Schiff-base consisting of a coumarin unit as a fluorescent sensor for Al^{3+} operable only in the alcoholic medium is synthesized to monitor dry alcoholate corrosion. The photo-induced electron transfer process in the probe molecule exhibits Al^{3+} induced large increase of fluorescence intensity, lifted by its complexation with Al^{3+}, which was further stabilized by the coordination and H-bonding interaction with the solvent molecule. The alcohol specific complex formation and subsequent fluorescence generation was suitably tuned to monitor the alcoholate corrosion by fluorometrically estimating aluminium alkoxide formation with a sensitivity of $\sim$10 μg L^{-1}. However, the simultaneous participation of small extent of the wet-process ($Al(OR)_3$ to $Al(OH)_3$ conversion) and its deposition in metal surface, particularly for the alloy, inhibits the dry alcoholate corrosion. The alloy specific detection of the early stage alcoholate corrosion is in progress to obtain suitable material useful as a biofuel container.

Conflicts of interest

There are no conflicts to declare.

Acknowledgements

Notes and references

1 (*a*) J. Xuan, D. Y. C. Leung, M. Ni and M. K. H. Leung, *Renew. Sustain. Energy Rev.*, 2009, **13**, 1301; (*b*) F. H. Shinya and Y. KenjiImou, *Bioresour. Technol.*, 2010, **101**, 109.

2 (*a*) L. Matejovsky, J. Macak, M. Pospisil, P. Baros, M. Stas and A. Krausova, *Energy Fuels*, 2017, **31**, 10880; (*b*) R. H. Borgwardt, *Ind. Eng. Chem. Res.*, 1998, **37**, 3760; (*c*) B. Shayan, S. M. Seyedpour, F. Ommi, S. H. Moosavy and

M. Alizadeh, *Int. J. Automot. Mech. Eng.*, 2011, **1**, 3; (*d*) J. H. Lunsford, *Catal. Today*, 2000, **63**, 165.

3 M. B. Çelik, B. Ozdalyan and F. Alkan, *Fuel*, 2011, **90**, 1591.

4 K. Wagner, K. Eppel, T. Troßmann and C. Berger, *Energy Mater. Mater. Sci. Eng. Energy Syst.*, 2008, **3**, 227.

5 K. Eppel, M. Scholz, T. Troßmann and C. Berger, *Proceedings: EUROCORR*, 2009, Nice, p. 9.

6 J. Linder, thesis on, Alcoholate corrosion of aluminium in ethanol blends, Master thesis, KTH Royal Institute of Technology, Div. Surface and Corrosion Science, Stockholm, 2012.

7 (*a*) P. B. L. Fregolente, M. R. Wolf Maciel and L. S. Oliveira, *Braz. J. Chem. Eng.*, 2015, **32**, 895; (*b*) S. K. Thangavelu, A. S. Ahmed and F. N. Ani, *Int. J. Energy Res.*, 2016, **40**, 1704.

8 (*a*) L. Kruger, F. Tuchscheerer, M. Mandel, S. Muller and S. Liebsch, *J. Mater. Sci.*, 2012, **47**, 2798; (*b*) O. Seri and Y. Kido, *Mater. Trans.*, 2009, **50**, 1433; (*c*) Corrosion resistance of aluminium and protective measures where appropriate, First Edition: 2011 © AFSA Compiled and published by the Aluminium Federation of South Africa; (*d*) G. R. Kramer, C. M. Mendez and A. E. Ares, *Mat. Res.*, 2018, **21**, 1.

9 (*a*) S. Das, Y. Sarkar, S. Mukherjee, J. Bandyopadhyay, S. Samanta, P. P. Parui and A. Ray, *Sens. Actuators, B*, 2015,

209, 545; (*b*) P. P. Parui, A. Ray, S. Das, Y. Sarkar, T. Paul, S. Roy, R. Majumder and J. Bandyopadhyay, *New J. Chem.*, 2019, **43**, 3750; (*c*) P. A. Anna, P. Paul and W. R. David, *Anal. Chem.*, 1997, **69**, 1635.

10 (*a*) A. Gupta and N. Kumar, *RSC Adv.*, 2016, **6**, 106413; (*b*) Q. Jiang, M. Li, J. Song, Y. Yang, X. Xu, H. Xu and S. Wang, *RSC Adv.*, 2019, **9**, 10414; (*c*) H. L. Nguyen, N. Kumar, J.-F. Audibert, R. Ghesami, J.-P. Lefevre, M.-H. Ha-Thi, C. Mongin and I. Leray, *New J. Chem.*, 2019, **43**, 15302.

11 I. A. Finneran, P. B. Carroll, G. J. Mead and G. A. Blake, *Phys. Chem. Chem. Phys.*, 2016, **18**, 22565.

12 S. Sahana, S. Bose, S. K. Mukhopadhyay and P. K. Bharadwaj, *J. Lumin.*, 2016, **169**, 334.

13 (*a*) R. Casasnovas, M. Adrover, J. Ortega-Castro, J. Frau, J. Donoso and F. Muñoz, *J. Phys. Chem. B*, 2012, **116**, 10665; (*b*) B. Setner, M. Wierzbicka, L. Jerzykiewicz, M. Lisowski and Z. Szewczuk, *Org. Biomol. Chem.*, 2018, **16**, 825.

14 V. Thomsen, D. Schatzlein and D. Mercuro, *Spectroscopy*, 2003, **18**, 112.

15 B. Tan, P. Melius and P. Ziegler, *J. Chromatogr. Sci.*, 1982, **20**, 213.

PAPER

Check for updates

An inquisitive fluorescence method for the real-time detection of trace moisture in polar aprotic solvents with the application of water rancidity in foodstuffs†

Snigdha Roy,[a] Sanju Das,[b] Ambarish Ray[c] and Partha Pratim Parui (ID) *[a]

A simple analytical technique for detection of trace water in organic solvents is indispensable for moisture-free organic synthesis, environmental research, and food monitoring industry. Using a simple 4-methyl-2,6-diformyl phenol molecule (AH), we report the convenient fluorometric detection of trace water in various polar aprotic organic solvents having detection limits within 0.01–0.04% (v/v). Phenolate-oxygen of deprotonated AH (A⁻) forms an H-bond with a water molecule to exhibit a large spectral blue-shift from ∼485 to 440 nm in the UV-vis absorption or fluorescence excitation spectra, while unchanged emission characteristics were detected apparently due to dissociation of the H-bond in the excited state. The gradual blue-shift of the excitation band with the increase in water% (v/v) in the solution affects an opposite emission intensity changing behavior, from an increasing to a decreasing trend, due to the change in the excitation wavelength from 440 to 485 nm. Emission intensity changes of free A⁻ and A⁻/H_2O H-bonded species for each water addition are combined together for the spectral normalization to achieve water% induced a highly manifested linear emission response. The improved sensitivity allows us to quantify real-time atmospheric moisture incorporations in various polar aprotic solvents. The normalized emission intensity does not depend on AH concentration, and thus the water detection process is very effective for the estimation of water% in the solution with heterogeneous probe distributions. With this advantage, we succeed to estimate water% in various moisture-sensitive edible oils and dairy foods produced from water-rich raw materials. Therefore, the method can be applied to prevent water rancidity in foods with greater than its permissible limits *via* identifying higher moisture contamination.

Introduction

An effective analytical procedure for the estimation of trace water in organic solvents displays a direct impact in chemical research, industry and food inspection.[1–5] For organic synthesis, in particular the synthesis of organometallic compounds, moisture-free solvents are essential to obtain the optimum product yield.[6,7] Carboxylic ester and imine functional compounds are highly susceptible to hydrolysis even in the presence of trace amounts of moisture during their storage in organic solvents.[8] The moisture contamination in oil can be a major problem in the petroleum industry due to emulsification and phase separation processes,[9,10] resulting in the blockage of fuel pipe, and subsequent engine damage or failure.[11,12] Furthermore, the estimation of water in food samples is very important for various reasons:[13–17] (a) optimum moisture level in foods is essential for to sustain an appropriate test, texture and appearance, and most vital nutritional values; (b) food manufacturers often incorporate inexpensive water ingredients illegally as much as possible in foods for their profit; (c) trace water affects microbial food degradation or water rancidity, especially for pure oil-based food materials;[15–17] (d) food processing operations such as transferring through pipes, packaging and mixing also affect the estimation.

The Karl Fischer titration is one of the best known methods for the estimation of moisture in organic solvents.[18] Gas chromatography is another well-acquainted classic option.[19,20] However, certain limitations in those methods such as time consumption, inability for real-time analysis, specialized equipment design requirement, difficulties in sample preparation, and rigorous data handling are major concerns for easy and cost-effective moisture

[a] *Department of Chemistry, Jadavpur University, Kolkata 700032, India.*
  E-mail: parthaparui@yahoo.com; Fax: +91-33-24146223; Tel: +91-9433490492
[b] *Department of Chemistry, Maulana Azad College, Kolkata 700013, India*
[c] *Department of Chemistry, Barasat Govt. College, Kolkata 700124, India*
† Electronic supplementary information (ESI) available. See DOI: 10.1039/d0nj06046a

detection for applied analytical samples.[21,22] Fluorescence technique may opt as a better alternative owing to its simplicity and rapid response, and non-destructive fabrication and most importantly its high sensitivity.[23–25] Consequently, a number of research groups currently switch their focus to various kinds of commercially viable fluorescence-based water sensing procedures. Up to now, a number of fluorosensing mechanisms, such as intramolecular charge transfer (ICT),[26,27] photo-induced electron transfer (PET),[1,28] excited-state intramolecular proton transfer (ESIPT),[29,30] hydrogen-bonding interaction,[5,31,32] aggregation-induced emission (AIE)[33–35] or Förster resonance energy transfer (FRET),[36,37] have been reported to detect trace water in organic solvents. Water fluorosensors based on chemical rearrangements such as ring-opening of cyclic rhodamine derivatives,[38] hydrolytic cleavage of Schiff bases[39,40] and hydration of aldehyde functionality[41] have also been reported. In addition, researchers constructed various metal/ligand complexes or metal organic frameworks (MOFs)[42,43] as water fluorosensors.

Among the various water sensing fluorescent probe molecules reported in the literature, some exhibit very high detection sensitivity ($\sim$0.001% or even below), although often the high detection accuracy is restricted to specific solvent systems.[14,44–46] However, the requirement of multi-step complex synthesis procedures for the preparation of probe molecules makes the overall moisture detection procedure inconvenient for routine analytical purpose.[34,37,41–43] In most cases, the detection methodologies are relying only upon a single emission/excitation band originated by the association/interaction of water with the recognition site of a probe molecule.[26–32,34–38,41,42] Therefore, it is not always straightforward to recognize the actual cause for the observed fluorescence response between the inhomogeneous probe distribution in the solution due to sample micro-heterogeneity and any moisture affected changes. In addition, photobleaching of the probe molecule and instrumental parameters[44] are often troublesome to assess the actual fluorosensing response induced by water incorporation.

In this study, a simple 4-methyl-2,6-diformyl phenol fluorescent probe (AH) was exploited to detect trace water in several polar aprotic organic solvents with high precision (detection limit $\sim$0.01–0.04% (v/v)). The phenolate form of the probe molecule (A^-) exhibits a water-induced spectral blue-shift to various extents in the UV-vis absorption and fluorescence excitation spectra from $\sim$470–490 nm to 440–450 nm depending on various polar aprotic organic solvents due to the formation of an A^-/H_2O H-bonded complex. Although both A^-/H_2O and free A^- show identical fluorescence emission characteristics, an opposite emission intensity changing pattern, from a gradually increasing to a decreasing trend with the increase in water%, was detected upon switching the excitation wavelength from 440 to 485 nm. Water induced emission intensity changes of A^- and A^-/H_2O species for each water% value were combined together to obtain a normalized single spectral profile, and thus the water% induced emission increase manifested considerably with eliminating the probe concentration dependency on the intensity response. Moreover, such normalization eventually produces linear intensity changes dependent on water%, which are effective

to estimate water% ratiometrically. In addition, a large spectral blue-shift of $\sim$25 nm in the excitation spectra induced by only a small quantity of water (2–5% v/v) can also be suitably tuned for its detection purpose. The water detection procedure was applied to monitor real-time atmospheric moisture incorporation in common polar aprotic solvents and moisture analysis studies in various food samples useful for water rancidity.

Experimental

Chemicals and general methods

Chemicals of analytical grade were purchased from different commercial sources. The chemical 4-methyl-2,6-diformyl phenol (AH) was synthesized according to a published procedure starting from p-cresol[47] (Sigma Aldrich (USA)), and the purity was checked by ^{1}H-NMR studies (Fig. S1, ESI†). Different commercially available food samples (butter, cheese, ghee and coconut oil) were collected from different local market sources. Molecular sieves of 3 Å pore size were obtained from Sigma-Aldrich (USA). HPLC-grade solvents (methanol, ethanol, acetone, MeCN, DMF and DMSO) and triethyl amine (TEA) were purchased from Sigma-Aldrich (USA), and the solvents were further dried over the 3 Å molecular sieves.[21] The solvents were stored in a dry nitrogen atmosphere in the presence of the molecular sieves. Throughout all experimental studies, Milli-Q water (Millipore) of conductivity 18.2 MΩ cm was used. ^{1}H-NMR studies were performed in DMSO-d_6 using a Bruker 300 MHz NMR spectrophotometer considering tetramethylsilane (0 ppm) as an internal standard.

UV-vis absorption and fluorescence studies

UV-vis absorption spectra were monitored using a 1 cm path-length quartz cell with a double-beam spectrophotometer (Shimadzu, Japan; model TCC-240A) equipped with a thermostatted cell holder. Steady-state fluorescence studies were carried out using a Perkin-Elmer LS-55 spectro-fluorimeter (PerkinElmer, USA) using a 1 cm path-length quartz cell. Fluorescence excitation and emission spectra were recorded for the fixed emission at 525 nm and excitation at 440 or 485 nm, respectively (excitation band pass: 11; emission band pass: 4). The measuring solutions were filtered using a 0.45 mm filter (Millex, Millipore). The spectral reproducibility was checked by measurements in triplicat.

The phenolic-OH deprotonated form of AH (A^-) acting as the actual water sensing probe was generated by addition of base (KOH or TEA) in different solvents. For the detection of water in polar aprotic solvents (acetone, MeCN, DMF and DMSO), the fluorescence spectral studies for A^- were monitored in the absence and presence of various water% (v/v) values.

The fluorometric limit of detection (LOD) for water was obtained using the following equation:[48]

$$\text{Detection limit (LOD)} = 3\sigma/k,$$

where σ and k represent the experimental standard deviation and slope value of the linear fitting curve, respectively.

The fluorescence quantum yield for the A^- form of AH (AH (0.5 μM + KOH (10 μM))) was evaluated according to the

procedure described earlier.[49] In brief, 9,10-diphenylanthracene in an ethanol medium was used as the reference fluorophore with an emission quantum yield (Φ_F^r) = 0.95. The Φ_F was estimated using the following equation:

$$\Phi_F^s = [A_r F_s n_s^2 / A_s F_r n_r^2] \Phi_F^r$$

where A represents the absorbance at the excitation wavelength, and the integrated emission area is designated by F. n is the refractive index of the medium. Subscripts refer to the reference (r) or sample (s) molecule.

Fluorescence transient decays were monitored by the time-correlated single-photon counting (TCSPC) method. Two separate nano-second diodes with excitation at $\sim$450 and 490 nm respectively (nano-LED; IBH, UK) were used as the light source. Fluorescence decays were monitored using a special Hamamastu photomultiplier tube (PMT) coupled with TBX4 detection module (IBH, UK). The solutions for analysis were passed through a 0.45 μm filter (Millex, Millipore) before all the experiments. All measurements were repeated at least three times to check the reproducibility. The decays were analyzed using the in-built software.

Theoretical calculations

To identify the solution structure of the hydrogen-bonded A^-/H_2O complex, density function theoretical (DFT) calculations were performed using the Gaussian 09 Program.[50] Furthermore, time-dependent DFT (TD-DFT) calculations were carried out to obtain UV-vis absorption parameters. The structural optimization was carried out by considering the B3LYP exchange–correlation functional. The 6-31G++(3d,3p) basis was set and the geometries were optimized in the solvent phase. The global minima of all these species were confirmed by the positive vibrational frequencies. The TD-DFT calculation in different solvents with the CPCM solvent model was performed to obtain the electronic properties of the singlet excited state using optimized geometries of the ground states (S_0) of the relevant species, along with the determination of vertical excitation energy and oscillator strength of the respective ground-state geometry.

Atmospheric moisture incorporation studies

First, 40 mL of dry acetone, MeCN, DMF and DMSO were taken separately in a 100 mL dry beaker with a diameter of $\sim$5 cm. Each solvent was incubated under open laboratory conditions with 75% ($\pm$5%) relative humidity at 25 $^\circ$C ($\pm$1 $^\circ$C) for different time intervals (12 to 120 min). To estimate atmospheric moisture incorporation in the medium, steady-state fluorescence emission and excitation spectra were monitored by addition of AH (0.5 μM) with KOH (10 μM) in the laboratory-exposed solvents at different intervals of time (12 to 120 min). For acetone and MeCN solvents, the effects of small amounts of solvent evaporation during the exposure in the open atmosphere on the moisture incorporation values evaluated from the fluorescence response at different time intervals were included to find the time-dependent actual moisture incorporation values.

Moisture detection in food samples

All the food samples (butter, cheese, ghee and coconut oil) were collected from local markets. The food samples were stored at 4 $^\circ$C in the same commercial seal container until use for the moisture analysis studies. To extract free moisture present in food samples, various amounts of different food samples were mixed separately with 100 mL DMSO in a stoppered container under dry nitrogen conditions at room temperature (25 $^\circ$C). Then, each mixture was heated at 60–70 $^\circ$C to completely liquefy the food samples, followed by vigorous vortexing at the same temperature for 10 min to relocate all the free water from the food sample to the DMSO medium. Then, the solution was settled until complete separation of the DMSO phase from the rest of the solution. The DMSO phase was separated using a separating funnel, and the fluorescence studies were conducted in the DMSO phase by addition of AH (0.5 μM) and KOH (10 μM).

Results and discussion

Solvent-induced spectral shifts of the phenolate form of AH

AH deprotonated partially around neutral pH ($pK_a \sim 7.1$) in an aqueous buffer according to the pH-dependent changeover of UV-vis absorption intensities between $\sim$350 nm for the phenol form (AH) and $\sim$440 nm for the phenolate form (A^-) (Fig. S2, ESI†). A^- exhibited a strong fluorescence intensity (quantum yield (Φ) $\sim$ 0.4) (cf. Experimental section), but AH did not (Fig. S3, ESI†).[51] Consistent with the earlier reports, an additional absorption intensity at $\sim$485 nm with appreciable quenching of the intensity at $\sim$350 nm for AH (6 μM) was identified in the DMF or DMSO medium even in the absence of the base[52,53] (Fig. S4A, ESI†). The appearance of band at $\sim$485 nm is mainly due to partial deprotonation of AH induced by the basic solvent character,[54] since the spectral shape and position did not change except a large increase in its intensity by an addition of base (KOH, 15 μM) in DMF or DMSO (Fig. S4B, ESI†). This proposition is further supported by the base-induced similar spectral shift from $\sim$350 nm to 470–480 nm for other non-basic aprotic solvents (acetone, MeCN) (Fig. S4B, ESI†). However, similar to the aqueous medium, a large blue-shifting of absorption band from 470–485 nm to 440–435 nm for the phenolate form (A^-) was detected by changing the medium from aprotic to protic methanol or ethanol (Fig. S5, ESI†). Previously, the solvent-induced large spectral blue-shift has been justified with presuming higher dipole moment of DMSO/DMF than the water molecule.[53] However, since the solvent-dependent absorption spectral shift is usually very nominal, the large spectral blue-shift is attributed to a specific A^-/solvent interaction (Fig. 1 and Fig. S5, ESI†).

Formation of A^-/H_2O complexes in aprotic solvents

The phenolic-OH deprotonated form of AH (A^-) was confirmed with forming UV-vis intensity at 470–485 nm by addition of any base (KOH or TEA) to polar aprotic solvents (Fig. 1). However, TEA (THF-solubilized base) induced no spectral change in a relatively nonpolar THF medium, suggesting no such deprotonation
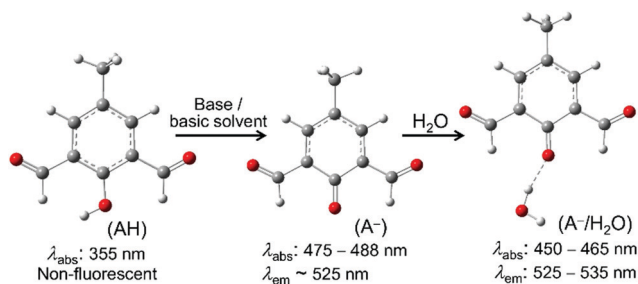
Fig. 1 Schematic of base or basic solvent (DMSO/DMF)-induced complete/partial deprotonation of AH (A$^-$) and its H-bonding interaction with water. The DFT-optimized structures are shown (color index: C, gray; O, red; and H, white). The experimental UV-vis absorption (λ_{abs}) and emission (λ_{em}) wavelengths for different species are depicted in the lower panel. (cf.) The calculated absorption parameters are shown in Table 1.

reaction of AH (Fig. S6, ESI†), presumably due to poor solvation of the negatively charged A$^-$ species. The water-induced large blue-shift of the absorption band for A$^-$ shows the interaction of A$^-$ with the water molecule (Fig. 2). A similar UV-vis spectral blue-shift by water interaction was reported by C. Pinheiro et al.[6] Instead, the presence of water causes no spectral changes for the protonated AH form (Fig. S7, ESI†), which excludes the possibility of water/AH interaction. Most probably, the large negative charge density at phenolate-O in A$^-$ may induce efficient H-bonding affinity with the water molecule to form an A$^-$/H$_2$O complex.

To avoid any significant change of general solvent properties, UV-vis absorption spectral changes of A$^-$ (AH (6 µM) + KOH (15 µM)) in different polar aprotic solvents (acetone, MeCN, DMF and DMSO) were monitored in the presence of low amounts of water up to ~6–12% (v/v). With the increase in water% in solvents (0.1–6.0 for acetone, 0.1–8% for MeCN, 0.1–12% for DMF and 0.3–12% DMSO), the absorption band of A$^-$ gradually

Fig. 2 UV-vis absorption spectra of AH (6 µM) in the presence of KOH (15 µM) and various water% (v/v) in different solvents: (A) acetone (water%: 0.1, 0.3, 0.6, 1.0, 1.5, 2.0, 3.5, 6.0, 8.5 and 11.0); (B) MeCN (water%: 0.1, 0.3, 0.6, 1.5, 2.5, 6.5 and 9.0); (C) DMF (water%: 0.1, 0.4, 1.0, 1.5, 2.7, 4.8, 6.5, 8.5 and 10.0) and (D) DMSO (water%: 0.3, 0.9, 1.4, 2.0, 3.2, 5.1, 6.3, 8.5, 6.3, 10.0 and 12.3). (A–D) The gradual spectral blue-shift with the increase in water% is depicted by arrows. The spectra in the absence of water are shown in black.

blue-shifted from 475 to 488 nm maximally up to ~445–450 nm (Fig. 2). The spectrum at the highest water% for each aprotic solvent was found to be closely similar to that obtained in a pure aqueous medium (Fig. 2 and Fig. S5, ESI†). Upon reverse solvent addition, i.e., each aprotic solvent (~10% (v/v)) in an aqueous medium causes an insignificantly small spectral wavelength shift (Fig. S8, ESI†), indicating that A$^-$ involves a specific interaction with water in the aprotic solvents. Notably, the observed small spectral changes between the aprotic medium in the presence of the highest water% and in pure water can be explained by their general solvent properties, even though the same species, namely, A$^-$/H$_2$O complex, can be expected in both types of solvents (Fig. 2 and Fig. S8, ESI†). However, the replacement of water with other protic solvents such as methanol or ethanol, in the aprotic solvents showed a similar spectral blue-shift up to ~435 nm (Fig. S9, ESI†), while the blue-shift requires much higher alcohol% (~23–25% (v/v)) than water% (6–12%) presumably due to weaker interaction ability of A$^-$ with the alcohol molecules. Most probably, A$^-$ participates in the H-bonding interaction with water molecules, which may increase the $S_0 \rightarrow S_1$ transition energy for the phenolate chromophore moiety to attribute for the 30–50 nm spectral blue-shift (Fig. 1). Since the water molecule itself participates in the H-bonding interaction with large affinity in the aprotic solvents, the fraction of H-bonded A$^-$ was found to be enhanced with the increase in water% due to the formation of more number of A$^-$/H$_2$O H-bonded complexes than its dissociation affected by the increased ratio of the water amount in the solvent composition.

The H-bonding interaction of A$^-$ with water molecules was also examined by steady-state and time-resolved fluorescence methods. The deprotonated A$^-$ species exhibited a strong emission intensity at 525–535 nm in different solvents (acetone, MeCN, DMF, DMSO and water) (Fig. S10, ESI†). The excitation spectra of deprotonated A$^-$ for the emission at 525 nm showed an intensity at 470–490 nm for different aprotic solvents, whereas in the water medium the peak shifted to ~440 nm (Fig. S11, ESI†), which is consistent with the observed absorption wavelength shift by changing an aprotic to water medium (Fig. 2 and Fig. S5, ESI†). Similar to the absorption studies, the fluorescence excitation band gradually blue-shifted up to ~445–450 nm by a gradual increase in water% up to 6–12% (v/v) in different aprotic solvents (Fig. 2 and Fig. S12, ESI†). These results corresponded well with that interpreted from the absorption studies for the formation of the H-bond in the A$^-$/H$_2$O complex (Fig. 1). However, no emission wavelength shift under a particular water% value in the aprotic media was detected by the change in the excitation wavelength from 440 to 485 nm (Fig. S13, ESI†). The result indicates that the emissive properties are similar between free A$^-$ and A$^-$/H$_2$O H-bonded complexes.

Different water%-dependent fluorescence transient decays for A$^-$ in the aprotic solvents were monitored at 530 nm for excitations at ~450 nm and ~490 nm. For either excitation, a mono-exponential decay with unchanged fluorescence lifetime (τ) values was noticed at each water% value (Fig. 3 and Fig. S14, ESI†), where the τ value was found to increase gradually with

Fig. 3 Excitation wavelength-dependent fluorescence transients of AH (6 μM) in the presence of KOH (15 μM) in acetone under various water% (v/v) values (water%: red, 1.0%; orange, 2%; green, 4%; purple, 8%). Excitation wavelengths were (A) 450 nm and (B) 490 nm. (A and B) The transient decay in pure water and acetone media is shown in blue and black, respectively, for comparison. The emission collected at 525 nm both excitation wavelengths. The scattering profile is shown in grey.

the increase in water% from 0 up to 8%; from ~3.3 to 5.7 ns for acetone, ~3.8 to 5.7 ns for MeCN, ~3.8 to 5.9 ns for DMF and 4.1 to 5.9 ns for DMSO (Table 1). The similar τ value between two different excitations (450 and 490 nm) especially when the A^-/H_2O complex and free A^- coexist at the water% value below 4% strongly justify our proposition that the emission of the A^-/H_2O complex originated from the excited state of free A^- after breaking of the H-bond in the excited state (Fig. 4 and Fig. S14, ESI†). However, an expected stronger electrostatic interaction of A^- with the water molecule than any of those aprotic solvent molecules may increase the local water concentration surrounded to A^- largely than remaining of the solution even for a small increase of water% in the solution. Presumably, the higher water accumulation around A^- may affect greater solvation induced its higher excited state stability to observe the gradual increase in the τ value with the increase in the water% value. Moreover, the τ value for the A^- species in a pure aqueous medium is ~4.7 ns which is significantly lower than that observed in various aprotic solvents containing 8% water (~5.9 ns) probably due to a significant decrease in non-radiative decay rate from the aprotic solvents to water (Fig. 3, Fig. S14, ESI† and Table 1).

Theoretical studies for H-bonding interaction in A^-/H_2O

To identify the probable H-bonding mode in the A^-/H_2O complex, DFT-based theoretical calculations were performed

Table 1 Emission lifetime values of A^- in different polar aprotic solvents containing various water% (v/v)[a]

| Solvent | Lifetime (τ/ns) | | | | |
| | Water% (v/v) | | | | |
	0.0	1.0	2.0	4.0	8.0
Acetone	3.34 (3.34)	4.03 (4.03)	4.22 (4.22)	4.77 (4.77)	5.71 (5.71)
MeCN	3.83 (3.83)	4.38 (4.38)	4.54 (4.54)	4.97 (4.97)	5.75 (5.75)
DMF	3.85 (3.85)	4.39 (4.39)	4.47 (4.77)	4.87 (4.87)	5.87 (5.87)
DMSO	4.09 (4.09)	4.57 (4.57)	4.60 (4.60)	4.86 (4.86)	5.87 (5.87)
Water[b]	4.75 (4.75)	—	—	—	—

[a] The emission collected at 525 nm for the excitations at 450 nm and 490 nm. The τ values in bracket are for the excitation at 490 nm. [b] τ values in pure water solvent.
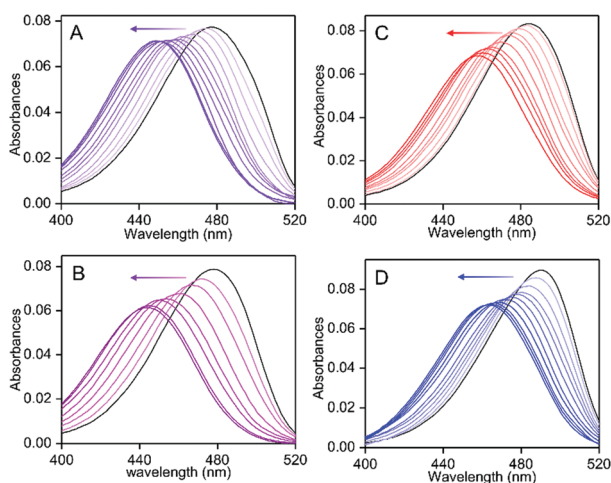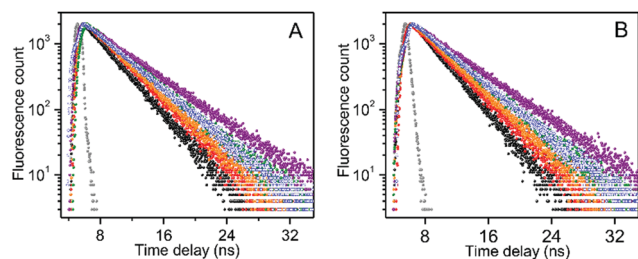

Fig. 4 Excitation wavelength-dependent fluorescence emission spectra of AH (0.5 μM) in the presence of KOH (10 μM) and various water% (v/v) values in different solvents: (A and E) acetone (water%: 0.1, 0.3, 0.6, 1.1, 1.8, 3.0, 4.5, 8.0 and 11.5); (B and F) MeCN (water%: 0.1, 0.2, 0.3, 0.4, 0.6 0.8, 1.0, 1.5, 2.0, 2.5, 3.0, 4.0, 4.7 and 5.5); (C and G) DMF (water%: 0.2, 0.4, 0.8, 1.5, 2.5, 4.0, 6.5, 8.0, 10.0 and 12.0); (D and H) DMSO (water%: 0.5, 1.0, 2.0, 3.5, 5.0, 7.5, 10.0 and 11.4). The spectra in the absence of water are depicted in black. The gradual increase or decrease in intensities with the increase in water% values is indicated by arrows. Excitation wavelengths were 440 nm (A–D) and 485 nm (E–H).

considering the most probable H-bonding interaction between phenolate-O and one hydrogen atom of water molecules (Fig. 1 and Fig. S15A, ESI†). The ground-state structures in the gas phase for free A^- and A^-/H_2O complex were optimized using the B3LYP 6-31G++(3d,3p) basis set (Fig. S15A, ESI†). To correlate the experimental UV-vis absorption parameters, TD-DFT calculations (B3LYP, 6-31G++(3d,3p) basis function) on the optimized ground-state geometries were performed in the solution phase considering the CPCM solvent model for acetone, MeCN and DMSO, and the calculated values of various absorption parameters are depicted in Table 2 and Fig. S15B (ESI†). The electric charge densities in HOMO/LUMO both for A^- and A^-/H_2O are centered within the diformyl-phenolate unit (Fig. S15B, ESI†). The excitation wavelengths for A^- species in different aprotic

Table 2 Solvent dependent experimental (exp.) and TD-DFT calculated (cal.) wavelengths of UV-vis absorption band (λ_{max}) and molar extinction coefficients (ε) for the deprotonated form of AH (A$^-$) and its H-bonded complex with water (A$^-$/H$_2$O)[a]

	Absorbance parameters						
	A$^-$				A$^-$/H$_2$O		
	λ_{max} (nm)		$\varepsilon \times 10^4$ (M^{-1} cm^{-1})		λ_{max} (nm)		$\varepsilon \times 10^4$ (M^{-1} cm^{-1})
Solvent	Exp.	Cal.	Exp.	Cal.	Exp.	Cal.	Exp.	Cal.
Acetone	477	458	1.32	0.91	450	444	1.19	0.80
MeCN	478	457	1.34	0.91	445	443	1.06	0.80
DMF	485	—	1.39	—	457	—	1.16	—
DMSO	489	460	1.50	0.95	463	445	1.21	0.90
Water	—	—	—	—	443	443	1.20	0.87

[a] Experimental UV-vis parameters for A$^-$ (absence of water) and A$^-$/H$_2$O (presence of highest water% value) obtained according to Fig. 2.

solvents (acetone, DMF and DMSO) were computed to be ∼455–460 nm due to the HOMO (43) to LUMO (44) electronic transition (Table 2). However, the A$^-$/H$_2$O H-bonded complex exhibited the absorption intensity at ∼443–445 nm for HOMO (48) to LUMO (49) transition (Table 2). Although the energy of LUMO is comparable between A$^-$ (−0.075 eV) and A$^-$/H$_2$O (−0.077 eV), a considerable decrease in the HOMO energy by 0.006 eV for A$^-$ upon its H-bond interaction with water causes for the spectral blue-shift (Fig. S15B, ESI†). The calculated spectral blue-shift from free A$^-$ species to its water-complex well corresponded with the water-induced experimental blue-shift of the UV-vis absorption (or fluorescence excitation) band of the A$^-$ species in the aprotic solvents (Table 2). In addition, the experimental UV-vis molar extinction coefficient (ε) values also well matched with those values calculated theoretically (Table 2). The results justify the proposed H-bonding mode of the water molecule with A$^-$.

Detection of water in polar aprotic solvents

Water-induced fluorescence response for A$^-$ remained similar on the nature of base (KOH or TEA) used in the polar aprotic solvents (Fig. S16, ESI†). Thus, the addition of base attributes no other role except for the deprotonation of the phenolic-OH moiety in AH. The conversion from free A$^-$ to H-bonded A$^-$/H$_2$O species by the addition of water attributes the blue-shifting of the fluorescence excitation (or UV-vis absorption) band from ∼485 to 440 nm for the fluorescence emission at 525 nm (Fig. S12, ESI†), where the excitation band intensity at ∼485 and ∼440 nm were assigned to the ground-state free A$^-$ and A$^-$/H$_2$O species, respectively. In contrast, their emissive properties, e.g., its intensity-wavelength (∼530 nm) and lifetime values for different excitation wavelengths at 440 and 485 nm are observed to be identical due to the excited-state H-bond dissociation, as discussed before (Fig. S13, S14, ESI† and Table 2). Consequently, with the increase in water% in the solution (up to 6–12% (v/v)), the more amount of free A$^-$ to A$^-$/H$_2$O conversion in the ground state resulted in a gradual increase in the emission intensity at ∼530 nm for a fixed wavelength excitation of the A$^-$/H$_2$O species at 440 nm (Fig. 4A–D), whereas the emission intensity was found to decrease gradually during the excitation of

reduced amount of free A$^-$ species with the 485 nm light (Fig. 4E–H). It is noteworthy to mention here that the base-induced formation of deprotonated A$^-$ species is not possible in relatively nonpolar aprotic solvents (THF) (Fig. S6, ESI†); thus, the operable solvent condition for the detection of moisture should be polar aprotic in nature.

The effect of water-induced changes in the equilibrium concentration of the free A$^-$ and A$^-$/H$_2$O complex on emission intensity changes for the two separate excitation (440 and 485 nm) can be combined together by including the effect of both the intensity changes in a single spectrum (Fig. 4 and 5A–D (right spectra)). For each water% value, the emission spectrum for excitation at 440 nm was divided by the maximum intensity value in the absence of water, and the resulting spectrum ($F(\lambda)/F_0$ (λ_{ex} = 440 nm)) was further divided by the extent of emission intensity decrease factor with respect to the zero water condition for excitation at 485 nm (F_{max}/F_0 (λ_{ex} = 485 nm)) to obtain the normalized emission spectrum (($F(\lambda)/F_0$)/(F_{max}/F_0)) (Fig. 5A–D (right spectra)). Such normalization procedure not only is helpful to manifest the water-induced emission response and its detection sensitivity, but also causes the water%-dependent linear emission response (Fig. 5E–H). In addition, such normalization procedure eliminates the AH concentration dependency during the ratiometric detection of water in the solution with heterogeneous distribution of probe molecules (Fig. 5). The maximum normalized intensity value at ∼530 nm increased more than 5.5- and 5.7-fold in the presence of 6.0% and 7.5% water in acetone and MeCN, respectively (Fig. 5E and F). However, the extent of increased intensities, maximally up to ∼3.5-fold for acetone and 3.3-fold for MeCN, in the presence of various amounts of added water% up to 2% (v/v), maintains a very well behaved linear correlation with a residual of fitting R^2 ∼ 0.995–0.997 and slope ∼ 1.24 volume%$^{-1}$ (acetone) or 1.20 volume%$^{-1}$ (acetonitrile) (Fig. 5E and F). In comparison, the water%-dependent normalized emission intensity increase was found to be relatively less for the other aprotic solvents (DMF and DMSO) (Fig. 5G and H); maximum up to ∼4.3-fold for DMF and 3.8-fold for DMSO. Nevertheless, the linear intensity increasing region expanded up to much higher water% value; ∼6% for DMF and ∼12% for DMSO medium (R^2 ∼ 0.995 and slope 0.34 volume%$^{-1}$ (DMF) or 0.21 volume%$^{-1}$ (DMSO)) than that observed for acetone or MeCN solvent (Fig. 5G and H).

The water amount-dependent linear emission intensity changes can be highly useful for the ratiometric detection of unknown water% in the aprotic solvents. Based on the water-induced minimum extent of detectable unambiguous fluorescence response, the limit of detection (LOD) was evaluated using the eqn. LOD = $3\sigma/k$, where σ and k represent the standard deviation for the emission measurements and the slope value of the linear fitting curve, respectively (Fig. 5E–H). The LOD values for the detection of water% were evaluated to be ∼0.01% for acetone and MeCN, whereas it was ∼0.04% (v/v) for DMF and DMSO. To check the reversibility in the water detection, fluorescence studies for AH (0.5 µM) in the presence of KOH (10 µM) were performed at a certain water% value (1.8% for acetone; 1.5% for MeCN; 2.5% for DMF and 3.5% for

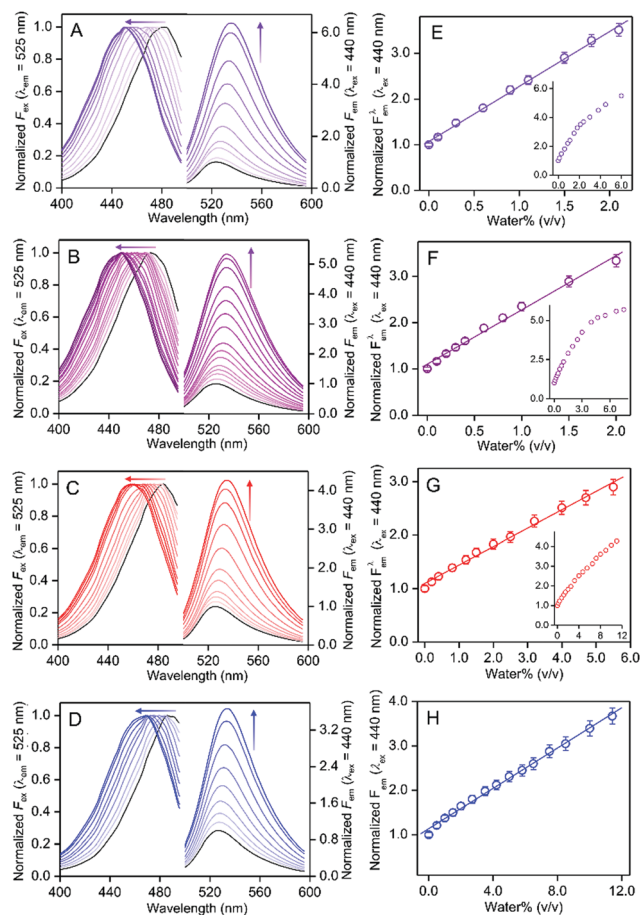Fig. 5 (A–D) Normalized fluorescence excitation (left side) and emission (right side) spectra of AH (0.5 μM) in the presence of KOH (10 μM) and various water% (v/v) values in different solvents: (A) acetone (water%: 0.1, 0.3, 0.6, 1.1, 1.8, 3.0, 4.5, 8.0 and 11.5); (B) MeCN (water%: 0.1, 0.2, 0.3, 0.4, 0.6 0.8, 1.0, 1.5, 2.0, 2.5, 3.0, 4.0, 4.7 and 5.5); (C) DMF (water%: 0.2, 0.4, 0.8, 1.5, 2.5, 4.0, 6.5, 8.0, 10.0 and 12.0) and (D) DMSO (water%: 0.5, 1.0, 2.0, 3.5, 5.0, 7.5, 10.0 and 11.4). The spectra in the absence of water are depicted in black. (E–H) The normalized intensities are plotted against water% (v/v) and fitted linearly up to certain water% range: (E) acetone; (F) acetonitrile; (G) DMF and (H) DMSO. The variations for other higher water% are shown in the *inset* of E–G. (A–D) Each fluorescence excitation spectrum for the emission at 525 nm is normalized by its maximum intensity value. For normalization of emission spectra, each emission spectrum for the excitation at 440 nm was divided by the maximum intensity value in the absence of water, and the resulting spectrum was further divided by the extent of emission intensity decrease factor with respect to zero water condition for excitation at 485 nm. The gradual blue-shift for the excitation spectra or the increase in the emission intensity with the increase in of water% are depicted in arrows.
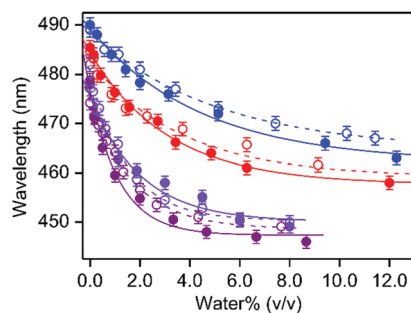
Fig. 6 Water% (v/v)-dependent shift in the fluorescence excitation wavelength (hollow circles, broken lines) for the emission at 525 nm and UV-vis absorption wavelength (solid circles, solid lines) for AH in the presence of KOH in different solvents is plotted: violet, acetone; purple, MeCN; red, DMF; blue, DMSO. The data points are fitted single exponential curves.

emission intensity changes, the wavelength shift of fluorescence excitation or UV-vis absorption band may also be beneficial for the detection of water%. About ∼25 nm blue-shift for the addition of ∼2% water in acetone and MeCN or ∼15 and 20 nm blue-shift for the addition of ∼5% water for DMF and DMSO, respectively, was detected (Fig. 6). The extent of blue-shift in the absorption or excitation spectra was plotted against the water% value in different aprotic media (Fig. 6), and the data points were fitted with a single exponential curve. The phenomenon of such a large wavelength shift induced by the presence of a relatively low water amount (<2% (v/v) for acetone and acetonitrile; <4% for DMF and DMSO) can be exploited for the detection of lower water amounts (Fig. 6).

Real-time moisture analysis in polar aprotic solvents

Polar aprotic organic solvents exhibit high moisture affinity, and thus, require special arrangement to preserve them under the moisture-free condition for prolonged period of time. It has been reported that a considerable extent of moisture incorporation in the solvents may happen even for their short-time exposure in an open atmosphere.[19,21] Using the present water detection protocol, the real-time atmospheric moisture incorporations in the aprotic solvents under the open laboratory atmospheric condition were monitored.

The amount of moisture incorporations is highly dependent on the relative atmospheric humidity and temperature.[21] As described in detail in the experimental section, all the solvents were dried meticulously and stored in a closed glass container in a nitrogen atmosphere with 3 Å molecular sieves up to not more than 12 hours. No moisture incorporation during the solvent preservation was confirmed from the unchanged emission response for A⁻ (Fig. S18, ESI†). We exposed each dried solvent (∼40 mL) containing A⁻ (AH (0.5 μM) + KOH (10 μM)) in a 100 mL beaker with a diameter of ∼5 cm for different time intervals up to 2 hours in the open laboratory atmosphere with 75% (±5%) relative humidity at 25 °C (±1 °C). The amount of moisture incorporation was estimated by evaluating the normalized excitation and emission spectra determined from

DMSO), and followed by the addition of a specific amount of the same solvent without water but containing identical probe concentrations to reach a certain value of water% below that of the respective initial value (0.6% for acetone and MeCN; 0.8% for DMF and 1.0% for DMSO). Fluorescence excitation and emission spectra of final water-diluted solutions were found to be nicely matched with the corresponding known spectra at an identical water% value (Fig. S17, ESI†), showing that the water association with A⁻ is reversible in nature. In addition to the
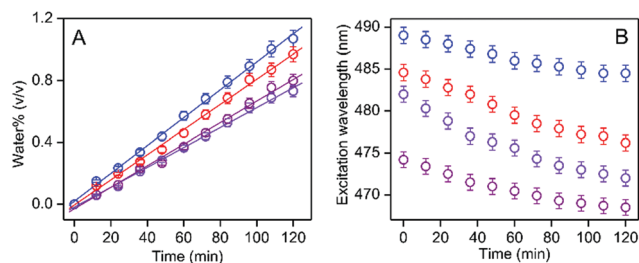
Fig. 7 (A) Plots of water% (v/v) incorporation and (B) the wavelength of fluorescence excitation band for the emission at 525 nm in various aprotic solvents over time upon exposure to an open laboratory atmosphere at 25 °C (±1 °C) and 75% (±5%) relative humidity condition: violet, acetone; purple, MeCN; red, DMF; blue, DMSO.

the time-dependent emission spectra of A^- upon excitation at 440 nm and 485 nm, as described in the previous section (Fig. S19, ESI†). The normalized emission intensity at its intensity maxima at 525–530 nm increased gradually with the increase in exposure time intervals up to 120 min, where the extent of intensity increase depends on the specific solvent system; 1.91-fold for acetone and 1.95-fold for MeCN, 1.40-fold for DMF and 1.37-fold for DMSO for 120 min exposure (Fig. S19, ESI†). The gradual increase in the normalized emission intensity with the time period of atmospheric exposure suggests a greater extent of atmospheric moisture incorporation (Fig. 7A). In addition, the gradual blue-shift in the excitation spectra (from ~474 to 467 nm for acetone; ~482 to 472 nm for MeCN; ~485 to 477 nm for DMF and ~489 to 484 nm for DMSO) with the increase in exposure time intervals also indicates an increase in the moisture content in solvents (Fig. 7B). However, the precise amount of atmospheric moisture incorporation for each solvent system was evaluated by correlating the time-dependent normalized emission intensities at 525–530 nm, according to Fig. 5E–H. It is noteworthy to mention here that the effect of small volume changes, particularly for acetone and MeCN, upon exposure to the open atmosphere, on the relative changes of normalized emission intensities was also considered during the estimation of moisture incorporation from the normalized emission intensity value. With the increase in the exposure time from 12 to 120 min, the amount of moisture intake increased along with maintaining a fairly well linear correlation from ~0.05 to 0.73% (v/v) for acetone, ~0.06 to 0.80% for MeCN, ~0.11 to 0.97% for DMF and ~0.14 to 1.07% for DMSO (Fig. 7A).

To justify the generality of the present methodology in terms of detection accuracy and applicability, we also performed similar atmospheric moisture incorporation studies in the presence of externally added water-spike of 1% before exposing each solvent to the open atmosphere (Fig. S20 and Table S1, ESI†). Notably, the subtracted amount of water-spike from the total recovered water% obtained fluorometrically was found to well match with that evaluated under the condition of without water-spikes (Table S1, ESI†). The results indicate the generality that various extents of contaminated water from different sources can be easily monitored by this method. Based on the

atmospheric moisture incorporation capabilities for different aprotic solvents, the relative hygroscopicity scale can be drawn as DMSO > DMF > MeCN > acetone, which is consistent with the earlier reports.[19,21]

Moisture analysis in different food samples

The moisture content in various processed food items is one of the key parameter from legal and economic point of view.[13,55] There are ample possibility to differ the total moisture content from its recommended tolerant limit particularly in diary food items (butter, cheese and ghee (commonly popular in India and south Asian countries)) or coconut oil, obtained from high water content raw materials. Moreover, higher moisture content than its tolerant limit of ~0.3% in pure oil-based ghee and coconut oil are highly susceptible to undergo microbial degradation or water rancidification during their preservation for prolonged time period.[15–17,56–58] Therefore, the quality control of the foods relies heavily on cost-effective convenient moisture detection methods.

The total moisture contents in those food items (butter, cheese, ghee and coconut oil) available in the market were estimated using the present water detection protocol. For the chosen food samples, most of the food components either insoluble or sparingly soluble in the DMSO medium, and thus, the general solvent properties of DMSO are not expected to differ appreciably even in their presence in large excess, making DMSO a preferred solvent over the other aprotic solvents. In addition, the water-induced linear emission response spanning up to the large water-ratio value of ~12% (v/v) for DMSO is an additional advantage for its use as a suitable medium to detect widely different moisture contents in different food items varying from the very low (ghee or coconut oil) to large value (butter or cheese). The moisture content of a food material is defined using the following equation:

$$\% \text{ Moisture} = (m_w/m_{sample}) \times 100$$

where m_w and m_{sample} represent the mass of water and mass of the sample, respectively.

The water% in various food samples was analysed by mixing different amounts of each food sample in 100 mL DMSO medium according to the protocol described in the Experimental section. The content of free water molecules in ghee or coconut oil is much lower than that in cheese or butter. Therefore, a lower amount of butter (10, 20 and 40 g) or cheese (4.0, 7.5 and 15 g) than ghee or coconut oil (100 g each) was mixed with the DMSO solvent for effective fluorescence studies to estimate the moisture content in those foodstuffs. Fluorescence spectra were recorded with the DMSO phase in the presence of AH (0.5 μM) and KOH (10 μM) (cf. experimental). The relative moisture amounts in different food samples obtained by evaluating the normalized fluorescence intensities are listed in Table 3 (Fig. S21, ESI†). The moisture amounts were found to be ~15% for butter and ~48% for cheese irrespective of different quantities of each sample taken (butter sample: 10, 20 and 40 g; cheese sample: 4.0, 7.5 and 15.0 g) in 100 mL DMSO medium (Table 3). However, low moisture

Table 3 Estimated water amounts in commercial food samples

Sample	Amount^a (g)	Water-spike^b (%, v/v)	Total water^c (%, w/w)	$A_T - A_0{}^d$ (%, w/w)
Butter	10.0	—	15.0 ± 0.2	—
	20.0	—	14.9 ± 0.2	—
	40.0	—	15.4 ± 0.2	—
Cheese	3.0	—	48.2 ± 0.3	—
	7.5	—	48.5 ± 0.3	—
	15.0	—	47.1 ± 0.3	—
Ghee	100	0	0.32 ± 0.04	—
		0.50	0.79 ± 0.04	0.47
		1.00	1.34 ± 0.06	1.02
		1.50	1.83 ± 0.06	1.51
Coconut oil	100	0	0.40 ± 0.04	—
		0.50	0.87 ± 0.05	0.47
		1.00	1.41 ± 0.06	1.01
		1.50	1.88 ± 0.06	1.48

^{a} Mass taken in 100 mL of DMSO solvent. ^{b} Volume% of water with respect to DMSO volume. ^{c} Amount of water with respect to 100 g of food sample. ^{d} Subtracted value of estimated water% without the water-spike from the total estimated water%.

amounts of ∼0.3% and 0.4% were estimated for ghee and coconut oil, respectively (Table 3 and Fig. S21(C and D), ESI†). As described earlier, higher moisture contamination in pure oil-based commercial ghee or coconut oils make them susceptible to water rancidity. To validate our method with detecting higher water%, we introduced additional 0.5, 1.0 or 1.5% water-spike in the DMSO medium containing ghee or coconut oil sample (Fig. S21(C and D), ESI†). The recovered moisture amount after subtracting the actual moisture present, *i.e.*, 0.3–0.4% (estimated without water-spike) in the commercial sample, from the estimated total found water% were closely similar to the amount of respective amounts of water-spikes (Table 3). The results strongly indicate that the present moisture detection protocol can be applied to arrest the water rancidity by identifying the contamination of higher moisture% than its permissible limit for those essentially moisture-free food items with great accuracy.

Conclusions

We demonstrated a sensitive fluorometric method for the detection of trace moisture in various common aprotic solvents using a simple aldehydic phenol probe molecule. The phenolate form of the probe participates in the H-bonding interaction with water in the aprotic medium to exhibit a large blue-shift, from ∼485 nm to 440 nm, in the absorption or fluorescence excitation spectra, although both H-bonded and free phenolate forms of probe show similar emission characteristics owing to the dissociation of the H-bond in the excited state. The water-induced spectral blue-shift and subsequent emission intensity increase and decrease for excitation at 440 nm and 485 nm, respectively, and they were utilized for the detection of moisture. Both those emission intensities changes for two different excitations were combined in a single spectral profile to enhance the detection sensitivity eliminating the dependency of the probe

concentration for the ratiometric detection of moisture even in complex heterogeneous samples. The atmospheric moisture incorporation kinetics was evaluated for various aprotic solvents. Moreover, we estimated the water amount in butter or cheese with a relatively high water content and edible coconut oil or ghee food samples with a low water content. We have also shown that the present water detection protocol is highly effective to check water rancidity in ghee and coconut oil during their manufacture from high-water content raw materials.

Conflicts of interest

The authors declare no competing financial interest.

Acknowledgements

Notes and references

1 H. S. Jung, P. Verwilst, W. Y. Kim and J. S. Kim, *Chem. Soc. Rev.*, 2016, **45**, 1242.
2 N. L. T. Padivitage, J. P. Smuts and D. W. Armstrong, *Specification of drug substances and products: development and validation of analytical methods*, Elsevier, Amsterdam, 2013.
3 T. Kodama, M. Takeuchi, N. Wakiyama and K. Terada, *Int. J. Pharm.*, 2014, **469**, 59.
4 W. E. Lee, Y. J. Jin, L. S. Park and G. Kwak, *Adv. Mater.*, 2012, **24**, 5604.
5 C. Pinheiro, J. C. Lima and A. J. Parola, *Sens. Actuators, B*, 2006, **114**, 978.
6 E. W. Abel, F. G. A. Stone and G. Wilkinson, *Comprehensive Organometallic Chemistry II*, Pergamon, Oxford, 1995.
7 H. W. Roesky, M. G. Walawalkar and R. Murugavel, *Acc. Chem. Res.*, 2001, **34**, 201.
8 S. Das, Y. Sarkar, S. Mukherjee, J. Bandyopadhyay, S. Samantab, P. P. Parui and A. Ray, *Sens. Actuators, B*, 2015, **209**, 545.
9 F. G. Golding, M. Giallorenzo, N. Moreno and V. Chang, *Sens. Actuators, A*, 1995, **47**, 337.
10 R. Liu, X. Xi and C. Liang, *Proc. SPIE-Int. Soc. Opt. Eng.*, 1991, **1572**, 399.
11 A. M. Araujo, L. M. Santos, M. Fortuny, R. L. F. V. Melo, R. C. C. Coutinho and A. F. Santos, *Energy Fuels*, 2008, **22**, 3450.
12 N. S. Foster, J. E. Amonette, T. Autrey and J. T. Ho, *Sens. Actuators, B*, 2001, **77**, 620.
13 J. M. deMan, J. W. Finley, W. J. Hurst and C. Y. Lee, *Principles of Food Chemistry, Food Science Text Series*, 2018, DOI: 10.1007/978-3-319-63607-8.
14 P. Kumar, R. Kaushik, A. Ghosh and D. A. Jose, *Anal. Chem.*, 2016, **88**, 11314.
15 K. Aysegul and J. Issa, *J. Dairy Technol.*, 2008, **61**, 300–306.

16 N. Suwarat and W. Tungjaroenchai, *Int. J. Biosci., Biochem. Bioinf.*, 2013, **3**, 332.

17 E. Lück and G. W. R. Lipinski, Foods, 3. Food Additives, *Ullmann's Encyclopedia of Industrial Chemistry*, 2002, Wiley-VCH, Weinheim, DOI: 10.1002/14356007.a11_561.

18 H. A. Frediani, *Anal. Chem.*, 1952, **24**, 1126.

19 B. Tan, P. Melius and P. Ziegler, *J. Chromatogr. Sci.*, 1982, **20**, 213.

20 J. M. Hogan, R. A. Engel and H. F. Stevenson, *Anal. Chem.*, 1970, **42**, 249.

21 Y. Hui and R. D. Webster, *Anal. Chem.*, 2011, **83**, 976.

22 H. S. Peng, X. H. Li, F. T. You, F. Teng and S. H. Huang, *Microchim. Acta*, 2013, **180**, 807.

23 P. P. Parui, Y. Sarakar, R. Majumder, S. Das, H. Yang, K. Yasuhara and S. Hirota, *Chem. Sci.*, 2019, **10**, 9140.

24 Y. Sarkar, R. Majumder, S. Das, A. Ray and P. P. Parui, *Langmuir*, 2018, **34**, 6271.

25 S. Roy, S. Das, R. Majumder, A. Ray and P. P. Parui, *RSC Adv.*, 2020, **10**, 23245.

26 A. P. de Silva, H. Q. N. Gunaratne, T. Gunnlaugsson, A. J. M. Huxley, C. P. McCoy, J. T. Rademacher and T. E. Rice, *Chem. Rev.*, 1997, **97**, 1515.

27 C. G. Niu, A. L. Guan, G. M. Zeng, Y. G. Liu and Z. W. Li, *Anal. Chim. Acta*, 2006, **577**, 264.

28 Y. Ooyama, M. Sumomogi, T. Nagano, K. Kushimoto, K. Komaguchi, I. Imae and Y. Harima, *Org. Biomol. Chem.*, 2011, **9**, 1314.

29 H. Mishra, V. Misra, M. S. Mehata, T. C. Pant and H. B. Tripathi, *J. Phys. Chem. A*, 2004, **108**, 2346.

30 W. Liu, Y. Wang, W. Jin, G. Shen and R. Yu, *Anal. Chim. Acta*, 1999, **383**, 299.

31 C. Pinheiro, J. C. Lima and A. J. Parola, *Sens. Actuators, B*, 2006, **114**, 978.

32 S. Cha, M. G. Choi, H. R. Jeon and S. K. Chang, *Sens. Actuators, B*, 2011, **157**, 14.

33 W. Chen, Z. Zhang, X. Li, H. Agren and J. Su, *RSC Adv.*, 2015, **5**, 12191.

34 D. W. Cho, *New J. Chem.*, 2014, **38**, 2233.

35 M. Tanioka, S. Kamino, A. Muranaka, Y. Shirasaki, Y. Ooyama, M. Ueda, M. Uchiyama, S. Enomoto and D. Sawada, *Phys. Chem. Chem. Phys.*, 2017, **19**, 1209.

36 D. Yang, X. J. Cao, X. T. Wu, Z. X. Yang and B. X. Zhao, *Anal. Methods*, 2019, **11**, 3079.

37 D. Yang, X. T. Wu, X. J. Cao and B. X. Zhao, *Dyes Pigm.*, 2019, **170**, 1075582.

38 M. G. Choi, M. H. Kim, H. J. Kim, J. E. Park and S. K. Chang, *Bull. Korean Chem. Soc.*, 2007, **28**, 1818.

39 G. Men, G. Zhang, C. Liang, H. Liu, B. Yang, Y. Pan, Z. Wang and S. Jiang, *Analyst*, 2013, **138**, 2847.

40 W. Y. Kim, H. Shi, H. S. Jung, D. Cho, P. Verwilst, J. Y. Lee and J. S. Kim, *Chem. Commun.*, 2016, **52**, 8675.

41 S. A. Poteet and F. M. MacDonnell, *Dalton Trans.*, 2013, **42**, 13305.

42 L. Chen, J. W. Ye, H. P. Wang, M. Pan, S. Y. Yin, Z. W. Wei, L. Y. Zhang, K. Wu, Y. N. Fan and C. Y. Su, *Nat. Commun.*, 2017, **8**, 15985.

43 B. Li, W. Wang, Z. Hong, E. S. M. E. Sayed and D. Yuan, *Chem. Commun.*, 2019, **55**, 6926.

44 R. Kaushik, R. Sakla, N. Kumar, A. Ghosh, V. D. Ghule and D. A. Jose, *Sens. Actuators, B*, 2021, **328**, 129026.

45 T. I. Kim and Y. Kim, *Anal. Chem.*, 2017, **89**, 3768.

46 M. H. Lee, J. S. Kim and J. L. Sessler, *Chem. Soc. Rev.*, 2015, **44**, 4185.

47 R. R. Gagne, C. L. Spiro, T. J. Smith, C. A. Hamann, W. R. Thies and A. K. Schiemke, *J. Am. Chem. Soc.*, 1981, **103**, 4073.

48 International Conference on Harmonization (ICH) of Technical Requirements for Registration of Pharmaceuticals for Human Use, Topic Q2 (R1): Validation of Analytical Procedures: Text and Methodology; http://www.ich.org, 2005.

49 J. V. Morris, M. A. Mahaney and J. R. Huber, *J. Phys. Chem.*, 1976, **80**, 969.

50 M. J. Frisch, *et al.*, *Gaussian 09 Rev. A.1*, Gaussian Inc., Wallingford, CT, 2009.

51 S. Mitra, R. Das and S. Mukherjee, *J. Photochem. Photobiol., A*, 1994, **79**, 49.

52 A. Mandal and S. Mukherjee, *Chem. Phys. Lett.*, 2001, **343**, 265.

53 M. Mukhopadhyay, D. Banerjee and S. Mukherjee, *J. Phys. Chem. A*, 2006, **110**, 12743.

54 H. Shen, L. Zhang and A. Eisenberg, *J. Am. Chem. Soc.*, 1999, **121**, 2728.

55 S. K. Lee, S. Anema and H. Klostermeyer, *Int. J. Food Sci. Technol.*, 2004, **39**, 763.

56 R. L. Bradley, *J. AOAC Int.*, 2001, **84**, 569.

57 M. L. Serunjogi, R. K. Abrahamsen and J. Narvhus, *Int. Dairy J.*, 1998, **8**, 677.

58 A. Kirazci and I. Javidipour, *Int. J. Dairy Technol.*, 2008, **61**, 300.

Fluorometric trace methanol detection in ethanol and isopropanol in a water medium for application in alcoholic beverages and hand sanitizers†

Snigdha Roy,[a] Sanju Das,[b] Ambarish Ray*[c] and Partha Pratim Parui [ID] *[a]

Detection of methanol (MeOH) in an ethanol (EtOH)/isopropanol (^{i}PrOH) medium containing water is crucial to recognize MeOH poisoning in alcoholic beverages and hand sanitizers. Although chemical sensing methods are very sensitive and easy to perform, the chemical similarities between the alcohols make MeOH detection very challenging particularly in the presence of water. Herein, the fluorometric detection of a trace amount of MeOH in EtOH/^{i}PrOH in the presence of water using alcohol coordinated Al(III)-complexes of an aldehydic phenol ligand containing a dangling pyrazole unit is described. The presence of MeOH in the EtOH/^{i}PrOH causes a change of the complex geometry from tetrahedral (Td) to octahedral (Oh) due to the replacement of the coordinated EtOH/^{i}PrOH by MeOH molecules. The Td-complex exhibited fluorescence but the Oh-species did not, because of the intramolecular photo-induced electron transfer (PET). By interacting the Oh species with water, its one MeOH coordination is replaced by a water molecule followed by the proton transfer from the water to pyrazole-N which generates strong fluorescence by inhibiting the PET. In contrast, the water interaction dissociates the Td-complex to exhibit fluorescence quenching. The water induced reversal of the fluorescence response from the decrease to increase between the absence and presence of MeOH is utilized to detect MeOH in an EtOH/^{i}PrOH medium containing water with a sensitivity of ~0.03–0.06% (v/v). The presence of water effected the MeOH detection and allows the estimation of the MeOH contamination in alcoholic beverages and hand sanitizers containing large amounts of water.

Introduction

Worldwide, hundreds of economically constrained people are dying every year because of consumption of methanol (MeOH) contaminated illicit liquors.[1–3] In the countryside, use of crude fermentation methods and improper distillation are the main culprits for the MeOH contamination in ethanol (EtOH). In some cases, unavoidable MeOH formation during standard fermentation processes is also a major concern.[4] Consumption of MeOH beyond a certain permissible limit (1−2 mL per kg body mass) directly affects the central nervous system, by inhibiting the activity of cytochrome c oxidase, causing hypoxia, acidosis or even a painful death.[5–9] Even a minute amount of MeOH ingestion, approximately 10 mL of dietary intake, is potent enough to cause some adverse effects.[10,11] The use of much less expensive MeOH is a very common illegal practice

used to alter the EtOH strength in alcoholic beverages to give a higher profit. Nevertheless, in recent times during the COVID-19 pandemic, a large number of poisonous MeOH containing hand sanitizers were seized worldwide, even after repeated warnings from the FDA.[12] Because the use of costly EtOH and isopropanol (^{i}PrOH) based hand sanitizers has significantly increased to help combat the COVID-19 pandemic, indiscriminate commercial production inevitably increases the chance of using MeOH containing cheaper hand sanitizers.[12]

The MeOH, EtOH and ^{i}PrOH are all chemically similar in nature.[13–15] Thus, using a reaction based chemical sensor, MeOH detection in commercial alcoholic beverages and hand sanitizers containing a large amount of EtOH/^{i}PrOH as well as water is an extremely challenging task.[16–18] In the search for an alternative method of detection, researchers focused on various other analytical procedures, such as different types of mass spectrometry (MS),[19–21] gas chromatography,[22–24] cyclic voltammetry,[25] capillary electrophoresis,[26] quartz crystal microbalances (QCMs) and so on.[27] However, costly sophisticated instrumentation, the requirement of skilled technicians or tedious standardizations for the previous methods are major disadvantages for using them in routine analysis. In view of their cost-effectiveness and easy detection protocol, the reaction

[a]Department of Chemistry, Jadavpur University, Kolkata 700032, India. E-mail: parthaparui@yahoo.com; Fax: +91-33-24146223; Tel: +91-9433490492

[b]Department of Chemistry, Maulana Azad College, Kolkata 700013, India

[c]Department of Chemistry, Barasat Govt. College, Kolkata 700124, India. E-mail: r_ambarish@yahoo.co.in; Tel: +91-9836650180

based chemical sensing methods are far superior detection techniques.

Fluorometric chemical sensing because of its ultra-high sensitivity is considered to be one of the most effective methods. Despite this, few organic fluorescent probes for MeOH are reported in the literature and those that are have certain limitations.[17,28–30] Different materials have also been used as MeOH fluorosensors such as a supramolecular ionic material by Zhang *et al.*,[31] a bimetallic lanthanide-organic framework by Du and co-workers,[32] and nitrogen-doped oxidized carbon dots by Latha *et al.*[33] In most of the cases MeOH is differentiated only from EtOH but not from ^{i}PrOH. The detection is based on either an increase or decrease of the relative intensity changes between MeOH and EtOH but never in the opposite direction, that is an increase for one and a decrease for the other. In addition, the effect of a large amount of water in the sample being analyzed for MeOH, although useful in the preparation of alcoholic beverages and hand sanitizers, has not been thoroughly investigated. Thus, it is proposed that the MeOH detection based on water induced a reverse fluorescence response for the probe such as an increase in intensity in the presence of MeOH but a decrease in intensity in its absence for a EtOH/^{i}PrOH medium.

The aldehydic phenol ligand (PPY) and its alcohol coordinated Al(III)-complexes were strategically synthesized, and they exhibited a water mediated MeOH selective fluorometric response. The presence of MeOH in EtOH/^{i}PrOH induces a change in the complex geometry from a fluorescent tetrahedral (Td) form to a weakly fluorescent octahedral (Oh) form, which is due to the exchange of coordinated EtOH/^{i}PrOH by MeOH. The interaction of water with the Oh-species exhibited a strong fluorescence intensity because of the exchange of its one coordinated MeOH with a water molecule followed by an intramolecular proton transfer from the coordinated water to the ligand moiety. However, the less stable Td-complex in the absence of MeOH is dissociated by the water interaction to exhibit an intensity decrease. Such water induced opposite intensity changes between the absence and presence of MeOH are utilized to detect MeOH in EtOH/^{i}PrOH and in alcoholic beverages/hand sanitizers in a water medium.

Experimental

The general experimental procedures and materials are described on page S2 of the ESI.†

Synthesis of PPY

Firstly, 3,5-dimethylpyrazole (**1**) and 2-hydroxy-3-(hydroxymethyl)-5-methylbenzaldehyde (**2**) were synthesized according to published procedures.[34,35] To synthesize 3-(chloromethyl)-2-hydroxy-5-methylbenzaldehyde (**3**), **2** (0.5 mol) was taken in 2 mL of dichloromethane (DCM, CH_2Cl_2) and the suspension obtained was stirred. Freshly distilled $SOCl_2$ in DCM was added drop wise (final ratio of $SOCl_2 : DCM = 1 : 1$) under constant stirring. The yellow colored solution obtained was then stirred for another hour. Then the unreacted $SOCl_2$

was removed. The solid residue was dissolved in 1 mL of DCM and the solution was further diluted in 1 mL of hexane. The diluted solution was then kept until it had evaporated to dryness, which produced white colored crystals. Next, 1.84 g (10 mmol) of **3** was dissolved in 5 mL of dry THF. Then, 0.96 g (10 mmol) of **1** was taken in 20 mM of TEA. The solution of **1** was added drop wise into the solution of **3**, and the mixture was stirred for 24 h. The solution was extracted with brine solution and activated by Na_2SO_4 to obtain the desired product (PPY), which was further purified using column chromatography. ^{1}H-NMR (DMSO-d_6, 400 MHz): 2.08 (s, 3H, ArC$\underline{H}_3$), 2.23 (s, 6H, Py-2C$\underline{H}_3$), 2.51 (solvent residual peak), 3.33 (due to trace H_2O), 5.14 (s, 2H, C$\underline{H}_2$-Ar), 5.86 (s,1H, Py-C=C$\underline{H}$), 6.98 (s,1H, Ar$\underline{H}$), 7.49 (s,1H, Ar$\underline{H}$), 10.08 (s, 1H, C$\underline{H}$=O), 11.12 (s,1H, Ar$O\underline{H}$) ppm. ^{13}C-NMR (DMSO-d_6, 75 MHz): 10.96, 13.82, 20.51, 39.51–40.90 (solvent residual peak), 46.51, 105.44, 121.82, 126.43, 129.27, 131.85, 136.95, 139.96, 139.79, 146.99, 156.36, 196.19 (Fig. S1 and S2, ESI†). ESI-MS$^+$ for PPY in methanol: m/z calc. for [PPY + H]$^+$: 245.281, found: 245.221 (Fig. S3A, ESI†).

Generation of PPY/Al^{3+} *in situ* complex and its reaction with water

For preparation of a stock solution of $AlCl_3$ (1 mM), appropriate amounts of anhydrous $AlCl_3$ were taken in different alcohol mediums and the mixture was vortexed until completely solubilized. Stock solutions of PPY (1 mM) in each alcohol medium were prepared separately. The alcohol medium was kept the same for the preparation of stock solutions and reaction medium. A portion (10 μL or 4 μL) of the stock solution of PPY (final concentration: 10 μM or 2 μM) was added to each reaction medium (final volume 2 mL) containing various amounts of $AlCl_3$ (5–200 μM) in the absence or presence of water and/or MeOH in alcohol mediums under constant stirring, and the time-dependent PPY/Al^{3+} complex formation kinetics were monitored using UV-vis absorption and fluorescence studies at 25 °C. A diluted solution of PPY/Al^{3+} (0.1 μM PPY + 5 μM $AlCl_3$) was used for the limit of detection (LOD) studies.

UV-vis absorption and fluorescence studies

The UV-vis absorption and fluorescence studies were carried out in a double beam spectrophotometer (TCC-240A, Shimadzu, Japan) and spectrofluorometer (LS 55, PerkinElmer). The fluorescence spectra were obtained upon excitation at 402 nm (excitation band-pass: 10 or 8, and emission band pass: 2 or 8). Time-dependent fluorescence intensities at 505 nm were monitored for up to 60 min upon excitation at 405 nm while maintaining the same excitation and emission band-pass. The measuring solutions were filtered using a 0.45 mm filter (Millex, Millipore). The data reproducibility was checked using multiple measurements.

The LOD for MeOH was obtained as:[36]

$$\text{Detection limit (LOD)} = 3\sigma/k,$$

where σ, and k represent the experimental standard deviation and slope value of the linear fitting, respectively.

The fluorescence quantum yields were measured according to a procedure described earlier.[37]

Theoretical calculations

For structural optimization, density function theory (DFT) calculations were performed with the Gaussian 09 Program.[38] Time-dependent DFT (TD-DFT) calculations were performed to obtain UV-vis absorption parameters of different species. The structural optimizations were carried out by considering the B3LYP exchange-correlation functional and the 6-31G basis function.
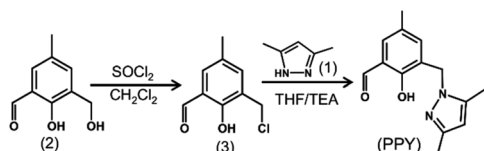
Results and discussion

Probe design for MeOH detection

The synthesis route of the Al^{3+} binding aldehydic phenol ligand consisting of a dangling pyrazole unit (PPY) is shown in Scheme 1. It has recently been reported that the Al^{3+} ion exhibits a strong complex formation affinity with phenolic Schiff-base molecules by binding to phenolic-O and imine-N in alcohol solvents, and the rest of the Al(III)-coordination sites were filled by alcohol molecules.[39] In this research, the aldehydic moiety was deliberately not converted into the corresponding imine functionality of PPY, in order to achieve a reduced complex formation affinity due to the weaker interaction ability of aldehydic-O than that of the imine-N. Thus, upon the addition of a trace amount of the MeOH in the EtOH/^{i}PrOH medium, a spontaneous conversion from a structurally fragile Td geometry to a relatively stable Oh symmetrical PPY/Al^{3+} complex is possible due to the exchange of coordinated EtOH/^{i}PrOH by MeOH molecules. The reaction of water with PPY/Al^{3+} induces a fluorescence increase for the Oh species, but an intensity decrease for the Td complex. The MeOH induced the reversal of the fluorescence intensity change due to the change of the Al(III) geometry which was utilized for the detection of trace MeOH in EtOH/^{i}PrOH.

The PPY/Al^{3+} complex formation and its interaction with water

In the presence of anhydrous $AlCl_3$ (200 μM), the UV-vis absorption intensity at ~340 nm for PPY (10 μM) in alcohol solvents decreased gradually with time (up to 60 min), upon the formation of a new intensity at 405−410 nm through an isosbestic point at ~378 nm (Fig. 1 and S4, ESI†), indicating that PPY was involved in a complex formation reaction with the Al^{3+} ion by a kinetically slow process. The amount of complex formation was evaluated directly by judging the relative
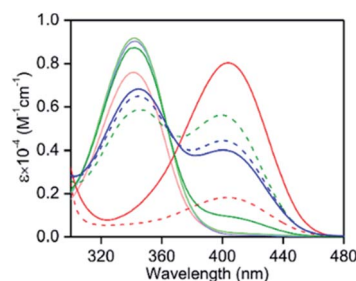

Fig. 1   The UV–vis absorption spectra of PPY (10 μM) in the presence (solid lines) and absence (broken lines) of 2.5% (v/v) water containing anhydrous $AlCl_3$ (200 μM) at 25 °C: red, MeOH; blue, EtOH and green, ^{i}PrOH. The spectra were collected during the 60 min of $AlCl_3$ addition. The spectra of PPY in the absence of $AlCl_3$ and water are depicted in their respective light colors for comparison.

intensity changeover from ~340 nm to the 405–410 nm absorption band, because both intensities are not overlapped by each other (Fig. 1). However, to estimate the equilibrium between PPY and its Al(III)-complex in the presence of various amount of $AlCl_3$ (20–200 μM), the intensity values when the reaction attained equilibrium in nearly in 60 min were evaluated (Fig. 1 and S5, ESI†). It should be noted that a large amount of Al^{3+} (~200 μM, 20 equiv.) was required to react all the PPY with Al^{3+} in an MeOH medium (Fig. 1 and S5, ESI†), which suggested that the interaction of PPY with the Al^{3+} ions was not only kinetically slow but also thermodynamically weak in nature. However, large fractions of unreacted PPY ~60% in EtOH and ~50% in ^{i}PrOH medium were identified in the presence of the same concentration of Al^{3+} (20 equiv.) (Fig. 1). This result indicates that the complex formation affinity was reduced even more in the EtOH/^{i}PrOH than in the MeOH medium.

In spite of inadequate complex formation in the EtOH or ^{i}PrOH solvents, the intensity at ~405 nm for the PPY/Al^{3+} complex was ~3-fold larger, $i.e.$, there was a 6–7 times higher molar extinction coefficient (ε) value (~1.1 × 10^4 M^{-1} cm^{-1}), than that observed in MeOH (~0.17 × 10^4 M^{-1} cm^{-1}) (Fig. 1). Although phenolate-O and Al^{3+} bond formation was quite obvious, the formation of aldehydic-O with the Al^{3+} bond was

Fig. 2   (A) Time–dependent fluorescence intensity changes at 505 nm upon the addition of anhydrous $AlCl_3$ addition (50 μM), and (B) fluorescence spectra in 60 min of $AlCl_3$ addition in various alcohol solvents in the presence (solid line) and absence (broken line) of 2.5% (v/v) water containing PPY (2 μM) at 25 °C: red, MeOH; blue, EtOH and green, ^{i}PrOH. The spectrum in the absence of PPY is shown in grey (B). The excitation wavelengths were 405 nm in both (A and B).

Scheme 1   Synthesis route of PPY.

assured by an up-field ^{1}H-NMR chemical shift from ~9.91 to 9.53 ppm, which was presumably due to an Al^{3+} binding induced, increased negative charge density at the aldehydic-O (Fig. S6 and S7 ESI,† compare with the theoretical calculation section). Furthermore, a 1 : 1 PPY to Al^{3+} binding with a reflection of coordinated alcohol molecules (maximum up to four MeOH molecules (m/z calc. for $[PPY + 4MeOH + Al + Cl]^+$: 433.873, found: 433.912) and two EtOH molecules (m/z calc. for $[PPY + 2EtOH + Al + Cl]^+$: 397.854, found: 397.823)) were recognized in the ESI-MS$^+$ studies (Fig. S3B and D ESI†)). The results indicated that the saturation of the Al(III)-coordination was effected by the solvent alcohol molecules. The reaction of MeOH (1–20% (v/v)) with the solvent coordinated PPY/Al^{3+} in the presence of unreacted PPY in EtOH/^{i}PrOH showed a gradual decrease of both UV-vis intensities at ~340 nm of unreacted PPY and at ~403 nm of the PPY/Al^{3+} complex due to newly formed MeOH coordinated complexes and a replacement of coordinated EtOH/^{i}PrOH by MeOH molecules in the solvent coordinated PPY/Al^{3+}, respectively, (Fig. S8, ESI†). The results justified the proposition that the stability or formation affinity was higher for MeOH coordinated PPY/Al^{3+} than for the EtOH/^{i}PrOH coordinated one.

The interaction of the PPY/Al^{3+} complex with water molecules in EtOH/^{i}PrOH medium showed an increase of absorption intensity at ~340 nm whereas a decrease in intensity at ~405 nm indicated the dissociation of the complex (Fig. S9, ESI†). However, a similar water interaction in the MeOH medium caused a large increase of absorption intensity (~4-fold) at 405 nm without generating any absorption band at ~340 nm for free PPY (Fig. 1). This result shows that water reacted with the Al(III) center in the MeOH coordinated PPY/Al^{3+} complex without disturbing the PPY and Al(III) interaction. Because of the greater stabilities of MeOH coordinated species, an incorporation of a water molecule in the Al(III) coordination site may occur by it replacing one coordinated MeOH molecule, and this phenomenon was verified from the ESI-MS$^+$ measurements (m/z calc. for $[PPY + 3MeOH + H_2O + Al + Cl]^+$: 419.842, found: 419.762) (Fig. S3C, ESI†).

Solvent alcohol/water induced fluorescence response for PPY/Al^{3+}

The PPY exhibited no fluorescence intensity. With an addition of AlCl$_3$ (50 μM, 25 equiv.) in separate different alcohol mediums (MeOH, EtOH or ^{i}PrOH) containing PPY (2 μM), the fluorescence intensity at ~510 nm was enhanced gradually with time until the intensity was nearly saturated in ~60 min of Al^{3+} addition (Fig. 2A). However, the saturated intensity value varied widely depending on the alcohol medium. Compared to MeOH, ~8- and 2-fold larger intensities were detected in ^{i}PrOH and EtOH, respectively, (ϕ_F ~ 0.013 for MeOH, ~0.025 for EtOH, and ~0.102 for ^{i}PrOH) (Fig. 2). Interestingly, the interaction of water with the PPY/Al^{3+} complex exhibited an increase of intensity in the MeOH medium but an intensity decrease in the EtOH/^{i}PrOH medium (Fig. 2). An intensity increase of about 6-fold was observed in the MeOH medium containing ~1.2% (v/v) water, whereas the intensity increased maximally up to ~6.7-fold (ϕ_F ~
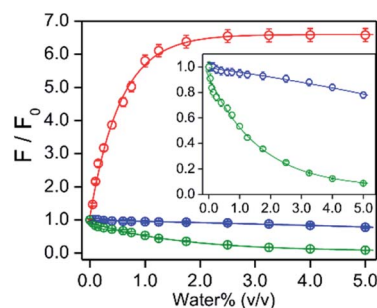

Fig. 3 The ratio of fluorescence intensities at 505 nm for the PPY/Al^{3+} complex in the presence of various amounts of water% and its absence are plotted with the value of water% (v/v) in different alcohol mediums at 25 °C: red, MeOH; blue, EtOH and green, ^{i}PrOH. The intensity values in the absence and presence of different water% are collected in 60 min of anhydrous AlCl$_3$ (50 μM) addition in the medium containing PPY (2 μM). Inset: the Y-axis expanded plots for EtOH and ^{i}PrOH medium are shown for clarity. Excitation and emission wavelength were 405 and 505 nm, respectively. The data points for each alcohol solvent are fitted using a single exponentially-fitted method. The average value for each data point is obtained from triplicate measurements ($n = 3$).

0.09) in the presence of ~2.5% water (Fig. 3). In contrast, intensity quenching, almost completely in ^{i}PrOH and ~20% in EtOH solvents was detected by the addition of 5% water (Fig. 3). Similarly to the EtOH/^{i}PrOH solvent, the water induced fluorescence decrease was noticed for other alcohols (n-PrOH, ^{t}BuOH, n-hexanol) (Fig. S10, ESI†). Therefore, MeOH is a unique alcohol to use to show the water induced fluorescence increase.

DFT theoretical calculations: complex structure *vs.* optical response

The Al(III) can exist as both Oh and Td geometric forms,[40–42] where the Oh symmetry is more preferred than the Td symmetry.[41,42] According to the results of the ESI-MS$^+$ studies, coordination of four MeOH and two EtOH molecules in the respective solvents were identified (Fig. S3, ESI†). Because PPY was acting as 1 : 1 bi-dentate ligand for Al^{3+}, the coordination of the four MeOH molecules was related to the Oh geometry of Al(III). However, the same number of alcohol molecules binding for bigger EtOH or ^{i}PrOH or any other alcohol molecules may not be a steric fit around the Al(III) coordination sphere, thus a less stable Td structure which would allow two EtOH/^{i}PrOH molecules was the most likely to occur (Scheme 2).

Using a DFT based theoretical calculation, it was identified that a possible Oh to Td structural interconversion for PPY/Al^{3+} was responsible for the alcoholic solvent dependent changes in UV-vis absorption and fluorescence properties, both in the presence and absence of water. The ground state geometries of four MeOH and two EtOH/^{i}PrOH molecules coordinated Oh and Td complexes, respectively, with common phenolic-O and aldehydic-O coordination were optimized using B3LYP density function and a 6-31G basis set. The UV-vis absorption properties for the Oh and Td structures were evaluated using the TD-DFT calculations on the optimized ground state structures. The calculated HOMO to LUMO electronic transitions at ~409 nm

for both Oh and Td structures corresponded well with the respective experimental absorption wavelengths (Fig. 1, 4 and Scheme 2). In a similar way to the experimentally observed UV-vis intensity increase at ~405 nm obtained by changing the solvent medium from MeOH to EtOH/^{i}PrOH, the HOMO → LUMO oscillator strength (f_{cal}) for the MeOH coordinated Oh geometry (~0.04) was found to be significantly lower than that detected for the EtOH/^{i}PrOH coordinated Td geometry (~0.07) (Fig. 4). When one coordinated MeOH close to the pyrazole-N was replaced by a water molecule, the optimized structure showed a proton transfer reaction from the coordinated water molecule to pyrazole-N, and a large increase of f_{cal} from ~0.04 to 0.09 was detected (Fig. 4 and Scheme 2). The increase of f_{cal} agreed well with the experimentally observed water induced large increase of UV-vis intensity in the MeOH medium (Fig. 1).

The efficient PET process from the pyrazole unit to the aldehydic phenol chromophore moiety made the PPY non-fluorescent (Fig. S11, ESI†). For the MeOH coordinated Oh structure, the PET process did not disturb it significantly, and thus a weak fluorescence intensity was observed experimentally (Fig. 2 and 4). However, the electron distribution in both HOMO and LUMO for EtOH or ^{i}PrOH coordinated Td-species centered mostly at the aldehydic phenol chromophore, and the resultant suppression of the PET process made the Td complex highly fluorescent (Fig. 2, 4 and Scheme 2). Most interestingly, the calculations also identified that the PET process in the water substituted Oh species was eliminated, which clarified the probable reason for the water induced large increase of fluorescence intensity in the MeOH medium. All these studies suggested that the change of Al(III) geometry from Oh to Td may

be responsible for the alcohol solvent dependent change in optical response for the PPY/Al^{3+} complex.

Detection of MeOH in EtOH or ^{i}PrOH in the presence of water

It was found that the addition of water induced a fluorescence increase for MeOH coordinated Oh PPY/Al^{3+}, whereas the intensity decreased for the EtOH/^{i}PrOH coordinated Td complex (Fig. 3). An intensity increase of about 6.7-fold was found in MeOH/water mixed medium, which remained unaffected within a water% of ~2.5%–11.0% (v/v), although the intensity decreased gradually as the water% was further increased (Fig. 3 and S12, ESI†). However, for the water% amount above ~75%, the intensity value was found to be less in comparison to that observed in the absence of water (Fig. S12, ESI†). It was also observed that the coordinated solvent in the PPY/Al^{3+} complex were replaced by MeOH from the EtOH/^{i}PrOH molecules with a subsequent change of complex geometry from Td to Oh by the addition of MeOH in EtOH/^{i}PrOH (Fig. 2, Scheme 2, and Fig. S8, ESI†). Additionally, the residual unreacted PPY existed after the completion of a complex formation in EtOH/^{i}PrOH medium reacted further with Al^{3+} to form MeOH coordinated PPY/Al^{3+} in the presence of MeOH (Fig. S8, ESI†). Moreover, the presence of 10% MeOH in the solution with various EtOH/^{i}PrOH to water ratios showed that the presence of water effected different extents of intensity increase up to 70% water (Fig. S13, ESI†). All these results strongly suggest that the relative percentage of MeOH
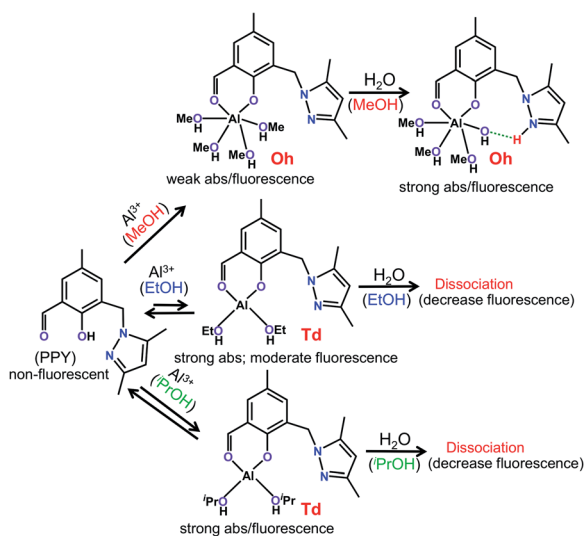
Scheme 2 Mechanistic view of alcoholic solvent selective formation of geometrically different PPY/Al^{3+} complexes and their reaction with water molecules. The Al(III) coordination saturation for the octahedral (Oh) geometry in MeOH and the tetrahedral (Td) geometry in EtOH/^{i}PrOH medium are achieved by the coordination of four MeOH and two EtOH/^{i}PrOH molecules, respectively. The coordination geometry dependent relative UV-vis absorption (abs), and the emission parameters of the PPY/Al^{3+} complex are shown.
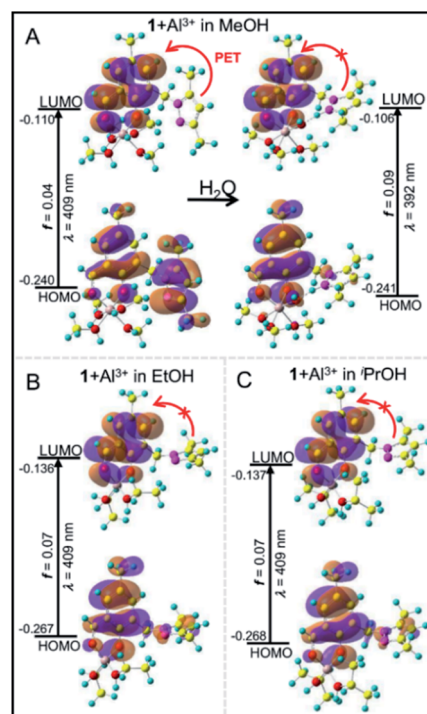

Fig. 4 Frontier molecular orbital (FMO) profiles including different calculated UV-vis absorption parameters of MeOH (A: left upper panel) and MeOH/H$_2$O (A: right upper panel) coordinated Oh. The EtOH (B: left lower panel) and ^{i}PrOH (C: right lower panel) coordinated Td complexes based on DFT and TD-DFT (B3LYP/6-31G) calculations.

coordinated Oh complex with respect to the EtOH/^{i}PrOH coordinated Td species should be much higher even in the presence of a low amount of MeOH in EtOH/^{i}PrOH. The water effected fluorescence intensity increased in the presence of various MeOH amounts was investigated for its potential use in the analytical detection of MeOH in EtOH/^{i}PrOH.

In the EtOH/^{i}PrOH medium containing water, the intensity ratios between the presence and absence of MeOH increased gradually with the increase of MeOH% (0.5–10% (v/v)) when the amount of any fixed water% value was within 2.5–55% (Fig. 5 and S14, ESI†). The relative intensity enhancements depended on the water%. For a solution containing 10% MeOH, the relative intensity increments were ∼2.0-, 3.1-, 2.5- and 1.5-fold for the EtOH system or ∼1.8-, 3.7-, 3.5- and 2.2-fold for the ^{i}PrOH system in the presence of 2.5%, 10%, 25%, and 55% (v/v) of water, respectively (Fig. 5). The extent of the relative intensity increase with increasing MeOH% under various water% (2.5–55%) values followed a fairly good linear correlation (residual of fitting $\chi^2 \sim 0.99$) for both the EtOH and ^{i}PrOH systems, where the water% dependent slope values were estimated to be ∼0.10, 0.21, 0.15 and 0.08 for EtOH or ∼0.08, 0.26, 0.25 and 0.12 for ^{i}PrOH in the presence of 2.5%, 10%, 25% and 55% water, respectively (Fig. 5). Using the linear calibration curve, the unknown amount of MeOH in the EtOH/^{i}PrOH solvent containing various water% can be evaluated ratiometrically. It was evident that the water amount present in the solution played the most critical role for the MeOH detection sensitivity, in which the sensitivity was at maximum at a water amount of ∼10% (v/v) for both EtOH and ^{i}PrOH. Notably, the MeOH (10% v/v) also induced an appreciable amount of increased fluorescence intensity for PPY/Al^{3+} and this was also observed in other alcohol mediums (n-PrOH, ^{t}BuOH and n-hexanol) containing 5% water (Fig. S15, ESI†), which indicated that the MeOH detection selectivity of the PPY/Al^{3+} complex did not alter with the change of alcohol systems. However, to detect a low amount of MeOH or low LOD values, fluorescence studies were

conducted in the presence of very low PPY/Al^{3+} concentrations (0.1 μM PPY and 4 μM Al^{3+}) so that an appreciable fluorescence response can be observed even in the presence of much lower amount of MeOH. The fluorescence intensity changes in the presence of much lower amounts of MeOH (0.05–0.30%) are shown in Fig. S16 (ESI†). The LOD was evaluated using the equation: LOD = $3\sigma/k$ (see Experimental section). The LOD values for MeOH detection were estimated to be ∼0.03%–0.06% depending on the solvent compositions.

The water% dependency variation of the fluorescence response for MeOH was interpreted by combining the water% dependent various extent of intensity increase for MeOH medium in the absence of EtOH/^{i}PrOH and the intensity decrease for EtOH/^{i}PrOH in the absence of MeOH (Fig. 3 and S12, ESI†). The presence of a small amount of MeOH in the EtOH/^{i}PrOH medium replaced coordinated EtOH/^{i}PrOH with MeOH molecules in PPY/Al^{3+} to obtain a Td to Oh structural change. However, the existence of an EtOH/^{i}PrOH coordinated Td complex and its water interaction induced intensity decrease cannot be neglected entirely in the interpretation of the fluorescence response values in the presence of various amounts of MeOH and water. The presence of a water induced ∼6.7-fold intensity increase remains unchanged between 2.5% and 10% of water for MeOH in the absence of EtOH/^{i}PrOH (Fig. 3 and S12, ESI†) and the observed intensity was decreased by increasing the water% (2.5% to 10%) for EtOH/^{i}PrOH in the absence of MeOH, which effects the enlargement of the MeOH detection slope value (∼0.10 to 0.21 for EtOH and ∼0.08 to 0.26 for ^{i}PrOH) by the increase of water%. Significantly higher slope changes for ^{i}PrOH medium: ∼3.7-fold compared to ∼2.1-fold for EtOH medium due to the increase of water% (2.5% to 10%) was rationalized by the increased water amount which induced a greater amount of intensity quenching for ^{i}PrOH (∼90%) than the EtOH medium (45%) in the absence of MeOH (Fig. 5 and S12, ESI†). However, any further increase of water% from 10% to 55% produced a larger intensity decrease for MeOH in the absence of EtOH/^{i}PrOH than for EtOH/^{i}PrOH in the absence of MeOH (Fig. S12, ESI†), and thus a gradual decrease of the MeOH detection slope value from ∼0.21 to 0.08 for EtOH and ∼0.26 to 0.12 for ^{i}PrOH was observed.
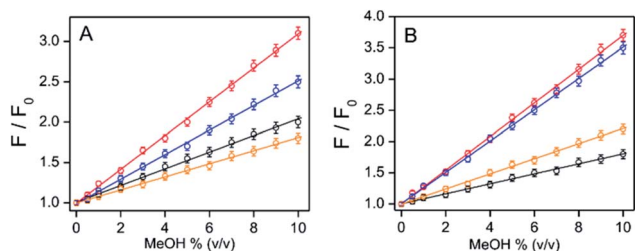
The MeOH detection in alcoholic samples and sanitizers

The EtOH% in alcoholic beverages are dependent (5–70% (v/v)) on their classifications, and usually water is the rest of the liquid volume. However, according to WHO guidelines, the composition of hand sanitizers should be ∼80% EtOH (v/v) or 75% ^{i}PrOH (v/v), glycerol (1.45% (v/v)), and H$_2$O$_2$ (0.125% (v/v)).[43] Spiked MeOH% in high and low EtOH% containing vodkas (∼45% (v/v)) and wine (∼15% (v/v)) samples, respectively, were estimated. As the MeOH detection sensitivity at above 55% (v/v) of water was comparatively low (Fig. S12 and S13, ESI†), an external EtOH addition is required for the detection of MeOH in the wine samples. In addition, spiked MeOH was estimated both in the presence and absence of externally added EtOH to show the applicability of the method for alcoholic beverages containing higher EtOH%. However, the

Fig. 5 Relative fluorescence intensity changes between the presence and absence of MeOH for PPY/Al^{3+} are plotted with MeOH% (v/v) in (A) EtOH/water and (B) ^{i}PrOH/water mixed medium containing various amounts of water (v/v): black, 2.5%; red, 10%; blue, 25%; orange, 55%. The identical value of water% before and after the MeOH spike was maintained by an addition of an appropriate amount of water in the spiked sample. The intensity values in the absence and presence of various MeOH% were collected during the addition of AlCl$_3$ (50 μM), over 60 min, to the medium containing PPY (2 μM). The data points for each solvent system are fitted with a linear equation. Excitation and emission wavelengths were 405 nm and 505 nm. The average value for each data point is obtained from triplicate measurements ($n = 3$).

spiked MeOH amounts were estimated in EtOH- and ^{i}PrOH-based hand sanitizers without any further addition of external EtOH/^{i}PrOH.

To observe the MeOH induced fluorescence intensity increase, the water% before and after MeOH spikes in the hand sanitizer samples were maintained by addition of an appropriate amount of water in the spiked MeOH sample. With the increase of MeOH spikes from 0.5% to 10% in the vodka sample in the presence and absence of externally added 30% EtOH (total water ~25%), the relative fluorescence intensity between the presence and absence of MeOH was found to increase linearly from 1.04- to 1.77-fold and 1.08- to 2.45-fold, respectively (Fig. 6A–C). For a wine sample with the externally added 30% EtOH, the relative intensity also increased linearly from 1.05- to 1.78-fold (Fig. S17, ESI†), where the slope value of the linear plots ~0.08 was found to be similar to that obtained for
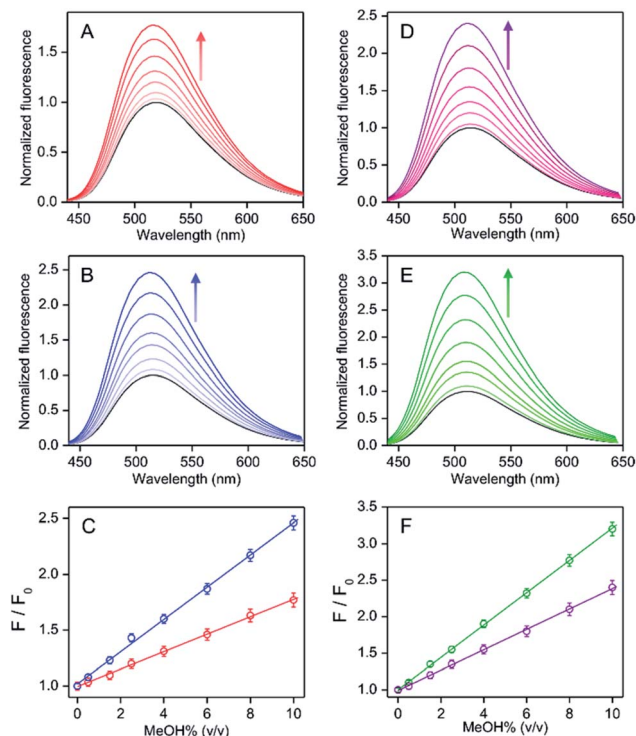

Fig. 6 The relative fluorescence spectral changes between the presence and absence of MeOH for PPY/Al^{3+} with various MeOH spikes (0.5–10% (v/v)) in an alcoholic beverage (vodka: labelled EtOH% ~ 45% (v/v)) in (A) the absence and (B) the presence of externally added 30% EtOH, and (D) EtOH or (E) ^{i}PrOH-based hand sanitizers (labelled ^{i}PrOH ~75% and EtOH ~80%) at 25 °C. The spectra in the absence of MeOH spikes are shown in black. The maximum intensity values for alcoholic beverages (C) and hand sanitizer (F) samples are plotted against the amount of the MeOH spikes. (A–C) Blue and red correspond to the presence and absence of externally added 30% EtOH, respectively. (D–F) Purple and green correspond to EtOH- and ^{i}PrOH-based hand sanitizer, respectively. (A–F) The identical value of water% before and after of MeOH spike was maintained by using an appropriate amount of water addition in the spiked sample. The intensity increases with the increase of MeOH% are shown by arrows. The excitation wavelength was 405 nm. The average value for each data point is obtained from triplicate measurements ($n = 3$).

a known EtOH/water mixed medium (45% EtOH) or vodka (45% EtOH) sample (Fig. 5A). In addition, the slope values for vodka samples with 30% EtOH added externally (total EtOH, 75%) were also similar to the results obtained for the known 75% EtOH medium (Fig. 5A, 6B and C). All these results clearly showed that the presence of other chemicals in alcoholic beverages did not disturb the detection ability of the MeOH. Even without knowing the accurate water% value in the test sample, the estimation of MeOH contamination was possible from the correlation of fluorescence response of the test sample with the linear calibration plots for the corresponding MeOH free alcoholic beverages (Fig. 6C).

The fluorescence spectra for PPY/Al^{3+} in EtOH (80%) or ^{i}PrOH (75%) and a water mixed medium remain unchanged by the addition of glycerol (1.45% (v/v)) or H$_2$O$_2$ (0.125% (v/v)), both in the presence and absence of MeOH (Fig. S18, ESI†), showing that the presence of glycerol and H$_2$O$_2$ in hand sanitizers did not affect the performance of the probe. The intensity increased linearly from ~1.05 to 2.38 for EtOH-based sanitizer or from ~1.08 to 3.22 for the ^{i}PrOH-based sanitizer because of the increase of the amount of MeOH spiking from 0.5% to 10% under the identical water% condition. The observed slope value of ~0.22 for the ^{i}PrOH-based sanitizer and of ~0.14 for the EtOH-based sanitizer were similar to that detected for the known 80% EtOH and 75% ^{i}PrOH medium, respectively (Fig. 5 and 6D–F). Therefore, an unknown amount of MeOH contamination in hand sanitizers could be estimated by correlating the intensity value of the test sample with the known linear calibration line obtained for the EtOH (or ^{i}PrOH) containing water or MeOH free standard for the EtOH (or ^{i}PrOH)-based hand sanitizer.

As in the procedure described previously, a low level of MeOH contamination in alcoholic beverages and sanitizer could be estimated using a low probe concentration (0.1 μM PPY and 4 μM Al^{3+}). The MeOH induced fluorescence spectral changes in the presence of a lower amount of MeOH spikes (0.06–0.18% for a vodka sample and 0.03–0.10% for the ^{i}PrOH hand sanitizer) revealed that even a MeOH contamination of below 0.1 μM in alcoholic beverages and sanitizer can be estimated accurately by the present protocols (Fig. S19, ESI†). The efficiency of probe recovery was also verified by conducting EDTA induced fluorescence intensity quenching studies in vodka and EtOH-based hand sanitizers. For both samples, MeOH induced ~90% of the increased intensity for PPY/Al^{3+} which was found to be quenched by the addition of EDTA, whereas the intensity recovered again upon further addition of Al^{3+} (Fig. S20, ESI†). The EDTA induced displacement of PPY from the PPY/Al^{3+} complex again participated in complexation with the freshly added Al^{3+} to regain the fluorescence intensity by the reaction with MeOH present in solution. Thus, the probe can be reused on several occasions.

Conclusions

A sensitive fluorometric MeOH detection method was demonstrated in EtOH/^{i}PrOH in a water medium using a 1 : 1 Al(III)-complex of an aldehydic phenol ligand containing a pyrazole

unit (PPY). The complex adopted the MeOH coordinated weakly fluorescent octahedral (Oh) geometry from the fluorescent tetrahedral (Td) structure by an addition of MeOH in the EtOH/^{i}PrOH. The interaction of water with the Oh species causes a large fluorescence intensity increase due to the exchange of one coordinated MeOH by a water molecule, whereas a similar water interaction for the Td complex resulted in an intensity decrease due to its dissociation. The water mediated fluorescence intensity reversal due to the change in complex geometries by the addition of MeOH was utilized to detect MeOH in EtOH/^{i}PrOH and various alcoholic beverages/hand sanitizers. Such water induced MeOH detection could be very useful industrially.

Author contributions

Snigdha Roy: experimental, analysis and review and editing. Sanju Das: synthesis. Ambarish Ray: conceptualization, supervision, editing. Partha Pratim Parui: experimental, conceptualization, writing – original draft, supervision.

Conflicts of interest

There are no conflicts of interest to declare.

Acknowledgements

Notes and references

1 S. B. Jarwani, P. D. Motiani and S. Sachdev, *J. Emerg. Trauma Shock*, 2016, **6**, 73.
2 G. A. Beauchamp and M. Valento, *Emerg. Med. Pract.*, 2016, **18**, 1.
3 R. Paasma, K. E. Hovda, A. Tikkerberi and D. Jacobsen, *Clin. Toxicol.*, 2007, **45**, 152.
4 F. Bindler, E. Voges and P. laugel, *Food Addit. Contam.*, 1988, **5**, 343.
5 P. E. Hantson, *Bull Mem Acad R Med Belg*, 2006, **161**, 425.
6 D. G. Barceloux, G. R. Bond, E. P. Krenzelok, H. Cooper and J. A. Vale, *J. Toxicol. Clin. Toxicol.*, 2002, **40**, 415.
7 J. J. Liu, M. R. Daya and N. C. Mann, *J. Toxicol., Clin. Toxicol.*, 1999, **37**, 69.
8 F. Onder, S. Ilker, T. Kansu, T. Tatar and G. Kural, *Int. Ophthalmol.*, 1998, **22**, 81.
9 J. A. Kruse, *Crit. Care Clin.*, 2012, **28**, 661.
10 C. S. Moon, *Ann Occup Environ Med*, 2017, **29**, 44.
11 D. Jacobsen and K. E. McMartin, *Med. Toxicol.*, 1986, **1**, 309.
12 L. Welle, A. Medoro and B. Warrick, *Ann. Emerg. Med.*, 2021, **77**, 131.
13 P. F. Pereira, R. M. F. Sousa, R. A. A. Munoz and E. M. Richter, *Fuel*, 2013, **103**, 725.
14 Methanol: colorless, mp $= -97.0\,^{\circ}\text{C}$, bp $= 64.7\,^{\circ}\text{C}$, $d = 0.79$ g dm^3, n_{D} (at 20 $^{\circ}$C) $= 1.33$, dipole moment $= 1.70$ D, dielectric constant $= 33$, p$K_{\text{a}} = 15.5$.
15 Ethanol: colorless, mp $= -114.3\,^{\circ}\text{C}$, bp $= 78.4\,^{\circ}\text{C}$, $d = 0.799$ g dm^3, n_{D} (at 20 $^{\circ}$C) $= 1.36$, dipole moment $= 1.69$ D, dielectric constant $= 24.6$, p$K_{\text{a}} = 15.9$.
16 G. J. Mohr, F. Lehmann, U. W. Grummt and U. E. Spichiger-Keller, *Anal. Chim. Acta*, 1997, **344**, 215.
17 S. H. Lim, L. Feng, J. W. Kemling, C. J. Musto and K. S. S. Suslick, *Nat. Chem.*, 2009, **1**, 562.
18 T. Qin, B. Liu, Y. Huang, K. Yang, K. Zhu, Z. Luo, C. Pan and L. Wang, *Sens. Actuators, B*, 2018, **277**, 484.
19 L. R. Cordell, H. Pandya, M. Hubbard, A. M. Turner and S. P. Monks, *Anal. Bioanal. Chem.*, 2013, **405**, 4139.
20 T. M. Allen, T. M. Falconer, M. E. Cisper, A. J. Borgerding and C. W. Wilkerson, *Anal. Chem.*, 2001, **73**, 4830.
21 V. Shestivska, V. Kolivoska, J. Kubista, D. Smith and P. Spanel, *Rapid Commun. Mass Spectrom.*, 2020, **34**, 1.
22 M. L. Wang, Y. M. Choong, N. W. Su and M. H. Lee, *J Food Drug Anal*, 2003, **11**, 133.
23 M. Bursova, T. Hlozek and R. Cabala, *J. Anal. Toxicol.*, 2015, **39**, 741.
24 J. V. D. Broek, S. Abegg, S. E. Prastsinis and A. T. Guntner, *Nat. Commun.*, 2019, **10**, 1.
25 D. S. Park, M. S. Won, R. N. Goyal and Y. B. Shim, *Sens. Actuators, B*, 2012, **174**, 45.
26 M. S. F. Santos, E. T. D. Costa, I. G. R. Gutz and C. D. Garcia, *Anal. Chem.*, 2017, **89**, 1362.
27 C. Wang, F. Chen, X. W. He, S. Z. Kang, C. C. You and Y. Liu, *Analyst*, 2001, **126**, 1716.
28 V. Kumar, A. Kumar, U. Diwan, M. K. Singh and K. K. Upadhyay, *Org. Biomol. Chem.*, 2015, **13**, 8822.
29 Z. Wu, X. Fu and Y. Wang, *Sens. Actuators, B*, 2017, **245**, 406.
30 M. Zhao, Y. Yue, C. Liu, P. Hui, S. He, L. Zhao and X. Zheng, *Chem. Commun.*, 2018, **54**, 8339.
31 L. Zhang, H. Qi, Y. Wang, L. Yang, P. Yu and L. Mao, *Anal. Chem.*, 2014, **86**, 7280.
32 D. M. Chen, C. X. Sun, Y. Peng, N. N. Zhang, H. H. Si, C. S. Liu and M. Du, *Sens. Actuators B*, 2018, **265**, 104.
33 M. Latha, R. A. Devi, N. K. R. Bogireddy, S. E. S. Rios, W. L. Mochan, J. C. Uribe and V. Agarwal, *RSC Adv.*, 2020, **10**, 22522.
34 R. H. Wiley and P. E. Hexner, *Org. Synth.*, 1951, **31**, 43.
35 R. R. Gagne, C. L. Spiro, T. J. Smith, C. A. Hamann, W. R. Thies and A. K. Schiemke, *J. Am. Chem. Soc.*, 1981, **103**, 4073.
36 *International Conference on Harmonization (ICH) of Technical Requirements for Registration of Pharmaceuticals for Human Use, Topic Q2 (R1): Validation of Analytical Procedures: Text and Methodology*, 2005, http://www.ich.org.

37 J. V. Morris, M. A. Mahaney and J. R. Huber, *J. Phys. Chem.*, 1976, **80**, 969.

38 M. J. Frisch, *et al.*, *Gaussian 09 Rev. A.1*, Gaussian Inc., Wallingford CT, 2009.

39 S. Roy, S. Das, R. Majumder, A. Ray and P. P. Parui, *RSC Adv.*, 2020, **10**, 23245.

40 J.-J. Delpuech, M. R. Khaddar, A. A. Peguy and P. R. Rubini, *J. Am. Chem. Soc.*, 1975, **97**(12), 3373.

41 E. Furia, A. Beneduci, N. Russo and T. Marino, *New J. Chem.*, 2018, **42**, 11006.

42 L. Malacaria, G. A. Corrente, A. Beneduci, E. Furia, T. Marino and G. Mazzone, *Molecules*, 2021, **26**, 2603.

43 *Guide to Local Production: WHO-recommended handrub formulations (PDF)*, World Health Organization, WHO/IER/PSP/2010.5, WHO April, 2010.